



M Ű E G Y E T E M 1 7 8 2

Budapesti Műszaki és Gazdaságtudományi Egyetem

MECHANICAL STUDY ON THE MESOSTRUCTURE OF HETEROGENEOUS MATERIALS

Tudományos Diákköri Konferencia

2014

Építőmérnöki Kar

Készítette:

Gábor Edit

Budapesti Műszaki és Gazdaságtudományi
Egyetem
Építőmérnöki Kar
Szerkezet-építőmérnök mesterszak
Szerkezet-informatika szakirány (angol nyelvű
képzés)
2. évfolyam

Konzulens:

Dr. Bojtár Imre

Egyetemi tanár
Budapesti Műszaki és Gazdaságtudományi
Egyetem
Építőmérnöki Kar
Tartószerkezetek Mechanikája Tanszék

Budapest, 2014. október

Contents

Introduction	5
1 The historical background of multiscale modeling	7
1.1 Multiple scales in heterogeneous materials	7
1.2 Historical overview of materials sciences and mechanics.....	8
1.2.1 History of materials sciences.....	8
1.2.2 History of continuum mechanics.....	9
1.2.3 History of micromechanics	9
1.3 Introduction to atomistic models of materials	11
1.3.1 Empirical atomistic models of materials	11
1.3.2 Molecular statics	11
1.3.3 Classical equilibrium statistical mechanics.....	13
1.3.4 Molecular dynamics	13
2 Description of the mathematical and continuum-mechanical background of the mechanical modeling of heterogeneous materials.....	14
2.1 Mathematical basis. Application of Green's functions	14
2.1.1 Fourier series and Fourier integrals.....	14
2.1.2 Green's function.....	22
2.2 Mechanical basis. Definitions of eigenstrains and eigenstresses, basic equations	26
2.2.1 General theory of eigenstrains.....	26
2.2.2 General expressions of elastic fields for given eigenstrain distributions	28
2.2.3 Static Green's functions	30
3 Mechanical study on the environment of inclusions and inhomogeneities. Analytical solutions for determination of the resulting elastic field.....	32
3.1 Inclusions.....	32
3.1.1 Definition of inclusion	32
3.1.2 Interface conditions	33
3.1.3 Some examples of eigenstrains	34
3.1.4 Ellipsoidal inclusion with uniform eigenstrains. Eshelby solution	35
3.1.5 Isotropic inclusions	38
3.1.6 Anisotropic inclusions.....	44
3.2 Inhomogeneities.....	48
3.2.1 Definition of inhomogeneity	48
3.2.2 Ellipsoidal inhomogeneities. Equivalent inclusion method	49

3.2.3	Inhomogeneous inclusions	52
3.2.4	Energies of inhomogeneities	56
4	Analytical and numerical model of the environment of inhomogeneities	59
4.1	Analytical model.....	59
4.2	Numerical model	68
4.3	Weak inhomogeneities	73
5	The effect of mesolevel inhomogeneities on macrolevel material properties.....	75
5.1	Definitions of effective moduli of heterogeneous materials	75
5.1.1	Representative volume element.....	76
5.1.2	Random media.....	76
5.1.3	Macroscopic averages	79
5.1.4	Hill's lemma	80
5.1.5	Definitions of effective moduli of heterogeneous media	81
5.2	Bounds for effective moduli	83
5.2.1	Classical variational theorems in linear elasticity	83
5.2.2	Voigt upper bound and Reuss lower bound	84
5.2.3	Hashin-Shtrikman variational principle under displacement boundary conditions	85
5.2.4	Hashin-Shtrikman bounds	89
5.2.5	Hashin-Shtrikman variational principle under traction boundary conditions	91
5.3	Determination of effective moduli	94
5.3.1	Basic ideas of micromechanics for effective properties.....	94
5.3.2	Eshelby method	96
5.3.3	Mori-Tanaka method.....	98
5.3.4	Self-consistent methods for composite materials.....	100
5.3.5	Differential schemes.....	102
6	Analytical and numerical homogenization.....	104
6.1	Analytical homogenization.....	104
6.1.1	Two-phase heterogeneous material	105
6.1.2	Three- and four-phase heterogeneous material	118
6.2	Numerical homogenization.....	120
6.2.1	Derivation of overall material properties by numerical homogenization	121
6.2.2	The applied numerical model	124
6.2.3	Two-phase model	125

6.2.4	Three- and four-phase model	131
7	Summary	133
	Bibliography	135

Introduction

Classical continuum-mechanics presumes the materials to be homogeneous, but as a matter of fact, all the materials are heterogeneous due to their microstructure. It is merely an engineering simplification that above a certain structural level, we regard them to be homogeneous, thereby facilitating mechanical computations. The aim of the most recent developments in material modeling is to describe a structure in such way that under a prescribed loading – regarding either its yielding or fatigue failure –, at the critical structural parts the macroscopically homogeneous material shall be replaced with its *micro-* or *mesolevel* model taking into account its heterogeneous behaviour. This type of material modeling is called *multiscale modeling*.

In case of composite (particle- or fiber-reinforced materials) and polycrystalline materials (metals, ceramics), the effective behaviour of the heterogeneous material can be determined in function of the *known material parameters of the individual phases* and the *volume fractions* of them. The connection between the physical properties on micro- and macrolevel is given by the so-called *homogenization methods*. The multiscale model needs the results of the micro-/mesolevel model to be transformed to the macrolevel structural model, therefore it applies homogenization methods and appropriate boundary conditions to connect the different modeling levels.

Studying the behaviour of heterogeneous materials is not only important in multiscale modeling, but it can also be applied at *designing structures against fatigue* failure. Based on the energies of inclusions and inhomogeneities, one can derive criterion for crack propagation also taking into account whether the individual phases or the interface between them is the weakest part of the material regarding fracture. Another remarkable application of micromechanical based design is to *produce new building materials* and to *develop* already existing ones. The *computer-aided material modeling* presented in this paper can replace the outdated trial-error procedures on a purely scientific basis, resulting in a faster and more economical design process.

Since the subject of micromechanics has not been involved in our university studies, first I had to get familiar with this vast field of mechanics. I reviewed a great amount of literature, both on the analytical and on the numerical background of the subject under consideration. The *scope of this work* is to give an *overall introduction to mesolevel material modeling* that I can continue studying and in the future benefit from this knowledge in the field of multiscale modeling.

In this paper, first I demonstrate the *mathematical* and *mechanical background* of the mesolevel mechanical modeling of heterogeneous materials. The disturbed stress- and strain field due to the presence of inclusions and inhomogeneities are described with the help of Green's functions. In order to interpret this disturbing effect from mechanical point-of-view, I introduce the definitions of *eigenstrains* and *eigenstresses*, that allow us to distinguish voids, inclusions, inhomogeneities and inhomogeneous inclusions inside a material.

In order to get acquainted with the future applications of multiscale modeling, I review the *international researches* made under the topic of atomistic- and mesolevel models so far.

The mechanical study of the environment of inhomogeneities is based both on *analytical solutions* from the literature and on *my own numerical models*. I pay special attention to Eshelby's analytical solution developed for ellipsoidal inhomogeneities, which allow me to make use of the *Eshelby tensor* – describing the connection between the strain- and eigenstrain field in heterogeneous materials – in the homogenization methods as well.

Finally, I compute the *macrolevel material properties* of a heterogeneous material with known physical properties of the individual phases, and given geometry and spatial distribution of heterogeneities. I compare the different analytical and numerical results and define the limit of applicability of the applied homogenization methods.

1 The historical background of multiscale modeling

1.1 Multiple scales in heterogeneous materials

I would like to introduce the importance of micromechanics by a discussion by Egon Orowan (Orowan, 1944):

„The tensile test is very easily and quickly performed, but it is not possible to do much with its results, because one does not know what they really mean. They are the outcome of a number of very complicated physical processes taking place during the extension of the specimen. The extension of a piece of metal is, in a sense, more complicated than the working of a pocket watch, and to hope to derive information about its mechanism from two or three data derived from measurements during the tensile test is perhaps as optimistic as would be an attempt to learn about the working of a pocket watch by determining its compressive strength.”

This statement summarizes the basic idea behind multiscale modeling: the answer of engineering materials to mechanical effects is **highly dependent on their microstructure**, and at critical parts of structures, the otherwise macrolevel structural model shall be replaced by its meso- or microlevel counterparts. When modeling the mechanical behavior of a structural element, a major requirement is to get the most accurate result besides investing in the least possible time and energy. That is the reason why we cannot model everything at its atomistic level: a very complex input would yield a very complex output while the whole process is immensely time-consuming as well. In Figure 1 the different length scales of materials are to be seen.

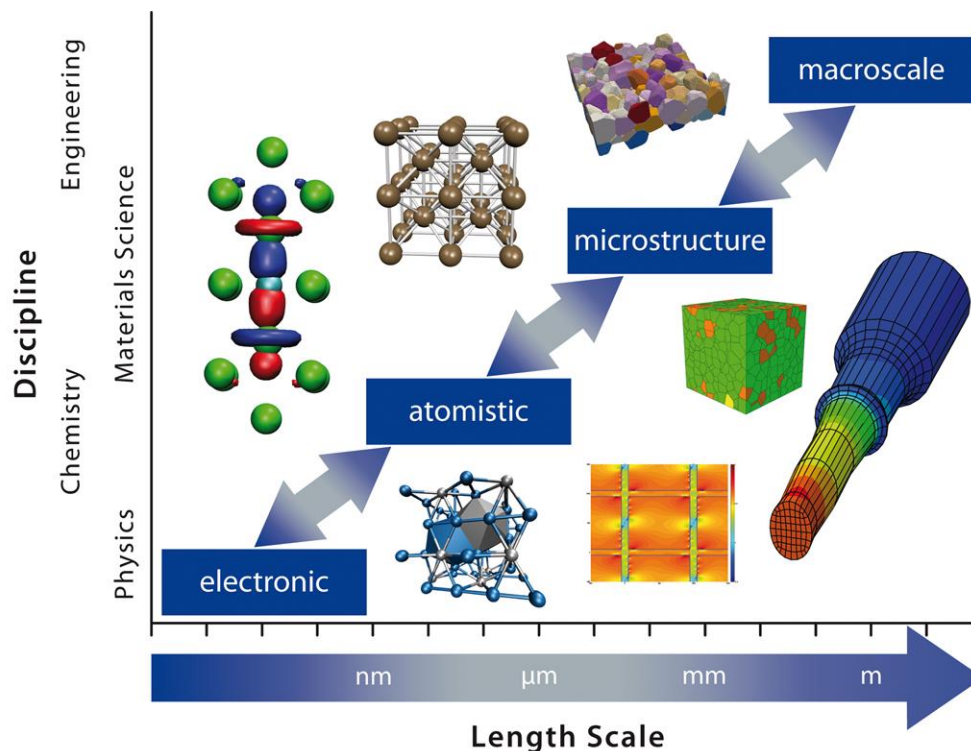


Figure 1 Multiple scales in heterogeneous materials

The *electronic scale* is considered only in very rare cases, for example at carbon nanotubes, but in general, this level is only a field of research, mainly investigated by physicists. The

next level is the *atomistic level*, which appears in mechanics occasionally, but it is more likely a subject of chemistry. On the other hand, in order to understand the connections between individual atoms to macromolecules, the atomistic level needs to be examined thoroughly. In materials science, we are interested in the *microstructure* of materials, which is quite a wide range consisting of individual dislocations and precipitates on the nanometer scale to e.g. the grain structure of polycrystalline materials on the scale of 0.1 mm. The latter structural level is usually called *mesolevel*. Most engineers only deal with the *macroscale*, which is the reason we need to apply homogenization methods in order to provide them macrolevel material properties based on the exact properties measured on smaller levels.

1.2 Historical overview of materials sciences and mechanics

1.2.1 History of materials sciences

The history of *materials sciences* is influenced by the culture of the peoples and by the history of the Earth itself.

Around 300,000 BC, in the *Stone Age*, the use of flint marked the beginning of the use of ceramics. From 5000 BC, in the *Bronze Age*, the utilization of metals became popular, continuously developing the science of metallurgy. In the years 3000 BC, the first alloy, bronze came into use. In the 10th century BC, glass production began to thrive in the Near East. The first steel, called wootz steel was invented in India near 300 BC.

The Roman Empire used local materials, such as pozzolana, a volcanic ash that served as a hydraulic-setting cement, in which they threw local stones, aggregates. This is the Roman concrete, the first man-made composite material.

The application of wood as building material became popular in the Middle Ages, when the Little Ice Age hit the northern hemisphere, resulting in the demand for warmer materials. In the 16th century, Italian metallurgist Vannoccio Biringuccio published his book *De la pirotechnia*, the first systematic book on metallurgy. At the same time in the Netherlands, glass lens were developed, a fundamental component of microscopes and telescopes.

In the 1600s, Italian polyhistor Galileo Galilei's book *Two new sciences* on strength of materials and kinematics included the first quantitative statements on material sciences, as a starting point of the *Age of Enlightenment*. In these years, throughout the 18th century, a great scientific development called *Scientific Revolution* took place with Isaac Newton, Robert Hooke, Charles-Augustin de Coulomb, Augustin-Louis Cauchy, Pierre-Simon Laplace, Joseph Fourier, Leonhard Euler and Joseph-Louis Lagrange.

The 19th century – based on the theoretical evolution of the 1700s – was the age of *Industrial Revolution* with new manufacturing processes, and thus, new artificial materials, such as rubber, metal alloys etc.

The modern materials sciences in the 20th century dealt with steel production, polymers, high temperature and/or high strength materials and soft materials such as gels, foams and organic matters. The first Materials Science Department was founded in 1955 at Northwestern University, Chicago.

1.2.2 History of continuum mechanics

Mechanics is a science of the behavior of physical bodies subjected to forces and displacements and the resulting effects of the bodies on their environment.

Based on the writings of Aristotle, Archimedes and Leonardo da Vinci, Galilei and Newton laid the foundation of *classical mechanics*, a branch of mechanics concerned with particles that are either at rest or moving with velocities much smaller than that of light. Although the atomic nature of matter was already accepted, these works concentrated on the mechanics of *rigid bodies*. Later on, scientists like Ukrainian engineer Stepan Timoshenko (Timoshenko & Goodier, 1934) emphasized in their works, that „Atomic structure will not be considered (...) It will be *assumed* that the *matter of an elastic body is homogeneous and continuously distributed over its volume* so that the *smallest element cut from the body possesses the same specific physical properties as the body*.” The *unifying theory of continuum mechanics* related to American mathematician Clifford Truesdell (Truesdell, 1960) came into use in the mid-1900s along with developments in thermodynamics and rheology. At the same time, *quantum mechanics* was born in 1925, which is not contradictory to classical mechanics, but it has a more general scope.

1.2.3 History of micromechanics

The first postulation of materials having discrete internal structure was found in the work of Leucippus that was later extended by his student, Democritus in the fifth century BC. According to Democritus, the world is built up by *atoms* (from the Greek word 'atomos' meaning 'indivisible') moving about incessantly in a void of emptiness. He stated that only the atoms and the void are real, the objects of sense are just supposed to be real. This perception can be expressed as the observed macroscopic properties being only consequences of the microstructure of materials, they cannot be the starting point of materials science. Democritus also took into account the shapes of atoms and the connections between them when defining the source of the observed properties of a particular material.

Despite being close to the real structure of materials, Democritus' philosophy was abandoned because of its secular nature, and his books were burned, his work is only known from references by others. In Classical Greek philosophy, Plato's view was the leading one, which stated that the basic particles the material is composed of, are made of four basic elements: earth, fire, water and air, and a fifth one, aether (also called quintessence meaning 'fifth element') filling the universe. These five *platonian solids* (Figure 2) were assumed to bear predefined shapes: cube for earth, tetrahedron for fire, icosahedron for water, octahedron for air and dodecahedron for aether.

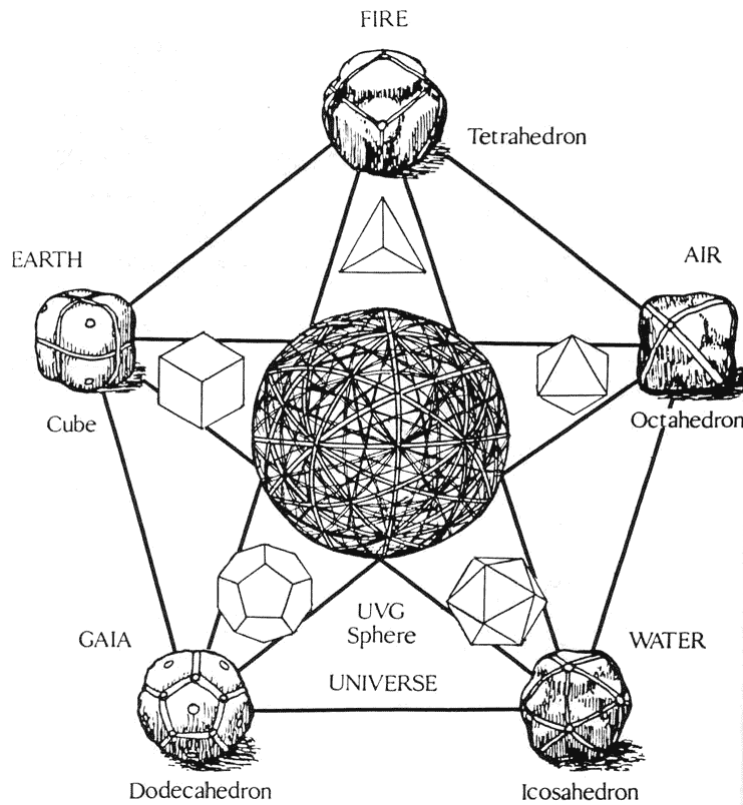


Figure 2 *The platonic solids*

In 1611 AD, German astronomer Johannes Kepler wrote a booklet *On the Six-cornered Snowflake* (Kepler, 1966) in which he ponders the persistent six-fold symmetry of snowflakes. He supposed that this constant shape of snowflake has something to do with the internal structure of snow. He compared it to other natural objects having the same symmetry, such as honeycomb and the seeds in a pomegranate. His observation, known as *Kepler's conjecture* is that the highest possible sphere packing density is obtained from *cubic* or *hexagonal close-packing* (Figure 3) – which was later proven by American mathematician Thomas Hales –, and is again an approach towards the modern materials science.

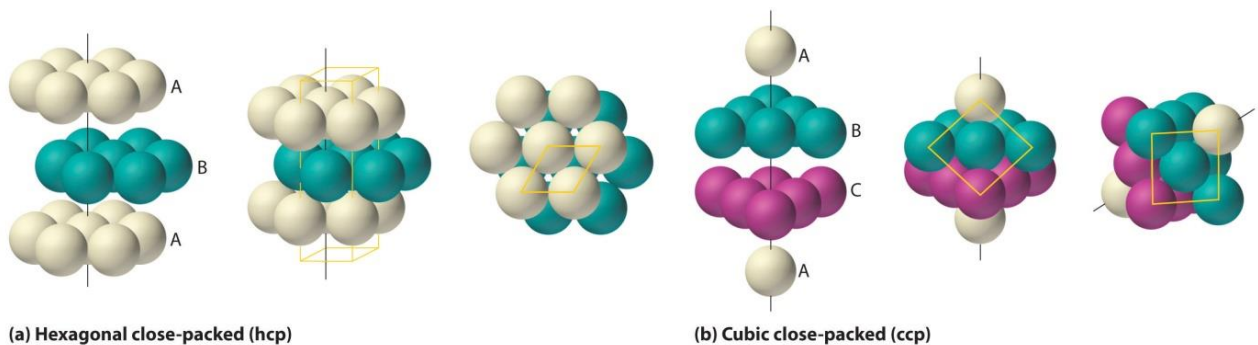


Figure 3 *Hexagonal and cubic close-packed spheres*

In the late 17th century, English scientist Robert Hooke examined materials through the newly-invented microscope. In his book *Micrographia* (Hooke, 1987), sketches of 'crystalline bodies' can be found, which he observed in stones, metals, minerals and salts. He claimed that these regular bodies are constructed by packing 'globular particles' together. Being a

contemporary of Hooke, English physicist Isaac Newton made the same perception on the existence of atoms in his book *Optics* (Newton, 1730) by saying that these indivisible solid particles of particular shapes, sizes and properties are always much harder than the porous bodies compounded by them, which is the basic idea of today's micromechanics as well.

In 1808, English scientist John Dalton proposed that each chemical element is composed of atoms of a unique type that cannot be altered or destroyed by chemical means, and his idea became the accepted *atomic theory of matter*. French crystallographer René-Just Haüy researched the *taxonomy of crystal structures*, and he stated that crystals are built up from polyhedral particles, hence, he did not accept the idea of the close-packed spherical particles. These two concepts were integrated by French scientist Gabriel Delafosse, who replaced Haüy's molecules by polyhedra with Dalton's spherical atoms at the vertices. These polyhedra were classified by French physicist August Bravais, also introducing the idea of *unit cells*.

The idea of *homogenization* arose in the 20th century, when scientists made effort to incorporate the inhomogeneous nature of materials in their calculations without the difficult mathematical part of solving differential equations. In 1957, Eshelby's paper (Eshelby, 1957) on a single ellipsoidal inclusion in isotropic media was a major breakthrough in micromechanics. In the next decade, Hill (Hill, 1963; 1965), Hashin, Shtrikman (Hashin & Shtrikman, 1961; 1963; Hashin, 1988), Budiansky and Tsai laid the foundation of homogenization. In the 1970s, these methods were extended to composites having *periodic microstructure*.

In the present, the main field of interest is to find better bounds, to design new materials or develop already existing ones with the help of homogenization. Due to the continuous advancements in computer science, *computational physics* – an application of numerical methods in solving problems of physics – became a major field of research, and without the support of homogenization, the modern *multi-scale modeling techniques* would not exist.

1.3 Introduction to atomistic models of materials

1.3.1 Empirical atomistic models of materials

In order to model properly the bonding problems of solids, one must apply quantum mechanics and solve *Schrödinger's equations* for the electronic wave functions. Since the methods of quantum mechanics is too complex even in the simplest cases, numerical solutions can be found using the so-called *density functional theory* (DFT) or its parametrized version, *tight-binding* (TB), but these methods need great computational time. To model the bonding problem of solids, we have to use *fitted functional forms* that gives an approximation to the atomic interactions. Even the TB formulations contain daring approximations comparing to quantum mechanics, therefore the empirical models should always be treated suspiciously.

1.3.2 Molecular statics

With the help of the methods of *molecular statics*, one can study the main features of the potential energy landscape of a configuration of atoms.

With the highly accurate methods of quantum mechanics – DFT or TB –, one can compute the total potential energy of a configuration of atoms. These empirical models approximate the electronic energy as a potential energy function dependent only on the interatomic distances. The common feature of these models is that we can calculate the potential energy $V = V(\underline{r})$ for any arbitrary set of N atoms with the positions $\underline{r} = (r^1, \dots, r^N)$. The configuration space of the system contains the set of all the possible coordinates $\{\underline{r}^\alpha\}$.

The potential energy function can be visualized as a $3N$ -dimensional *potential energy landscape*, that can be *characterized by its extremal points*, i.e. minima, maxima and saddle points. In order to find these particular points, numerical techniques must be applied, such as the method of the steepest descent. This way the configuration space can be divided into disjoint regions, corresponding to the set of points that quench to the same minimum. These regions are called the *basins of attraction*. They are separated by dividing surfaces that intersect each other in the saddle points. The deepest minima on the energy landscape refers to the defect-free crystalline structures. Minima with higher energies are associated with crystalline containing internal defects. Even higher energies denotes the amorphous structures and finite clusters. The *curvature of the energy function* around a minimum point determines the *elastic modulus* of the particular solid. The *transition paths*, which is the lowest-energy trajectory between two minima, predict how the material deforms.

In numerical mathematics, finding the global minimum of a nonconvex, multi-dimensional function quickly is still an open field of research. These *nonlinear optimization problems* are usually solved with the help of the steepest descent (SD), conjugate gradient (CG) or Newton-Raphson (NR) method. These methods are also called *local optimization methods*, since there is no guarantee that the result coming from these methods is truly the global minimum of the function, usually they result only in local minima. When talking about *relaxation*, it is the process that takes us from the unrelaxed, i.e. starting configuration or initial guess to the local minimum, which is the relaxed structure. There are *global optimization techniques* such as simulated annealing, that uses Monte Carlo sampling.

When solving nonlinear optimization problems, the solution is highly dependent on the initial guess. It is not always needed to find the global minimum, for example in solids, it would be associated with the perfect crystal, but we are more interested in crystals with internal defects, therefore finding local minima is more suitable.

Dislocation motions, fracture, chemical reactions and diffusion are some of the processes that follow the transition paths of the potential energy landscape. Finding saddle points are even more difficult than finding local minima. The general feature of saddle points is that they have positive curvature in one direction and negative curvature in another. The so-called eigenvector-following methods analyze the Hessian matrix of the system, which is very time consuming. Transition paths are easy to find, once the saddle points are known. The most widely used method is the so-called nudged elastic band (NEB) method.

In molecular statics, we are able to predict the atomic behavior at zero temperature. Though, the atoms in the crystals are always *vibrating with a velocity* that is highly *dependent on*

temperature. On microscale, the thermal fluctuations are of random and chaotic nature, thus we need to resort to *statistical methods* to understand the effect of this motion on the macroscopic level of materials science. The *numerical realization of statistical mechanics* is the *equilibrium molecular dynamics*.

1.3.3 Classical equilibrium statistical mechanics

Statistical mechanics is a 'bridge' between atomistic and continuum mechanical models. It is based on the fact that continuum variables represent the averages over sufficiently large number of atoms. Molecular dynamics simulations on the macrolevel give us information about the positions and velocities of the atoms of a system, that should be translated to the level of engineering design, i.e. how can the engineers use this data for designing an airplane against fatigue failure.

The most important reason to connect these two models is the application of '*multiscale methods*', that concurrently *couple continuum and atomistic descriptions in one model*. At the interface of the micro- and macrolevel, *appropriate boundary conditions* need to be set.

The key to averaging over the dynamical behavior of a large number of *atoms* is the fact that *as a set, they exhibit highly regular statistical behavior*.

Phenomenological theories, such as continuum mechanics use variables that can be measured at macrolevel, like volume, energy, temperature, stress and entropy. These variables are referred to as *macroscopic observables*. In continuum mechanics the macroscopic observables are called *state variables*. At the microscale, a system is fully characterized by the set of *positions* and *momenta* ($\underline{q}, \underline{p}$) of its atoms. It is then convincing to assume that a macroscopic observable \mathcal{A} is related to a function $A(\underline{q}, \underline{p})$ called *phase function*. The aim of statistical mechanics is to make an *explicit connection* between the state variable \mathcal{A} and the phase function $A(\underline{q}, \underline{p})$.

1.3.4 Molecular dynamics

Molecular dynamics simulations follow the motion of all the atoms in the system by treating them as classical Newtonian particles, writing the *equations of motion*

$$(1.1) \quad m^\alpha \ddot{\underline{r}}^\alpha = \underline{f}^\alpha, \quad \alpha = 1, \dots, N,$$

where N is the number of atoms in the system, m^α is the mass of the α -th atom, \underline{r}^α is its position and \underline{f}^α is the time-dependent force acting on it due to both external and internal effects.

MD simulations are used to replace the limited molecular statics simulations, because the latter cannot take into account that at finite temperature, the real systems of atoms are in constant motion. Molecular dynamics is a branch of science evolved from statistical mechanics.

2 Description of the mathematical and continuum-mechanical background of the mechanical modeling of heterogeneous materials

2.1 Mathematical basis. Application of Green's functions

The analytical solutions of problems related to the existence of inclusions and inhomogeneities are based on the application of Green's functions. In order to understand the formulae given in the forthcoming chapters, I introduce the most important mathematical expressions from the Fourier series to Green's functions through the integral transforms.

2.1.1 Fourier series and Fourier integrals

2.1.1.1 Fourier series

The **Fourier series** of a function $f(x)$, where $f(x)$ is a continuous, integrable function defined on the interval $[-c, c]$:

$$(2.1) \quad f(x) = \left(\frac{a_0}{2} \right) + \sum_{k=1}^{\infty} \left(a_k \cos\left(\frac{k\pi x}{c}\right) + b_k \sin\left(\frac{k\pi x}{c}\right) \right).$$

The coefficients a_k and b_k (k : integer):

$$(2.2) \quad a_k = \frac{1}{c} \int_{-c}^c f(x) \cos\left(\frac{k\pi x}{c}\right) dx, \quad n = 0, 1, 2, \dots,$$

$$(2.3) \quad b_k = \frac{1}{c} \int_{-c}^c f(x) \sin\left(\frac{n\pi x}{c}\right) dx, \quad n = 1, 2, \dots$$

If $f(x)$ were an odd function (Figure 4): $f(-x) = -f(x)$, then $a_n = 0$ ($n = 0, 1, 2, \dots$), thereby we can express $f(x)$ as a sinusoidal function with the help of its Fourier series extension. If $f(x)$ were an even function (Figure 5): $f(-x) = f(x)$, then $b_n = 0$ ($n = 1, 2, \dots$), hence its Fourier series extension will not include the sinusoidal term.

2.1.1.2 Double Fourier series

Let $\varphi_n(\alpha, \beta)$ be a set of continuous functions defined on the region $-a \leq \alpha \leq a$, $-b \leq \beta \leq b$. The set of functions is

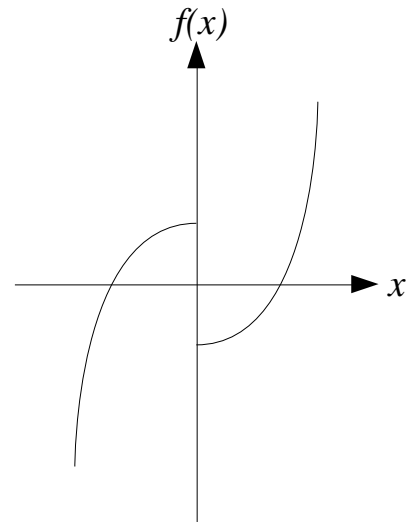


Figure 4 Odd function

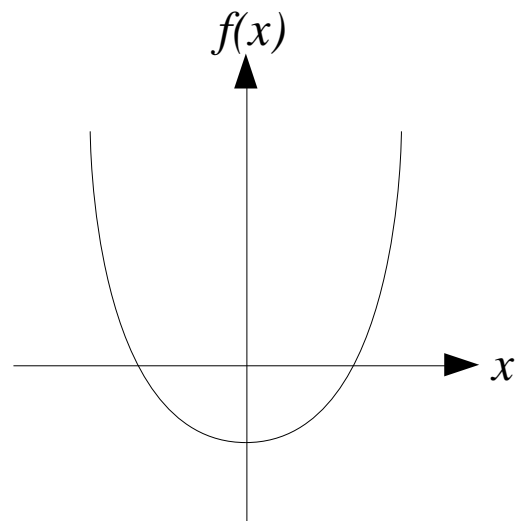


Figure 5 Even function

orthogonal, if

$$(2.4) \quad \int_{\beta} \int_{\alpha} \varphi_n(\alpha, \beta) \varphi_m(\alpha, \beta) d\alpha d\beta = 0, \quad n \neq m.$$

The norm of $\varphi_n(\alpha, \beta)$:

$$(2.5) \quad \|\varphi_n\| = \left(\int_{\beta} \int_{\alpha} \varphi_n^2(\alpha, \beta) d\alpha d\beta \right)^{\frac{1}{2}}.$$

We say that a set of function is normalized, if: $\|\varphi_n\| = 1$.

It is possible to extend a function of two variables $f(\alpha, \beta)$ in terms of $\varphi_n(\alpha, \beta)$ orthogonal functions:

$$(2.6) \quad f(\alpha, \beta) = \sum_{n=0}^{\infty} c_n \varphi_n(\alpha, \beta).$$

The coefficients can be calculated based on the orthogonality of the functions:

$$(2.7) \quad c_n = \frac{\int_{\beta} \int_{\alpha} f(\alpha, \beta) \varphi_n(\alpha, \beta) d\alpha d\beta}{\int_{\beta} \int_{\alpha} \varphi_n^2(\alpha, \beta) d\alpha d\beta}.$$

If the orthogonal set of functions are normalized, the denominator in (2.7) is $\int_{\beta} \int_{\alpha} \varphi_n^2(\alpha, \beta) d\alpha d\beta = 1$, and the coefficients become:

$$(2.8) \quad c_n = \int_{\beta} \int_{\alpha} f(\alpha, \beta) \varphi_n(\alpha, \beta) d\alpha d\beta.$$

2.1.1.3 Double trigonometric series

Considering the orthogonal set of functions

$$1, \cos(mx), \sin(mx), \cos(ny), \sin(ny), \\ \cos(mx)\cos(ny), \sin(mx)\cos(ny), \\ \cos(mx)\sin(ny), \sin(mx)\sin(ny), \dots \quad (n, m = 1, 2, 3, \dots)$$

defined on the region $-\pi \leq x \leq \pi$, $-\pi \leq y \leq \pi$, it is leading to the system

$$(2.9) \quad a_{mn} = \frac{1}{\pi^2} \int_{y} \int_{x} f(x, y) \cos(mx) \cos(ny) dx dy,$$

$$(2.10) \quad b_{mn} = \frac{1}{\pi^2} \int_{y} \int_{x} f(x, y) \sin(mx) \cos(ny) dx dy,$$

$$(2.11) \quad c_{mn} = \frac{1}{\pi^2} \int_0^\pi \int_0^\pi f(x, y) \cos(mx) \sin(ny) dx dy,$$

$$(2.12) \quad d_{mn} = \frac{1}{\pi^2} \int_0^\pi \int_0^\pi f(x, y) \sin(mx) \sin(ny) dx dy,$$

with $m, n = 1, 2, \dots$. Extending the possible values that m, n can take by either $m = 0$ or $n = 0$, the series expansion of function $f(x, y)$ can be written as:

(2.13)

$$f(x, y) = \sum_{m, n=0}^{\infty} \lambda_{mn} (a_{mn} \cos(mx) \cos(ny) + b_{mn} \sin(mx) \cos(ny) + c_{mn} \cos(mx) \sin(ny) + d_{mn} \sin(mx) \sin(ny))$$

with the coefficients

$$(2.14) \quad \lambda_{mn} = \begin{cases} \frac{1}{4} & \text{for } m = n = 0, \\ \frac{1}{2} & \text{for } m > 0, n = 0 \text{ or } m = 0, n > 0, \\ 1 & \text{for } m, n > 0. \end{cases}$$

The $x, y \in [-\pi, \pi \times -\pi, \pi]$ variables and domain can be transformed into $\alpha, \beta \in [-a, a \times -b, b]$, where $x = \frac{\pi\alpha}{a}$, $y = \frac{\pi\beta}{b}$.

2.1.1.4 Integral transforms

The function $f(x)$ has convergent integral¹ on $[0, \infty]$ if

$$(2.15) \quad I_f(\alpha) = \int_0^\infty f(x) K(\alpha x) dx$$

¹ An infinite series $\sum_{n=0}^{\infty} f(n)$ of non-negative terms $f(x)$ defined on the unbounded interval $[0, \infty]$ on which

it is monotone decreasing, converges to a real number if and only if the improper integral $\int_0^\infty f(x) dx$ is finite.

In this case, the *improper integral* is the limit of a definite integral as the endpoint of the interval of integration approaches to infinity: $\lim_{b \rightarrow \infty} \int_a^b f(x) dx$. If the improper integral is finite, then the proof also gives the lower

and upper bound for the infinite series: $\int_0^\infty f(x) dx \leq \sum_{n=0}^{\infty} f(n) \leq f(0) + \int_0^\infty f(x) dx$.

is convergent. $I_f(\alpha)$ is the *integral transform* of function $f(x)$ by kernel² $K(\alpha x)$.

If (2.15) is satisfied by only one particular $f(x)$, then the integral (2.15) has an inverse form:

$$(2.16) \quad f(x) = \int_0^{\infty} I_f(\alpha) H(\alpha x) d\alpha.$$

If $K(\alpha x) = H(\alpha x)$, then $K(\alpha x)$ is a *Fourier kernel*, and the integral transform of function $f(x)$ by a Fourier kernel $K(\alpha x)$ is called the **Fourier transform** $F(\alpha)$ of the function:

$$(2.17) \quad F(\alpha) = \int_0^{\infty} f(x) K(\alpha x) dx.$$

The *Mellin transform* $K(s)$ of kernel $K(x)$:

$$(2.18) \quad K(s) = \int_0^{\infty} K(x) x^{s-1} dx,$$

where the kernel $K(x)$ itself is transformed by the Mellin kernel

$$(2.19) \quad M(x, s) = x^{s-1}.$$

If $K(\alpha x)$ is a Fourier kernel, it has the property

$$(2.20) \quad K(s)K(1-s) = 1.$$

2.1.1.5 Dirichlet's conditions

Dirichlet's conditions give integrability properties of a given function $f(x)$.

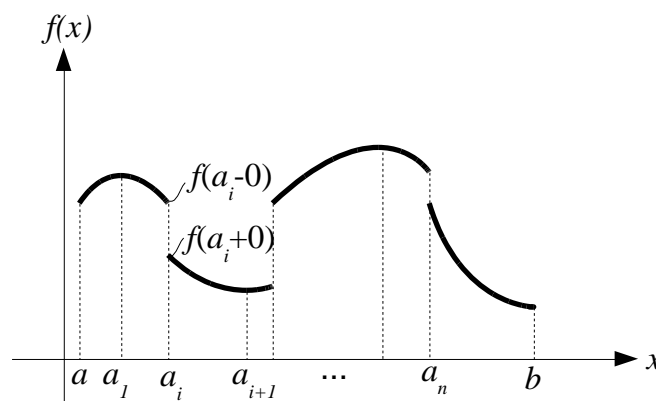


Figure 6 A function $f(x)$ satisfying Dirichlet's conditions

² An integral transform is a particular type of mathematical operator, where the input is a function $f(x)$, the output is another function $I_f(\alpha)$ dependent on the choice of the kernel function $K(\alpha x)$ of variables x and α . There are some special integral transforms, such as Fourier transform, Mellin transform, identity transform, they are dependent only on the applied kernel function.

A function $f(x)$ satisfies *Dirichlet's conditions* if $f(x)$ has only finite number n of extrema and of finite discontinuities in interval $[a, b]$ (Figure 6). If $f(x)$ satisfies Dirichlet's conditions in $[a, b]$, then in each subinterval defined between an extremum or discontinuity a_i and a_{i+1} , the function is monotone increasing or decreasing and

$$(2.21) \quad \lim_{\omega \rightarrow \infty} \int_a^b f(x) \sin(\omega x) dx = 0,$$

$$(2.22) \quad \lim_{\omega \rightarrow \infty} \int_a^b f(x) \cos(\omega x) dx = 0$$

where $\omega \rightarrow \infty$ means that the upper bound b of the definite integral approaches infinity, resulting in an improper integral¹.

The function $f(x)$ can be expanded in a Fourier series which converges to the function $f(x)$ at continuous points, and to the mean of the positive and negative limits $\frac{1}{2}(f(x+0) + f(x-0))$ at points of discontinuity:

$$(2.23) \quad \lim_{\omega \rightarrow \infty} \frac{2}{\pi} \int_a^b f(x+u) \frac{\sin(\omega u)}{u} du = \begin{cases} f(x+0) + f(x-0) & \text{if } a < 0 < b, \\ f(x+0) & \text{if } a = 0 < b, \\ f(x-0) & \text{if } a < 0 = b, \\ 0 & \text{if } 0 < a < b \text{ or } a < b < 0. \end{cases}$$

If $f(x)$ satisfies Dirichlet's conditions, then

$$(2.24) \quad \frac{1}{2}(f(x+0) + f(x-0)) = \frac{1}{\pi} \int_0^{\infty} d\alpha \int_{-\infty}^{\infty} f(u) \cos(\alpha(u-x)) du,$$

at points of discontinuity and at continuous points

$$(2.25) \quad f(x) = \frac{1}{2}(f(x+0) + f(x-0)) = \frac{1}{\pi} \int_0^{\infty} d\alpha \int_{-\infty}^{\infty} f(u) \cos(\alpha(u-x)) du.$$

2.1.1.6 Integral theorems

If a function $f(x)$ has a convergent integral in interval $[0, \infty]$ and satisfies Dirichlet's conditions, we can extend $f(x)$ in interval $[-\infty, 0]$ such that $f(-x) = f(x)$, i.e. by constructing an even function. In this case, from (2.24) comes

$$(2.26) \quad f(x) = \frac{2}{\pi} \int_0^{\infty} \cos(\alpha x) d\alpha \int_0^{\infty} f(\eta) \cos(\alpha \eta) d\eta = \sqrt{\frac{2}{\pi}} \int_0^{\infty} F_c(\alpha) \cos(\alpha x) d\alpha,$$

where the Fourier cosine transform of $f(x)$ is defined as

$$(2.27) \quad F_c(\alpha) = \sqrt{\frac{2}{\pi}} \int_0^{\infty} f(\eta) \cos(\alpha \eta) d\eta .$$

If we extend $f(x)$ in the interval $[-\infty, 0]$ such that $f(-x) = -f(x)$, i.e. by constructing an odd function, then, similarly to (2.26):

$$(2.28) \quad f(x) = \frac{2}{\pi} \int_0^{\infty} \sin(\alpha x) d\alpha \int_0^{\infty} f(\eta) \sin(\alpha \eta) d\eta = \sqrt{\frac{2}{\pi}} \int_0^{\infty} F_s(\alpha) \sin(\alpha x) d\alpha ,$$

where the Fourier sine transform of $f(x)$ is

$$(2.29) \quad F_s(\alpha) = \sqrt{\frac{2}{\pi}} \int_0^{\infty} f(\eta) \sin(\alpha \eta) d\eta .$$

Noting that

$$(2.30) \quad \int_{-m}^m \cos(\alpha(\eta - x)) d\alpha = 2 \int_0^m \cos(\alpha(\eta - x)) d\alpha ,$$

$$(2.31) \quad \int_{-m}^m \sin(\alpha(\eta - x)) d\alpha = 0 ,$$

from (2.25) it can be written that

$$(2.32) \quad f(x) = \lim_{m \rightarrow \infty} \frac{1}{\pi} \int_{-\infty}^{\infty} f(\eta) d\eta \int_0^m \cos(\alpha(\eta - x)) d\alpha = \lim_{m \rightarrow \infty} \frac{1}{\pi} \int_{-\infty}^{\infty} f(\eta) d\eta \cdot \frac{1}{2} \int_{-m}^m e^{i\alpha(\eta - x)} d\alpha$$

which further implies

$$(2.33) \quad f(x) = \frac{1}{2\pi} \int_{-\infty}^{\infty} e^{-i\alpha x} d\alpha \int_{-\infty}^{\infty} f(\eta) e^{i\alpha \eta} d\eta .$$

The **Fourier integral** of a function $f(x)$ is defined as

$$f(x) = \frac{1}{\sqrt{2\pi}} \int_{-\infty}^{\infty} F(\alpha) e^{-i\alpha x} d\alpha ,$$

where

$$(2.34) \quad F(\alpha) = \frac{1}{\sqrt{2\pi}} \int_{-\infty}^{\infty} f(x) e^{i\alpha x} dx .$$

The Fourier integrals can be considered as limiting cases of the Fourier series, where $c \rightarrow \infty$ in (2.1).

2.1.1.7 Convolution integrals

The convolution theorems can be used to evaluate integrals.

The *convolution* of functions $f(x)$ and $g(x)$ is defined as

$$(2.35) \quad (f * g)(x) = \int_{-\infty}^{\infty} f(x - \eta)g(\eta)d\eta .$$

Let us consider the Fourier transforms

$$(2.36) \quad F(t) = \frac{1}{\sqrt{2\pi}} \int_{-\infty}^{\infty} f(x)e^{itx} dx ,$$

$$(2.37) \quad G(t) = \frac{1}{\sqrt{2\pi}} \int_{-\infty}^{\infty} g(x)e^{itx} dx .$$

The convolution of $f(x)$ and $g(x)$ can be written with the help of their Fourier transforms $F(t)$ and $G(t)$ as

$$(2.38) \quad (f * g)(x) = \int_{-\infty}^{\infty} F(t)G(t)e^{-itx} dt = \int_{-\infty}^{\infty} f(x - \eta)g(\eta)d\eta .$$

In a special case, when $x = 0$, the convolution $(f * g)(x)$ can be written as

$$(2.39) \quad (f * g)(0) = \int_{-\infty}^{\infty} F(t)G(t)dt = \int_{-\infty}^{\infty} f(-\eta)g(\eta)d\eta .$$

If $f(x)$ is an even function, i.e. $f(-x) = f(x)$, then we can replace $F(t)$ with the Fourier cosine transform $F_c(t)$ and $G(t)$ with $G_c(t)$, respectively (see (2.27)). Hence, (2.39) becomes

$$(2.40) \quad (f * g)(0) = \int_0^{\infty} F_c(t)G_c(t)dt = \int_0^{\infty} f(\eta)g(\eta)d\eta .$$

2.1.1.8 *Fourier transforms of derivatives of a function*

The formula for the Fourier transform of the r -th derivative of a function $f(x)$ can be obtained by integrating by parts

$$(2.41) \quad F^{(r)}(\alpha) = \frac{1}{\sqrt{2\pi}} \int_{-\infty}^{\infty} \frac{d^r f(x)}{dx^r} e^{i\alpha x} dx .$$

The general formula can be written as

$$(2.42) \quad F^{(r)}(\alpha) = (-i\alpha)^r F(\alpha) .$$

2.1.1.9 Dirac delta function

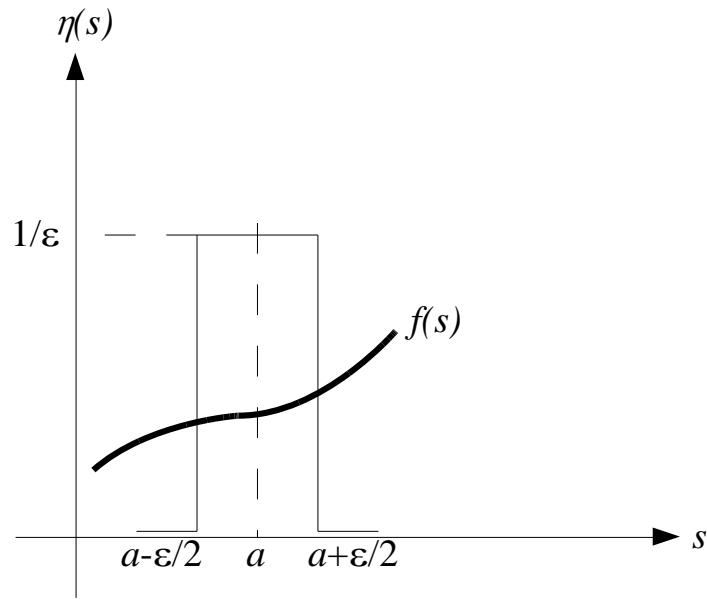


Figure 7 Identity transform of function $f(s)$ by kernel $\eta(s, a)$

It can be seen in Figure 7 that the improper integral of the step function $\eta(s, a)$ along s yields

$$(2.43) \quad \int_{-\infty}^{\infty} \eta(s, a) ds = 2 \cdot \frac{1}{2} \cdot \varepsilon \cdot \frac{1}{\varepsilon} = 1.$$

By expanding $f(s)$ around point $s = a$, only the first term of its Taylor series will nonzero be. Thus,

$$(2.44) \quad \lim_{\varepsilon \rightarrow 0} \int_{-\infty}^{\infty} \eta(s, a) f(s) ds = f(a).$$

Note that

$$(2.45) \quad \lim_{\varepsilon \rightarrow 0} \eta(s, a) = \infty \text{ at } s = a$$

and

$$(2.46) \quad \lim_{\varepsilon \rightarrow 0} \eta(s, a) = 0 \text{ at } s \neq a.$$

Let us define the Dirac delta function such that

$$(2.47) \quad \lim_{\varepsilon \rightarrow 0} \eta(s, a) \equiv \delta(s - a),$$

and

$$(2.48) \quad \int_{-\infty}^{\infty} f(s) \delta(s - a) ds = f(a),$$

with

$$(2.49) \quad \delta(s - a) = \begin{cases} \infty & \text{if } s = a, \\ 0 & \text{if } s \neq a. \end{cases}$$

Regarding the case $a = 0$, the Dirac delta function can be written as

$$(2.50) \quad \delta(s) = \begin{cases} \infty & \text{if } s = 0, \\ 0 & \text{if } s \neq 0, \end{cases}$$

hence, from (2.43), the integral of the Dirac delta function over an unbounded region is always of unit magnitude:

$$(2.51) \quad \int_{-\infty}^{\infty} \delta(s) ds = 1.$$

From the property (2.48) the Dirac delta function $\delta(s - a)$ is also considered as the kernel function of the identity transform (Figure 7).

2.1.2 Green's function

2.1.2.1 General definition of Green's function

In general, **Green's function** $G(x, s)$ is the impulse response of an *inhomogeneous partial differential equation*

$$(2.52) \quad Lu(x) = f(x)$$

defined on a domain with *prescribed boundary or initial conditions*:

$$(2.53) \quad Du(x) = 0.$$

At time-invariant, linear problems, the *impulse response* $G(x, s)$ of a linear transformation $L = L(x)$ acting at point $x = s$, is the image of the Dirac delta function $\delta(x - s)$ under the transformation:

$$(2.54) \quad LG(x, s) = \delta(x - s),$$

where the case $x \neq s$ results in a homogeneous equation due to the property of Dirac's delta function given in (2.49). If the kernel of L is non-trivial, then the Green's function of the problem is not unique. In general, due to the prescribed boundary or initial conditions, Green's function is always unique.

The convolution of Green's function $G(x, s)$ with any arbitrary function $f(s)$ on that domain is the solution for the inhomogeneous differential equation for $f(s)$:

$$(2.55) \quad \int LG(x, s) f(s) ds = \int \delta(x - s) f(s) ds = f(x),$$

where the Dirac delta function appeared as a kernel function of the identity transform (see (2.48)). Substituting (2.52) into (2.55) we have

$$(2.56) \quad Lu(x) = \int LG(x, s) f(s) ds.$$

Since the linear operator L is only a function of x , it can be taken out from the integration along s and

$$(2.57) \quad Lu(x) = L \int G(x, s) f(s) ds,$$

which implies

$$(2.58) \quad u(x) = \int G(x, s) f(s) ds.$$

It is the exact solution of the inhomogeneous partial differential equation (2.52). The difficult part of finding the solution with the help of Green's function is finding the Green's function itself for a given linear operator L . Moreover, the evaluation of the integration in (2.57) is quite complicated, but this method gives a theoretically exact result for inhomogeneous partial differential equations.

2.1.2.2 Mechanical interpretation of Green's function

In applied physics, Green's functions are used to solve *inhomogeneous boundary value problems*, such as the boundary value problem in mechanics defined in the following, where *body forces* appearing in the elastic media *are also considered*.

In anisotropic elastic media, the equilibrium equations:

$$(2.59) \quad \sigma_{ij,j} + b_i = 0,$$

where b_i is the vector of body force per unit volume.

The constitutive equations:

$$(2.60) \quad \sigma_{ij} = C_{ijkl} e_{kl} = C_{ijkl} u_{k,l},$$

where e_{ij} denotes the small elastic strains and C_{ijkl} stands for the elastic stiffness tensor of the media. Substituting the stresses in (2.60) into the equilibrium equation (2.59), we obtain:

$$(2.61) \quad C_{ijkl} u_{k,lj} = -b_i.$$

If b_i is concentrated, acts at point $\underline{x} = \underline{x}'$ in direction x_m , and its magnitude is unity, then

$$(2.62) \quad b_i = \begin{cases} 0 & \text{if } i \neq m, \\ \delta(\underline{x} - \underline{x}') & \text{if } i = m, \end{cases}$$

or it can be written as:

$$(2.63) \quad b_i = \delta_{im} \delta(\underline{x} - \underline{x}') \quad (i = 1, 2, 3),$$

where $\delta(\underline{x} - \underline{x}')$ is the Dirac delta function and δ_{ij} indicates the Kronecker delta tensor:

$$(2.64) \quad \delta_{ij} = \begin{cases} 1 & \text{if } i = j, \\ 0 & \text{if } i \neq j. \end{cases}$$

Based on (2.63), equation (2.61) can be rewritten in a form

$$(2.65) \quad C_{ijkl} u_{k,lj}^{(m)} = -\delta_{im} \delta(\underline{x} - \underline{x}'),$$

where the physical meaning of $u_k^{(m)}$ is (Figure 8): the component of displacement u in the k -th direction at point \underline{x} , caused by a point force acting in the m -th direction at point \underline{x}' . Displacement $u_k^{(m)}$ generates a connection between two vectors, thereby this quantity is a tensor, and this is the Green's function G_{mk} of the boundary value problem under consideration:

$$(2.66) \quad u_k^{(m)} = G_{mk}.$$

Green's function is always symmetric, $G_{mk} = G_{km}$, therefore (2.65) can be written in the form

$$(2.67) \quad C_{ijkl} G_{km,lj}(\underline{x}, \underline{x}') = -\delta_{im} \delta(\underline{x} - \underline{x}').$$

The requirement for Green's function is the influence of the point force to vanish sufficiently rapid in the physical space:

$$(2.68) \quad G_{km} \sim \frac{1}{|\underline{x} - \underline{x}'|} = \frac{1}{r} \text{ as } r \rightarrow \infty,$$

i.e. the displacements at \underline{x} caused by the point force at \underline{x}' vanish as the distance $|\underline{x} - \underline{x}'|$ tends to infinity. The solution of (2.59) can be obtained with the help of the Fourier transform of Green's function:

$$(2.69) \quad g_{km}(\underline{K}) = \int_{-\infty}^{\infty} G_{km}(\underline{x}, \underline{x}') e^{i\underline{K}\underline{x}} d^3 \underline{x},$$

hence, the Fourier-integral of Green's function is:

$$(2.70) \quad G_{km}(\underline{x}, \underline{x}') = \frac{1}{(2\pi)^3} \int_{-\infty}^{\infty} g_{km}(\underline{K}) e^{-i\underline{K}\underline{x}} d^3 \underline{K},$$

where \underline{K} is the Fourier vector in Fourier space. Multiplying (2.67) by $e^{i\underline{K}(\underline{x}-\underline{x}')}$ and integrating over the unbounded domain, we have

$$(2.71) \quad \int_{-\infty}^{\infty} C_{ijkl} G_{km,lj}(\underline{x}, \underline{x}') e^{i\underline{K}(\underline{x}-\underline{x}')} d^3 \underline{x} = - \int_{-\infty}^{\infty} \delta_{im} \delta(\underline{x} - \underline{x}') e^{i\underline{K}(\underline{x}-\underline{x}')} d^3 \underline{x},$$

where $d^3 \underline{x} = d^3(\underline{x} - \underline{x}')$ because of the fixed position of \underline{x}' . Taking into account (2.68), integration by parts yield

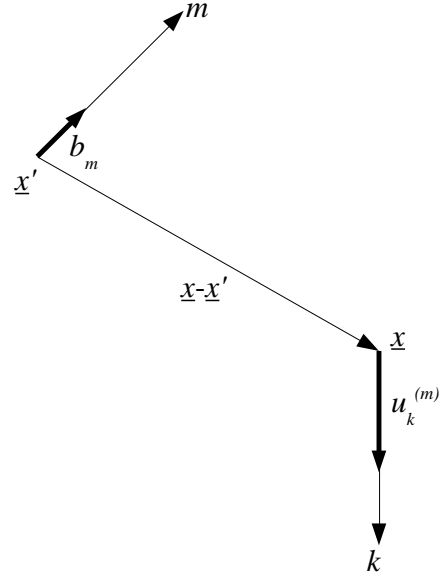


Figure 8 Physical meaning of displacement $u_k^{(m)}$

$$(2.72) \quad - \int_{-\infty}^{\infty} K_j K_l C_{ijkl} G_{km}(\underline{x}, \underline{x}') d^3(\underline{x} - \underline{x}') = -\delta_{im}.$$

If we define a unit vector \underline{T} along vector $\underline{x} - \underline{x}'$, we can express Green's function as

$$(2.73) \quad G_{km}(\underline{x}, \underline{x}') = G_{km}(s\underline{T}) = \frac{\text{sgn}(s)}{s} G_{km}(\underline{T}),$$

and the α_n -th derivative of Green's function:

$$(2.74) \quad G_{km, \alpha_1 \alpha_2 \dots \alpha_n}(\underline{x}, \underline{x}') = G_{km, \alpha_1 \alpha_2 \dots \alpha_n}(s\underline{T}) = \frac{\text{sgn}(s)}{s^n} G_{km, \alpha_1 \alpha_2 \dots \alpha_n}(\underline{T}),$$

where s is an algebraically signed scalar expressing the distance between \underline{x} and \underline{x}' .

2.1.2.3 Isotropic Green's function

In case of isotropic elastic media, we can define the elastic stiffness tensor C_{ijkl} with the help of the Kronecker delta tensor δ_{ij} and Lamé's constants λ and μ :

$$(2.75) \quad C_{ijkl} = \lambda \delta_{ij} \delta_{kl} + \mu (\delta_{ik} \delta_{jl} + \delta_{il} \delta_{jk}).$$

The isotropic Green's function can be expressed by

$$(2.76) \quad G_{km}(\underline{x} - \underline{x}') = \frac{1}{8\pi\mu} \left(\delta_{km} \nabla^2 - \frac{\lambda + \mu}{\lambda + 2\mu} \frac{\partial^2}{\partial x_k \partial x_m} \right) |\underline{x} - \underline{x}'|$$

with

$$(2.77) \quad \nabla^2 |\underline{x} - \underline{x}'| = \frac{2}{|\underline{x} - \underline{x}'|}.$$

The displacement $u_k^{(m)}$ is independent of the positions \underline{x} and \underline{x}' , it is only the function of the distance $|\underline{x} - \underline{x}'|$ between them, resulting in Green's function being translation invariant. At linear, time-invariant problems, Green's function is always translation-invariant, and due to this property, it acts as a convolution operator:

$$(2.78) \quad G(\underline{x}, \underline{x}') = G(\underline{x} - \underline{x}').$$

2.2 Mechanical basis. Definitions of eigenstrains and eigenstresses, basic equations

2.2.1 General theory of eigenstrains

2.2.1.1 Definition of eigenstrains

Eigenstrains are such nonelastic strains as thermal expansion, phase transformation, initial strains, plastic strains or misfit strains. This type of strain appears in a body even if there is no external load acting on it.

Eigenstresses are such self-equilibrated internal stresses caused by eigenstrains in bodies which are free from any other external force and surface constraints. This stress field is created by the incompatibility of the eigenstrains.

2.2.1.2 Fundamental equations of elasticity

If a free body D is subjected to a given distribution of eigenstrains, otherwise it is free from any external surface or body force, then the actual strain (ε_{ij}) can be computed as the sum of the eigenstrains (ε_{ij}^*) and the elastic strains (e_{ij}) defined by Hooke's law in elastic bodies:

$$(2.79) \quad \varepsilon_{ij} = e_{ij} + \varepsilon_{ij}^* .$$

The compatibility equation written for the total strain:

$$(2.80) \quad \varepsilon_{ij} = \frac{1}{2} (u_{i,j} + u_{j,i}) .$$

The connection between the elastic strains and stresses:

$$(2.81) \quad \sigma_{ij} = C_{ijkl} e_{kl} = C_{ijkl} (\varepsilon_{kl} - \varepsilon_{kl}^*) ,$$

and its inverse form:

$$(2.82) \quad \varepsilon_{ij} - \varepsilon_{ij}^* = C_{ijkl}^{-1} \sigma_{kl} ,$$

which – for isotropic materials – can be expressed with the help of Lamé's constant (also known as shear modulus) μ and Poisson's ratio ν :

$$(2.83) \quad \varepsilon_{ij} - \varepsilon_{ij}^* = \frac{1}{2\mu} \left(\sigma_{ij} - \frac{\delta_{ij} \sigma_{kk} \nu}{1 + \nu} \right) .$$

If body D is not free from external forces, then the actual stress field is the sum of the eigenstress of the free body and the solution of the boundary value problem. The equations of equilibrium if we neglect the body forces:

$$(2.84) \quad \sigma_{ij,j} = 0, \quad i = 1, 2, 3 .$$

The boundary conditions for free external surface forces:

$$(2.85) \quad \sigma_{ij} n_j = 0,$$

where n_i is the outward unit normal vector on the surface of D .

We can express the stress field with the help of eigenstrains and the displacement field based on (2.80) and (2.81):

$$(2.86) \quad \sigma_{ij} = C_{ijkl} (u_{k,l} - \varepsilon_{kl}^*).$$

The conditions (2.84) and (2.85) yield:

$$(2.87) \quad C_{ijkl} u_{k,lj} = C_{ijkl} \varepsilon_{kl,j}^*,$$

$$(2.88) \quad C_{ijkl} u_{k,l} n_j = C_{ijkl} \varepsilon_{kl}^* n_j.$$

From (2.87) we can see that the eigenstrain contributes as a body force X_i :

$$(2.89) \quad C_{ijkl} u_{k,lj} = -X_i.$$

It is also visible that in (2.88) the eigenstrain behaves like a surface force on the boundary of D . Summarizing these two observations, the elastic displacement field in an elastic body caused by a given eigenstrain ε_{ij}^* is equivalent to that caused by a body force $-C_{ijkl} \varepsilon_{kl,j}^*$ and surface force $C_{ijkl} \varepsilon_{kl}^* n_j$.

In most cases, D is considered as an infinitely extended body, thus (2.85) can be replaced with the following condition:

$$(2.90) \quad \sigma_{ij}(\underline{x}) \rightarrow 0 \text{ as } \underline{x} \rightarrow \infty.$$

The compatibility conditions can be given with the help of the third-order permutation tensor ε_{pki} :

$$(2.91) \quad \varepsilon_{pki} \varepsilon_{qij} \varepsilon_{ij,kl} = 0.$$

The fundamental equations to be solved are equations (2.87). Several methods for calculating the associated elastic fields under a given distribution of eigenstrains were developed. The most important one was made by Eshelby (Eshelby, 1951; 1957; 1959; 1961), when a uniform eigenstrain is given in an ellipsoidal domain Ω in an infinitely extended medium D (Figure 9). The results are useful regarding the mechanical properties of solids that contain precipitates, inclusions, voids and/or cracks.

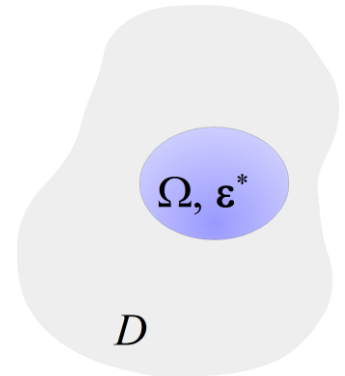


Figure 9 Uniform eigenstrain ε_{ij}^* in an ellipsoidal domain Ω in an infinitely extended body D

2.2.2 General expressions of elastic fields for given eigenstrain distributions

2.2.2.1 Periodic solutions

If the eigenstrain is given in the form of a single wave of amplitude $\bar{\varepsilon}_{ij}^*$, which is a function of the wave vector $\underline{\xi}$:

$$(2.92) \quad \varepsilon_{ij}^*(\underline{x}) = \bar{\varepsilon}_{ij}^*(\underline{\xi}) e^{i\underline{\xi}\underline{x}},$$

the corresponding displacement field can also be written in the form:

$$(2.93) \quad u_i(\underline{x}) = \bar{u}_i(\underline{\xi}) e^{i\underline{\xi}\underline{x}}.$$

In (Mura, Micromechanics of defects in solids, 1987) one can find explicit expressions for the resulting elastic field:

$$(2.94) \quad u_i(\underline{x}) = -i C_{jlmn} \bar{\varepsilon}_{mn}^*(\underline{\xi}) \xi_l N_{ij}(\underline{\xi}) D^{-1}(\underline{\xi}) e^{i\underline{\xi}\underline{x}},$$

$$(2.95) \quad \varepsilon_{ij}(\underline{x}) = \frac{1}{2} C_{klmn} \bar{\varepsilon}_{mn}^*(\underline{\xi}) \xi_l (\xi_j N_{ik}(\underline{\xi}) + \xi_i N_{jk}(\underline{\xi})) D^{-1}(\underline{\xi}) e^{i\underline{\xi}\underline{x}},$$

$$(2.96) \quad \sigma_{ij}(\underline{x}) = C_{ijkl} \left(C_{pqmn} \bar{\varepsilon}_{mn}^*(\underline{\xi}) \xi_q \xi_l N_{kp}(\underline{\xi}) D^{-1}(\underline{\xi}) e^{i\underline{\xi}\underline{x}} - \varepsilon_{kl}^*(\underline{x}) \right),$$

with

$$(2.97) \quad K_{ik}(\underline{\xi}) = C_{ijkl} \xi_j \xi_l,$$

$$(2.98) \quad D(\underline{\xi}) = \varepsilon_{mnl} K_{m1} K_{n2} K_{l3},$$

$$(2.99) \quad N_{ij}(\underline{\xi}) = \frac{1}{2} \varepsilon_{ikl} \varepsilon_{jmn} K_{km} K_{ln}.$$

The periodic solution was used by Mura (Mura, 1964) for periodic distributions of dislocations and by Khachaturyan (Khachaturyan, 1967) for a coherent inclusion of a new phase.

2.2.2.2 Method of Fourier series and Fourier integrals

If the eigenstrain is given in the Fourier series form (see Appendix):

$$(2.100) \quad \varepsilon_{ij}^*(\underline{x}) = \sum \bar{\varepsilon}_{ij}^*(\underline{\xi}) e^{i\underline{\xi}\underline{x}},$$

its solution is the superposition of the elastic fields of single waves of the form (2.92):

$$(2.101) \quad u_i(\underline{x}) = -i \sum C_{jlmn} \bar{\varepsilon}_{mn}^*(\underline{\xi}) \xi_l N_{ij}(\underline{\xi}) D^{-1}(\underline{\xi}) e^{i\underline{\xi}\underline{x}},$$

$$(2.102) \quad \varepsilon_{ij}(\underline{x}) = \frac{1}{2} \sum C_{klmn} \bar{\varepsilon}_{mn}^*(\underline{\xi}) \xi_l (\xi_j N_{ik}(\underline{\xi}) + \xi_i N_{jk}(\underline{\xi})) D^{-1}(\underline{\xi}) e^{i\underline{\xi}\underline{x}},$$

$$(2.103) \quad \sigma_{ij}(\underline{x}) = C_{ijkl} \left(\sum C_{pqmn} \bar{\varepsilon}_{mn}^*(\underline{\xi}) \xi_q \xi_l N_{kp}(\underline{\xi}) D^{-1}(\underline{\xi}) e^{i\underline{\xi}\underline{x}} - \varepsilon_{kl}^*(\underline{x}) \right).$$

If ε_{ij}^* is given in the Fourier integral form (see Appendix):

$$(2.104) \varepsilon_{ij}^*(\underline{x}) = \int_{-\infty}^{\infty} \bar{\varepsilon}_{ij}^*(\underline{\xi}) e^{i\underline{\xi}\underline{x}} d\underline{\xi}$$

where

$$(2.105) \bar{\varepsilon}_{ij}^*(\underline{\xi}) = (2\pi)^{-3} \int_{-\infty}^{\infty} \varepsilon_{ij}^*(\underline{x}) e^{-i\underline{\xi}\underline{x}} d\underline{x},$$

the corresponding displacement, strain and stress field:

$$(2.106) u_i(\underline{x}) = -i \int_{-\infty}^{\infty} C_{jlmn} \bar{\varepsilon}_{mn}^*(\underline{\xi}) \xi_l N_{ij}(\underline{\xi}) D^{-1}(\underline{\xi}) e^{i\underline{\xi}\underline{x}} d\underline{\xi},$$

$$(2.107) \varepsilon_{ij}(\underline{x}) = \frac{1}{2} \int_{-\infty}^{\infty} C_{klmn} \bar{\varepsilon}_{mn}^*(\underline{\xi}) \xi_l (\xi_j N_{ik}(\underline{\xi}) + \xi_i N_{jk}(\underline{\xi})) D^{-1}(\underline{\xi}) e^{i\underline{\xi}\underline{x}} d\underline{\xi},$$

$$(2.108) \sigma_{ij}(\underline{x}) = C_{ijkl} \left(\int_{-\infty}^{\infty} C_{pqmn} \bar{\varepsilon}_{mn}^*(\underline{\xi}) \xi_q \xi_l N_{kp}(\underline{\xi}) D^{-1}(\underline{\xi}) e^{i\underline{\xi}\underline{x}} d\underline{\xi} - \varepsilon_{kl}^*(\underline{x}) \right).$$

2.2.2.3 Method of Green's functions

The integral representations of the elastic field can also be given with the help of Green's functions, it is called the fundamental solution. If Green's function³ $G_{ij}(\underline{x}, \underline{x}')$ (see Appendix) is defined as:

$$(2.109) G_{ij}(\underline{x} - \underline{x}') = (2\pi)^{-3} \int_{-\infty}^{\infty} N_{ij}(\underline{\xi}) D^{-1}(\underline{\xi}) e^{i\underline{\xi}(\underline{x} - \underline{x}')} d\underline{\xi},$$

the solution:

$$(2.110) u_i(\underline{x}) = - \int_{-\infty}^{\infty} C_{jlmn} \varepsilon_{mn}^*(\underline{x}') G_{ij,l}(\underline{x} - \underline{x}') d\underline{x}',$$

$$(2.111) \varepsilon_{ij}(\underline{x}) = - \frac{1}{2} \int_{-\infty}^{\infty} C_{klmn} \varepsilon_{mn}^*(\underline{x}') (G_{ik,lj}(\underline{x} - \underline{x}') + G_{jk,li}(\underline{x} - \underline{x}')) d\underline{x}',$$

$$(2.112) \sigma_{ij}(\underline{x}) = -C_{ijkl} \left(\int_{-\infty}^{\infty} C_{pqmn} \varepsilon_{mn}^*(\underline{x}') G_{kp,ql}(\underline{x} - \underline{x}') d\underline{x}' + \varepsilon_{kl}^*(\underline{x}) \right).$$

Explicit expressions for Green's functions are only available for isotropic and transversely isotropic materials, otherwise the Fourier integral forms are more convenient.

³ Having the property of translation invariance, Green's function $G_{ij}(\underline{x}, \underline{x}')$ is only a function of the distance between x_i and x_i' , thus it can be written as $G_{ij}(\underline{x} - \underline{x}')$.

2.2.3 Static Green's functions

The equations of equilibrium with respect to a displacement $G_{km}(\underline{x} - \underline{x}')$ when the body force $\delta_{im}\delta(\underline{x} - \underline{x}')$ is applied:

$$(2.113) C_{ijkl}G_{km,lj}(\underline{x} - \underline{x}') + \delta_{im}\delta(\underline{x} - \underline{x}') = 0.$$

2.2.3.1 Isotropic materials

For isotropic materials, Lord Kelvin found the Green's function, expressing it with the help of Lamé's constants λ , μ and/or Poisson's ratio ν :

$$(2.114) G_{ij}(\underline{x}) = (2\pi)^{-3} \int_{-\infty}^{\infty} \frac{(\lambda + 2\mu)\delta_{ij}\xi^2 - (\lambda + \mu)\xi_i\xi_j}{\mu(\lambda + 2\mu)\xi^4} e^{i\underline{\xi}\cdot\underline{x}} d\underline{\xi} = \frac{1}{16\pi\mu(1-\nu)x} \left((3-4\nu)\delta_{ij} + \frac{x_i x_j}{x^2} \right),$$

where x'_i is taken as zero without the loss of generality, and $x = (x_i x_i)^{\frac{1}{2}}$.

The expression for Green's function is usually given as a line integral. Let us define a unit sphere S^2 in the ξ -space centered at the origin of the coordinates ξ_i (Figure 10). Green's function at point x_i can be expressed by a line integral along the unit circle S^1 which lies on the plane perpendicular to x_i :

$$(2.115)$$

$$G_{ij}(\underline{x}) = \frac{(2\pi)^{-2}}{2} \int_{S^2} \delta(x\underline{\xi} - \underline{x}) \frac{(\lambda + 2\mu)\delta_{ij} - (\lambda + \mu)\bar{\xi}_i \bar{\xi}_j}{\mu(\lambda + 2\mu)} dS(\underline{\xi}) = \frac{(2\pi)^{-2}}{2x} \oint_{S^1} \frac{(\lambda + 2\mu)\delta_{ij} - (\lambda + \mu)\bar{\xi}_i \bar{\xi}_j}{\mu(\lambda + 2\mu)} d\phi,$$

where $\bar{\xi}_i = \xi_i/x$ and $x_i = x\bar{x}_i$. ϕ is an angle on the plane perpendicular to x_i , bounded by the unit circle S^1 , and the starting line of measuring this angle is arbitrary.

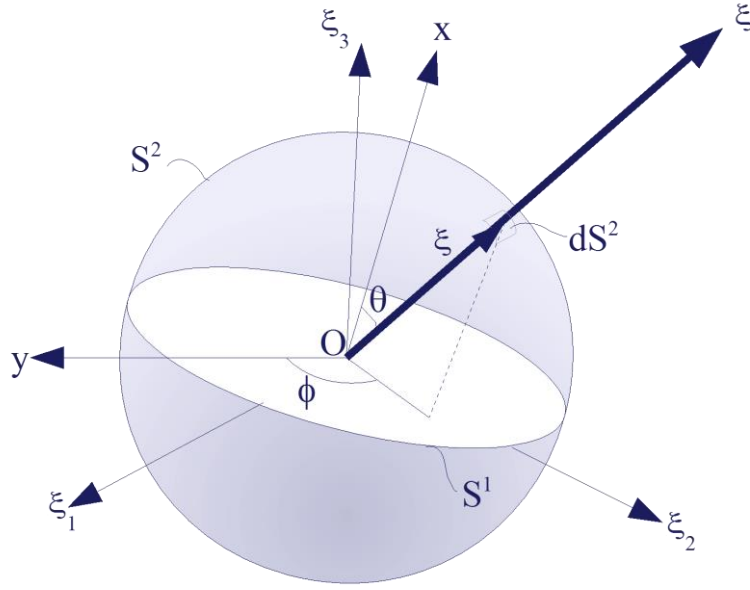


Figure 10 Unit sphere S^2 and unit circle S^1 in ξ -space

2.2.3.2 Anisotropic materials

For anisotropic materials, the surface- and line integral expression of Green's functions are the following:

$$(2.116) G_{ij}(\underline{x}) = \frac{1}{8\pi^2} \int_{S^2} \delta(x\xi \bar{x}) N_{ij}(\underline{\xi}) D^{-1}(\underline{\xi}) dS(\underline{\xi}) = \frac{1}{8\pi^2 x} \oint_{S^1} N_{ij}(\underline{\xi}) D^{-1}(\underline{\xi}) d\phi.$$

2.2.3.3 Kröner's formula

Since $N_{ij}(\underline{\xi}) D^{-1}(\underline{\xi})$ is a continuous function on S^2 , it can be extended into a series of surface harmonic functions, which is any linear combination of spherical harmonics (set of solution of Laplace's equation):

$$(2.117) N_{ij}(\underline{\xi}) D^{-1}(\underline{\xi}) = \sum_{n=0}^{\infty} U_n(\underline{\xi}),$$

where

$$(2.118) U_n(\underline{\xi}) = \frac{2n+1}{4\pi} \int_{S^2} P_n(\underline{\xi}\underline{\xi}') N_{ij}(\underline{\xi}') D^{-1}(\underline{\xi}') dS(\underline{\xi}'), \quad n = 0, 1, 2, \dots$$

and P_n is the Legendre polynomial. The solution of Legendre's differential equation for $n = 0, 1, 2, \dots$ form a polynomial sequence of orthogonal polynomials called the Legendre polynomials. Each $P_n(z)$ polynomial is an n -th degree polynomial:

$$(2.119) P_n(z) = \frac{1}{2^n n!} \frac{d^n}{dz^n} \left((z^2 - 1)^n \right).$$

Kröner's formula is a series expression of Green's function for general anisotropic materials using surface harmonic functions:

$$(2.120) \quad G_{ij}(\underline{x}) = \frac{1}{4\pi x} \sum_{n=0}^{\infty} P_n(0) U_n(\bar{x}).$$

Kröner's formula was modified by Mura and Kinoshita (Mura & Kinoshita, 1971), their solution is continuously differentiable:

$$(2.121) \quad G_{ij}(\underline{x}) = \frac{1}{16\pi^2} \Delta \int_{S^2} N_{ij}(\bar{\xi}) D^{-1}(\bar{\xi}) \left| \frac{\underline{x}\bar{\xi}}{|\underline{x}\bar{\xi}|} \right| dS(\bar{\xi}).$$

2.2.3.4 Derivatives of Green's functions

In the solution of eigenstrain problems, we usually need the derivatives of Green's function. The formulae can be found in the previous section in (2.74), furthermore in (Mura, 1987) found by Barnett (Barnett, 1972) and Willis (Willis, 1975).

3 Mechanical study on the environment of inclusions and inhomogeneities. Analytical solutions for determination of the resulting elastic field

3.1 Inclusions

3.1.1 Definition of inclusion

When an eigenstrain is prescribed in a finite subdomain Ω in a homogeneous material D , and it is zero in the matrix defined by $D - \Omega$, then Ω is called an inclusion and $D - \Omega$ is called matrix (Figure 11). The elastic moduli in the inclusion and in the matrix is assumed to be the same.

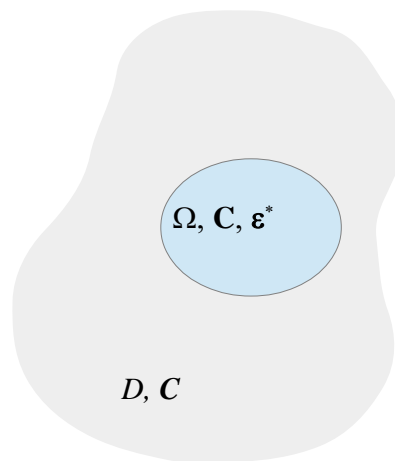


Figure 11 Inclusion Ω with eigenstrain ε_{ij}^* in homogeneous body D

The elastic field due to the inclusion can be written with the help of Green's functions:

$$(3.1) \quad u_i(\underline{x}) = - \int_{\Omega} C_{jlmn} \varepsilon_{mn}^*(\underline{x}') G_{ij,l}(\underline{x} - \underline{x}') d\underline{x}',$$

$$(3.2) \quad \varepsilon_{ij}(\underline{x}) = -\frac{1}{2} \int_{\Omega} C_{klmn} \varepsilon_{mn}^*(\underline{x}') (G_{ik,ij}(\underline{x} - \underline{x}') + G_{jk,li}(\underline{x} - \underline{x}')) d\underline{x}',$$

$$(3.3) \quad \sigma_{ij}(\underline{x}) = -C_{ijkl} \left(\int_{\Omega} C_{pqmn} \varepsilon_{mn}^*(\underline{x}') G_{kp,ql}(\underline{x} - \underline{x}') d\underline{x}' + \varepsilon_{kl}^*(\underline{x}) \right),$$

or, considering its Fourier integral forms:

$$(3.4) \quad u_i(\underline{x}) = -i(2\pi)^{-3} \int_{-\infty}^{\infty} \int_{\Omega} C_{jlmn} \varepsilon_{mn}^*(\underline{x}') \xi_l N_{ij}(\underline{\xi}) D^{-1}(\underline{\xi}) e^{i\underline{\xi}(\underline{x}-\underline{x}')} d\underline{\xi} d\underline{x}',$$

$$(3.5) \quad \varepsilon_{ij}(\underline{x}) = (2\pi)^{-3} \int_{-\infty}^{\infty} \int_{\Omega} \frac{1}{2} C_{klmn} \varepsilon_{mn}^*(\underline{x}') \xi_l (\xi_j N_{ik}(\underline{\xi}) + \xi_i N_{jk}(\underline{\xi})) D^{-1}(\underline{\xi}) e^{i\underline{\xi}(\underline{x}-\underline{x}')} d\underline{\xi} d\underline{x}',$$

$$(3.6) \quad \sigma_{ij}(\underline{x}) = C_{ijkl} \left((2\pi)^{-3} \int_{-\infty}^{\infty} \int_{\Omega} C_{pqmn} \varepsilon_{mn}^*(\underline{x}') \xi_q \xi_l N_{kp}(\underline{\xi}) D^{-1}(\underline{\xi}) e^{i\underline{\xi}(\underline{x}-\underline{x}')} d\underline{\xi} d\underline{x}' - \varepsilon_{kl}^*(\underline{x}) \right),$$

where $\varepsilon_{kl}^*(\underline{x}) = 0$ for $\underline{x} \in D - \Omega$.

When the eigenstrain is uniform in an inclusion and Ω has an arbitrary shape, it is convenient to rewrite (3.1) as a surface integral, where $|\Omega|$ is the boundary of Ω :

$$(3.7) \quad u_i(\underline{x}) = - \int_{|\Omega|} C_{jlmn} \varepsilon_{mn}^* G_{ij}(\underline{x} - \underline{x}') n_l dS.$$

3.1.2 Interface conditions

The eigenstrain field is discontinuous on the boundary of the inclusion, but some quantities must be continuous, like displacements and tractions. The continuity conditions:

$$(3.8) \quad (u_i)_{jump} \equiv u_i(S^+) - u_i(S^-) = 0,$$

$$(3.9) \quad (\sigma_{ij})_{jump} n_j \equiv (\sigma_{ij}(S^+) - \sigma_{ij}(S^-)) n_j = 0,$$

where S denotes the interface between the matrix and Ω . The positive side is the one belonging to the matrix. The displacements can be discontinuous only if the inclusion can slide on the interfacial surface.

The displacement gradient or distortion is discontinuous at the interface:

$$(3.10) \quad (u_{i,j})_{jump} \equiv u_{i,j}(S^+) - u_{i,j}(S^-) = \lambda_i n_j,$$

where λ is the proportionality constant, which gives the magnitude of the jump. It is shown in (Mura, 1987) that the displacement gradient, the strain and the stress field can be calculated from

$$(3.11) \quad (u_{i,j})_{jump} = -C_{lkmn} \varepsilon_{mn}^* n_k n_j N_{il}(\underline{n}) D^{-1}(\underline{n}),$$

$$(3.12) \quad (\varepsilon_{ij})_{jump} = -\frac{1}{2} C_{ikmn} \varepsilon_{mn}^* (S^-) n_k (n_j N_{il}(\underline{n}) + n_i N_{jl}(\underline{n})) D^{-1}(\underline{n}),$$

(3.13)

$$(\sigma_{ij})_{jump} \equiv \sigma_{ij}(S^+) - \sigma_{ij}(S^-) = C_{ijkl} \left((u_{k,l})_{jump} - (\varepsilon_{kl}^*)_{jump} \right) = C_{ijkl} (-C_{pqmn} \varepsilon_{mn}^* n_q n_l N_{kp}(\underline{n}) D^{-1}(\underline{n}) + \varepsilon_{kl}^*).$$

Equation (3.13) is applicable when computing the strains and stresses just outside the inclusion, if the strain and stress field is given inside the inclusion. The *uniqueness theorem* for inclusion-matrix interface states that if the stress or strain is known locally at one side of the interface between an inclusion and the surrounding matrix, then their jumps and consequent values at the other side of the interface are explicitly determinable in terms of the matrix moduli, the eigenstrain in the inclusion and the interface normal.

3.1.3 Some examples of eigenstrains

Let us consider an *aluminum* ball under given eigenstrain, let it be thermal strain. First, there is no constraint, hence no stress is induced by the temperature change. Consequently, the elastic strain is zero:

$$(3.14) \quad e_{ij} = \varepsilon_{ij} - \varepsilon_{ij}^* = M_{ijkl} \sigma_{kl} = 0,$$

where M_{ijkl} is the fourth-order flexibility matrix⁴.

The total strain is then equals to the eigenstrain:

$$(3.15) \quad \varepsilon_{ij} = e_{ij} + \varepsilon_{ij}^* = \varepsilon_{ij}^* = \alpha_{Al} \Delta T \delta_{ij},$$

where α_{Al} is the thermal coefficient of aluminum and ΔT is the change of temperature in the aluminum ball.

Next, let this ball be embedded in a *rigid* matrix. In this case, the total strain must be zero because of the rigid constraint:

$$(3.16) \quad \varepsilon_{ij} = e_{ij} + \varepsilon_{ij}^* = 0.$$

Hence, the elastic strain is no longer zero, which results in a nonzero stress field in the aluminum ball:

$$(3.17) \quad e_{ij} = \varepsilon_{ij} - \varepsilon_{ij}^* = -\varepsilon_{ij}^* = -\alpha_{Al} \Delta T \delta_{ij},$$

⁴ The 6-by-6 compliance matrix is the inverse of the 6-by-6 stiffness matrix, but this statement does not hold for the fourth-order compliance and stiffness tensors. In this case, we can use the following equality:

$(C_{ij})^{-1} = R_{ik} (C_{kl}^{-1}) R_{lj}$, where $(C_{ij})^{-1}$ is the inverse of the stiffness matrix, thus, it is the 6-by-6 compliance matrix, (C_{ij}^{-1}) is the contracted form of the inverse of the fourth-order stiffness tensor and $R_{ij} = \langle 1, 1, 1, 2, 2, 2 \rangle$ is the diagonal Reuter-matrix.

$$(3.18) \quad \sigma_{ij} = C_{ijkl} e_{kl} = -\alpha_{Al} C_{nmij} \Delta T .$$

Finally, the aluminum ball is embedded in *deformable copper* matrix. In both material, the total strain is nonzero. Due to the deformability, the elastic strain is also nonzero:

$$(3.19) \quad \varepsilon_{ij,Al} = e_{ij,Al} + \alpha_{Al} \Delta T_{Al} \delta_{ij} ,$$

$$(3.20) \quad \varepsilon_{ij,Cu} = e_{ij,Cu} + \alpha_{Cu} \Delta T_{Cu} \delta_{ij} ,$$

thereby stresses are induced in the ball and in the matrix, too. The associated stress field cannot be obtained easily, but it is shown above, that stresses exist due to the different physical behavior of the materials.

3.1.4 Ellipsoidal inclusion with uniform eigenstrains. Eshelby solution

Consider an ellipsoidal inclusion Ω with given uniform eigenstrain ε_{ij}^* in an infinite domain D . The inclusion is defined by its semi-axes a_1, a_2, a_3 (Figure 12):

$$(3.21) \quad \Omega = \left\{ x_1, x_2, x_3; \left(\frac{x_1}{a_1} \right)^2 + \left(\frac{x_2}{a_2} \right)^2 + \left(\frac{x_3}{a_3} \right)^2 \leq 1 \right\} .$$

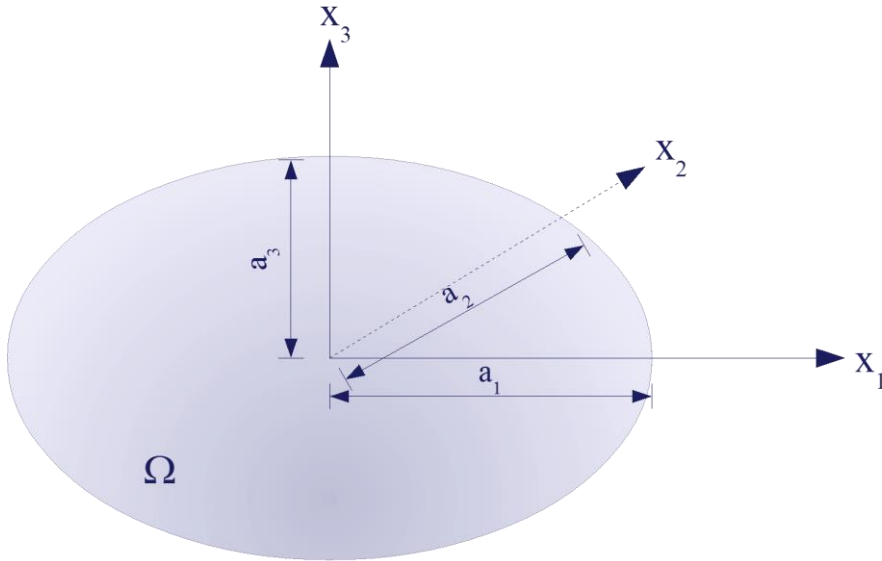


Figure 12 Eshelby's solution: Ellipsoidal inclusion Ω in x -space with semi-axes a_1, a_2, a_3

The eigenstrain distribution is given in the form

$$(3.22) \quad \varepsilon_{ij}^*(\underline{x}) = \begin{cases} \varepsilon_{ij}^* & \text{for } \underline{x} \in \Omega \\ 0 & \text{for } \underline{x} \notin \Omega \end{cases} .$$

Applying the Green's function for the solution of the eigenstrain problem, we have

$$(3.23) \quad u_i(\underline{x}) = C_{mjkl} \varepsilon_{kl}^* \int_{\Omega} \frac{\partial G_{mi}^{\infty}(\underline{x} - \underline{x}')}{\partial x'_j} dV(\underline{x}') ,$$

$$(3.24) \quad \varepsilon_{ij}(\underline{x}) = C_{klmn} \varepsilon_{mn}^* P_{ijkl}^\Omega(\underline{x}),$$

$$(3.25) \quad \sigma_{ij}(\underline{x}) = C_{ijkl} \left(C_{pqmn} \varepsilon_{mn}^* P_{klpq}^\Omega(\underline{x}) - \varepsilon_{kl}^* \right),$$

where $G_{ij}^\infty(\underline{x}, \underline{x}')$ is the infinite domain Green's function and

$$(3.26) \quad P_{ijkl}^\Omega(\underline{x}) = \int_{\Omega} \Gamma_{ijkl}^\infty(\underline{x}, \underline{x}') dV(\underline{x}').$$

The fourth-order tensor $\Gamma_{ijkl}^\infty(\underline{x}, \underline{x}')$ is defined by

$$(3.27) \quad \Gamma_{ijkl}^\infty(\underline{x}, \underline{x}') = \frac{1}{4} \left(\frac{\partial^2 G_{ki}^\infty(\underline{x}, \underline{x}')}{\partial x_j \partial y_l} + \frac{\partial^2 G_{kj}^\infty(\underline{x}, \underline{x}')}{\partial x_i \partial y_l} + \frac{\partial^2 G_{li}^\infty(\underline{x}, \underline{x}')}{\partial x_j \partial y_k} + \frac{\partial^2 G_{lj}^\infty(\underline{x}, \underline{x}')}{\partial x_i \partial y_k} \right).$$

These expressions are valid for \underline{x} both inside and outside the inclusion. For $\underline{x} \in \Omega$ the $P_{ijkl}^\Omega(\underline{x})$ is a constant fourth-order tensor:

$$(3.28) \quad P_{ijkl}^\Omega(\underline{x}) = P_{ijkl} = \frac{a_1 a_2 a_3}{4\pi} \int_{\hat{s}} H_{ijkl}(\underline{\xi}) a^{-3} D^{-1}(\underline{\xi}) dS^2(\underline{\xi}), \quad \underline{x} \in \Omega,$$

where P_{ijkl} is the Hill polarization tensor and

$$(3.29) \quad H_{ijkl}(\underline{\xi}) = N_{ik}(\underline{\xi}) \xi_j \xi_l + N_{jk}(\underline{\xi}) \xi_i \xi_l + N_{il}(\underline{\xi}) \xi_j \xi_k + N_{jl}(\underline{\xi}) \xi_i \xi_k,$$

$$(3.30) \quad a = \sqrt{(a_1 \bar{\xi}_1)^2 + (a_2 \bar{\xi}_2)^2 + (a_3 \bar{\xi}_3)^2}.$$

The integration is carried out over the surface of a unit sphere S^2 in $\underline{\xi}$ -space (Figure 10), where

$$(3.31) \quad \xi = (\xi_1^2 + \xi_2^2 + \xi_3^2)^{\frac{1}{2}},$$

$$(3.32) \quad \bar{\xi} = \frac{\xi}{\xi}.$$

Let us introduce a fourth-order tensor

$$(3.33) \quad S_{ijkl}(\underline{x}) = C_{mnlk} P_{ijmn}^\Omega(\underline{x}),$$

thus the strain and stress field in D can be rewritten as

$$(3.34) \quad \varepsilon_{ij}(\underline{x}) = S_{ijkl}(\underline{x}) \varepsilon_{kl}^*,$$

$$(3.35) \quad \sigma_{ij}(\underline{x}) = C_{ijkl} \left(S_{klmn}(\underline{x}) \varepsilon_{mn}^* - \varepsilon_{kl}^* \right) = C_{ijkl} \left(S_{klmn}(\underline{x}) - I_{klmn} \right) \varepsilon_{mn}^*$$

with I_{ijkl} fourth-order identity tensor:

$$(3.36) \quad I_{ijkl} = \frac{1}{2} (\delta_{ik} \delta_{jl} + \delta_{il} \delta_{jk}).$$

From equation (3.28) and (3.33), for $\underline{x} \in \Omega$, $S_{ijkl}(\underline{x})$ is also constant, thereby the total strain and stress field is uniform inside the ellipsoidal inclusion given that the eigenstrain is uniform:

$$(3.37) \quad \varepsilon_{ij}(\underline{x}) = S_{ijkl} \varepsilon_{kl}^*, \quad \underline{x} \in \Omega .$$

The S_{ijkl} fourth-order tensor is the **Eshelby inclusion tensor** and equation (3.37) is called the Eshelby ellipsoidal inclusion solution. From Hooke's law, the stress field can easily be obtained:

$$(3.38) \quad \sigma_{ij} = C_{ijkl}(\varepsilon_{kl} - \varepsilon_{kl}^*) = C_{ijkl} \varepsilon_{kl} + \tau_{ij}^* ,$$

$$(3.39) \quad \tau_{ij}^* = -C_{ijkl} \varepsilon_{kl}^* .$$

τ_{ij}^* indicates the stress polarization, which is the stress inside the inclusion caused by eigenstrain ε_{ij}^* when the inclusion is not allowed to deform, that is, the total strain e_{ij} is zero. It is the case, when the aluminum ball with given thermal strains was embedded into a rigid matrix.

The Eshelby tensor S_{ijkl} is nonsingular, independent of the eigenstrain but it is dependent on the material of the matrix. About the symmetry of the tensor, in general the Eshelby tensor does not possess the diagonal symmetry $S_{ijkl} \neq S_{klij}$, but the minor symmetry $S_{ijkl} = S_{jikl} = S_{ijlk} = S_{jilk}$ always holds. In case of general anisotropic materials, the integration in the Eshelby tensor needs to be carried out numerically. For isotropic materials, the integral can be rewritten as elliptical integrals and for special shaped inclusions, explicit expressions can be obtained (see (Mura, 1987)).

Please note, that Eshelby's ellipsoidal inclusion solution is only valid for material points inside the inclusion, hence, when computing the strain and stress field in the surrounding matrix, one has to carry out the integration in (3.26) or it is also convenient to use the solution based on the uniqueness theorem, namely if we know the elastic field inside the inclusion, we can compute the jump in the required quantities and we get the solution of the problem for exterior points. Another solution was obtained by Tanaka and Mura (Tanaka & Mura, 1982). For a given stress field $\sigma_{ij}(S^-)$ inside the inclusion, find the stress field $\sigma_{ij}(S^+)$ of the exterior points by assuming that Ω is a void and the applied stress is $-\sigma_{ij}(S^-)$. The stress field of the exterior points for the inclusion problem is the sum of $\sigma_{ij}(S^-)$ and $\sigma_{ij}(S^+)$.

A different approach to determine the elastic field of exterior points is to use Green's functions. In this case, two integrals should be carried out in order to obtain the associated stress and strain field:

$$(3.40) \quad \psi(\underline{x}) = \int_{\Omega} |\underline{x} - \underline{x}'| d\underline{x}' ,$$

$$(3.41) \quad \phi(\underline{x}) = \int_{\Omega} \frac{1}{|\underline{x} - \underline{x}'|} d\underline{x}'.$$

Norman Macleod Ferrers (Ferrers, 1877) and Frank Watson Dyson (Dyson, 1891) expressed the above integrals in terms of the following elliptic integrals (the so-called I -integrals):

$$(3.42) \quad I(\lambda) = 2\pi a_1 a_2 a_3 \int_{\lambda}^{\infty} \frac{ds}{\Delta(s)},$$

$$(3.43) \quad I_i(\lambda) = 2\pi a_1 a_2 a_3 \int_{\lambda}^{\infty} \frac{ds}{(a_i^2 + s)\Delta(s)},$$

$$(3.44) \quad I_{ij}(\lambda) = 2\pi a_1 a_2 a_3 \int_{\lambda}^{\infty} \frac{ds}{(a_i^2 + s)(a_j^2 + s)\Delta(s)},$$

where

$$(3.45) \quad \Delta(s) = \left((a_1^2 + s)(a_2^2 + s)(a_3^2 + s) \right)^{\frac{1}{2}}$$

and λ is the largest positive root of the equation

$$(3.46) \quad \frac{x_1^2}{(a_1^2 + \lambda)} + \frac{x_2^2}{(a_2^2 + \lambda)} + \frac{x_3^2}{(a_3^2 + \lambda)} = 1.$$

For interior points, $\lambda = 0$. In order to define the elastic field for both exterior and interior points, one must compute the higher order derivatives of (3.40) and (3.41). If the I -integrals are applied, due to the fact, that the lower bound of the integrals (3.42)-(3.44) are only a function of \underline{x} , the derivatives of $I(\lambda)$, $I_i(\lambda)$ and $I_{ij}(\lambda)$ can be reduced to the derivatives of λ . The I -integrals are given for ellipsoids (see (Mura, 1987)), therefore this is the easiest way to determine the elastic field in a material caused by the presence of inclusions.

3.1.5 Isotropic inclusions

3.1.5.1 Ellipsoidal inclusions with polynomial eigenstrains

Consider an elastic infinite body D with an ellipsoidal inclusion Ω . The eigenstrain on the inclusion is given in the form

$$(3.47) \quad \varepsilon_{ij}^*(\underline{x}) = B_{ijk} x_k + B_{ijkl} x_k x_l + \dots,$$

where B_{ijk}, B_{ijkl}, \dots are constants symmetric with respect to the free indices i and j (e.g. $B_{ijkl} = B_{ijlk}$) and the constant term was excluded for the sake of simplicity. The displacement field of both the interior and exterior points can be expressed with the help of functions

$$(3.48) \quad \Psi_{ij}(\underline{x}) = \int_{\Omega} |\underline{x} - \underline{x}'| \varepsilon_{ij}^*(\underline{x}') d\underline{x}',$$

$$(3.49) \quad \Phi_{ij}(\underline{x}) = \int_{\Omega} \frac{\varepsilon_{ij}^*(\underline{x}')}{|\underline{x} - \underline{x}'|} d\underline{x}'.$$

$\Phi_{ij}(\underline{x})$ and $\Psi_{ij}(\underline{x})$ are the harmonic and biharmonic potentials due to a body Ω of density $\varepsilon_{ij}^*(\underline{x})$. Substituting the polynomial eigenstrain into the potential functions, we have

$$(3.50) \quad \Psi_{ij}(\underline{x}) = B_{ijk}\psi_k + B_{ijkl}\psi_{kl} + \dots,$$

$$(3.51) \quad \Phi_{ij}(\underline{x}) = B_{ijk}\phi_k + B_{ijkl}\phi_{kl} + \dots$$

with

$$(3.52) \quad \psi_{ij\dots k}(\underline{x}) = \int_{\Omega} x'_i x'_j \dots x'_k |\underline{x} - \underline{x}'| d\underline{x}',$$

$$(3.53) \quad \phi_{ij\dots k}(\underline{x}) = \int_{\Omega} \frac{x'_i x'_j \dots x'_k}{|\underline{x} - \underline{x}'|} d\underline{x}'.$$

The harmonic potentials (3.52) and (3.53) can be expressed in terms of the following elliptic integrals:

$$(3.54) \quad V(\underline{x}) = \pi a_1 a_2 a_3 \int_{\lambda}^{\infty} \frac{U(s)}{\Delta(s)} ds,$$

$$(3.55) \quad V_i(\underline{x}) = \pi a_1 a_2 a_3 \int_{\lambda}^{\infty} \frac{U(s)}{(a_i^2 + s)\Delta(s)} ds,$$

$$(3.56) \quad V_{ij}(\underline{x}) = \pi a_1 a_2 a_3 \int_{\lambda}^{\infty} \frac{U(s)}{(a_i^2 + s)(a_j^2 + s)\Delta(s)} ds,$$

where

$$(3.57) \quad U(s) = 1 - \left(\frac{x_1^2}{(a_1^2 + s)} + \frac{x_2^2}{(a_2^2 + s)} + \frac{x_3^2}{(a_3^2 + s)} \right).$$

According to (Dyson, 1891), the potentials (3.52) and (3.53) are related to the V -integrals in the following way:

$$(3.58) \quad \phi = V,$$

$$(3.59) \quad \phi_n = a_n^2 x_n V_n,$$

$$(3.60) \quad \phi_{mn} = a_M^2 \left(x_m x_n a_N^2 V_{MN} + \frac{1}{4} \delta_{mn} (V - x_r x_r V_R - a_M^2 (V_M - x_r x_r V_{RM})) \right).$$

The I -integrals ((3.42)-(3.44)) and V -integrals ((3.54)-(3.56)) are related:

$$(3.61) \quad V(x) = \frac{1}{2} (I(\lambda) - x_r x_r I_R(\lambda)),$$

$$(3.62) \quad V_i(x) = \frac{1}{2} (I_i(\lambda) - x_r x_r I_{Ri}(\lambda)),$$

$$(3.63) \quad V_{ij}(x) = \frac{1}{2} (I_{ij}(\lambda) - x_r x_r I_{Rij}(\lambda)).$$

Eshelby pointed out in (Eshelby, 1961) that in case of an eigenstrain which is a homogeneous polynomial of x_i with degree n , the total strain inside the inclusion becomes an inhomogeneous polynomial of x_i with terms of degree $n, (n-2), (n-4), \dots$. The same result was obtained for anisotropic materials by Asaro and Barnett (Asaro & Barnett, The non-uniform transformation strain problem for an anisotropic ellipsoidal inclusion, 1975). The I -integrals are of great importance in the explicit expressions of the solutions of special shaped inclusions.

3.1.5.2 Energies of inclusions

Consider a finite body D with homogeneous and isotropic or anisotropic material. The body D contains inclusions Ω_i (Figure 13), the sum of domains occupied by them is denoted by Ω , and the volume of Ω is V .

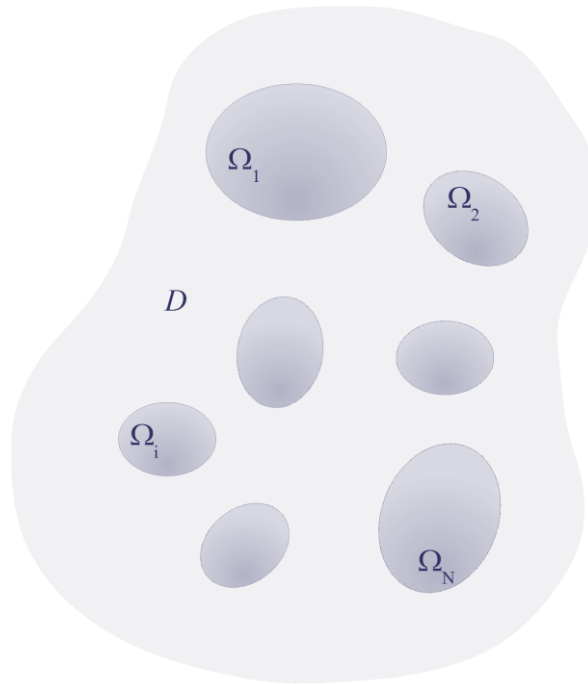


Figure 13 Inclusions Ω_i in finitely extended body D

3.1.5.2.1 Elastic strain energy

If the body D is free from any external force and surface constraint, but eigenstrains are prescribed in Ω , the elastic strain energy:

$$(3.64) \quad W^* = \frac{1}{2} \int_D \sigma_{ij} e_{ij} dD = -\frac{1}{2} \int_{\Omega} \sigma_{ij} \varepsilon_{ij}^* dD .$$

If Ω is an ellipsoidal inclusion and the eigenstrain is uniform, the stress field will also be uniform, thus the strain energy becomes

$$(3.65) \quad W^* = -\frac{1}{2}V\sigma_{ij}\varepsilon_{ij}^*.$$

If Ω is the sum of two inclusions Ω_1 and Ω_2 , the strain energy can be written in the form

$$(3.66) \quad \begin{aligned} W^* &= -\frac{1}{2}\left(\int_{\Omega_1}(\sigma_{ij}^{(1)} + \sigma_{ij}^{(2)})\varepsilon_{ij}^{(1)}dD + \int_{\Omega_2}(\sigma_{ij}^{(1)} + \sigma_{ij}^{(2)})\varepsilon_{ij}^{(2)}dD\right) = \\ &= -\frac{1}{2}\left(\int_{\Omega_1}\sigma_{ij}^{(1)}\varepsilon_{ij}^{(1)}dD + \int_{\Omega_2}\sigma_{ij}^{(2)}\varepsilon_{ij}^{(2)}dD + 2\int_{\Omega_1}\sigma_{ij}^{(2)}\varepsilon_{ij}^{(1)}dD\right), \end{aligned}$$

where $\varepsilon_{ij}^{(1)}$ and $\varepsilon_{ij}^{(2)}$ are the eigenstrains in the first and second inclusion, and $\sigma_{ij}^{(1)}$ and $\sigma_{ij}^{(2)}$ are the stress fields caused by $\varepsilon_{ij}^{(1)}$ and $\varepsilon_{ij}^{(2)}$, respectively. Then consider the case when body D is subjected to given surface tractions F_i . The displacement field is the sum of the displacements u_i^0 caused by F_i only and the displacements u_i caused by the eigenstrains only. The elastic strain energy in this case

$$(3.67) \quad W^* = \frac{1}{2}\int_D(\sigma_{ij}^0 + \sigma_{ij})(u_{i,j}^0 + u_{i,j} - \varepsilon_{ij}^*)dD = \frac{1}{2}\int_D\sigma_{ij}^0u_{i,j}^0dD - \frac{1}{2}\int_{\Omega}\sigma_{ij}\varepsilon_{ij}^*dD,$$

where σ_{ij}^0 is the stress field caused by u_i^0 and σ_{ij} is that caused by the eigenstrains. Please note, that the elastic strain energy is the sum of the energies caused by the external force and the eigenstrain, respectively, which is a Colonetti's theorem⁵.

3.1.5.2.2 Interaction energy

The total potential energy of a finite body D containing inclusions Ω with external surface tractions F_i on S and eigenstrain ε_{ij}^* in Ω :

$$(3.68) \quad W = W^* - \int_S F_i(u_i^0 + u_i)dS.$$

If there is no eigenstrain in D , the total potential energy becomes

$$(3.69) \quad W_0 = \frac{1}{2}\int_D\sigma_{ij}^0u_{i,j}^0dD - \int_S F_iu_i^0dS.$$

If the external forces are zero, the total potential energy of D :

$$(3.70) \quad W_1 = \frac{1}{2}\int_D\sigma_{ij}(u_{i,j} - \varepsilon_{ij}^*)dD = -\frac{1}{2}\int_{\Omega}\sigma_{ij}\varepsilon_{ij}^*dD.$$

⁵ Colonetti's theorem states that if a body containing an inclusion is subjected to traction forces on its boundary, there will be no cross term in the total elastic energy of the body, between the internal stress field and the applied stress field.

The interaction between the traction forces and the eigenstrain appears in the total potential energy as well. The interaction energy is defined as

$$(3.71) \quad \Delta W = W - W_0 - W_1 = -\int_S F_i u_i dS = -\int_{\Omega} \sigma_{ij}^0 \varepsilon_{ij}^* dD .$$

In case of uniform eigenstrain in an ellipsoidal inclusion Ω , the interaction energy:

$$(3.72) \quad \Delta W = -V \sigma_{ij}^0 \varepsilon_{ij}^* .$$

Under constant temperature, the elastic strain energy of a body is the Helmholtz free energy of the body. The Gibbs free energy of a body is the total potential energy of it, which is defined as the sum of the elastic strain energy of the body and the potential energy of an external force. W_0 is the Gibbs free energy of D when only the external force is the source of the stress field. W_1 is the Gibbs free energy of the body when there is no external force but there is an internal stress field due to the inclusion. Thus, ΔW is an additional term in the Gibbs free energy when not only an external force acts on the body, but also there is an eigenstrain-induced stress field in it. It represents the coexistence of the two effects acting on the body.

For example, in fracture mechanics, we are interested in the energy that is produced in a body initially subjected to external tractions F_i , when due to inclusions, eigenstrain is introduced in the material as well:

$$(3.73) \quad \Delta \bar{W} = W - W_0 = W_1 + \Delta W .$$

This energy is formed due to the eigenstrain and the interaction between the inclusions and the external forces. Please note that all the expressions for energy calculations are given by integrals over Ω , thus, the calculations become easier.

For *dilatational* eigenstrains

$$(3.74) \quad \varepsilon_{ij}^* = \delta_{ij} \varepsilon^*(\underline{x}) ,$$

the elastic strain energy per unit volume of an inclusion is constant independently of the shape of the inclusion, and can be expressed in terms of Lamé's constant μ and Poisson's ratio ν of the material under consideration:

$$(3.75) \quad \frac{W^*}{V} = 2\mu (\varepsilon^*)^2 \frac{1+\nu}{1-\nu} ,$$

with the volume of Ω

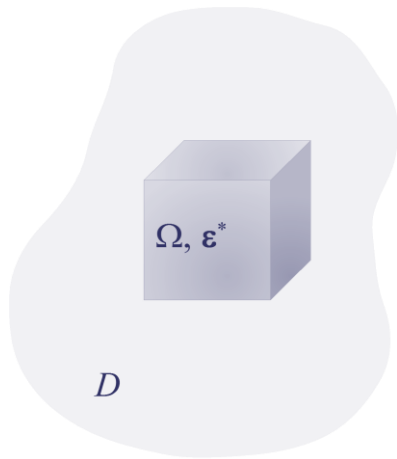
$$(3.76) \quad V = \frac{4}{3} \pi a_1 a_2 a_3 .$$

As a result, the hydrostatic pressure $\frac{\sigma_{ii}}{3}$ is uniform for any shape of inclusion in case of dilatational eigenstrain – that can be constant or a function of \underline{x} as well –:

$$(3.77) \quad \sigma_{ii} = \begin{cases} -4\mu \frac{1+\nu}{1-\nu} \varepsilon^* & \text{in } \Omega \\ 0 & \text{outside } \Omega \end{cases} .$$

The stress field inside an inclusion is only a function of the dilatational eigenstrain inside this particular inclusion, hence in case of several simultaneous inclusions, the dilatational eigenstrains do not interact. This observation holds only for isotropic materials and only for inclusions.

3.1.5.3 Cuboidal inclusions



In this thesis, cuboidal shaped inclusions (Figure 14) are not expounded, but they are interesting from that point of view, that the stress field inside the cuboidal inclusion will not be uniform in case of uniform eigenstrains. There are also logarithmic singularities in shear stresses in certain edges and corners of the cuboidal inclusion when ε_{ij}^* has no shear strain components.

Figure 14 Cuboidal inclusion Ω in body D

3.1.5.4 Inclusions in a half space

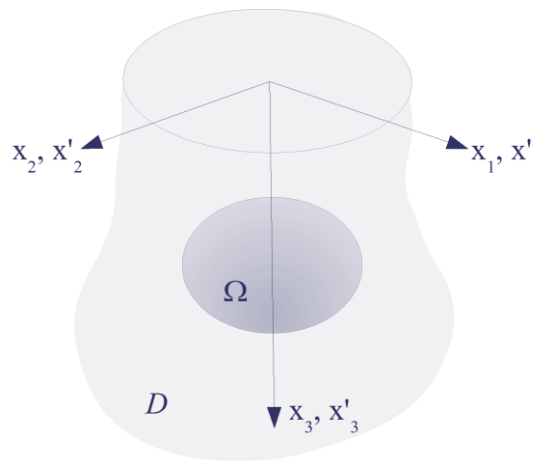


Figure 15 Inclusion Ω in a semi-infinite medium D bounded by the free surface $x_3 = 0$

Consider a semi-infinite domain where $x_3 \geq 0$ and the plane $x_3 = 0$ with unit normal n_i is free from external tractions (Figure 15). The Green's functions of the half-space have the properties

$$(3.78) \quad C_{ijkl} G_{km,lj}(\underline{x}, \underline{x}') + \delta_{im} \delta(\underline{x}, \underline{x}') = 0$$

on $x_3 \geq 0$, and

$$(3.79) \quad C_{ijkl} G_{km,l}(\underline{x}, \underline{x}') n_j = \delta_{im} \delta_S(\underline{x}, \underline{x}')$$

on $x_3 = 0$. In the above equations, δ_{ij} is the Kronecker delta, while $\delta(\underline{x}, \underline{x}')$ and $\delta_S(\underline{x}, \underline{x}')$ are the three- and two-dimensional Dirac delta functions. S indicates the surface $x_3 = 0$ and

$$(3.80) \quad \int_0^{\infty} f(\underline{x}') \delta(\underline{x}, \underline{x}') d\underline{x}' = f(\underline{x}),$$

$$(3.81) \quad \int_S f(\underline{x}') \delta_S(\underline{x}, \underline{x}') dS(\underline{x}') = f(\underline{x}) \text{ at } x_3 = 0,$$

$$(3.82) \quad \delta(\underline{x}, \underline{x}') = \delta_S(\underline{x}, \underline{x}') = 0 \text{ if } \underline{x} \neq \underline{x}'.$$

The explicit expression for the Green's function of an isotropic semi-infinite body was found by Mindlin (Mindlin, 1953). One can look up the formulae in (Mura, 1987).

3.1.5.4.1 Ellipsoidal inclusion with a dilatational uniform eigenstrain

The elastic field of the ellipsoidal inclusion with given dilatational uniform eigenstrain close to the free surface of the half-space (Figure 15) can be calculated with the help of the V -integrals (see (Mura, 1987)). It was shown by Seo and Mura (Seo & Mura, 1979) that the stresses in the inclusion and the surrounding matrix depends on the shape of the inclusion – sphere or ellipsoid –, and on the depth of the inclusion. Also the uniformity of the stresses inside the inclusion is mitigated by the existence of the free surface and tensile stresses may appear in the matrix. The free surface has less effect on the spherical inclusions, moreover, it was observed that this effect ceases, if the distance between the free surface and the centroid of the inclusion is greater than the diameter of the sphere. On the other hand, in case of spherical inclusions, there are large tensile stresses in the matrix close to the free surface. This behavior diminishes when the inclusion is embedded *deeper* in the semi-finite body. These tensile stresses are smaller when considering ellipsoidal inclusions, but they do not disappear with Ω being deeper in the matrix.

The elastic strain energy of a semi-infinite body with given dilatational eigenstrain is extended by a correction factor that represents the effect of free surface. The force acting on the inclusion is negative, thus *the free surface attracts the inclusion*.

3.1.6 Anisotropic inclusions

Since explicit expression for Green's functions of anisotropic materials are not available, one must carry out the integrals either in the Fourier space or in the physical space.

For any type of eigenstrain distribution in an ellipsoidal shaped inclusion embedded in an infinitely extended anisotropic material, the resulted elastic field both inside and outside the inclusion can be calculated from

$$(3.83) \quad u_i(\underline{x}) = -\frac{a_1 a_2 a_3}{8\pi^2} \int_{-1}^1 dz \int_0^{2\pi} d\phi \int_0^R r dr \int_{S^2} C_{klmn} \varepsilon_{nm}^*(\underline{x}') N_{ik}(\underline{\xi}) D^{-1}(\underline{\xi}) \xi_i \delta'(\underline{\xi} \cdot \underline{y} - \zeta z) dS(\underline{\xi}),$$

$$(3.84) \quad u_{i,j}(\underline{x}) = -\frac{a_1 a_2 a_3}{8\pi^2} \int_{-1}^1 dz \int_0^{2\pi} d\phi \int_0^R r dr \int_{S^2} C_{klmn} \varepsilon_{nm}^*(\underline{x}') N_{ik}(\underline{\xi}) D^{-1}(\underline{\xi}) \bar{\xi}_i \bar{\xi}_j \delta''(\zeta \bar{\xi}_i y - \zeta z) dS(\underline{\xi}).$$

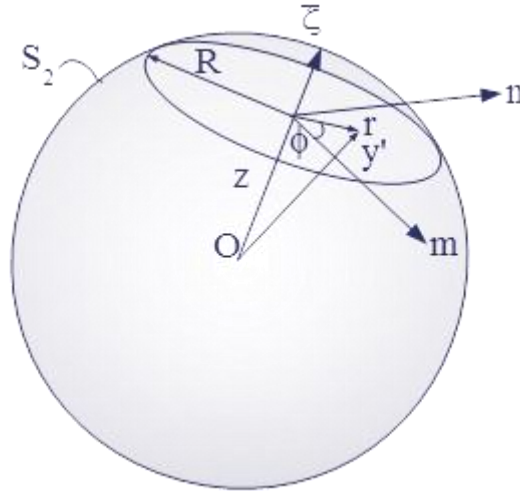


Figure 16 The polar coordinate system used in case of ellipsoidal shaped anisotropic inclusions transformed into unit sphere S^2

The new coordinates y_i and ζ_i (Figure 16) come from

$$(3.85) \quad \left. \begin{aligned} y_i &= \frac{x_i}{a_i}, \\ y_i' &= \frac{x_i'}{a_i}, \\ \zeta_i &= \frac{a_i}{\xi_i} \end{aligned} \right\} i = 1, 2, 3; \quad \bar{\zeta} = \frac{\zeta}{\xi}, \quad \text{with } \zeta = (\zeta_1^2 + \zeta_2^2 + \zeta_3^2)^{\frac{1}{2}} = (a_1^2 \bar{\xi}_1^2 + a_2^2 \bar{\xi}_2^2 + a_3^2 \bar{\xi}_3^2)^{\frac{1}{2}}.$$

The transformation from the ellipsoid to the unit sphere S^2 can be written in the form

$$(3.86) \quad \bar{\zeta}_i y_i = \frac{\bar{\xi}_i x_i}{\zeta}$$

and the distance between the observed plane and the centroid of the unit sphere becomes

$$(3.87) \quad z = \bar{\zeta}_i y_i' = \frac{\bar{\xi}_i x_i'}{\zeta}.$$

Likewise, in the polar coordinate system we have

$$(3.88) \quad d\underline{x}' = dx_1' dx_2' dx_3' = a_1 a_2 a_3 dy_1' dy_2' dy_3' = a_1 a_2 a_3 r dr d\phi dz,$$

and the following property has also been applied in the derivation of (3.83) and (3.84):

$$(3.89) \quad \frac{\partial}{\partial x_i} \delta(\bar{\xi}_i (\underline{x} - \underline{x}')) = \bar{\xi}_i \delta'(\bar{\xi}_i (\underline{x} - \underline{x}')).$$

For constant eigenstrains, $u_{i,j}$ will also be constant, and for linear ε_{ij}^* , the distortions will be linear. In case of uniform eigenstrains, we can write the displacements inside the inclusion in the form

$$(3.90) \quad u_i(\underline{x}) = \frac{1}{4\pi} C_{jlmn} \varepsilon_{nm}^* x_k \int_{-1}^1 d\zeta_3 \int_0^{2\pi} G_{ijkl}(\underline{\zeta}) d\theta,$$

where θ is measured counter-clockwise from the ζ_1 -axis () and

$$(3.91) \quad G_{ijkl}(\underline{\zeta}) = \zeta_k \zeta_l N_{ij}(\underline{\zeta}) D^{-1}(\underline{\zeta}).$$

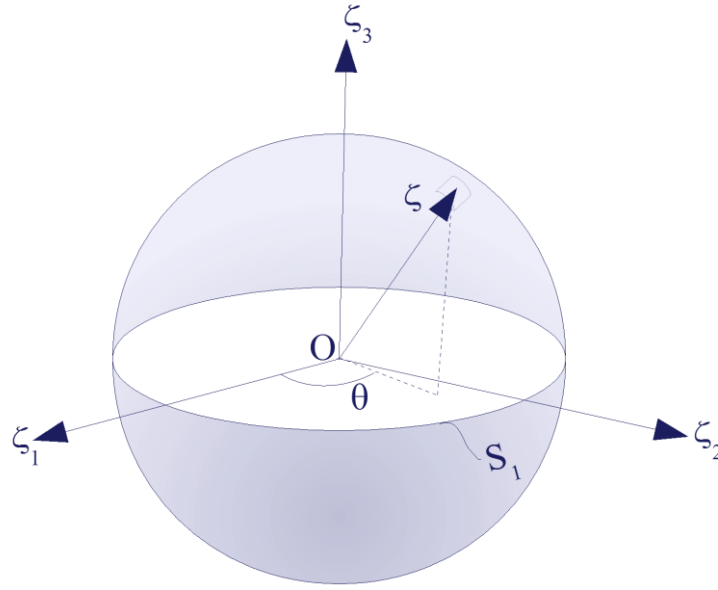


Figure 17 Unit sphere in ζ -space

This way, we can write Eshelby's solution for ellipsoidal inclusions with the Eshelby tensor for anisotropic materials and uniform eigenstrain:

$$(3.92) \quad S_{ijmn} = \frac{1}{8\pi} C_{pqmn} \int_{-1}^1 d\zeta_3 \int_0^{2\pi} (G_{ipjq}(\underline{\zeta}) + G_{jpiq}(\underline{\zeta})) d\theta.$$

Formulae for the elastic field of exterior points in an anisotropic media due to eigenstrain ε_{ij}^* can be found in (Mura, 1987).

The stress jump on the boundary of the inclusion can be computed from

$$(3.93) \quad (\sigma_{ij})_{jump} = \sigma_{ij}(S^+) - \sigma_{ij}(S^-) = C_{ijkl} \left(-C_{pqmn} \varepsilon_{nm}^*(\underline{x}) N_{kp}(\underline{n}) D^{-1}(\underline{n}) n_q n_l + \varepsilon_{kl}^*(\underline{x}) \right),$$

which can be used in the evaluation of the stress concentration factor of a lens-shaped void and its relation to the stress intensity factor of a crack.

When examining the interaction of two ellipsoidal inhomogeneities subjected to an applied stress, it is convenient to give the eigenstrain as a solid harmonic function of \underline{y} in the ellipsoidal inclusion Ω :

$$(3.94) \quad \varepsilon_{ij}^*(\underline{x}) = \bar{\varepsilon}_{ij}^*(\underline{\omega}) y^n P_n \left(\frac{y\omega}{y} \right),$$

where $\underline{\omega}$ is an arbitrary vector on the unit sphere S^2 and P_n is the Legendre polynomial of degree n .

3.1.6.1 Periodic distribution of spherical inclusions

Consider a periodic distribution of spherical inclusions with a period $2L$ in all three directions of a Cartesian coordinate-system (Figure 18). The eigenstrain distribution is given in its Fourier series form:

$$(3.95) \quad \varepsilon_{ij}^*(\underline{x}) = \sum_{v_1, v_2, v_3 = -\infty}^{\infty} \bar{\varepsilon}_{ij}^*(\underline{\xi}) e^{i\underline{\xi}\underline{x}},$$

where

$$(3.96) \quad \xi_i = \frac{\pi v_i}{L}, \quad v_i \neq 0,$$

$$(3.97) \quad \bar{\varepsilon}_{ij}^*(\underline{\xi}) = \frac{1}{8L^3} \int_{-L}^L \int_{-L}^L \int_{-L}^L \varepsilon_{ij}^*(\underline{x}) e^{i\underline{\xi}\underline{x}} d\underline{x}.$$

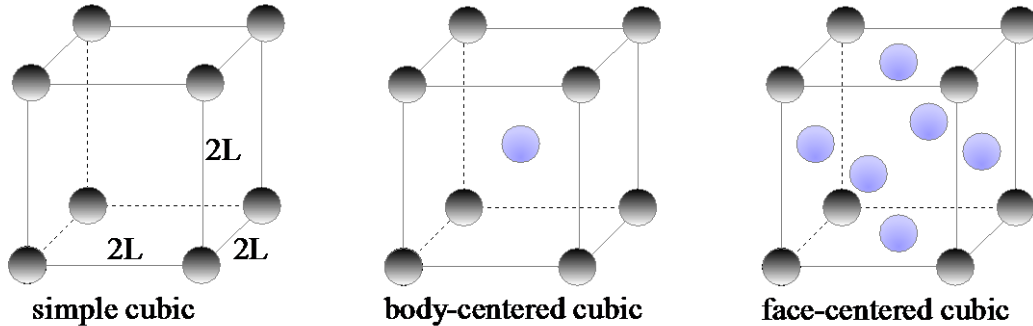


Figure 18 Unit cells of cubic crystals with edge lengths $2L$, modelled as periodic distribution of spherical inclusions with period $2L$ in three orthogonal directions

The resulting elastic field of a simple cubic, a body-centered cubic and a face-centered cubic crystal can be found in (Mura, 1987). Based on these expressions, one can study the stability of periodic arrangements of atoms in alloys. The atoms tend to array in such formulation, that the elastic strain energy to be the possible minimum. In some formulation, with decreasing period $2L$ the elastic strain energy decreases monotonically to the asymptotic value. The difference between the actual elastic energy and the asymptotic value is the interaction energy among the spherical precipitates. On the other hand there are arrangements in which the elastic strain energy decreases until a certain value, then increases to the asymptotic value. On this specific minimum energy level, formations of intermediate phases occur. We can see that phase transformations can be interpreted on the basis of the elastic strain energy associated of the clustering of contaminants.

3.2 Inhomogeneities

3.2.1 Definition of inhomogeneity

If a finite subdomain Ω in a material D has an elastic modulus different from those of the matrix, Ω is called inhomogeneity (Figure 19). Applied stresses are disturbed by the existence of the inhomogeneity. The disturbed stress field can be simulated as an eigenstress field by applying a fictitious eigenstrain in Ω , while considering a homogeneous material. At composite problems (plane strain or plane stress problems) the complex potential method by Muskhelishvili (Muskhelishvili, 1953) is more effective than the generally applied equivalent inclusion method.

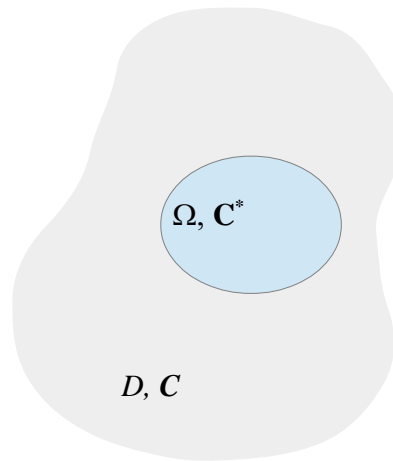


Figure 19 Inhomogeneity Ω embedded in medium D having different material properties than that of body D

A material containing inhomogeneities is free from any stress field unless a load is applied. On the other hand, a material containing inclusions is subjected to an eigenstress field even if it is free from external loading. When uniformly distributed stress is applied in infinity, at the neighbourhood of the inhomogeneity the stress field will not be uniform.

An inhomogeneity can also bear its own eigenstrain, this type of inhomogeneity is called inhomogeneous inclusion. As an example, most of the precipitates in alloys and martensitic blades in phase transformations are inhomogeneous inclusions with misfit and phase transformation strains as eigenstrains.

The inhomogeneity problem appears in other engineering problems, such as in a certain geotechnical problem, where a deep anchor embedded in soil or rock can be modelled as needle-type inhomogeneity and its load-deflection characteristics can be investigated. Another example is concrete, which can be modeled as ellipsoidal aggregates embedded in cement.

Considering an inhomogeneity under applied stress, the displacements and tractions across the boundary must be continuous. Indicating the elastic modulus of the inhomogeneity by C_{ijkl}^* , the stress field in the matrix (S^+) and in the inhomogeneity (S^-) can be written as

$$(3.98) \quad \sigma_{ij}(S^+) = C_{ijkl} u_{k,l}(S^+),$$

$$(3.99) \quad \sigma_{ij}(S^-) = C_{ijkl}^* u_{k,l}(S^-),$$

therefore the continuity condition

$$(3.100) \quad (\sigma_{ij})_{jump} n_j \equiv (\sigma_{ij}(S^+) - \sigma_{ij}(S^-)) n_j = 0$$

becomes

$$(3.101) \quad C_{ijkl} u_{k,l}(S^+) n_j = C_{ijkl}^* u_{k,l}(S^-) n_j.$$

The distortion field is discontinuous on the boundary, thereby equation (3.10) holds for the inhomogeneity problem, too:

$$(3.102) \quad (u_{i,j})_{jump} \equiv u_{i,j}(S^+) - u_{i,j}(S^-) = \lambda_i n_j.$$

Substituting (3.102) into (3.101) we have

$$(3.103) \quad C_{ijkl} \lambda_k n_i n_j = (C_{ijkl}^* - C_{ijkl}) u_{k,l}(S^-) n_j,$$

from which the unknown vector λ_i can be determined:

$$(3.104) \quad \lambda_i = N_{ij}(\underline{n}) n_k (C_{ijkl}^* - C_{ijkl}) u_{l,m}(S^-) D^{-1}(\underline{n}).$$

Substituting (3.104) into (3.102):

$$(3.105) \quad u_{i,j}(S^+) = u_{i,j}(S^-) + N_{ik}(\underline{n}) n_j n_l (C_{klmn}^* - C_{klmn}) u_{m,n}(S^-) D^{-1}(\underline{n}).$$

The resulting stress field just outside the inhomogeneity, if the elastic field is known inside Ω :

$$(3.106) \quad \sigma_{ij}(S^+) = C_{ijkl} (u_{k,l}(S^-) + N_{kp}(\underline{n}) n_l n_q (C_{pqmn}^* - C_{pqmn}) u_{m,n}(S^-) D^{-1}(\underline{n})).$$

These results hold for any shape of inhomogeneity and are applicable when computing the strains and stresses just outside the inhomogeneity, if the strain and stress field is given inside the inhomogeneity. The *uniqueness theorem* for inhomogeneity-matrix interface states that if the stress or strain is known locally at one side of the interface between an inhomogeneity and the surrounding matrix, then their jumps and consequent values at the other side of the interface are explicitly determinable in terms of the moduli of the inhomogeneity and the matrix and the interface normal.

3.2.2 Ellipsoidal inhomogeneities. Equivalent inclusion method

Consider an infinite elastic body D containing an ellipsoidal shaped inhomogeneity Ω . The fourth-order elastic stiffness tensors of the matrix and inhomogeneity is $\underline{\underline{C}}$ and $\underline{\underline{C}}^*$, respectively. On the boundary of D , the body is under surface traction forces $\underline{p}^0 = \underline{\underline{\sigma}}^0 \underline{n}$ (Figure 20).

When the two elastic moduli are identical, the elastic body D is homogeneous. In this case, the total stress field is uniform

$$(3.107) \underline{\underline{\sigma}}' = \underline{\underline{\sigma}}^0 .$$

Applying the linear superposition of the elastic theory, let us write the stress field of the elastic body D consisting inhomogeneity Ω as the sum of the stress field of the homogeneous body and the so-called stress perturbation due to the presence of the inhomogeneity:

$$(3.108) \underline{\underline{\sigma}}' = \underline{\underline{\sigma}}^0 + \underline{\underline{\sigma}} .$$

The perturbed stress field is in self-equilibrium, it satisfies the equilibrium equations and the homogeneous boundary condition

$$(3.109) \nabla \underline{\underline{\sigma}} = \underline{\underline{0}} ,$$

$$(3.110) \underline{\underline{\sigma}} \underline{\underline{n}} = \underline{\underline{0}} \text{ on } S ,$$

$$(3.111) \underline{\underline{\sigma}} = \underline{\underline{0}} \text{ in infinity .}$$

The strain field can also be divided into two parts. Let us denote the one corresponding to the *homogeneous material* by the superscript '0' such that

$$(3.112) \underline{\underline{\sigma}}^0 = \underline{\underline{C}} \underline{\underline{\varepsilon}}^0 ,$$

where – due to their symmetric behavior – the second order tensors are in Voigt form and the fourth-order tensors are reordered into 6-by-6 matrices.

The total strain field of the body including *inhomogeneity* can be written as

$$(3.113) \underline{\underline{\varepsilon}}' = \underline{\underline{\varepsilon}}^0 + \underline{\underline{\varepsilon}} ,$$

where $\underline{\underline{\varepsilon}}$ denotes the perturbed strain field due to the presence of the inhomogeneity. Applying Hooke's law for both the inhomogeneity Ω and the matrix $D - \Omega$:

$$(3.114) \underline{\underline{\sigma}}' = \underline{\underline{\sigma}}^0 + \underline{\underline{\sigma}} = \underline{\underline{C}}^* (\underline{\underline{\varepsilon}}^0 + \underline{\underline{\varepsilon}}) \text{ in } \Omega ,$$

$$(3.115) \underline{\underline{\sigma}}' = \underline{\underline{\sigma}}^0 + \underline{\underline{\sigma}} = \underline{\underline{C}} (\underline{\underline{\varepsilon}}^0 + \underline{\underline{\varepsilon}}) \text{ in } D - \Omega .$$

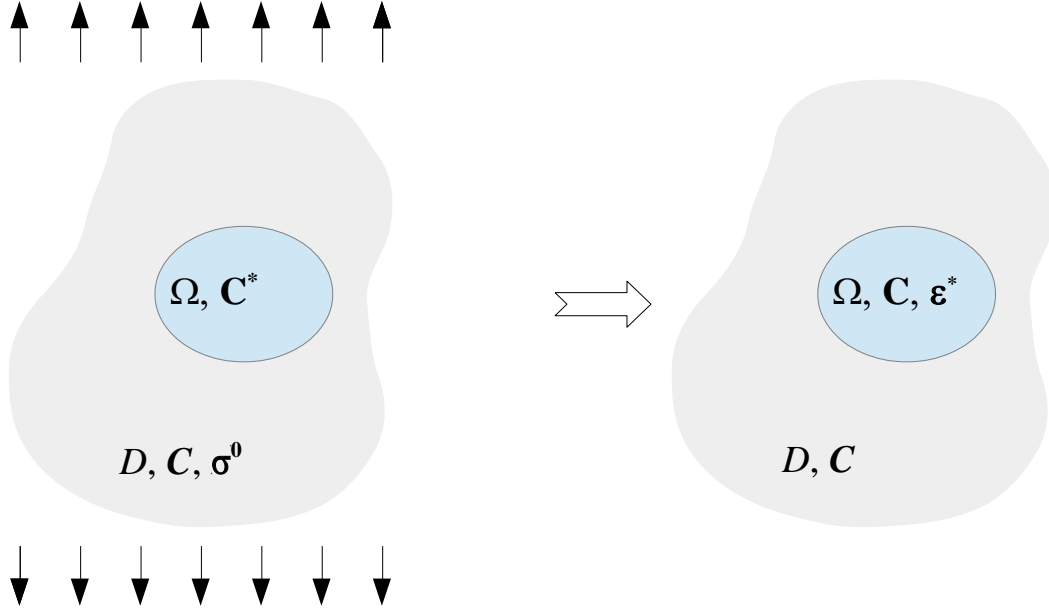


Figure 20 *Equivalent inclusion method: Ellipsoidal inhomogeneity Ω embedded in infinitely extended material D under applied stresses σ_{ij}^0 modelled as an ellipsoidal inclusion Ω with appropriate eigenstrain ε_{ij}^* in body D free from any external load*

This problem will be solved with the so-called equivalent inclusion method. Consider an elastic body D with an ellipsoidal inclusion Ω (Figure 20). In this case the elastic modulus is the same in the whole body. The eigenstrain $\underline{\varepsilon}^*$ is uniformly distributed in the inclusion. The value of the eigenstrain must be determined such that the stress field induced by the inclusion is the same as the stress field of the inhomogeneity problem presented above. We can say that the equivalent method *substitutes the inhomogeneity problem with an inclusion problem* by applying a proper eigenstrain field.

Writing Hooke's law for the inclusion problem:

$$(3.116) \quad \underline{\sigma}' = \underline{\sigma}^0 + \underline{\sigma} = \underline{\underline{C}}(\underline{\varepsilon}^0 + \underline{\varepsilon} - \underline{\varepsilon}^*) \text{ in } \Omega ,$$

$$(3.117) \quad \underline{\sigma}' = \underline{\sigma}^0 + \underline{\sigma} = \underline{\underline{C}}(\underline{\varepsilon}^0 + \underline{\varepsilon}) \text{ in } D - \Omega ,$$

but in this case $\underline{\sigma}$ and $\underline{\varepsilon}$ indicates the stress and strain field due to the eigenstrain in the inclusion, respectively. Substituting Eshelby's ellipsoidal inclusion solution into equations (3.116) and (3.117), and given that the stress field of the inhomogeneity is the same as that of the inclusion, we have the necessary and sufficient condition for the equivalency of the stresses and strains of the inhomogeneity and inclusion problem:

$$(3.118) \quad \underline{\sigma}' = \underline{\sigma}^0 + \underline{\sigma} = \underline{\underline{C}}(\underline{\varepsilon}^0 + \underline{\underline{S}}\underline{\varepsilon}^* - \underline{\varepsilon}^*) \text{ in } \Omega ,$$

where $\underline{\underline{S}}$ denotes the fourth-order Eshelby tensor reordered into a 6-by-6 matrix. Substituting (3.118) into (3.114):

$$(3.119) \quad \underline{\underline{C}}(\underline{\varepsilon}^0 + \underline{\underline{S}}\underline{\varepsilon}^* - \underline{\varepsilon}^*) = \underline{\underline{C}}^*(\underline{\varepsilon}^0 + \underline{\varepsilon}) \text{ in } \Omega .$$

Making use of the Eshelby-tensor providing a connection between the strain and eigenstrain field once again, we have

$$(3.120) \underline{\underline{C}}(\underline{\underline{\varepsilon}}^0 + \underline{\underline{S}}\underline{\underline{\varepsilon}}^* - \underline{\underline{\varepsilon}}^*) = \underline{\underline{C}}^*(\underline{\underline{\varepsilon}}^0 + \underline{\underline{S}}\underline{\underline{\varepsilon}}^*) \text{ in } \Omega .$$

This is the equivalent inclusion equation. The eigenstrain needed to simulate the inhomogeneity in the inclusion problem:

$$(3.121) \underline{\underline{\varepsilon}}^* = -\left(\underline{\underline{S}} + (\underline{\underline{C}}^* - \underline{\underline{C}})^{-1} \underline{\underline{C}}\right)^{-1} \underline{\underline{\varepsilon}}^0 ,$$

the total strain on the inclusion:

$$(3.122) \underline{\underline{\varepsilon}}' = \underline{\underline{\varepsilon}}^0 + \underline{\underline{\varepsilon}} = \underline{\underline{\varepsilon}}^0 + \underline{\underline{S}}\underline{\underline{\varepsilon}}^* = \underline{\underline{T}}\underline{\underline{\varepsilon}}^0$$

with

$$(3.123) \underline{\underline{T}} = \left(\underline{\underline{I}} + \underline{\underline{S}}\underline{\underline{C}}^{-1}(\underline{\underline{C}}^* - \underline{\underline{C}})\right)^{-1} .$$

The stresses in the inhomogeneity can be computed from the equivalent inclusion equation (3.118).

3.2.3 Inhomogeneous inclusions

An eigenstrain can be prescribed not only in an inclusion but also in an inhomogeneity. These types of inhomogeneities are called inhomogeneous inclusions, they appear for example at the formation of martensitic blades in quenched carbon steels and precipitations in alloys.

In this case, the elastic body D is under surface traction forces $\underline{p}^0 = \underline{\underline{\sigma}}^0 \underline{n}$ on its boundary and in Ω a given eigenstrain $\underline{\underline{\varepsilon}}^p$ is also prescribed (Figure 21). The stress field in the homogeneous material is $\underline{\underline{\sigma}}^0$. Applying Hooke's law in D , the total stress field:

$$(3.124) \underline{\underline{\sigma}}' = \underline{\underline{\sigma}}^0 + \underline{\underline{\sigma}} = \underline{\underline{C}}^*(\underline{\underline{\varepsilon}}^0 + \underline{\underline{\varepsilon}} - \underline{\underline{\varepsilon}}^p) \text{ in } \Omega ,$$

$$(3.125) \underline{\underline{\sigma}}' = \underline{\underline{\sigma}}^0 + \underline{\underline{\sigma}} = \underline{\underline{C}}(\underline{\underline{\varepsilon}}^0 + \underline{\underline{\varepsilon}}) \text{ in } D - \Omega .$$

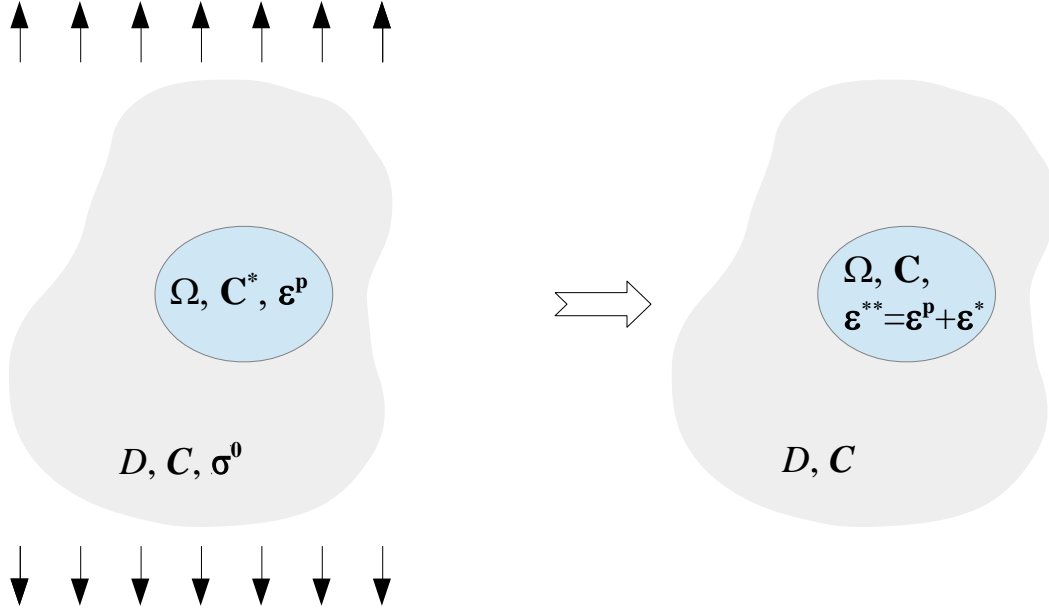


Figure 21 *Equivalent inclusion method in case of inhomogeneous inclusions: Ellipsoidal inhomogeneous inclusion Ω with prescribed eigenstrain ε_{ij}^p embedded in infinitely extended material D under applied stresses σ_{ij}^0 modelled as an ellipsoidal inclusion Ω with appropriate eigenstrain ε_{ij}^{**} in body D free from any external load*

The perturbed stress field $\underline{\sigma}$ and strain field $\underline{\varepsilon}$ is due to the presence of both the inhomogeneity and the eigenstrain field in the inhomogeneity. We can simulate these two effects by a homogeneous material containing an inclusion with a uniform eigenstrain field of $\underline{\varepsilon}^* + \underline{\varepsilon}^p$, namely applying the equivalent inclusion method here as well (Figure 21).

The total stress field in the equivalent inclusion:

$$(3.126) \quad \underline{\sigma}' = \underline{\sigma}^0 + \underline{\sigma} = \underline{\underline{C}}(\underline{\varepsilon}^0 + \underline{\varepsilon} - \underline{\varepsilon}^p - \underline{\varepsilon}^*) \text{ in } \Omega ,$$

$$(3.127) \quad \underline{\sigma}' = \underline{\sigma}^0 + \underline{\sigma} = \underline{\underline{C}}(\underline{\varepsilon}^0 + \underline{\varepsilon}) \text{ in } D - \Omega .$$

Eshelby's ellipsoidal inclusion solution becomes

$$(3.128) \quad \underline{\varepsilon} = \underline{\underline{S}}\underline{\varepsilon}^{**}$$

with

$$(3.129) \quad \underline{\varepsilon}^{**} = \underline{\varepsilon}^p + \underline{\varepsilon}^* .$$

The equivalent inclusion equation at the inhomogeneous inclusion problem is

$$(3.130) \quad \underline{\sigma}' = \underline{\underline{C}}^*(\underline{\varepsilon}^0 + \underline{\underline{S}}\underline{\varepsilon}^{**} - \underline{\varepsilon}^p) = \underline{\underline{C}}(\underline{\varepsilon}^0 + \underline{\underline{S}}\underline{\varepsilon}^{**} - \underline{\varepsilon}^{**}) \text{ in } \Omega .$$

The eigenstrain in the inclusion is written in the form

$$(3.131) \quad \underline{\varepsilon}^{**} = \left(\underline{\underline{C}}(\underline{\underline{S}} - \underline{\underline{I}}) - \underline{\underline{C}}^*\underline{\underline{S}} \right)^{-1} \left((\underline{\underline{C}}^* - \underline{\underline{C}})\underline{\underline{M}}\underline{\sigma}^0 - \underline{\underline{C}}^*\underline{\varepsilon}^p \right) .$$

Since

$$(3.132) \underline{\underline{S}} \left(\underline{\underline{C}} (\underline{\underline{S}} - \underline{\underline{I}}) - \underline{\underline{C}}^* \underline{\underline{S}} \right)^{-1} = - \left(\underline{\underline{C}} \underline{\underline{S}}^{-1} - \underline{\underline{C}} + \underline{\underline{C}}^* \right)^{-1} = - \left(\underline{\underline{H}} + \underline{\underline{C}}^* \right)^{-1},$$

where $\underline{\underline{H}}$ denotes Hill's constraint tensor

$$(3.133) \underline{\underline{H}} = \underline{\underline{C}} \underline{\underline{S}}^{-1} - \underline{\underline{C}} = \underline{\underline{C}} (\underline{\underline{S}}^{-1} - \underline{\underline{I}}) = \underline{\underline{P}}^{-1} - \underline{\underline{C}}.$$

Therefore the eigenstrain $\underline{\underline{\varepsilon}}^{**}$ can be written also as

$$(3.134) \underline{\underline{\varepsilon}}^{**} = - \underline{\underline{S}}^{-1} \left(\underline{\underline{H}} + \underline{\underline{C}}^* \right)^{-1} \left(\left(\underline{\underline{C}}^* - \underline{\underline{C}} \right) \underline{\underline{M}} \underline{\underline{\sigma}}^0 - \underline{\underline{C}}^* \underline{\underline{\varepsilon}}^p \right).$$

The total strain on the inhomogeneous inclusion:

$$(3.135) \underline{\underline{\varepsilon}}' = \underline{\underline{\varepsilon}}^0 + \underline{\underline{\varepsilon}} = \underline{\underline{\varepsilon}}^0 + \underline{\underline{S}} \underline{\underline{\varepsilon}}^{**} = \underline{\underline{\varepsilon}}^0 - \left(\underline{\underline{H}} + \underline{\underline{C}}^* \right)^{-1} \left(\left(\underline{\underline{C}}^* - \underline{\underline{C}} \right) \underline{\underline{M}} \underline{\underline{\sigma}}^0 + \underline{\underline{\tau}}^p \right),$$

where the stress polarization is defined by

$$(3.136) \underline{\underline{\tau}}^p = - \underline{\underline{C}}^* \underline{\underline{\varepsilon}}^p.$$

The total stress field in Ω becomes

$$(3.137) \underline{\underline{\sigma}}' = \underline{\underline{C}} (\underline{\underline{\varepsilon}}^0 + \underline{\underline{S}} \underline{\underline{\varepsilon}}^{**} - \underline{\underline{\varepsilon}}^{**}) = \underline{\underline{\sigma}}^0 - \underline{\underline{H}} \left(\underline{\underline{H}} + \underline{\underline{C}}^* \right)^{-1} \left(\left(\underline{\underline{C}}^* - \underline{\underline{C}} \right) \underline{\underline{M}} \underline{\underline{\sigma}}^0 + \underline{\underline{\tau}}^p \right),$$

which can be written in a simple form:

$$(3.138) \underline{\underline{\sigma}}' = \underline{\underline{\sigma}}^0 - \underline{\underline{H}} (\underline{\underline{\varepsilon}}' - \underline{\underline{\varepsilon}}^0) \text{ in } \Omega.$$

If there is no applied loading, only the given eigenstrain in the inhomogeneity, the total strain field becomes

$$(3.139) \underline{\underline{\varepsilon}}' = - \left(\underline{\underline{H}} + \underline{\underline{C}}^* \right)^{-1} \underline{\underline{\tau}}^p,$$

and the stresses in the inhomogeneity become

$$(3.140) \underline{\underline{\sigma}}' = \underline{\underline{H}} \left(\underline{\underline{H}} + \underline{\underline{C}}^* \right)^{-1} \underline{\underline{\tau}}^p = - \underline{\underline{H}} \underline{\underline{\varepsilon}}' \text{ in } \Omega.$$

When an anisotropic inhomogeneous inclusion is contained in an isotropic matrix, we take $\underline{\underline{C}}$ and $\underline{\underline{S}}$ for the isotropic material.

The displacement and stress field for exterior points can be obtained with the help of the equivalent eigenstrain, but these calculations are quite complicated. Tanaka and Mura (Tanaka & Mura, 1982) proposed an alternative method for computing the elastic fields outside the inhomogeneity (Figure 22). Let us consider an ellipsoidal inhomogeneity in an infinitely extended matrix with applied stress $\underline{\underline{\sigma}}^0$ at infinity. The stress field in Ω shall be computed and denoted by $\underline{\underline{\sigma}}^0 + \underline{\underline{\sigma}}(S^-)$, where the negative side of the boundary S of Ω belongs to the inhomogeneity, and the positive side to the matrix.. Then find the stress field $\underline{\underline{\sigma}}(S^+)$ in the matrix assuming that Ω is a void and the applied stress is $-\underline{\underline{\sigma}}(S^-)$. The stress field of the inhomogeneity problem for the exterior points is the sum of the above stress

fields, namely $\underline{\underline{\sigma}}^0 + \underline{\underline{\sigma}}(S^-) + \underline{\underline{\sigma}}(S^+)$ where solutions for the void problem are available in the literature.

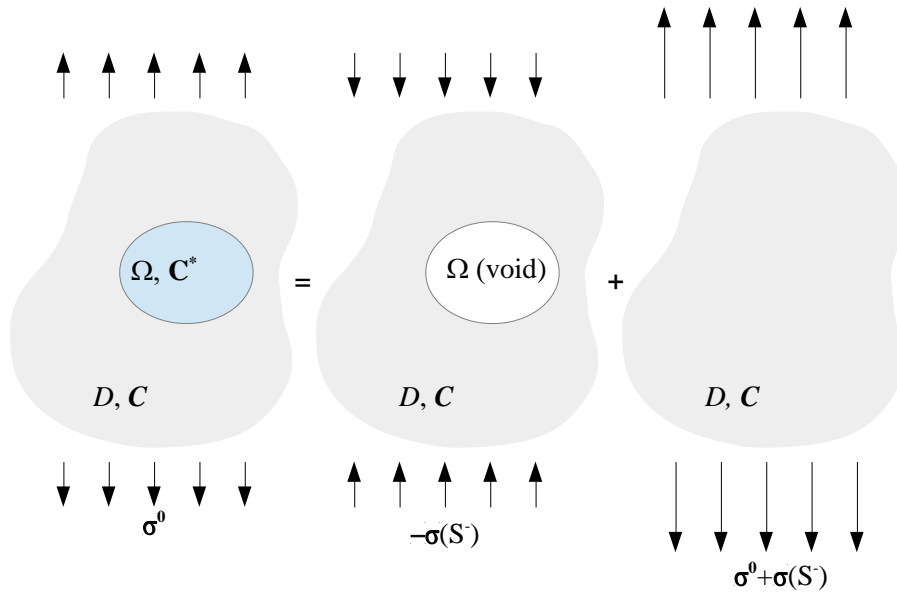


Figure 22 Calculation of the elastic field caused by the presence of inhomogeneity Ω at points $x_i \in D - \Omega$

The system of equations in the equivalent inclusion equation becomes *singular* when an inhomogeneity is taken as a *void*. The solution of this system of equations is not unique, which means that there are an infinite number of eigenstrains which do not generate any stress field within the material. These eigenstrains are called impotent eigenstrains. To avoid such a problem in numerical calculations, cavities can be modelled as weak inhomogeneities with their elastic moduli significantly smaller than that of the matrix: $\underline{\underline{C}}^* \ll \underline{\underline{C}}$.

Assuming a material with two inhomogeneities Ω_1 and Ω_2 , even if $\underline{\underline{\varepsilon}}^0$ is uniform, the strain field $\underline{\underline{\varepsilon}}$ due to the inhomogeneities is no longer uniform, because the interior points of Ω_1 are exterior points of Ω_2 and the stress in Ω_1 is disturbed by Ω_2 (Figure 23). Numerical calculations performed by Moschovidis (Moschovidis, 1975) show that in case of two spherical cavities under uniform tension field, the interaction between the two cavities become negligible if the distance between their centroids are at least four times larger than their radii.

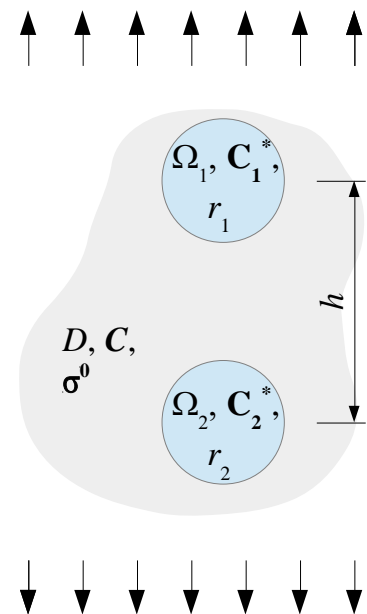


Figure 23 Interaction between spherical inhomogeneities Ω_1 and Ω_2

The equivalent inclusion method can be applied even in case of non-uniform stresses. When an applied stress is a function of the coordinates, and a polynomial of degree n , the equivalent eigenstrain is also function of the coordinates and chosen to be a polynomial of degree n .

3.2.4 Energies of inhomogeneities

3.2.4.1 Elastic strain energy

3.2.4.1.1 Elastic energy of a body containing inhomogeneous inclusion

The elastic strain energy of a body D free from any external force or constraint, but containing inhomogeneous inclusion Ω with prescribed eigenstrain ε_{ij}^p :

$$(3.141) W^* = \frac{1}{2} \int_D \sigma_{ij} e_{ij} dD = -\frac{1}{2} \int_{\Omega} \sigma_{ij} \varepsilon_{ij}^p dD ,$$

where the elastic strain is

$$(3.142) e_{ij} = \varepsilon_{ij} - \varepsilon_{ij}^p = \frac{1}{2} (u_{i,j} - u_{j,i}) - \varepsilon_{ij}^p .$$

If Ω is an ellipsoidal heterogeneity with volume V and the prescribed eigenstrain ε_{ij}^p is uniform, the elastic strain energy of D becomes

$$(3.143) W^* = -\frac{1}{2} V \sigma_{ij} \varepsilon_{ij}^p .$$

If the elastic modulus C_{ijkl}^* of the inhomogeneity is slightly different from that of the matrix, we can approximate the elastic strain energy of the body containing inhomogeneous inclusion based on a homogeneous inclusion problem. Given a homogeneous body of elastic modulus C_{ijkl} with prescribed eigenstrain ε_{ij}^p , the resulting displacement, elastic strain, stress and elastic strain energy for the homogeneous inclusion problem is denoted by \tilde{u}_i , \tilde{e}_{ij} , $\tilde{\sigma}_{ij}$ and \tilde{W} , respectively. Making use of (3.142) and the fact that

$$(3.144) \int_D \tilde{\sigma}_{ij} u_{i,j} dD = \int_D \sigma_{ij} \tilde{u}_{i,j} dD = 0 ,$$

the elastic strain energy of the homogeneous inclusion problem becomes

$$(3.145) \tilde{W} = -\frac{1}{2} \int_{\Omega} \tilde{\sigma}_{ij} \varepsilon_{ij}^p dD = -\frac{1}{2} \int_D \tilde{\sigma}_{ij} (\varepsilon_{ij}^p - u_{i,j} + u_{j,i}) dD = \frac{1}{2} \int_D \tilde{\sigma}_{ij} e_{ij} dD .$$

Similarly, the elastic strain energy of the inhomogeneous inclusion problem is

$$(3.146) W^* = \frac{1}{2} \int_D \sigma_{ij} \tilde{e}_{ij} dD .$$

If $e_{ij} - \tilde{e}_{ij}$ is small quantity compared to e_{ij} , the difference in the elastic strain energy of the inhomogeneous and homogeneous inclusion problem can be approximated by

$$(3.147) W^* - \tilde{W} = \frac{1}{2} \int_{\Omega} (C_{ijkl}^* - C_{ijkl}) \tilde{e}_{kl} \tilde{e}_{ij} dD .$$

Equations (3.145) and (3.147) can be used as an approximation of the inhomogeneous inclusion problem, where Ω can be the sum of several inclusions Ω_i . This method was proposed by Eshelby. In case of two inhomogeneities, the interaction energy between these two inhomogeneities:

$$(3.148) \Delta W^* = - \int_{\Omega_1} \sigma_{ij}^{(2)} \varepsilon_{ij}^p dD = - \int_{\Omega_2} \sigma_{ij}^{(1)} \varepsilon_{ij}^p dD ,$$

where $\sigma_{ij}^{(m)}$ is the stress caused by the prescribed eigenstrain in Ω_m .

3.2.4.1.2 Elastic energy of a body containing inhomogeneous inclusion under traction boundary condition

The elastic strain energy in a body D under applied surface force F_i and containing inhomogeneous inclusion Ω with eigenstrain ε_{ij}^p :

$$(3.149) W^* = \frac{1}{2} \int_D (\sigma_{ij}^0 + \sigma_{ij}) (u_{i,j}^0 + u_{i,j} - \varepsilon_{ij}^p) dD ,$$

where the displacement and stress field is denoted by $u_i^0 + u_i$ and $\sigma_{ij}^0 + \sigma_{ij}$, respectively. The superscript '0' indicates the elastic field when F_i acts in the absence of the inhomogeneous inclusion Ω . Hence,

$$(3.150) \sigma_{ij}^0 = C_{ijkl} u_{k,l}^0 ,$$

$$(3.151) \sigma_{ij}^0 + \sigma_{ij} = C_{ijkl}^* (u_{k,l}^0 + u_{k,l} - \varepsilon_{kl}^p) .$$

Since

$$(3.152) \int_D \sigma_{ij} (u_{i,j}^0 + u_{i,j}) dD = 0 ,$$

$$(3.153) \int_D \sigma_{ij} u_{i,j}^0 dD = 0$$

and applying the equivalent inclusion method with fictitious eigenstrain ε_{ij}^*

$$(3.154) \sigma_{ij}^0 (u_{i,j} - \varepsilon_{ij}^p) = C_{ijkl} u_{k,l}^0 (u_{i,j} - \varepsilon_{ij}^p - \varepsilon_{ij}^* + \varepsilon_{ij}^*) = \sigma_{ij}^0 u_{i,j}^0 + \sigma_{ij}^0 \varepsilon_{ij}^*$$

with

$$(3.155) \sigma_{ij} = C_{ijkl} (u_{k,l} - \varepsilon_{kl}^p - \varepsilon_{kl}^*) \text{ in } \Omega .$$

It follows that

$$(3.156) \int_D \sigma_{ij}^0 (u_{i,j} - \varepsilon_{ij}^p) dD = \int_{\Omega} \sigma_{ij}^0 \varepsilon_{ij}^* dD .$$

The elastic strain energy of the inhomogeneous inclusion problem with given traction boundary condition:

$$(3.157) W^* = \frac{1}{2} \int_D \sigma_{ij}^0 u_{i,j}^0 dD + \frac{1}{2} \int_{\Omega} \sigma_{ij}^0 \varepsilon_{ij}^* dD - \frac{1}{2} \int_{\Omega} \sigma_{ij} \varepsilon_{ij}^p dD .$$

If body D under applied traction forces F_i contains inhomogeneity Ω without eigenstrain ($\varepsilon_{ij}^p = 0$), the elastic strain energy becomes

$$(3.158) W^* = \frac{1}{2} \int_D \sigma_{ij}^0 u_{i,j}^0 dD + \frac{1}{2} \int_{\Omega} \sigma_{ij}^0 \varepsilon_{ij}^* dD .$$

On the contrary, the elastic strain energy of body D with inhomogeneous inclusion Ω ($\varepsilon_{ij}^p \neq 0$) in the absence of external loading becomes

$$(3.159) W^* = -\frac{1}{2} \int_{\Omega} \sigma_{ij} \varepsilon_{ij}^p dD .$$

According to Colonetti's theorem⁵, the elastic strain energy W^* of body D due to the coexisting eigenstrain ε_{ij}^p and external loading F_i is the sum of the individual elastic strain energies (3.158) and (3.159). It is the same as the originally derived strain energy expressed in (3.157).

When considering an infinite anisotropic matrix containing ellipsoidal anisotropic precipitate, which is an inhomogeneous inclusion, based on the calculation of the elastic strain energy, it was shown that the resulted elastic field is strongly dependent on the orientation and shape of the precipitates.

3.2.4.2 Interaction energy

Given a body D with inhomogeneity Ω and external surface tractions F_i on boundary S . The total potential energy or Gibbs free energy of this body is the sum of the elastic strain energy and the potential energy of the external loading:

$$(3.160) W = \frac{1}{2} \int_D \sigma_{ij}^0 u_{i,j}^0 dD + \frac{1}{2} \int_{\Omega} \sigma_{ij}^0 \varepsilon_{ij}^* dD - \int_S F_i (u_i^0 + u_i) dS .$$

If body D is homogeneous, the total potential energy can be written as

$$(3.161) W_0 = \frac{1}{2} \int_D \sigma_{ij}^0 u_{i,j}^0 dD - \int_S F_i u_i^0 dS .$$

The interaction energy between the external surface tractions and the inhomogeneity is defined as

$$(3.162) \Delta W = W - W_0 = \frac{1}{2} \int_{\Omega} \sigma_{ij}^0 \varepsilon_{ij}^* dD - \int_S F_i u_i dS = -\frac{1}{2} \int_{\Omega} \sigma_{ij}^0 \varepsilon_{ij}^* dD .$$

If σ_{ij}^0 is uniform and Ω is an ellipsoidal inhomogeneity, ε_{ij}^* becomes uniform and the interaction energy can be written as

$$(3.163) \Delta W = -\frac{1}{2} V \sigma_{ij}^0 \varepsilon_{ij}^* .$$

As a remark the interaction energy can also be used in fracture mechanics for the derivation of Griffith's fracture criterion, when Ω is a crack and $V \varepsilon_{ij}^*$ is held constant as $V \rightarrow 0$ and $\varepsilon_{ij}^* \rightarrow \infty$. The interaction energy can be expressed as an integral over the surface of Ω , denoted by Σ , bypassing the problem that Ω has no volume (the derivation can be found in (Mura, 1987)):

$$(3.164) \Delta W = \frac{1}{2} \int_{\Sigma} \sigma_{ij}^0 n_j (u_i)_{jump} dS ,$$

with outward normal vector n_i of the upper surface of the crack and crack opening displacement

$$(3.165) (u_i)_{jump} = u_i(\text{upper}) - u_i(\text{lower}) .$$

When a body D contains an inhomogeneous inclusion Ω with prescribed eigenstrain ε_{ij}^p and external surface tractions F_i on boundary S , the total potential energy or Gibbs free energy of the body:

$$(3.166) W = \frac{1}{2} \int_D (\sigma_{ij}^0 + \sigma_{ij}) (u_{i,j}^0 + u_{i,j} - \varepsilon_{ij}^p) dD - \int_S F_i (u_i^0 + u_i) dS .$$

The interaction energy between the inhomogeneous inclusion and the external loading is the difference between the Gibbs free energy of the body given in (3.166) and that of the homogeneous body from equation (3.161):

$$(3.167) \Delta W = -\frac{1}{2} \int_{\Omega} \sigma_{ij}^0 \varepsilon_{ij}^* dD - \frac{1}{2} \int_{\Omega} \sigma_{ij} \varepsilon_{ij}^p dD - \int_{\Omega} \sigma_{ij}^0 \varepsilon_{ij}^p dD .$$

These expressions are valid also for the interaction between an inhomogeneous inclusion Ω and any kind of different internal stress σ_{ij}^0 .

4 Analytical and numerical model of the environment of inhomogeneities

4.1 Analytical model

In the following I calculate the effect of applied stress in case of isotropic inhomogeneities inside an infinitely extended isotropic matrix material. The analytical solution is based on Eshelby's equivalent inclusion method. The Matlab™ code was provided by Chunfang Meng (Meng & Pollard, 2014; Meng, Heltsley, & Pollard, 2012). It calculates the Eshelby tensor of an inhomogeneity based on the geometry of the heterogeneity and the material properties of the individual phases of the composite under consideration. It makes use of the I -integrals provided for specially shaped inhomogeneities in (Mura, 1987).

Let us consider an ellipsoidal inhomogeneity in an infinitely extended matrix material under applied stresses (Figure 24). The semi-axes a_1, a_2, a_3 ($a_1 \geq a_2 \geq a_3$) of the ellipsoidal heterogeneity are parallel to the x , y and z axes, respectively. First, I compute the resulting stress field inside the heterogeneous material when a compressive stress in x direction of unit magnitude is applied.

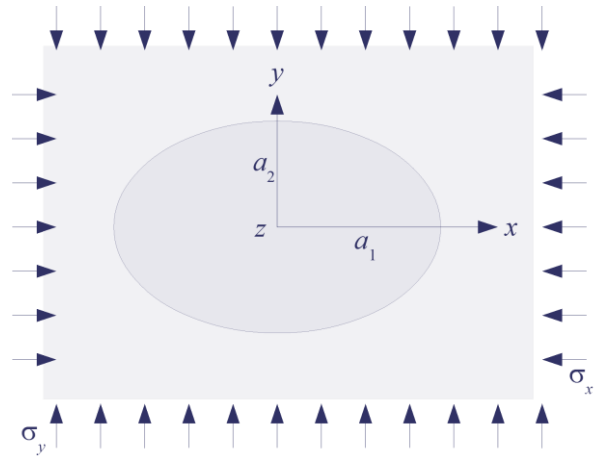


Figure 24 Heterogeneous material under applied stresses

The inhomogeneity is of spherical shape and bears the material properties of a strong inhomogeneity. Let us consider contaminants with elastic modulus $E_c = 200$ GPa and Poisson's ratio $\nu_c = 0.3$. In case of strong inhomogeneities, the inhomogeneity is stiffer than the surrounding matrix. Hence, I considered an infinite medium with elastic modulus $E_m = 20$ GPa and Poisson's ratio $\nu_m = 0.15$. (Later on, at homogenization methods, I use the same material properties to model steel reinforcing fibers embedded in portland cement, i.e. fiber-reinforced concrete.)

The dimensions of the inhomogeneity is dependent on its shape. I start the calculation with spherical shape, where the radius of heterogeneity is $r = 10$ mm and I continue with

ellipsoids, where the major to minor semi-axes ratio is of $\frac{a_1}{a_2} = 1.25, 2.5, 10$, respectively (the lengths in y and z directions are set to be the same, therefore the minor axis can be indicated by a_2 instead of a_3).

Before considering inhomogeneities, I check the Matlab™ code whether it gives correct results. I set the material properties of both the heterogeneity and the matrix to be the same ($E = E_m, \nu = \nu_m$), and loaded this specimen by $\sigma_x = -1 \frac{\text{kN}}{\text{mm}^2}$. If the calculation is correct, the resulting stress field must be constant inside the material, since I made the originally heterogeneous material to be homogeneous. This verification was successful (Figure

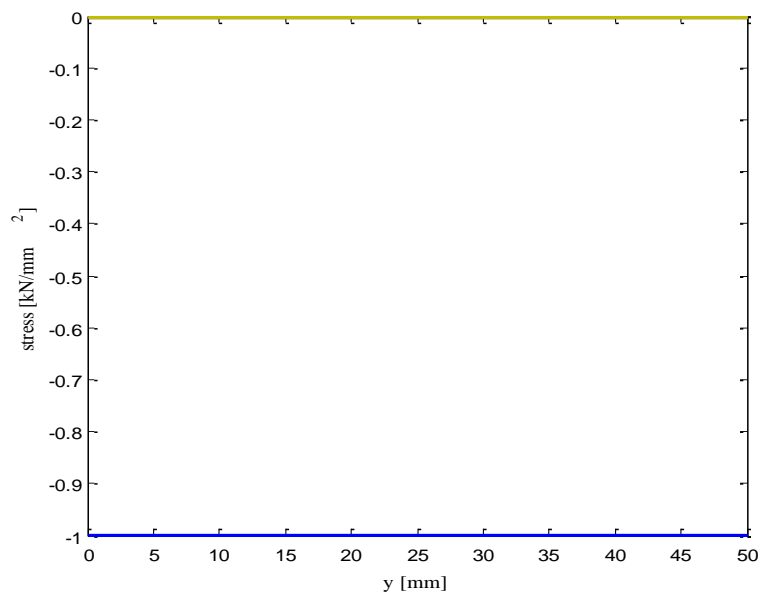


Figure 25 Verification of Matlab™ code by considering a homogeneous material under applied stress $\sigma_x = -1$

25). The vertical axis shows the value of the resulting stress field which is just the same as the applied stress, and the horizontal axis indicates the x axis of the three-dimensional space.

Figure 26 shows the stress field when the heterogeneity is of spherical shape. The horizontal axis shows the distance from the heterogeneity in millimetres, orthogonal to the distance of the applied stress, where the origin coincides with the centroid of the sphere. The vertical axis indicates the magnitude of the resulting stress field (dark blue: σ_x , light blue: σ_y and green: σ_z).

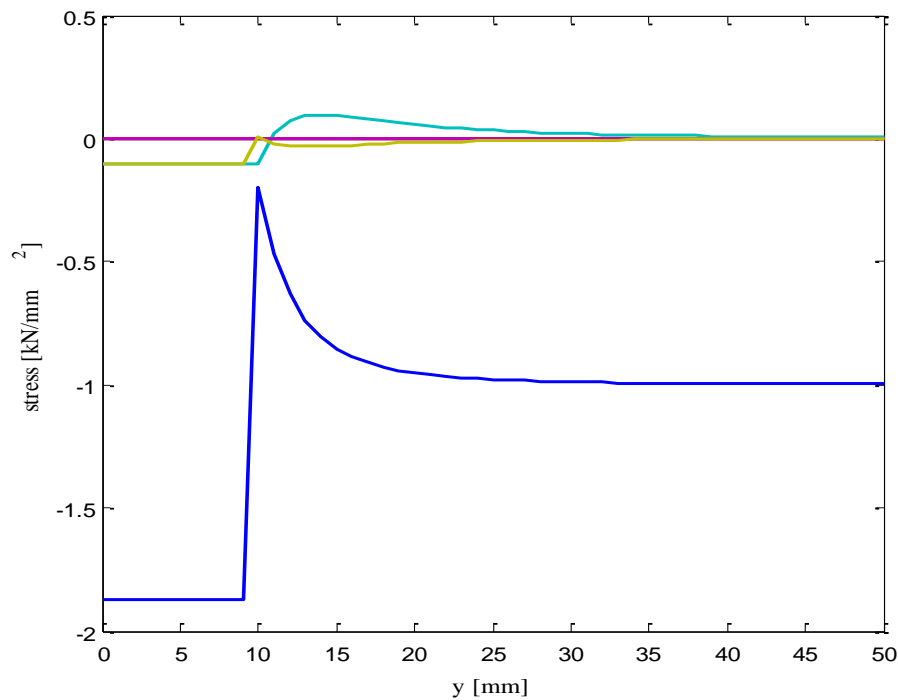


Figure 26 Resulting stress field (dark blue: σ_x , light blue: σ_y , green: σ_z) in case of spherical heterogeneity with $r = 10$ mm, under applied stress $\sigma_x = -1$

Due to the existence of the inhomogeneity, the applied stress σ_x (in infinity) almost doubles inside the inhomogeneity and at the interface of the inhomogeneity and the matrix material, a sudden jump appears. It is interesting that the stress field just outside the inhomogeneity falls to almost zero value. It is also visible that a constant applied stress in infinity causes constant stress field inside the heterogeneity. As for the normal stresses in the other two directions, inside the heterogeneity, σ_z has some constant nonzero value, but it decreases to zero in the matrix material quickly. The normal stress in y direction behaves similarly, except the fact that just outside the inhomogeneity, it changes its sign and becomes tensile stress which is quite undesirable in a lot of heterogeneous engineering materials, such as concrete or soil.

When varying the shape of the inhomogeneity to be $a_1 = 10$ mm and $a_2 = a_3 = 8$ mm, i.e. it is the case when the major-to-minor axis ratio equals 1.25, the resulting stress field becomes (Figure 27):

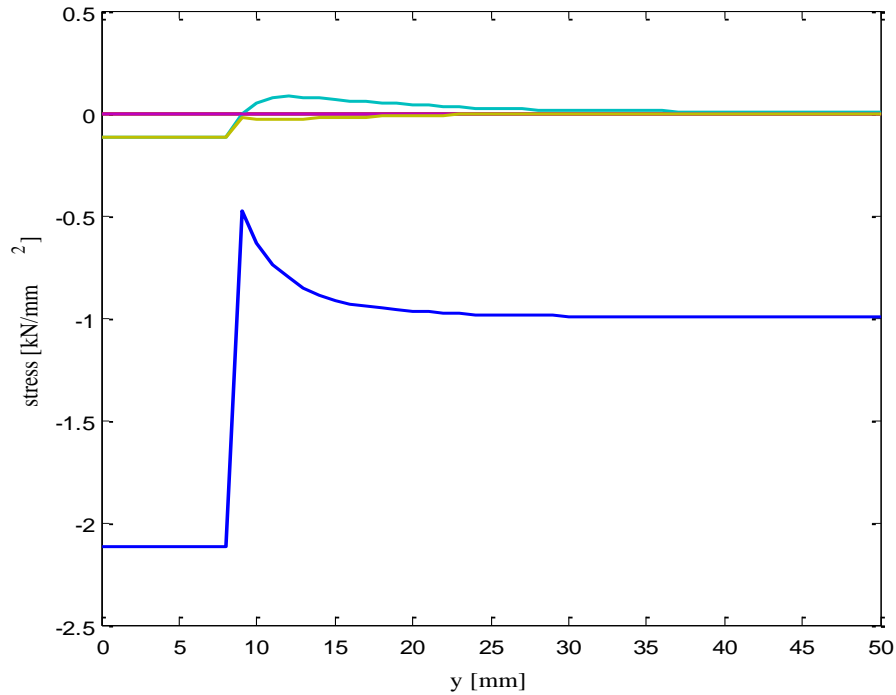


Figure 27 Resulting stress field (dark blue: σ_x , light blue: σ_y , green: σ_z) in case of ellipsoidal

heterogeneity with $\frac{a_1}{a_2} = 1.25$, under applied stress $\sigma_x = -1$

The same applied stress field causes 13% larger compressive stress σ_x inside the inhomogeneity when its size in cross directions y and z decreases to 80% of its original value. On the other hand, the stress jump at the interface halved due to this change of geometry. In the first case, the stresses just outside the heterogeneity were approximately -0.2 kN/mm^2 and inside the heterogeneity became -2 kN/mm^2 , which is ten times larger than at the exterior points. At the ellipsoidal one, this was only a fivefold increase. The σ_y and σ_z stress field has almost the same values than in case of a spherical heterogeneity.

Let us see what happens, when the major-to-minor axis ratio is increased again to be 2.5, 10 and the cross-directional semi-axes has the lengths of $a_2 = a_3 = 4 \text{ mm}$ and $a_2 = a_3 = 1 \text{ mm}$, respectively (Figure 28-Figure 29):

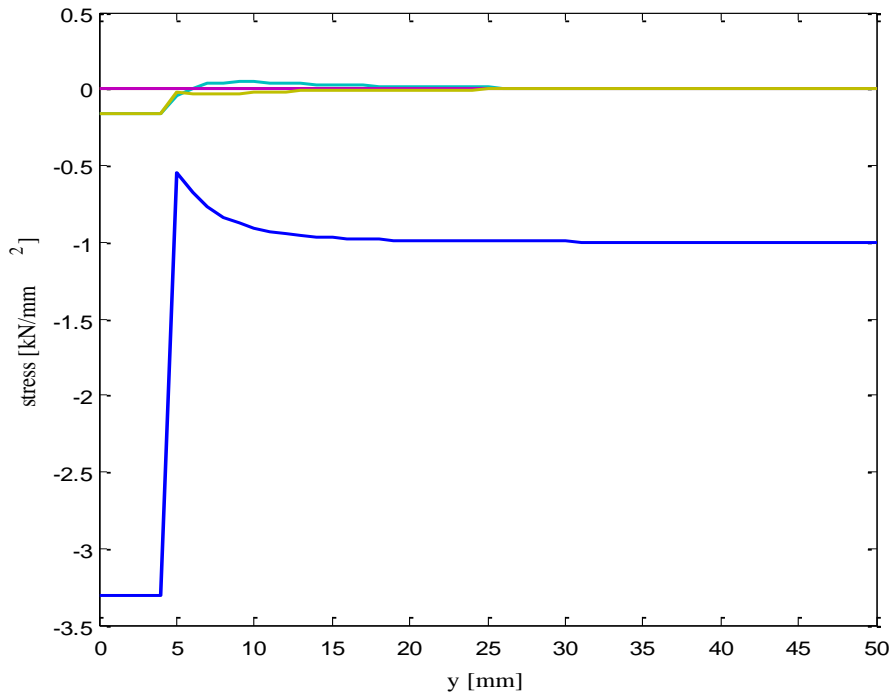


Figure 28 Resulting stress field (dark blue: σ_x , light blue: σ_y , green: σ_z) in case of ellipsoidal

heterogeneity with $\frac{a_1}{a_2} = 2.5$, under applied stress $\sigma_x = -1$

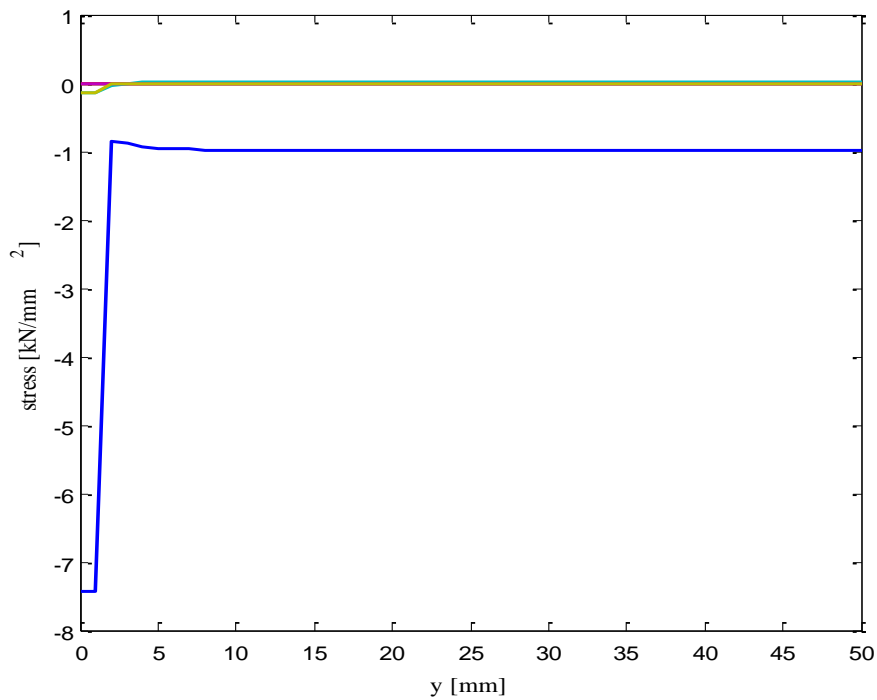


Figure 29 Resulting stress field (dark blue: σ_x , light blue: σ_y , green: σ_z) in case of ellipsoidal

heterogeneity with $\frac{a_1}{a_2} = 10$, under applied stress $\sigma_x = -1$

The tendency in having larger compressive stress σ_x inside the inclusion continued, and at the same time, the tensile stress σ_y tends to zero as the ratio of major to minor axes becomes larger. Obviously, the stresses outside the inhomogeneity fall back to their ‘undisturbed’ value faster as the ellipsoid gets flatter.

Now let us see what happens, when we consider the same major-to-minor axes ratios, but this time the applied stress will be $\sigma_y = -1 \frac{\text{kN}}{\text{mm}^2}$. Therefore, the resulting stress field is plotted against the distance measure from the centre of the ellipsoid in x direction:

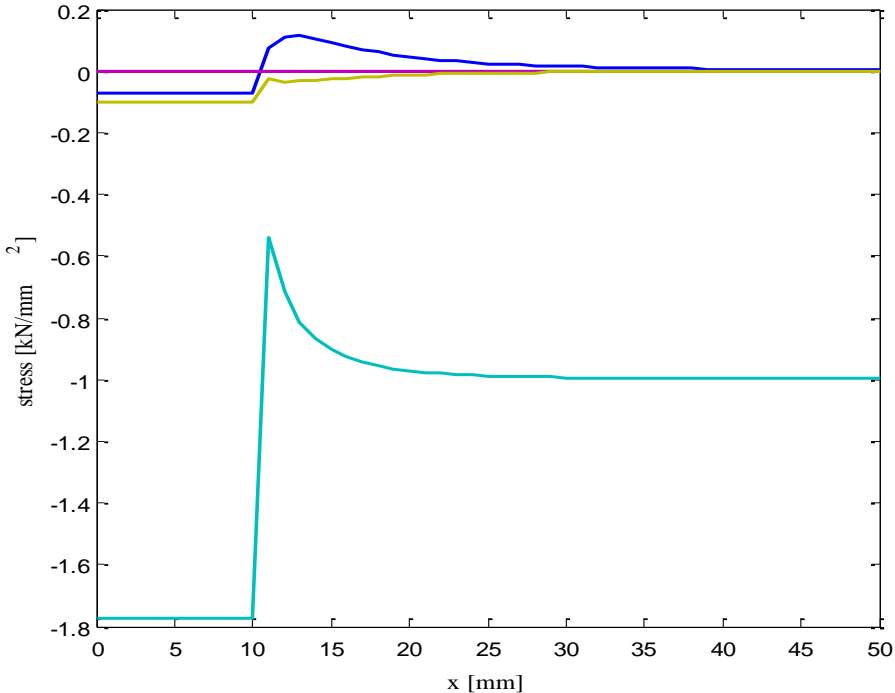


Figure 30 Resulting stress field (dark blue: σ_x , light blue: σ_y , green: σ_z) in case of ellipsoidal

heterogeneity with $\frac{a_1}{a_2} = 1.25$, under applied stress $\sigma_y = -1$

While in Figure 27-Figure 29, the ellipsoid became more and more elongated in the direction of the applied stress, show the resulted stress field in case of such major-to minor axes ratios when the ellipsoid is getting flatter in the direction of the applied loading. The constant (applied) compressive stress inside the inhomogeneity is smaller in case of flat ellipsoids, but the normal stress of the orthogonal direction changes into a relatively high value of tensile stress.

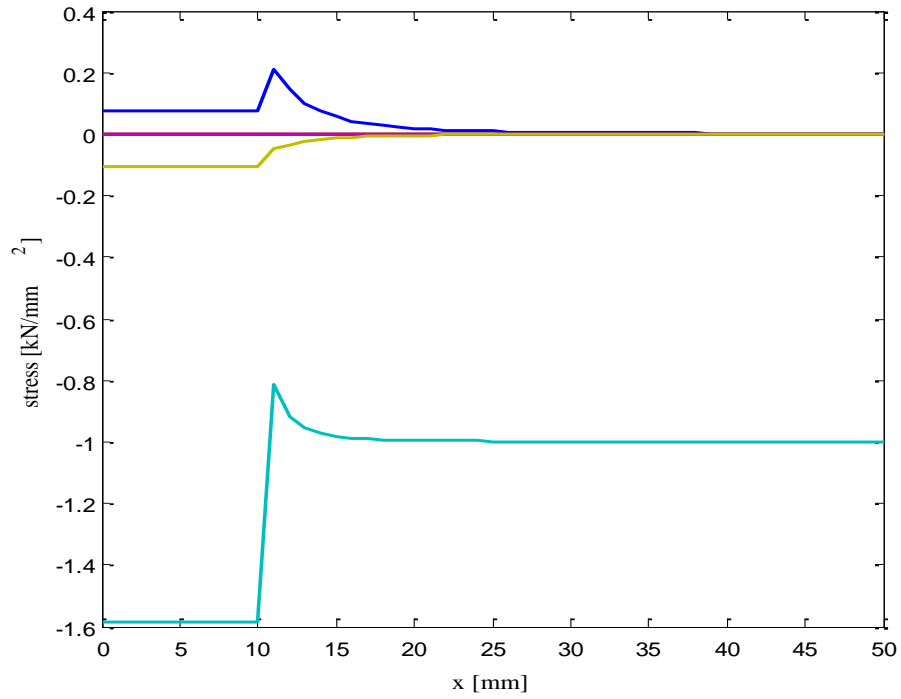


Figure 31 Resulting stress field (dark blue: σ_x , light blue: σ_y , green: σ_z) in case of ellipsoidal

heterogeneity with $\frac{a_1}{a_2} = 2.5$, under applied stress $\sigma_y = -1$

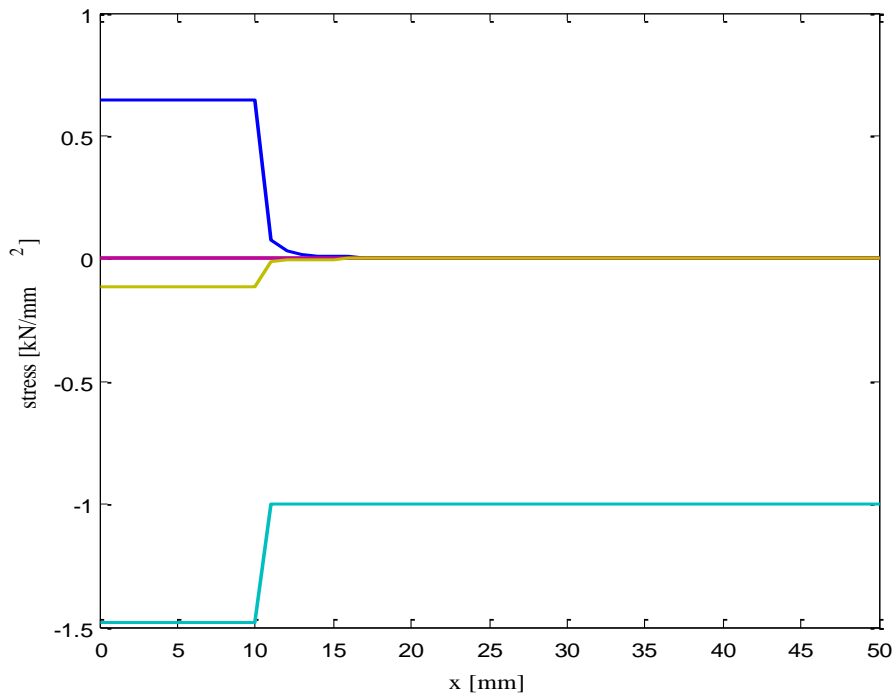


Figure 32 Resulting stress field (dark blue: σ_x , light blue: σ_y , green: σ_z) in case of ellipsoidal

heterogeneity with $\frac{a_1}{a_2} = 10$, under applied stress $\sigma_y = -1$

Considering the case when not only $\sigma_x = -1 \frac{\text{kN}}{\text{mm}^2}$, but $\sigma_y = -1 \frac{\text{kN}}{\text{mm}^2}$ are also applied in infinity, let us observe the changes in the resulting elastic field in case of heterogeneities of size $a_1 = a_2 = a_3 = 10 \text{ mm}$ and $a_1 = 10 \text{ mm}$, $a_2 = a_3 = 4 \text{ mm}$. The results of the spherical case (Figure 33):

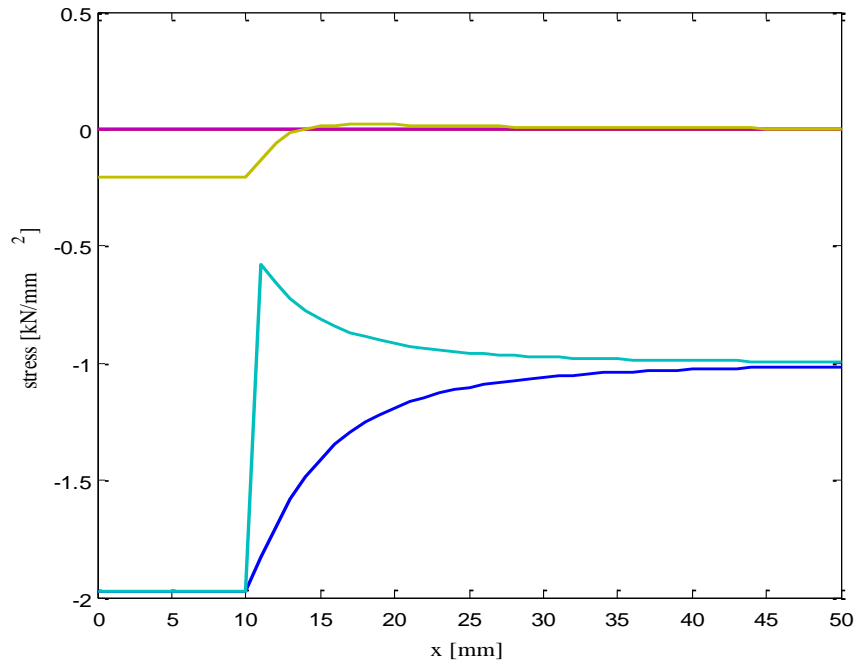


Figure 33 Resulting stress field (dark blue: σ_x , light blue: σ_y , green: σ_z) in case of spherical heterogeneity with $r = 10 \text{ mm}$, under applied stresses $\sigma_x = -1$ and $\sigma_y = -1$ in x direction

The stress field in y direction will be the same, except that the sudden jump at the matrix-inhomogeneity interface occurs in the σ_x stresses. The resulting stress field of a heterogeneous material with ellipsoidal inhomogeneity under hydrostatic pressure is depicted in Figure 34 and Figure 35. Due to the type of the applied loading, i.e. it is of the same magnitude in every direction, there is no significant tensile stress even in the out-of-plane direction. The normal stress in the direction belonging to the longer axis of the ellipsoid always bears higher values of compressive stress inside the heterogeneity. The applied stress observed in the direction orthogonal to it, shows a sudden jump at the interface of the heterogeneity and the matrix, but just outside the inhomogeneity, the absolute value of the resulting stresses are always smaller than that of the applied stress. The magnitude of the interfacial jump is dependent on the direction of the applied stress and the major-to-minor axes ratio. If we observe the direction where the size of the heterogeneity decreases (Figure 27-Figure 29), the magnitude of the jump increases greatly. On the other hand, when the size of the ellipsoid does not change in the observed direction orthogonal to the applied stress, while its shape becomes flatter, the jump in the resulting stress field becomes smaller (Figure 30-Figure 32).

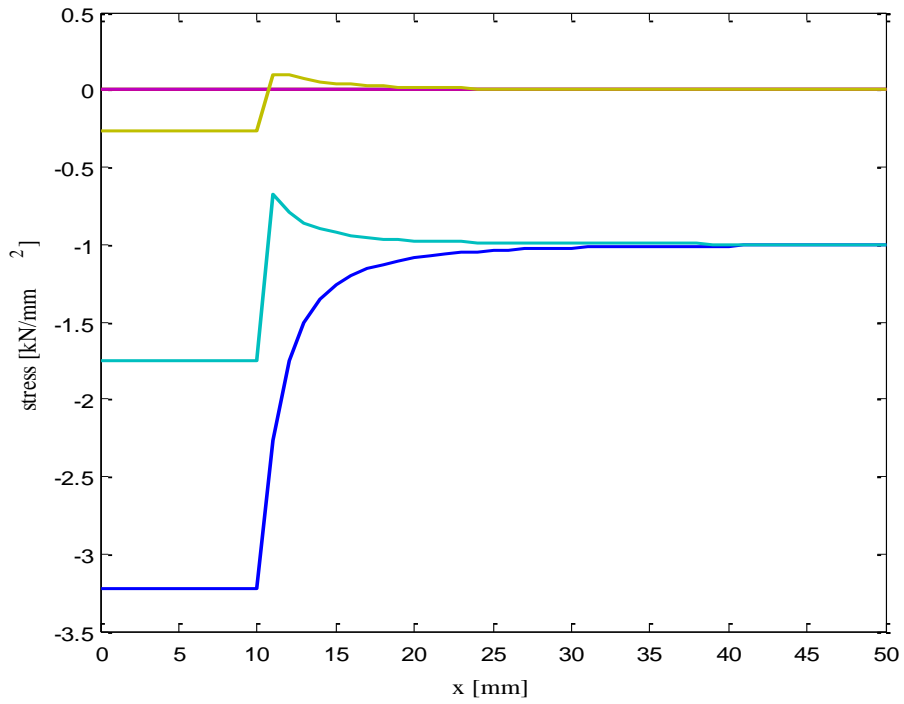


Figure 34 Resulting stress field (dark blue: σ_x , light blue: σ_y , green: σ_z) in case of ellipsoidal heterogeneity with $\frac{a_1}{a_2} = 2.5$, under applied stresses $\sigma_x = -1$ and $\sigma_y = -1$ in x direction

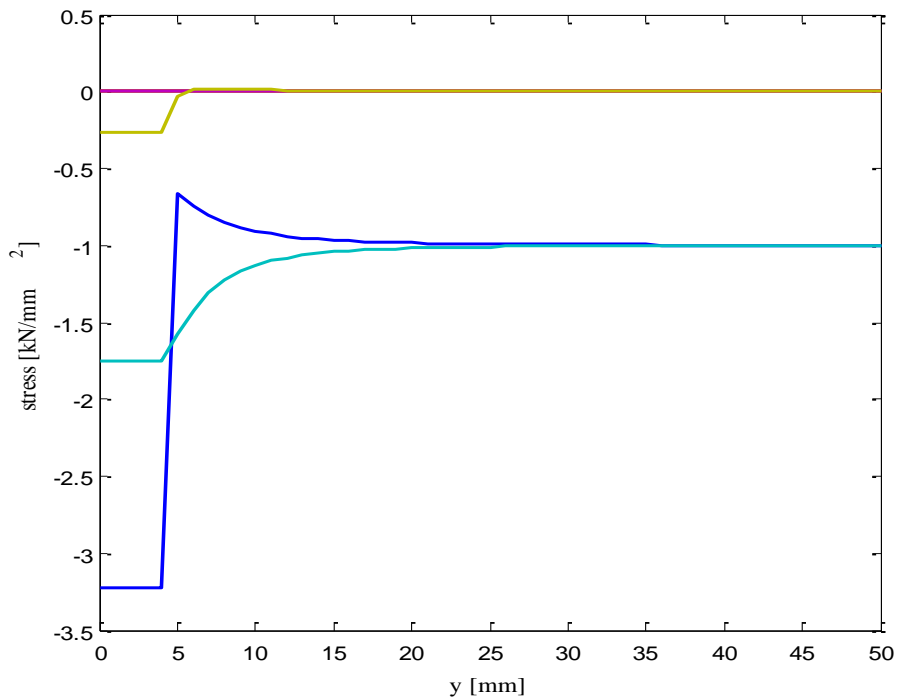


Figure 35 Resulting stress field (dark blue: σ_x , light blue: σ_y , green: σ_z) in case of ellipsoidal heterogeneity with $\frac{a_1}{a_2} = 2.5$, under applied stresses $\sigma_x = -1$ and $\sigma_y = -1$ in y direction

4.2 Numerical model

In order to verify the analytical solutions, I run some numerical analyses in finite element software Mechanical APDL 14.5 by Ansys™, where the inhomogeneity lies in xy plane, and has the same geometry as shown before, i.e. $a_1 = a_2 = 10$ mm and its variations as the major-to-minor axis varies as $\frac{a_1}{a_2} = 1.25, 2.5, 10$. The investigated distance from the centroid of the

initially examined sphere is also 50 mm, and due to the symmetry of the problem, I modelled only the half of the inhomogeneity in the infinite space. The material properties are the same as before: $E_c = 200$ GPa, $\nu_c = 0.3$ of the contaminants and $E_m = 20$ GPa, $\nu_m = 0.15$ of the matrix. I applied SHELL181, which is a four-node shell element with six degrees-of-freedom at every node (three translational and three rotational). The triangular version of this orogonally rectangular element is applied only as a filler element in mesh generation.

The verification of the numerical model occurred similarly to that of the analytical one, the material properties of the inhomogeneity are set to be the same as the properties of the matrix, hence the material is homogenous and an applied stress $\sigma_x = 1 \frac{\text{kN}}{\text{mm}^2}$ causes constant stress field inside the material (Figure 36):

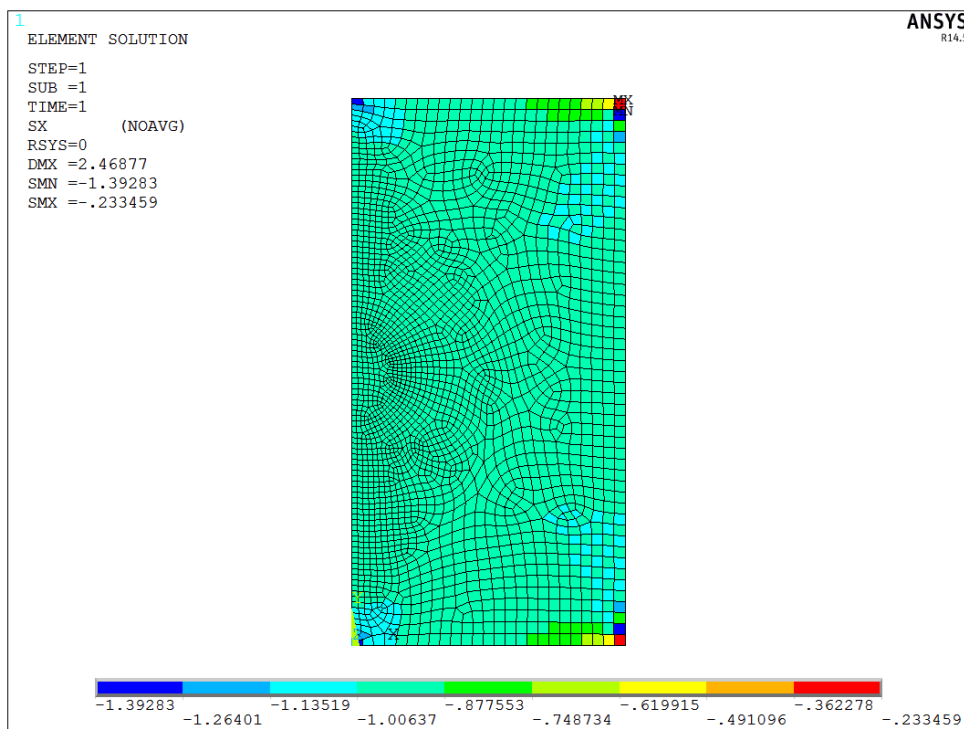


Figure 36 Verification of the numerical model

The stress field $\sigma_x ()$ and $\sigma_y ()$ of the heterogeneous material consisting spherical inhomogeneity when applying $\sigma_x = -1 \frac{\text{kN}}{\text{mm}^2}$ in infinity:

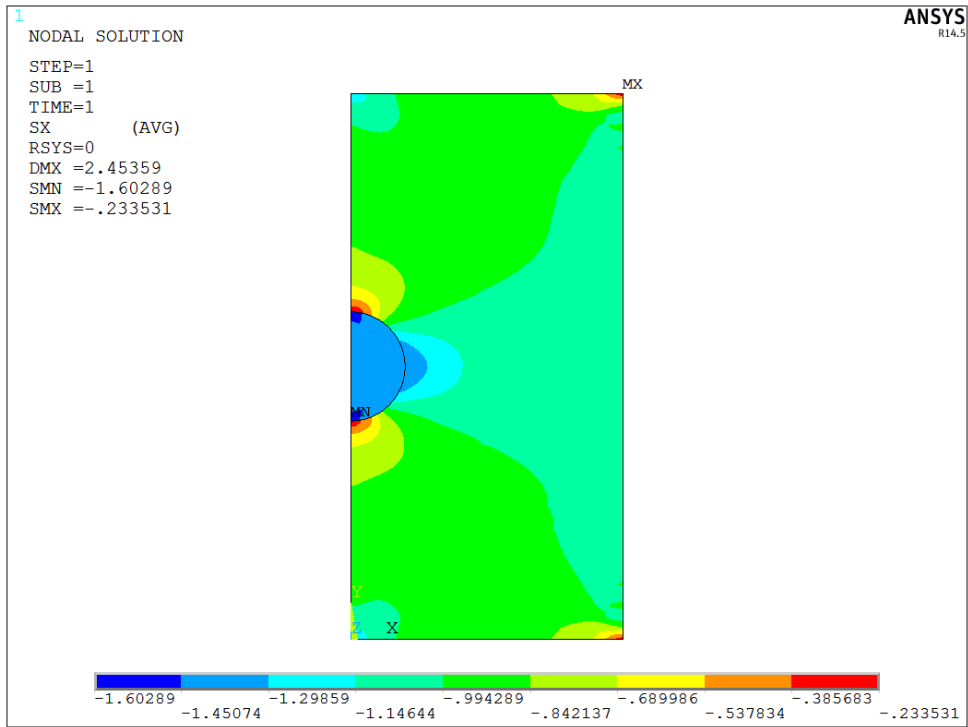


Figure 37 Resulting stress field σ_x in case of spherical heterogeneity with $r = 10$ mm , under applied stress $\sigma_x = -1$

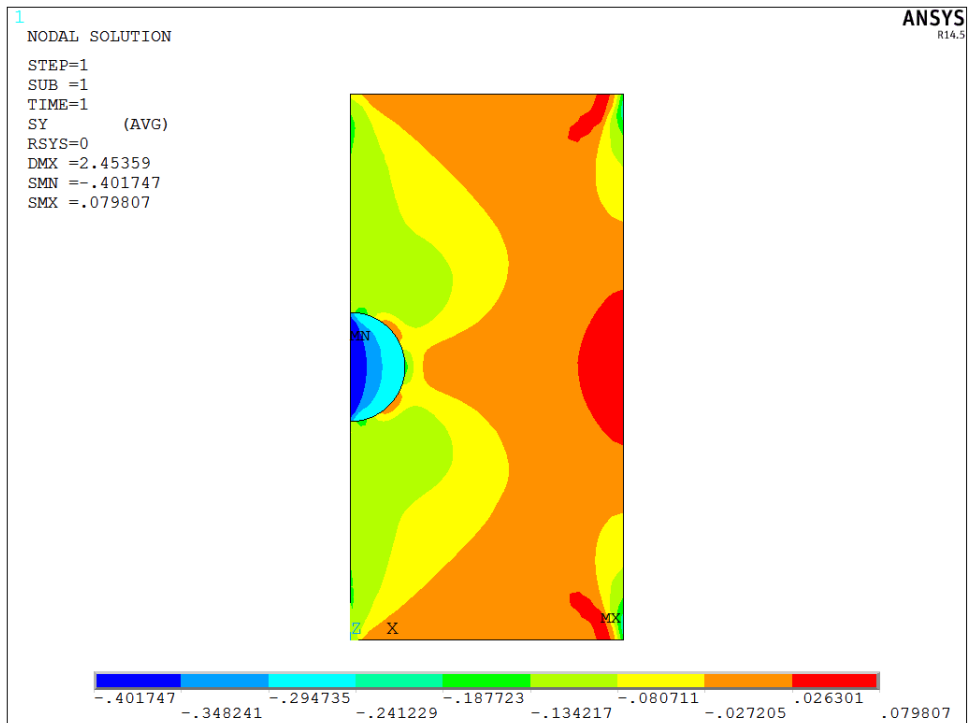


Figure 38 Resulting stress field σ_y in case of spherical heterogeneity with $r = 10$ mm , under applied stress $\sigma_x = -1$

Comparing Figure 37 to Figure 26, the compressive stress inside the inhomogeneity is approximately 17% smaller in absolute value at the numerical results, just inside the inhomogeneity, they become higher, then at the interface, the huge jump in the stress field can be observed here as well. Just outside the stress is about -0.2 kN/mm^2 , and the disturbed stress field is equilibrated in $\sim 22 \text{ mm}$ measured from the centre of the inhomogeneity in y direction (at the numerical result, it is the vertical axis), which is just the same as coming from the analytical solution. In Figure 38, the stress σ_y is -0.4 kN/mm^2 inside the inhomogeneity, and at the interface it changes to -0.13 kN/mm^2 , it does not change sign, there is no tensile stress in the $x = 0$ section under consideration.

Now let us examine the numerical results coming from a heterogeneous material consisting a strong, ellipsoidal shaped inhomogeneity with major-to-minor axes ratio $\frac{a_1}{a_2} = 10$, under applied stress $\sigma_x = -1 \frac{\text{kN}}{\text{mm}^2}$. The ellipsoid is elongated in x direction.

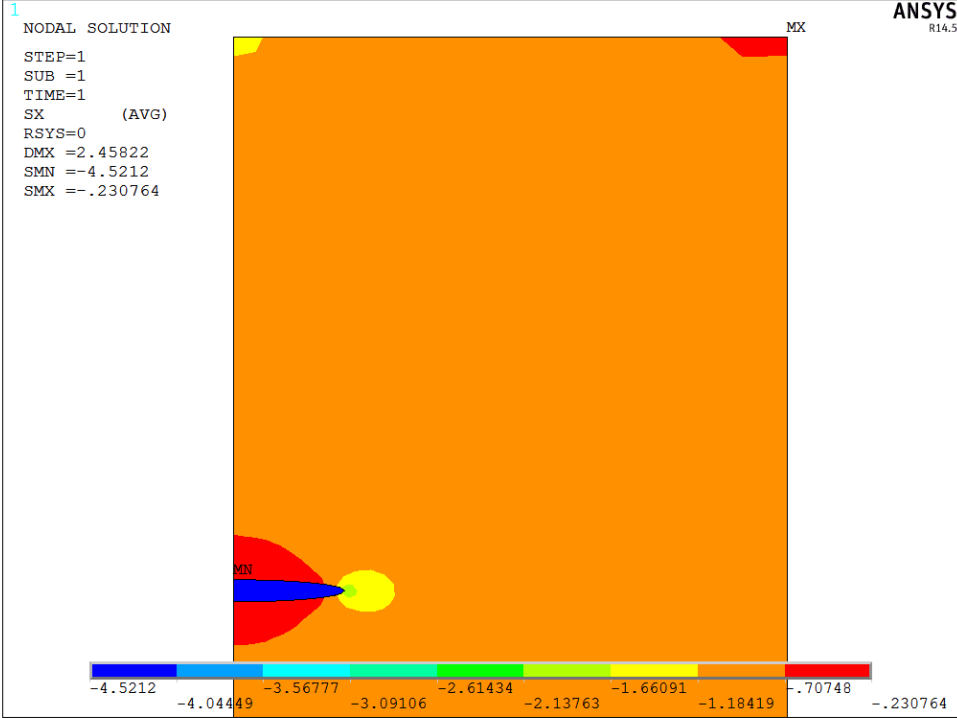


Figure 39 Resulting stress field σ_x in case of ellipsoidal heterogeneity with major-to-minor axes ratio

$$\frac{a_1}{a_2} = 10, \text{ under applied stress } \sigma_x = -1$$

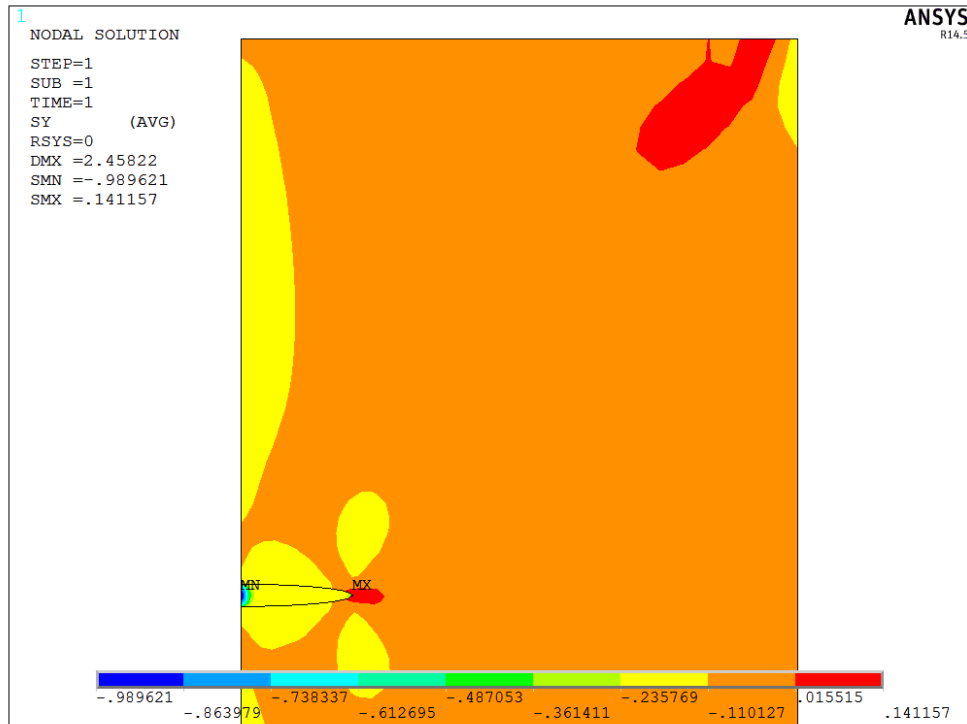


Figure 40 Resulting stress field σ_y in case of ellipsoidal heterogeneity with major-to-minor axes ratio

$$\frac{a_1}{a_2} = 10, \text{ under applied stress } \sigma_x = -1$$

Comparing Figure 39 to Figure 32, the numerical solution predicts 40% smaller compressive stress once again, and the disturbed stress field is balanced in ~ 7 mm from the centre of the ellipsoid, just like at the analytical solution. In Figure 40, σ_y is $(-0.9) \div (-0.3)$ kN/mm² inside the inhomogeneity and decreases to -0.1 kN/mm² at the exterior points. It is the same as the results coming from analytical methods. In x direction (horizontal axis), at the tip of the elongated inhomogeneity, σ_y tensile stresses appear, as one might expect.

The flat-shaped ellipsoidal inhomogeneity was examined such that the applied stress remained $\sigma_x = -1 \frac{\text{kN}}{\text{mm}^2}$, but this time the minor axis is parallel to the x axis. Let the major-to-minor

axes ratio be $\frac{a_1}{a_2} = 2.5$. In Figure 41, σ_x is -1.2 kN/mm² inside the heterogeneity, at the

interface it decreases to -0.8 kN/mm² and in 15 mm from the centre of the ellipsoid, it becomes -1 kN/mm², which is almost exactly the same as in Figure 31 at the analytical results.

In Figure 42, σ_y is -0.3 kN/mm² inside and -0.15 kN/mm² outside the inhomogeneity.

Comparing to the analytical results, there is some difference, that can be explained by the fact that the analytical solution applies a three-dimensional, meanwhile the numerical analysis applies only a two-dimensional model.

Comparing the analytical and numerical results in general, it is observed that the analytical solution yields surprisingly exact results, both regarding the values of the stresses and also the distance needed to equilibrate the disturbed elastic field.

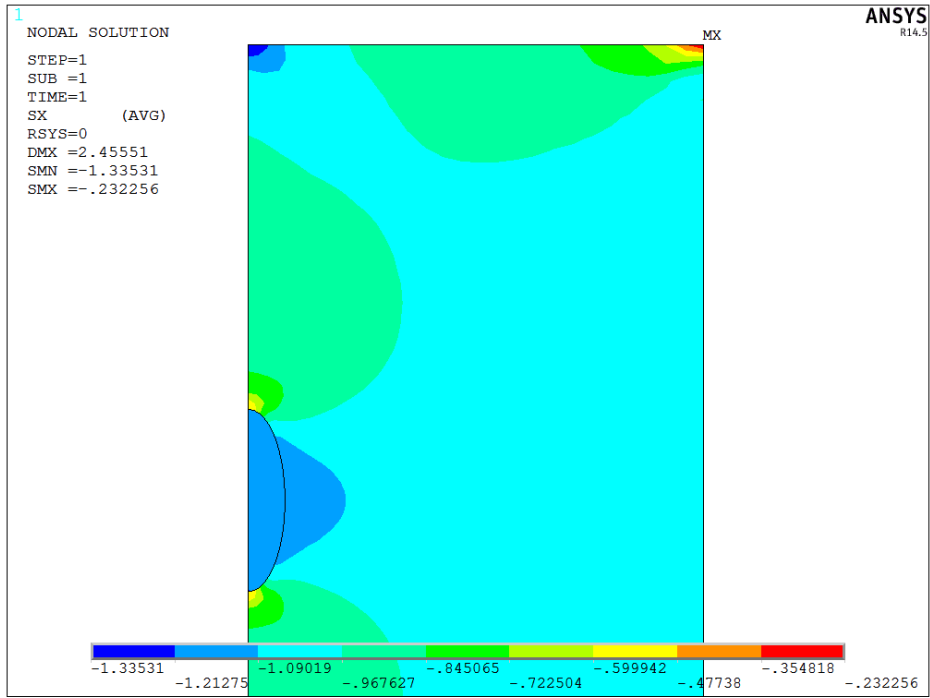


Figure 41 Resulting stress field σ_x in case of ellipsoidal heterogeneity with major-to-minor axes ratio

$$\frac{a_1}{a_2} = 2.5, \text{ under applied stress } \sigma_x = -1$$

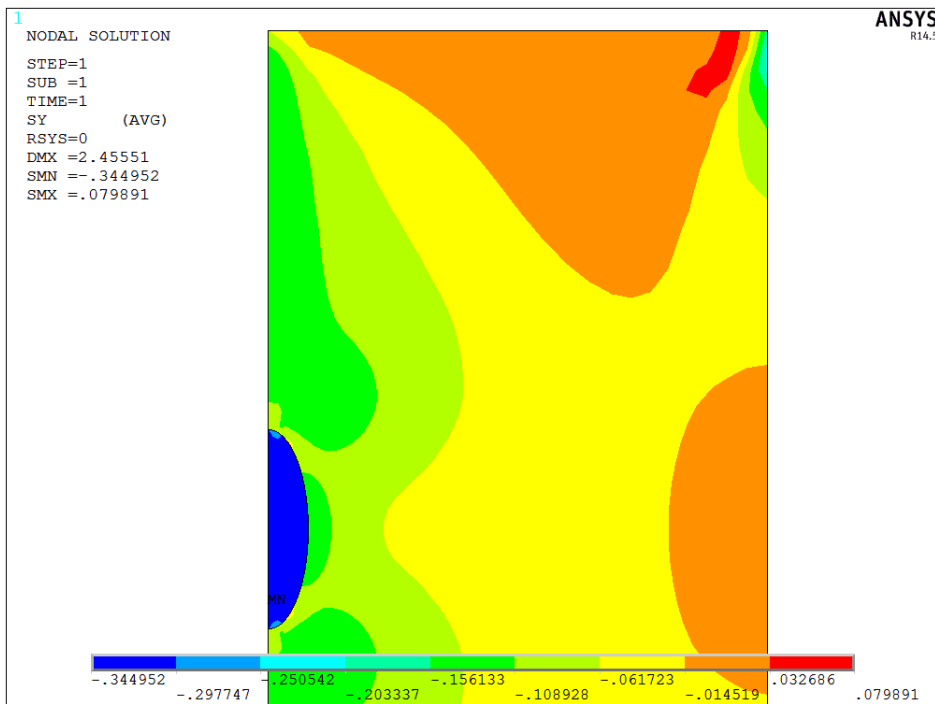


Figure 42 Resulting stress field σ_y in case of ellipsoidal heterogeneity with major-to-minor axes ratio

$$\frac{a_1}{a_2} = 2.5, \text{ under applied stress } \sigma_x = -1$$

4.3 Weak inhomogeneities

When modelling voids, one has to avoid the singularities caused by setting the values of material properties of voids to be zero by modelling them as very weak inhomogeneities. Let us define the Young's modulus and Poisson's ratio of the inhomogeneity (void) as $E_v = 0.01 \text{ GPa}$ and $\nu_v = 0.01$. The inhomogeneity is of ellipsoidal shape and its major-to-minor axes ratio is $\frac{a_1}{a_2} = 2.5$.

First, let us compare the analytical and numerical results when the heterogeneous material is loaded by a compressive stress of unit magnitude parallel to its major axis.

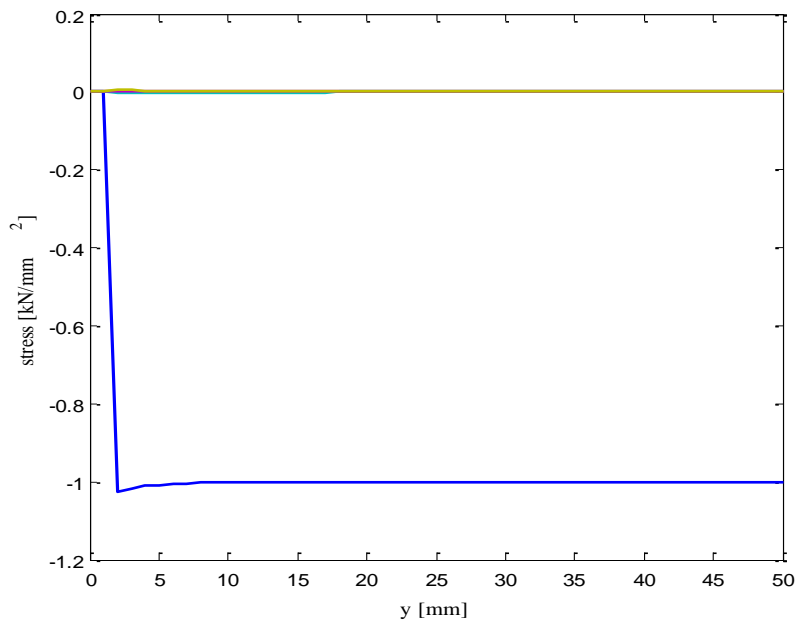


Figure 43 Analytical results of a heterogeneous material containing an elongated void

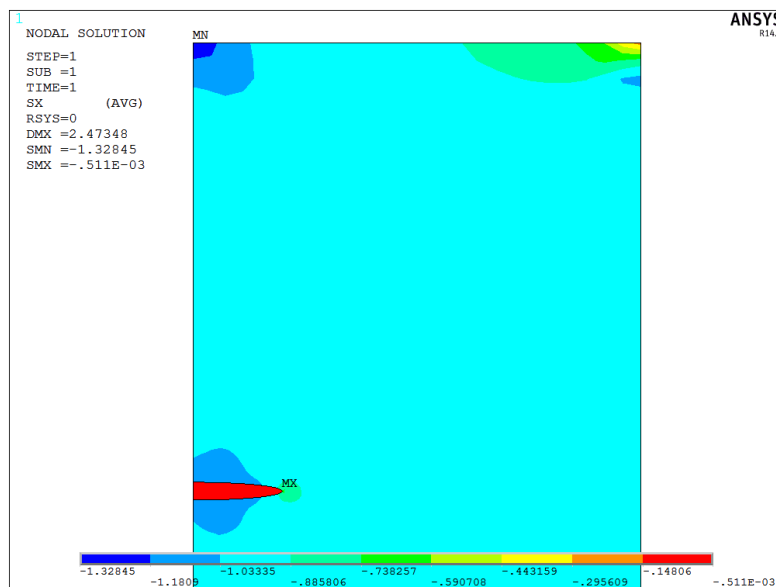


Figure 44 Numerical results of a heterogeneous material containing an elongated void

In Figure 43, the blue line shows that in the first 0.4 mm, that is inside the void, the applied stress becomes zero. At the interface it exceeds its applied value, but in 7 mm distance from the centre of the void, the disturbing effect of the void ceases. In Figure 44, the same results are obtained with the help of the finite element analysis, the only difference is that at the interface the stress reaches the magnitude of -1.2 kN/mm^2 .

When comparing the results of a flat ellipsoid, the difference is greater between the analytical (Figure 45) and numerical solutions (Figure 46). According to the analytical results, at the interface of the void and matrix, the stress in the direction of the applied stress is only -1.08 kN/mm^2 , while at the finite element analysis, it becomes -3 kN/mm^2 and 15 mm from the centre of the void the value of this stress is still -1.5 kN/mm^2 . The analytical solution cannot predict the stress field at the tip of the inhomogeneity as much as the numerical analysis.

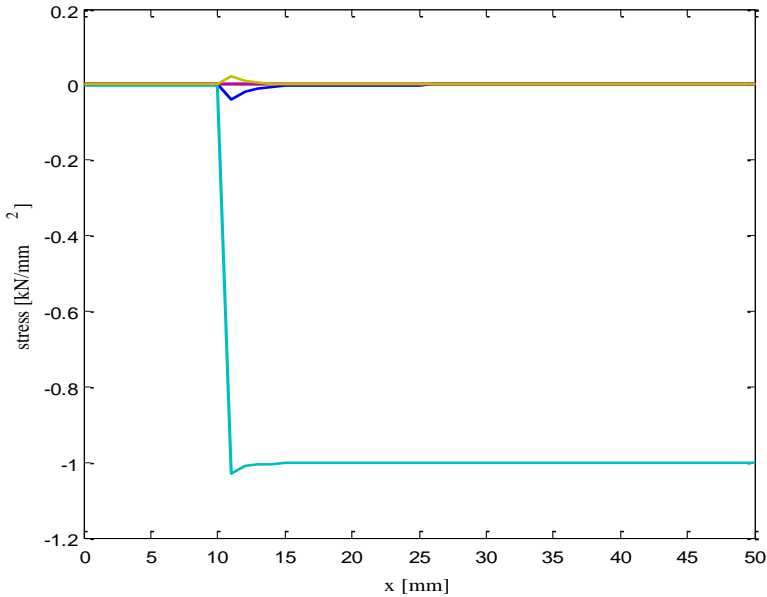


Figure 45 Analytical results of a heterogeneous material containing a flat void

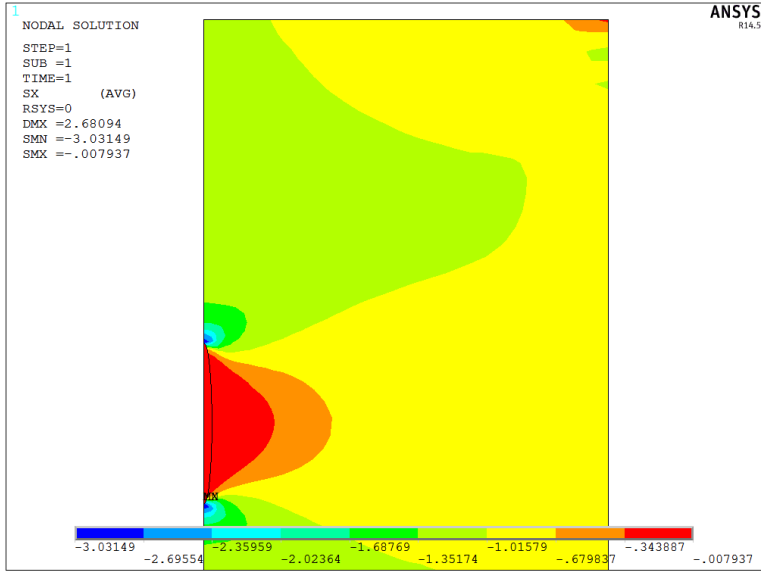


Figure 46 Numerical results of a heterogeneous material containing a flat void

5 The effect of mesolevel inhomogeneities on macrolevel material properties

5.1 Definitions of effective moduli of heterogeneous materials

Heterogeneous materials generally consist of several different constituents or phases, and each of them has different material properties. In engineering problems, when dealing with heterogeneous materials at the length scale of interest, we cannot deal with all the properties of the different materials, we would like to define an overall or so-called **effective property** of the whole material, that describes its behavior against mechanical effects.

Heterogeneous materials can be classified into two groups: materials with **periodic** (Figure 47) and **nonperiodic** (Figure 48) microstructures. In this thesis, I will only deal with the latter one, which includes most of the fiber and particulate reinforced materials. The materials with periodic microstructures cannot be treated as random media, thereby the different constituents' interactions need to be investigated more seriously.

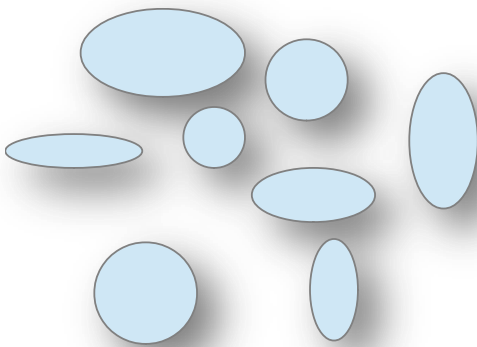


Figure 48 Nonperiodic microstructure

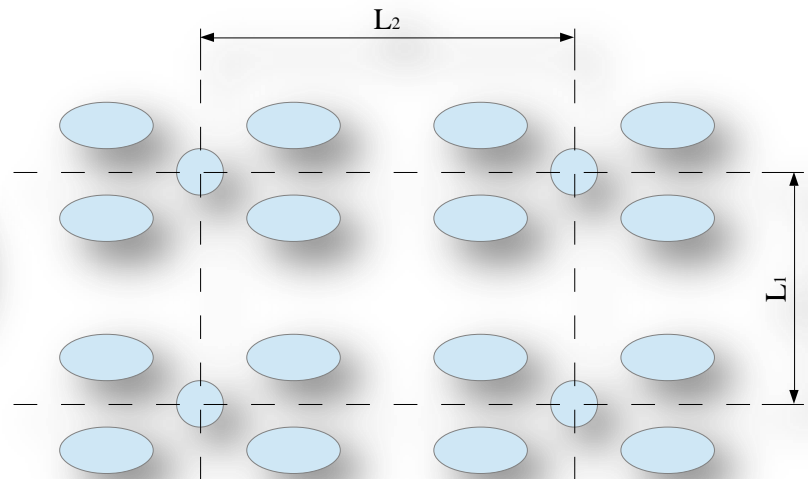


Figure 47 Periodic microstructure

All the materials are heterogeneous by nature. In engineering problems, we need to define a **length scale** at which the properties of the material are relevant. At this specific length scale, one can identify different constituents, that might seem homogeneous at a larger length scale, but would be heterogeneous itself at a smaller length scale.

In case of heterogeneous materials we can speak of overall properties, which is the properties differing from point-to-point averaged over a certain volume of the material. We say a material is macroscopically homogeneous, when for its overall properties, the average taken over any arbitrary volume element comparable with the relevant length scale is the same as the heterogeneous material sample under consideration.

When defining the *microscale* length d , which corresponds to the smallest constituent whose material properties have direct first-order effects on the macroscopic overall properties of the heterogeneous material, an optimum should be reached, by taking into consideration the

balance between the exact definition of what has first-order effects on the overall properties and the simplicity of the resulting model. The *macroscale* length D should be large enough, that the difference from point-to-point of the elastic field on microlevel influences the overall properties only through its average value. It must be true conversely, that the fluctuations of the elastic field should not be significant on the microscale, the macro-fields are locally uniform. In general, to satisfy these conditions, the microlevel must be orders of magnitude smaller than the macrolevel: $d / D \ll 1$.

5.1.1 Representative volume element

When a macroscopically heterogeneous material can be described by its microscopic length parameter d and macroscopic length parameter D (Figure 49) such that $d / D \ll 1$, then the heterogeneous material is said to be microscopically homogeneous at the macroscopic length scale D . A volume element of characteristic length D is called representative volume element (RVE). The overall properties of each RVE of a material are the same and represent the overall properties of the heterogeneous material itself.

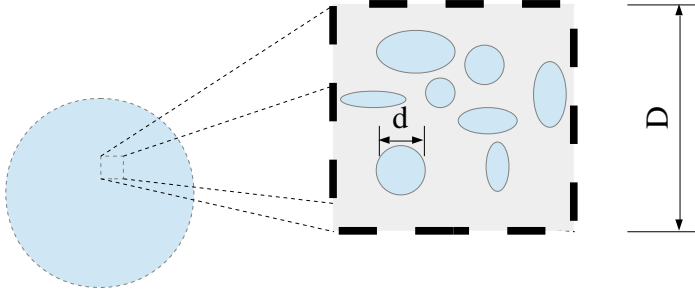


Figure 49 Definition of microscopic (d) and macroscopic (D) length parameter

5.1.2 Random media

Most of the engineering materials are of quite complex and random nature. It would be impossible or at least impractical to know every detail of its microstructure. We are interested in the **average properties** of the material, which is usually determined stochastically of a representative volume element. We distinguish two kinds of averages: the *ensemble average* and the volume or *spatial average*.

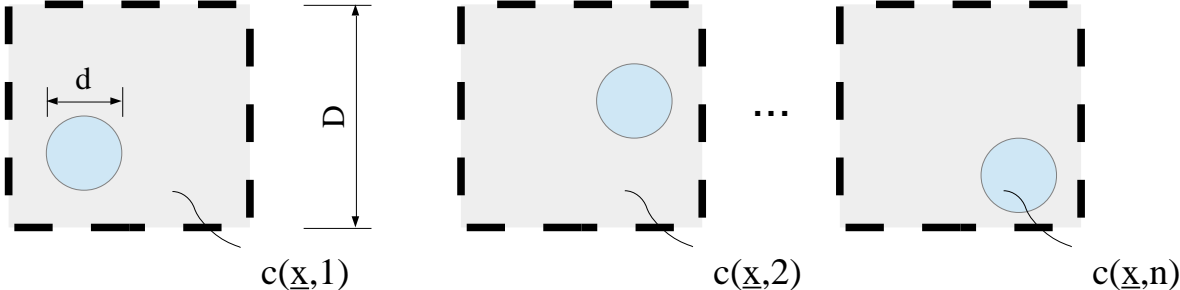


Figure 50 Inhomogeneity content at fixed positions in different samples

Consider N pieces of samples R , assuming that they were made under same processing conditions. The block dimension is D for every R and the size of an inhomogeneity d is such that $d / D \ll 1$, thus the macroscopically heterogeneous material is microscopically

homogeneous. Let us denote the volume fraction of inhomogeneities in each sample by c . Due to the different distribution of the inhomogeneities in the samples, when we examine a small volume at the same location \underline{x} in the α -th sample, the inhomogeneity content $c(\underline{x}, \alpha)$ will not be the same in all the specimens, the average will depend on N (Figure 50):

$$(5.1) \quad \langle c(\underline{x}) \rangle = \frac{1}{N} \sum_{\alpha=1}^N c(\underline{x}, \alpha).$$

In the limit case $N \rightarrow \infty$, the summation can be replaced by an integral over the sample space R , thus the average will be independent of the number of samples:

$$(5.2) \quad \langle c(\underline{x}) \rangle = \lim_{N \rightarrow \infty} \frac{1}{N} \sum_{\alpha=1}^N c(\underline{x}, \alpha) = \int_R c(\underline{x}, \alpha) d\alpha,$$

where $\langle c(\underline{x}) \rangle$ ⁶ indicates the *ensemble average*.

In the following, let us consider a sample from the R -space with a total volume of V . By dividing this specimen into M subdomains, we denote the volume of the i -th subdomain by V_i , where $\sum_{i=1}^M V_i = V$. In each subdomain the inhomogeneity content can be calculated in a particular representative point \underline{x}_i , for example in the centroid of the α -th subdomain: $c(\underline{x}_i, \alpha)$. The average volume fraction of a particular sample depends on M :

$$(5.3) \quad \overline{c(\alpha)} = \frac{1}{V} \sum_{i=1}^M c(\underline{x}_i, \alpha) V_i.$$

In the limit case $M \rightarrow \infty$, the summation can be replaced by an integral over the total volume V , thus the average will not depend on the number of subdomains any more:

$$(5.4) \quad \overline{c(\alpha)} = \lim_{M \rightarrow \infty} \frac{1}{V} \sum_{i=1}^M c(\underline{x}_i, \alpha) V_i = \frac{1}{V} \int_V c(\underline{x}) dV,$$

where $\overline{c(\alpha)}$ ⁷ denotes the *volume average*.

Please note, that the ensemble average gives the mean value of the volume fraction among all the samples in the sample space, while the spatial average is carried out over one specific sample in the sample space. The volume fraction can be regarded as a *random function* of both the sample α and the position \underline{x} that is measured. According to the ergodic⁸ hypothesis the inhomogeneity distribution can be such that these two averages give the same value:

$$(5.5) \quad \langle c(\underline{x}) \rangle = \overline{c(\alpha)},$$

⁶ The mathematical symbol $\langle \rangle$ in statistics represents the average $\langle S \rangle$ of all the elements of a set S .

⁷ In statistics, the overbar denotes the mean value \bar{x} of a set consisting of x_i , $i = 1, 2, \dots, N$.

⁸ Ergodic theory is a branch of mathematics that studies dynamical systems with an invariant measure and related problems. The development of ergodic theory was necessitated by problems of statistical physics.

$$(5.6) \quad \int_R c(\underline{x}, \alpha) d\alpha = \frac{1}{V} \int_V c(\underline{x}, \alpha) dV(\underline{x}) .$$

Generalizing the ergodic hypothesis to the microstructure features in heterogeneous materials, we should slightly modify the above expressions. Assuming there is a probability distribution function $p(\alpha)$ defined over R which satisfies

$$(5.7) \quad \int_R p(\alpha) d\alpha = 1 .$$

Suppose there are N different types of inhomogeneities or phases in each member of the group, where the r -th inhomogeneity has the volume of $V_r(\alpha)$, $r = 1, 2, \dots, N$. To describe the spatial distribution of the inhomogeneities, it is convenient to introduce a characteristic function that takes the value of 1 if \underline{x} is inside $V_r(\alpha)$ and zero otherwise:

$$(5.8) \quad f_r(\underline{x}, \alpha) = \begin{cases} 1 & \text{if } \underline{x} \in V_r(\alpha) \\ 0 & \text{if } \underline{x} \notin V_r(\alpha) \end{cases} .$$

In a specific sample,– at position \underline{x} ,– there can only be one kind of material phase, but there must be a phase, thus the characteristic function has the property

$$(5.9) \quad \sum_{r=1}^N f_r(\underline{x}, \alpha) = 1 .$$

The ensemble average of the characteristic function defines the probability $P_r(\underline{x})$ of finding phase r at position \underline{x} :

$$(5.10) \quad P_r(\underline{x}) = \langle f_r(\underline{x}, \alpha) \rangle = \int_R f_r(\underline{x}, \alpha) p(\alpha) d\alpha .$$

Similarly, finding phase r at \underline{x} and phase s at \underline{x}' simultaneously has the probability of $P_{rs}(\underline{x}, \underline{x}')$:

$$(5.11) \quad P_{rs}(\underline{x}, \underline{x}') = \langle f_r(\underline{x}, \alpha) f_s(\underline{x}', \alpha) \rangle = \int_R f_r(\underline{x}, \alpha) f_s(\underline{x}', \alpha) p(\alpha) d\alpha .$$

The functions $P_r(\underline{x})$ and $P_{rs}(\underline{x}, \underline{x}')$ are the *one-* and *two-point correlation functions* of $f_r(\underline{x}, \alpha)$, respectively. A heterogeneous medium is said to be **statistically homogeneous**, if its correlation functions are **translation invariant**. In this case the one-point correlation function $P_r(\underline{x})$ is a constant, thus the inhomogeneities are uniformly distributed in each sample, and the two-point correlation function will have the property $P_{rs}(\underline{x}, \underline{x}') = P_{rs}(\underline{x} - \underline{x}')$, which means $P_{rs}(\underline{x}, \underline{x}')$ will only depend on the distance between \underline{x} and \underline{x}' , regardless the exact location of these points. If the characteristic function of a heterogeneous material satisfies the ergodic hypothesis, the material is statistically uniform.

The microstructure or the distribution of the inhomogeneities of a heterogeneous material can be characterized by the correlation functions $P_r(\underline{x})$ and $P_{rs}(\underline{x}, \underline{x}')$. The spatial average gives the volume fraction c_r of the r -th phase:

$$(5.12) \quad \overline{f_r(\underline{x}, \alpha)} = \frac{1}{V} \int_V f_r(\underline{x}, \alpha) dV(\underline{x}) = \frac{V_r}{V} \equiv c_r.$$

The ergodic hypothesis states

$$(5.13) \quad P_r(\underline{x}) = \langle f_r(\underline{x}, \alpha) \rangle = \overline{f_r(\underline{x}, \alpha)} = c_r.$$

The volume average of the two-point correlation:

$$(5.14) \quad \overline{f_r(\underline{x}, \alpha) f_s(\underline{x}', \alpha)} = \frac{1}{V} \int_V f_r(\underline{x}, \alpha) f_s(\underline{x}', \alpha) dV(\underline{x}) = \frac{1}{V} \int_{V_r} f_s(\underline{x} - (\underline{x} - \underline{x}'), \alpha) dV(\underline{x}) = g_{rs}(\underline{x} - \underline{x}'),$$

therefore, according to the ergodic hypothesis

$$(5.15) \quad P_{rs}(\underline{x}, \underline{x}') = \langle f_r(\underline{x}, \alpha) f_s(\underline{x}', \alpha) \rangle = \overline{f_r(\underline{x}, \alpha) f_s(\underline{x}', \alpha)} = g_{rs}(\underline{x} - \underline{x}').$$

Applying the above introduced characteristics, we can say that the *representative volume element* must be defined so that it includes a very large number of inhomogeneities and in the meanwhile be *statistically homogeneous* and representative of the local continuum properties, so that the averaging schemes over this domain determine the overall mechanical properties of the heterogeneous material.

5.1.3 Macroscopic averages

Consider a statistically homogeneous material with domain D , where the average stresses and strains over D is defined as

$$(5.16) \quad \bar{\sigma}_{ij} = \frac{1}{D} \int_D \sigma_{ij} dV,$$

$$(5.17) \quad \bar{\varepsilon}_{ij} = \frac{1}{D} \int_D \varepsilon_{ij} dV,$$

respectively. Due to the statistically homogeneous behavior, the volume and the ensemble averages are the same. Note that domain D does not need to be a single domain and the volume of domain D is denoted by V .

Let us consider a given constant stress tensor σ_{ij}^0 with the traction boundary condition

$$(5.18) \quad \sigma_{ij} n_j \Big|_S = p_j^0 = \sigma_{ij}^0 n_j$$

prescribed on the entire boundary S of the domain D with outward normal vector n_j . The average stress on D is given by

$$(5.19) \quad \bar{\sigma}_{ij} = \sigma_{ij}^0,$$

this is called the *average-stress theorem*. According to this theorem, when a body is subjected to traction boundary condition (5.18) with σ_{ij}^0 being constant, the resulting stress averaged over the entire body is the same as σ_{ij}^0 , regardless the complexity of the stress field within the domain. Thus, the traction boundary condition can be written as

$$(5.20) \quad \sigma_{ij} n_j \Big|_S = \bar{\sigma}_{ij} n_j,$$

where $\bar{\sigma}_{ij}$ is the average stress tensor in the body enclosed by S .

Similarly, considering a given constant strain tensor ε_{ij}^0 with displacement boundary condition

$$(5.21) \quad u_i \Big|_S = \varepsilon_{ij}^0 x_j$$

prescribed on the entire boundary S of the domain D . The average strain on D is given by

$$(5.22) \quad \bar{\varepsilon}_{ij} = \varepsilon_{ij}^0,$$

this is called the *average-strain theorem*. According to this theorem, when a body is subjected to displacement boundary condition (5.21) with ε_{ij}^0 being constant, the resulting strain averaged over the entire body is the same as ε_{ij}^0 , regardless the complexity of the strain field within the domain. Thus, the displacement boundary condition can be written as

$$(5.23) \quad u_i \Big|_S = \bar{\varepsilon}_{ij} x_j,$$

where $\bar{\varepsilon}_{ij}$ is the average strain tensor in the body enclosed by S .

5.1.4 Hill's lemma

Consider a representative volume element with volume V and boundary S with prescribed displacement or traction boundary condition. For any stress and strain fields σ_{ij} and ε_{ij} at a given point in the RVE the following statement always holds

$$(5.24) \quad \overline{\sigma_{ij} \varepsilon_{ij}} - \bar{\sigma}_{ij} \bar{\varepsilon}_{ij} = \frac{1}{D} \int_S (u_i - x_j \bar{\varepsilon}_{ij}) (\sigma_{ik} n_k - \bar{\sigma}_{ik} n_k) dS,$$

where

$$(5.25) \quad \overline{\sigma_{ij} \varepsilon_{ij}} = \frac{1}{V} \int_V \sigma_{ij} \varepsilon_{ij} dV.$$

Equation (5.24) is **Hill's lemma**. A corollary of Hill's lemma states

$$(5.26) \quad \overline{\sigma_{ij} \varepsilon_{ij}} = \bar{\varepsilon}_{ij} \bar{\sigma}_{ij},$$

which is also known as *Hill's macrohomogeneity condition* or Mandel-Hill condition. It states that the twice of the value of the volume averaged strain energy density of a heterogeneous material can be obtained from the product of the volume averages of the strain field and stress field of the material, respectively.

5.1.5 Definitions of effective moduli of heterogeneous media

Assuming that a statistically homogeneous heterogeneous medium can be represented by an RVE consisting of N different phases dispersed throughout the RVE as inhomogeneities, with the size of an inhomogeneity being much smaller than the size of the RVE. Let us suppose that the interfaces between the distinct phases are perfectly bonded.

Note that heterogeneous materials with distinct matrix phase are called *composite materials*, while for example a polycrystalline material can be modelled as a *heterogeneous material* with infinitely many different phases without any particular matrix phase in which the inhomogeneities are embedded.

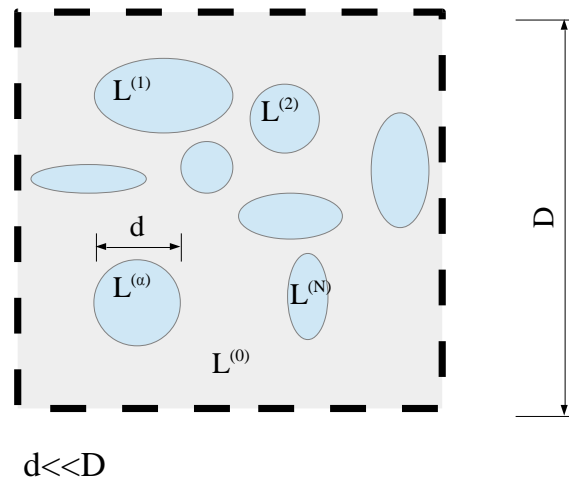


Figure 51 Stiffness tensors of the inhomogeneities and of the matrix in a heterogeneous material

Consider a heterogeneous body D bounded by surface S . The inhomogeneities are randomly oriented and shaped embedded in a matrix material with material stiffness tensor $\underline{\underline{L}}_0$ ⁹. The stiffness tensors of the inhomogeneities are denoted by $\underline{\underline{L}}_r$, $r = 1, 2, \dots, N$, (Figure 51). The *effective modulus* or stiffness tensor $\bar{\underline{\underline{L}}}$ of a heterogeneous material is defined by the relation

$$(5.27) \quad \bar{\underline{\underline{\sigma}}} = \bar{\underline{\underline{L}}} \bar{\underline{\underline{\varepsilon}}},$$

⁹ Please note that the material stiffness tensor is a fourth-order tensor, which can be converted to a 6-by-6 matrix due to the minor symmetry of the tensor: $L_{ijkl} = L_{ijlk} = L_{jikl} = L_{jilk}$. This 6-by-6 matrix can be related to the symmetric stress and strain tensors, if the stresses and strains are written in Voigt notation. In the previous chapters, the elastic modulus was indicated by C_{ijkl} , however, regarding the homogenization methods, I incorporated a distinct notation L_{ijkl} also used in the literature.

where $\bar{\underline{\sigma}}$ and $\bar{\underline{\varepsilon}}$ are the average stress and strain tensors of the heterogeneous body in Voigt form, respectively. The effective material *compliance tensor* $\bar{\underline{\underline{M}}}$ ¹⁰ of a heterogeneous material is defined similarly:

$$(5.28) \quad \bar{\underline{\varepsilon}} = \bar{\underline{\underline{M}}} \bar{\underline{\sigma}}.$$

The effective stiffness and compliance tensors must satisfy the condition

$$(5.29) \quad \bar{\underline{\underline{L}}} \bar{\underline{\underline{M}}} = \bar{\underline{\underline{M}}} \bar{\underline{\underline{L}}} = \underline{\underline{I}},$$

that is

$$(5.30) \quad \bar{\underline{\underline{L}}}^{-1} = \bar{\underline{\underline{M}}}.$$

Under given displacement boundary condition (5.23), the effective stiffness tensor of a composite can be given by the formula

$$(5.31) \quad \bar{\underline{\underline{L}}} = \underline{\underline{L}}_0 + \sum_{r=1}^N c_r (\underline{\underline{L}}_r - \underline{\underline{L}}_0) \underline{\underline{A}}_r,$$

where $\underline{\underline{A}}_r$ is the *strain concentration tensor* for the r -th inhomogeneity. The average strain in the r -th inhomogeneity $\bar{\underline{\varepsilon}}_r$ is defined as

$$(5.32) \quad \bar{\underline{\varepsilon}}_r = \underline{\underline{A}}_r \bar{\underline{\varepsilon}}.$$

Similarly, under given traction boundary condition(5.20), the effective compliance tensor of a composite can be calculated from

$$(5.33) \quad \bar{\underline{\underline{M}}} = \underline{\underline{M}}_0 + \sum_{r=1}^N c_r (\underline{\underline{M}}_r - \underline{\underline{M}}_0) \underline{\underline{B}}_r,$$

with $\underline{\underline{B}}_r$ being the *stress concentration tensor* of the r -th inhomogeneity. The average stress in the r -th inhomogeneity $\bar{\underline{\sigma}}_r$ is defined by

$$(5.34) \quad \bar{\underline{\sigma}}_r = \underline{\underline{B}}_r \bar{\underline{\sigma}}.$$

The concentration tensors defined above compare the elastic field of the r -th inhomogeneity and the averaged value of that of the entire sample. These are the so-called *global concentration* tensors. In composite materials, where there is a distinct matrix phase in which the inhomogeneities are embedded, one can compare the elastic fields of the r -th inhomogeneity and that of the matrix material through the *local concentration* tensors:

$$(5.35) \quad \bar{\underline{\varepsilon}}_r = \underline{\underline{G}}_r \bar{\underline{\varepsilon}}_0,$$

$$(5.36) \quad \bar{\underline{\sigma}}_r = \underline{\underline{H}}_r \bar{\underline{\sigma}}_0,$$

¹⁰ Similarly to the material stiffness tensor, the fourth-order material compliance tensor can also be converted to a 6-by-6 matrix, which can be related to the stress and strain tensors written in Voigt form.

where $\bar{\underline{\varepsilon}}_0$ and $\bar{\underline{\sigma}}_0$ are the averaged strain and stress tensors of the matrix in Voigt form, respectively, and $\underline{\underline{G}}_r$ is the local strain concentration tensor and $\underline{\underline{H}}_r$ is the local stress concentration tensor of the r -th inhomogeneity. The relation between the global and local concentration tensors:

$$(5.37) \quad \underline{\underline{A}}_r = \underline{\underline{G}}_r \left(c_0 \underline{\underline{I}} + \sum_{r=1}^N c_r \underline{\underline{G}}_r \right)^{-1},$$

$$(5.38) \quad \underline{\underline{B}}_r = \underline{\underline{H}}_r \left(c_0 \underline{\underline{I}} + \sum_{r=1}^N c_r \underline{\underline{H}}_r \right)^{-1}.$$

These known relations allow us to determine the effective stiffness and/or compliance tensors of the composite material from solely the local concentration tensors.

5.2 Bounds for effective moduli

The exact values of the effective moduli are not always easy to find, thereby knowing the bounds for these moduli can also be enough. These bounds can be derived based on the application of variational principles.

5.2.1 Classical variational theorems in linear elasticity

First, let us write two of the classical variational theorems of linear elasticity.

According to the minimum potential energy theorem, among all the kinematically admissible displacement fields, the solution of the problem makes the potential energy minimum:

$$(5.39) \quad \Pi(u_i) = \frac{1}{2} \int_D L_{ijkl} u_{k,l} u_{i,j} dV - \int_{S_\sigma} p_i^0 u_i dS,$$

where D is the total volume of the body under consideration and S_σ is the part of the boundary of D where p_i^0 traction forces are prescribed.

The minimum complementary energy theorem states that among all the statically admissible stress fields, the solution of the boundary value problem makes the complementary energy minimum:

$$(5.40) \quad \tilde{\Pi}(\sigma_{ij}) = \frac{1}{2} \int_D M_{ijkl} \sigma_{kl} \sigma_{ij} dV - \int_{S_u} u_i^0 \sigma_{ij} n_j dS,$$

where D is the total volume of the body under consideration and S_u is the part of the boundary of D where u_i^0 displacements are prescribed.

The above theorems can be applied to heterogeneous materials, because the tensors L_{ijkl} and M_{ijkl} does not need to be constant throughout body D .

Next, consider a body D under *prescribed displacements* on S (5.23) and no prescribed traction forces. Making use of the average strain theorem and Hill's lemma, the average strain energy density in the heterogeneous material can be written as

$$(5.41) \quad \bar{U} = \frac{1}{2D} \int_D L_{ijkl} \varepsilon_{kl} \varepsilon_{ij} dV = \frac{1}{2} \bar{\varepsilon}_{ij} \bar{L}_{ijkl} \bar{\varepsilon}_{kl} ,$$

where \bar{L}_{ijkl} is the effective stiffness tensor of the heterogeneous material. According to the minimum potential energy theorem, the following inequality holds for any kinematically admissible displacement field \hat{u}_i :

$$(5.42) \quad \bar{U} \leq \frac{1}{2D} \int_D L_{ijkl} \hat{u}_{k,l} \hat{u}_{i,j} dV .$$

Making use of the minimum complementary energy theorem, for any statically admissible stress field $\hat{\sigma}_{ij}$, the complementary energy becomes

$$(5.43) \quad \tilde{\Pi}(\sigma_{ij}) = \frac{1}{2} \int_D M_{ijkl} \sigma_{kl} \sigma_{ij} dV - \bar{\varepsilon}_{ij} \int_D \sigma_{ij} dV = -D\bar{U} ,$$

and the following inequality always holds

$$(5.44) \quad \bar{U} \geq \bar{\varepsilon}_{ij} \frac{1}{D} \int_D \hat{\sigma}_{ij} dV - \frac{1}{2D} \int_D M_{ijkl} \hat{\sigma}_{kl} \hat{\sigma}_{ij} dV .$$

Combining the inequalities (5.42) and (5.44), we have

$$(5.45) \quad 2\bar{\varepsilon}_{ij} \int_D \hat{\sigma}_{ij} dV - \int_D M_{ijkl} \hat{\sigma}_{kl} \hat{\sigma}_{ij} dV \leq 2D\bar{U} \leq \int_D L_{ijkl} \bar{\varepsilon}_{ij} \bar{\varepsilon}_{kl} dV ,$$

where the statically admissible stress field $\hat{\sigma}_{ij}$ satisfy

$$(5.46) \quad \hat{\sigma}_{ij,j} = 0 \text{ in } D ,$$

and the kinematically admissible displacements \hat{u}_i satisfy

$$(5.47) \quad \hat{u}_i = \bar{\varepsilon}_{ij} x_j \text{ on } S .$$

5.2.2 Voigt upper bound and Reuss lower bound

Let a heterogeneous body be subjected to the displacement boundary condition

$$(5.48) \quad u_i = \bar{\varepsilon}_{ij} x_j \text{ on } S ,$$

$$(5.49) \quad \hat{u}_i = \bar{\varepsilon}_{ij} x_j \text{ in } D ,$$

where $\bar{\varepsilon}_{ij}$ is a given constant strain tensor which is, according to the average strain theorem equals to the average strain over body D . The kinematical admissible strain field corresponding to \hat{u}_i is $\bar{\varepsilon}_{ij}$. For the boundary condition (5.48), any constant stress tensor $\hat{\sigma}_{ij}$ would be statically admissible. Thus, we can write the inequality (5.45) – simplifying with D – in the form

$$(5.50) \quad 2\bar{\varepsilon}_{ij} \hat{\sigma}_{ij} - \bar{M}_{ijkl}^R \hat{\sigma}_{ij} \hat{\sigma}_{kl} \leq 2\bar{U} \leq \bar{L}_{ijkl}^V \bar{\varepsilon}_{ij} \bar{\varepsilon}_{kl} ,$$

where

$$(5.51) \quad \bar{L}_{ijkl}^V = \frac{1}{D} \int_D L_{ijkl} dV ,$$

$$(5.52) \quad \bar{M}_{ijkl}^R = \frac{1}{D} \int_D M_{ijkl} dV .$$

To obtain the optimal lower bound, we shall find the stress tensor $\hat{\sigma}_{ij}$ that maximizes $2\bar{\varepsilon}_{ij}\hat{\sigma}_{ij} - \bar{M}_{ijkl}^R \hat{\sigma}_{kl}\hat{\sigma}_{ij}$. The solution is

$$(5.53) \quad \hat{\sigma}_{ij} = \bar{L}_{ijkl}^R \bar{\varepsilon}_{kl} = \left(\bar{M}_{ijkl}^R \right)^{-1} \bar{\varepsilon}_{kl} .$$

The following inequality holds for any constant strain tensor $\bar{\varepsilon}_{ij}$:

$$(5.54) \quad \bar{L}_{ijkl}^R \bar{\varepsilon}_{ij} \bar{\varepsilon}_{kl} \leq \bar{L}_{ijkl} \bar{\varepsilon}_{ij} \bar{\varepsilon}_{kl} \leq \bar{L}_{ijkl}^V \bar{\varepsilon}_{ij} \bar{\varepsilon}_{kl} ,$$

thus, we can conclude

$$(5.55) \quad \bar{L}_{ijkl}^R \leq \bar{L}_{ijkl} \leq \bar{L}_{ijkl}^V ,$$

where

$$(5.56) \quad \bar{L}_{ijkl}^R = \left(\bar{M}_{klmn}^R \right)^{-1} = \left(\frac{1}{D} \int_D M_{klmn} dV \right)^{-1} .$$

\bar{L}_{ijkl}^R is called the **Reuss lower bound** and \bar{L}_{ijkl}^V is the **Voigt upper bound**. When the stiffness tensor L_{ijkl}^r ($r = 1, 2, \dots, N$) of the r -th inhomogeneity of volume Ω_r is uniform, the upper and lower bound can be computed from

$$(5.57) \quad \bar{L}_{ijkl}^V = \sum_{r=0}^N c_r L_{ijkl}^r ,$$

$$(5.58) \quad \bar{L}_{ijkl}^R = \left(\sum_{r=0}^N c_r M_{ijkl}^r \right)^{-1} ,$$

$$(5.59) \quad c_r = \frac{\Omega_r}{D}, \quad r = 0, 1, \dots, N .$$

Note that when determining the bounds of the effective moduli, only the volume fraction of the phases are taken into consideration, they are independent of the geometry and the distribution of the inhomogeneities.

5.2.3 Hashin-Shtrikman variational principle under displacement boundary conditions

In the previous section, we have seen that in order to find bounds for the elastic moduli, we have to find suitable admissible fields. In order to define tighter bounds, one must specify admissible fields that make explicit allowance for the microstructure of the composite. First, let us develop an alternative to the classical variational principles, then find a *kinematically admissible displacement* field instead of a constant tensor as seen at the Voigt upper bound, and a *statically admissible stress* tensor rather than a constant stress field as seen at the Reuss lower bound. The stiffness tensor $L_{ijkl}(x)$ of a heterogeneous material can be decomposed

into a constant tensor L_{ijkl}^h representing the homogeneous '*comparison*' material and a stiffness tensor $L_{ijkl}^p(\underline{x})$ dependent on position \underline{x} which stands for the perturbation of the heterogeneous material from the homogeneous one:

$$(5.60) \quad L_{ijkl}(\underline{x}) = L_{ijkl}^h + L_{ijkl}^p(\underline{x}).$$

The body is under prescribed displacements as seen in (5.23).

The corresponding stress field can be written in the form

$$(5.61) \quad \sigma_{ij}(\underline{x}) = L_{ijkl}^h \varepsilon_{kl}(\underline{x}) + \tau_{ij}(\underline{x}),$$

where the actual strain tensor in D is

$$(5.62) \quad \varepsilon_{ij}(\underline{x}) = \frac{1}{2} \left(\frac{\partial u_i(\underline{x})}{\partial x_j} + \frac{\partial u_j(\underline{x})}{\partial x_i} \right)$$

and the second-order, symmetric *stress-polarization tensor* is given by

$$(5.63) \quad \tau_{ij}(\underline{x}) = L_{ijkl}^p(\underline{x}) \varepsilon_{kl}(\underline{x}).$$

The equations of equilibrium can be written as

$$(5.64) \quad L_{ijkl}^h u_{k,lj}(\underline{x}) + \tau_{ij,j}(\underline{x}) = 0 \text{ in } D.$$

Treating the first derivative of the stress polarization tensor as a body force, the solution of the boundary value problem can be computed with the help of Green's functions:

$$(5.65) \quad u_i(\underline{x}) = \int_S L_{ijkl}^h \frac{\partial G_{kl}(\underline{x}, \underline{y})}{\partial x_i} \bar{\varepsilon}_{pq} y_q n_j dS(\underline{y}) + \int_D G_{mi}(\underline{x}, \underline{y}) \frac{\partial \tau_{mn}(\underline{y})}{\partial y_n} dV(\underline{y}),$$

where $G_{ij}(\underline{x}, \underline{y})$ is Green's function (see Appendix) in the homogeneous comparison material satisfying the conditions

$$(5.66) \quad L_{ijkl}^h \frac{\partial^2 G_{km,lj}(\underline{x}, \underline{y})}{\partial x_i \partial x_j} + \delta_{im} \delta(\underline{x} - \underline{y}) = 0 \text{ in } V,$$

$$(5.67) \quad G_{ij}(\underline{x}, \underline{y}) \Big|_{\underline{x} \in S} = 0.$$

After some rearrangements, we can write the displacement field as

$$(5.68) \quad u_i(\underline{x}) = \bar{\varepsilon}_{iq} x_q - \int_D G_{mi}(\underline{x}, \underline{y}) \frac{\partial \tau_{mn}(\underline{y})}{\partial y_n} dV(\underline{y}) = \bar{\varepsilon}_{iq} x_q - \int_D \frac{\partial G_{mi}(\underline{x}, \underline{y})}{\partial y_n} \tau_{mn}(\underline{y}) dV(\underline{y})$$

and the strain tensor as

$$(5.69) \quad \varepsilon_{ij}(\underline{x}) = \bar{\varepsilon}_{ij} - \int_D \Gamma_{ijkl}(\underline{x}, \underline{y}) \tau_{kl}(\underline{y}) dV(\underline{y}),$$

where the second derivatives of the Green's function are embedded into the fourth-order tensor

$$(5.70) \quad \Gamma_{ijkl}(\underline{x}, \underline{y}) = \frac{1}{4} \left(\frac{\partial^2 G_{ki}(\underline{x} - \underline{y})}{\partial x_j \partial y_l} + \frac{\partial^2 G_{kj}(\underline{x} - \underline{y})}{\partial x_i \partial y_l} + \frac{\partial^2 G_{li}(\underline{x} - \underline{y})}{\partial x_j \partial y_k} + \frac{\partial^2 G_{lj}(\underline{x} - \underline{y})}{\partial x_i \partial y_k} \right).$$

Substituting (5.67) into (5.68) we have

$$(5.71) \quad u_i(\underline{x}) \Big|_{\underline{x} \in S} = \bar{\varepsilon}_{iq} x_q \Big|_{\underline{x} \in S} + \int_D G_{mi}(\underline{x}, \underline{y}) \Big|_{\underline{x} \in S} \frac{\partial \tau_{mn}(\underline{y})}{\partial y_n} dV(\underline{y}) = \bar{\varepsilon}_{iq} x_q \Big|_{\underline{x} \in S}$$

independently of the stress polarization tensor $\tau_{ij}(\underline{y})$. Therefore for any given $\hat{\tau}_{ij}(\underline{y})$, the displacement field coming from (5.71) and the strain tensor

$$(5.72) \quad \hat{\varepsilon}_{ij}(\underline{x}) = \bar{\varepsilon}_{ij} - \int_D \Gamma_{ijkl}(\underline{x}, \underline{y}) \hat{\tau}_{kl}(\underline{y}) dV(\underline{y})$$

are kinematically admissible displacement and strain fields, respectively. According to the minimum potential energy theorem we have

$$(5.73) \quad 2D\bar{U} \leq \int_D L_{ijkl}^h \hat{\varepsilon}_{ij} \hat{\varepsilon}_{kl} dV + \int_D L_{ijkl}^p \hat{\varepsilon}_{ij} \hat{\varepsilon}_{kl} dV.$$

Making use of the properties of the integral operator $\Gamma_{ijkl}(\underline{x}, \underline{y})$ and carrying out some simplifications, we arrive at

$$(5.74) \quad 2D(\bar{U} - \bar{U}^h) \leq -H(\underline{\hat{\tau}}) + \int_D L_{ijkl}^p \eta_{ij}(\underline{\hat{\tau}}) \eta_{kl}(\underline{\hat{\tau}}) dV,$$

where

$$(5.75) \quad \bar{U}^h = \frac{1}{2D} \int_D L_{ijkl}^h \bar{\varepsilon}_{ij} \bar{\varepsilon}_{kl} dV,$$

$$(5.76) \quad \eta_{ij}(\underline{\hat{\tau}}) = \left(L_{ijkl}^p \right)^{-1} \hat{\tau}_{kl} + \int_D \Gamma_{ijkl}(\underline{x}, \underline{y}) \hat{\tau}_{kl}(\underline{y}) dV(\underline{y}) - \bar{\varepsilon}_{ij},$$

$$(5.77) \quad H(\underline{\hat{\tau}}) = \int_D \hat{\tau}_{ij} \eta_{ij}(\underline{\hat{\tau}}) dV - \int_D \bar{\varepsilon}_{ij} \hat{\tau}_{ij} dV.$$

If the stress polarization tensor is the actual one of the problem, that is $\hat{\tau}_{ij} = \tau_{ij}$, we have

$$(5.78) \quad \eta_{ij}(\underline{\hat{\tau}}) = 0,$$

$$(5.79) \quad H(\underline{\hat{\tau}}) = - \int_D \bar{\varepsilon}_{ij} \tau_{ij} dV = - \int_D \bar{\varepsilon}_{ij} (L_{ijkl} - L_{ijkl}^h) \varepsilon_{kl} dV = -2D(\bar{U} - \bar{U}^h),$$

in other words, the right-hand side of (5.74) is **minimized**.

From (5.74) follows the theorem: among all the symmetric second-order tensors, the *real solution to the stress polarization tensor* $\hat{\tau}_{ij}$ renders the following functional minimum:

$$(5.80) \quad I(\underline{\hat{\tau}}) = \bar{U}^h - \frac{1}{2D} H(\underline{\hat{\tau}}) + \frac{1}{2D} \int_D L_{ijkl}^p \eta_{ij}(\underline{\hat{\tau}}) \eta_{kl}(\underline{\hat{\tau}}) dV,$$

and the minimum value of the functional gives the strain energy density of the heterogeneous material under the displacement boundary condition (5.23):

$$(5.81) \quad \min \{I(\underline{\hat{\tau}})\} = \bar{U} = \frac{1}{2} \bar{L}_{ijkl} \bar{\varepsilon}_{ij} \bar{\varepsilon}_{kl}.$$

The **Hashin-Shtrikman variational principle** states that if L_{ijkl}^p is negative semi-definite, the functional (5.80) simplifies to

$$(5.82) \quad I(\underline{\hat{\tau}}) = \bar{U}^h - \frac{1}{2D} H(\underline{\hat{\tau}}),$$

due to the attribute

$$(5.83) \quad \int_D L_{ijkl}^p \eta_{ij}(\underline{\hat{\tau}}) \eta_{kl}(\underline{\hat{\tau}}) dV \leq 0.$$

Substituting (5.69) into (5.61) we have

$$(5.84) \quad \sigma_{ij}(\underline{x}) = L_{ijkl}^h \bar{\varepsilon}_{kl} - L_{ijkl}^h \int_D \Gamma_{klmn}(\underline{x}, \underline{y}) \tau_{mn}(\underline{y}) dV(\underline{y}) + \tau_{ij}(\underline{x}),$$

and the divergence of the stress field is

$$(5.85) \quad \nabla(\sigma_{ij}(\underline{x})) = L_{ijkl}^h \int_D \Gamma_{klmn}(\underline{x}, \underline{y}) \nabla(\tau_{mn}(\underline{y})) dV(\underline{y}) + \nabla(\tau_{ij}(\underline{x})).$$

Therefore, for any statically admissible stress polarization tensor $\hat{\tau}_{ij}$, where $\nabla(\hat{\tau}_{ij}(\underline{x})) = 0$, the stress tensor $\hat{\sigma}_{ij}$ calculated from (5.84) will also be statically admissible, that is

$$(5.86) \quad \nabla(\hat{\sigma}_{ij}(\underline{x})) = \nabla(L_{ijkl}^h \varepsilon_{kl}(\underline{x}) + \hat{\tau}_{ij}(\underline{x})) = \nabla(L_{ijkl}^h \varepsilon_{kl}(\underline{x})) = 0.$$

The following inequality for the complementary potential energy holds for the statically admissible stress field $\hat{\sigma}_{ij}$:

$$(5.87) \quad 2D\bar{U} \geq 2\bar{\varepsilon}_{ij} \int_D \hat{\sigma}_{ij} dV - \int_D M_{ijkl} \hat{\sigma}_{ij} \hat{\sigma}_{kl} dV = 2\bar{\varepsilon}_{ij} \int_D \hat{\sigma}_{ij} dV - \int_D (M_{ijkl}^h + M_{ijkl}^p) \hat{\sigma}_{ij} \hat{\sigma}_{kl} dV,$$

where the compliance tensor is decomposed into a *constant part* of the homogeneous 'comparison' material and a *position-dependent perturbed part*:

$$(5.88) \quad M_{ijkl}(\underline{x}) = M_{ijkl}^h + M_{ijkl}^p(\underline{x}).$$

Similarly as shown before, for any statically admissible tensor $\hat{\tau}_{ij}$ holds that

$$(5.89) \quad 2D(\bar{U} - \bar{U}^h) \geq -H(\underline{\hat{\tau}}) - \int_D L_{ijkl}^h M_{ijkl}^p L_{ijkl}^h \eta_{ij}(\underline{\hat{\tau}}) \eta_{kl}(\underline{\hat{\tau}}) dV.$$

If the stress polarization tensor is the actual one of the problem, that is $\hat{\tau}_{ij} = \tau_{ij}$, the right-hand side of the (5.89) is **maximized**.

From (5.89) follows the theorem: among all the statically admissible stress fields, the *real solution to the stress polarization tensor* $\hat{\tau}_{ij}$ renders the following functional maximum:

$$(5.90) \quad \tilde{I}(\underline{\hat{\tau}}) = \bar{U}^h - \frac{1}{2D} H(\underline{\hat{\tau}}) - \frac{1}{2D} \int_D L_{ijkl}^h M_{ijkl}^p L_{ijkl}^h \eta_{ij}(\underline{\hat{\tau}}) \eta_{kl}(\underline{\hat{\tau}}) dV ,$$

and the maximum value of the functional gives the strain energy density of the heterogeneous material under the displacement boundary condition (5.23):

$$(5.91) \quad \max \{ \tilde{I}(\underline{\hat{\tau}}) \} = \bar{U} = \frac{1}{2} \bar{L}_{ijkl} \bar{\varepsilon}_{ij} \bar{\varepsilon}_{kl} .$$

The **Hashin-Shtrikman variational principle** states that if M_{ijkl}^p is negative semi-definite, or, equivalently, L_{ijkl}^p is positive semi-definite, the functional (5.90) simplifies to

$$(5.92) \quad \tilde{I}(\underline{\hat{\tau}}) = \bar{U}^h - \frac{1}{2D} H(\underline{\hat{\tau}}) ,$$

due to the attribute

$$(5.93) \quad \int_D L_{ijkl}^h M_{ijkl}^p L_{ijkl}^h \eta_{ij}(\underline{\hat{\tau}}) \eta_{kl}(\underline{\hat{\tau}}) dV \leq 0 .$$

5.2.4 Hashin-Shtrikman bounds

In order to develop bounds specifically for heterogeneous materials, one must find an appropriate statically admissible stress tensor $\hat{\tau}_{ij}$. Instead of a uniform stress field throughout the whole composite material, let us consider a *piecewise uniform field* for $\hat{\tau}_{ij}$:

$$(5.94) \quad \hat{\tau}_{ij}(\underline{x}) \Big|_{\underline{x} \in \Omega_r} = \tau_{ij}^r, \quad r = 0, 1, 2, \dots, N ,$$

in other words, the stress tensor is uniform only inside the r -th phase individually. Substituting this piecewise constant stress polarization tensor into the Hashin-Shtrikman variational principle, we arrive at $H(\underline{\hat{\tau}})$ being a quadratic function of τ_{ij}^r . The required τ_{ij}^r

gives the extreme value of $H(\underline{\hat{\tau}})$ which can be determined from the equation $\frac{\partial H(\underline{\hat{\tau}})}{\partial \tau_{ij}^r} = 0$. It

results in a system of linear algebraic equations for τ_{ij}^r :

$$(5.95) \quad \left(\bar{L}_{ijkl}^{p,r} \right)^{-1} \tau_{kl}^r + D \sum_{s=0}^N c_s P_{ijkl}^{rs} \tau_{kl}^s = \bar{\varepsilon}_{ij}, \quad r = 0, 1, \dots, N ,$$

where

$$(5.96) \quad \left(\bar{L}_{ijkl}^{p,r} \right)^{-1} = \frac{1}{\Omega_r} \int_{\Omega_r} \left(L_{ijkl}^p \right)^{-1} dV ,$$

$$(5.97) \quad P_{ijkl}^{rs} = \frac{1}{\Omega_r \Omega_s} \int_{\Omega_r} \int_{\Omega_s} \Gamma_{ijkl}(\underline{x}, \underline{y}) dV(\underline{y}) dV(\underline{x}) .$$

The solution for stress tensor τ_{ij}^r which gives extreme value for $H(\hat{\underline{\tau}})$ can be written in the form

$$(5.98) \quad \tau_{ij}^r = R_{ijkl}^r \bar{\varepsilon}_{kl} .$$

Substituting the solution (5.98) into (5.77) the extreme value of $H(\hat{\underline{\tau}})$ can be computed from

$$(5.99) \quad H(\hat{\underline{\tau}}) \Big|_{\tau_{ij}^r = R_{ijkl}^r \bar{\varepsilon}_{kl}} = -D \bar{\varepsilon}_{ij} \sum_{r=0}^N c_r R_{ijkl}^r \bar{\varepsilon}_{kl} = D \bar{\varepsilon}_{ij} (L_{ijkl}^h - \tilde{L}_{ijkl}) \bar{\varepsilon}_{kl} ,$$

with

$$(5.100) \quad \tilde{L}_{ijkl} = L_{ijkl}^h + \sum_{r=0}^N c_r R_{ijkl}^r .$$

If L_{ijkl}^p is negative semi-definite, substituting into (5.74) yields

$$(5.101) \quad 2\bar{U} = \bar{L}_{ijkl} \bar{\varepsilon}_{ij} \bar{\varepsilon}_{kl} \leq \tilde{L}_{ijkl} \bar{\varepsilon}_{ij} \bar{\varepsilon}_{kl} ,$$

providing an upper bound for the effective stiffness tensor

$$(5.102) \quad \bar{L}_{ijkl} \leq \tilde{L}_{ijkl} = L_{ijkl}^h + \sum_{r=0}^N c_r R_{ijkl}^r ,$$

which is called the *Hashin-Shtrikman upper bound*.

If L_{ijkl}^p is positive semi-definite, substituting (5.99) into (5.89) we have the dual pair of the bound for the effective stiffness tensor \bar{L}_{ijkl} , called as the *Hashin-Shtrikman lower bound*:

$$(5.103) \quad \bar{L}_{ijkl} \geq \tilde{L}_{ijkl} = L_{ijkl}^h + \sum_{r=0}^N c_r R_{ijkl}^r .$$

In general the Hashin-Shtrikman bounds are *more restrictive* than the Voigt upper and Reuss lower bounds.

When carrying out the double integral in (5.97) one might face some difficulties due to the large number of inhomogeneities and the statistical nature of their distribution. Willis (Willis, 1981) proposed a good approximation by replacing the Green's function in the finite domain D by its counterpart in the infinite domain which yields

$$(5.104) \quad P_{ijkl}^{rs} \approx \frac{1}{\Omega_r \Omega_s} \int_{\Omega_r} \int_{\Omega_s} \Gamma_{ijkl}^{\infty}(\underline{x}, \underline{y}) dV(\underline{y}) dV(\underline{x}) ,$$

where $\Gamma_{ijkl}^{\infty}(\underline{x}, \underline{y})$ is counterpart of the integral operator $\Gamma_{ijkl}(\underline{x}, \underline{y})$ in the infinite domain. For statistically homogeneous heterogeneous materials with isotropic distribution of inhomogeneities the integral can be written in the form

$$(5.105) P_{ijkl}^{rs} \approx \frac{1}{\Omega_s} (\delta_{rs} - c_s) P_{ijkl},$$

where the following integral is carried out over a unit sphere \hat{S}^2 :

$$(5.106) P_{ijkl}(\underline{x}) = \int_{\hat{S}^2} \Gamma_{ijkl}^{\infty}(\underline{x}, \underline{y}) dV(\underline{y}), \underline{x} \in \hat{S}^2.$$

The tensor P_{ijkl} is related to the Eshelby-tensor S_{ijkl} through

$$(5.107) P_{ijkl} = S_{ijmn} (L_{klpq}^h)^{-1}.$$

The stress polarization tensor can be calculated from

$$(5.108) \tau_{mnrs}^r = \left((\bar{L}_{ijkl}^{p,r})^{-1} + P_{klmn} \right)^{-1} \left(\bar{\varepsilon}_{pqrs} + P_{pqij} \sum_{s=0}^N c_s \tau_{ijrs}^s \right), r = 0, 1, \dots, N.$$

The Hashin-Shtrikman bound therefore

$$(5.109) \tilde{L}_{pqtv} = L_{pqtv}^h + \left(\sum_{r=0}^N c_r (\delta_{ijmn} + \bar{L}_{ijkl}^{p,r} P_{klmn})^{-1} \right)^{-1} \sum_{r=0}^N c_r (\delta_{ijrs} + \bar{L}_{ijkl}^{p,r} P_{klrs})^{-1} \bar{L}_{mntv}^{p,r}.$$

5.2.5 Hashin-Shtrikman variational principle under traction boundary conditions

Similarly to the Hashin-Shtrikman variational principle under displacement boundary conditions, one can develop variational principles for a heterogeneous body under given *traction boundary conditions*

$$(5.110) \sigma_{ij}(\underline{x}) n_j \Big|_{\underline{x} \in S} = \bar{\sigma}_{ij} n_j,$$

where $\bar{\sigma}_{ij}$ is a constant stress tensor. Let us introduce a strain polarization tensor ε_{ijkl}^* – that is, the uniform eigenstrain – as

$$(5.111) \varepsilon_{ij} = M_{ijkl}^h \sigma_{kl} + \varepsilon_{ij}^*$$

or

$$(5.112) \sigma_{kl} = (M_{ijkl}^h)^{-1} (\varepsilon_{mn} - \varepsilon_{mn}^*),$$

where M_{ijkl}^h is defined in (5.88) and ε_{ij} is the actual strain in the heterogeneous material. Substituting Hooke's law into (5.111) we have

$$(5.113) \varepsilon_{ij}^* = M_{ijkl}^p \sigma_{kl}.$$

Substituting (5.112) into the equations of equilibrium yields

$$(5.114) (M_{ijkl}^h)^{-1} u_{m,ni}(\underline{x}) - (M_{ijkl}^h)^{-1} \varepsilon_{mn,i}^*(\underline{x}) = 0 \text{ in } D.$$

For the solution of this boundary value problem let us introduce the following *Green's function*

$$(5.115) \left(M_{ijkl}^h \right)^{-1} \frac{\partial^2 \tilde{G}_{km}(\underline{x}, \underline{y})}{\partial x_i \partial x_j} + \delta_{im} \delta(\underline{x} - \underline{y}) = 0 \text{ in } D,$$

$$(5.116) \left(M_{ijkl}^h \right)^{-1} \frac{\partial \tilde{G}_{km}(\underline{x}, \underline{y})}{\partial x_i} n_j \Big|_{\underline{x} \in S} = 0.$$

Similarly to the problem with given displacement boundary conditions, one can derive the solution applying Green's functions. In this case, the stress tensor simplifies to

$$(5.117) \sigma_{rs}(\underline{x}) = \bar{\sigma}_{rs} - L_{rsij} \int_D \frac{\partial \tilde{G}_{mi}(\underline{x}, \underline{y})}{\partial x_j} \frac{\partial \left(M_{klmn}^h \right)^{-1} \varepsilon_{pq}^*(\underline{y})}{\partial y_n} dV(\underline{y}).$$

Due to the properties of Green's function the following equations hold:

$$(5.118) \sigma_{kp,p}(\underline{x}) = \left(M_{ijkl}^h \right)^{-1} \varepsilon_{mn,l}^*(\underline{x}),$$

$$(5.119) \sigma_{pq}(\underline{x}) n_q \Big|_{\underline{x} \in S} = \bar{\sigma}_{pq} n_q.$$

Therefore, independently from the eigenstrain ε_{ijkl}^* , the stress tensor computed from (5.117) is *always statically admissible*, satisfying the equations of equilibrium (5.114) and the traction boundary conditions (5.110).

Let us introduce

$$(5.120) L_{rsij} \int_D \frac{\partial \tilde{G}_{mi}(\underline{x}, \underline{y})}{\partial x_j} \frac{\partial \left(M_{klmn}^h \right)^{-1} \varepsilon_{pq}^*(\underline{y})}{\partial y_n} dV(\underline{y}) \equiv \int_D \tilde{\Gamma}_{rspq}(\underline{x}, \underline{y}) \varepsilon_{pq}^*(\underline{y}) dV(\underline{y}).$$

The stress tensor can be written as

$$(5.121) \sigma_{ij}(\underline{x}) = \bar{\sigma}_{ij} - \int_D \tilde{\Gamma}_{ijkl}(\underline{x}, \underline{y}) \varepsilon_{kl}^*(\underline{y}) dV(\underline{y}).$$

From (5.113) the constant stress tensor is

$$(5.122) \bar{\sigma}_{kl} = \left(M_{ijkl}^p \right)^{-1} \varepsilon_{mn}^*(\underline{x}) + \int_D \tilde{\Gamma}_{klmn}(\underline{x}, \underline{y}) \varepsilon_{mn}^*(\underline{y}) dV(\underline{y}).$$

Let $\hat{\varepsilon}_{ij}^*(\underline{y})$ be any strain polarization tensor, then the corresponding statically admissible stress field is

$$(5.123) \hat{\sigma}_{ij}(\underline{x}) = \bar{\sigma}_{ij} - \int_D \tilde{\Gamma}_{ijkl}(\underline{x}, \underline{y}) \hat{\varepsilon}_{kl}^*(\underline{y}) dV(\underline{y}).$$

The minimum complementary energy theorem yields

$$(5.124) 2D \bar{U}_c \leq \int_D M_{ijkl}(\underline{x}) \hat{\sigma}_{ij}(\underline{x}) \hat{\sigma}_{kl}(\underline{x}) dV(\underline{x})$$

with

$$(5.125) \bar{U}_c = \frac{1}{2D} \int_D M_{ijkl} \bar{\sigma}_{ij} \bar{\sigma}_{kl} dV = \frac{1}{2} \bar{M}_{ijkl} \bar{\sigma}_{ij} \bar{\sigma}_{kl}.$$

Substituting the statically admissible stress field into (5.124) we have

$$(5.126) 2D (\bar{U} - \bar{U}_c^h) \leq -\tilde{H}(\underline{\hat{\varepsilon}}^*) + \int_D M_{ijkl}^p(\underline{x}) \gamma_{ij}(\underline{x}) \gamma_{kl}(\underline{x}) dV(\underline{x}),$$

where

$$(5.127) \bar{U}_c^h = \frac{1}{2} \bar{M}_{ijkl}^h \bar{\sigma}_{ij} \bar{\sigma}_{kl},$$

$$(5.128) (M_{ijkl}^h)^{-1} \gamma_{mn}(\underline{x}) = \int_D \tilde{\Gamma}_{klmn}(\underline{x}, \underline{y}) \varepsilon_{mn}^*(\underline{y}) dV(\underline{y}) + (\bar{M}_{ijkl}^h)^{-1} \hat{\varepsilon}_{mn}^*(\underline{x}) - \bar{\sigma}_{kl},$$

$$(5.129) \tilde{H}(\underline{\hat{\varepsilon}}^*) = -\int_D \hat{\varepsilon}_{ij}^*(\underline{x}) (M_{ijkl}^h)^{-1} \gamma_{kl}(\underline{x}) dV(\underline{x}) + \int_D \hat{\varepsilon}_{ij}^*(\underline{x}) \bar{\sigma}_{ij} dV.$$

If the strain polarization tensor is the *actual one* of the problem, that is $\hat{\varepsilon}_{ij}^* = \varepsilon_{ij}^*$, we have

$$(5.130) \gamma_{ij}(\underline{x}) = 0,$$

$$(5.131) \tilde{H}(\underline{\varepsilon}^*) = \int_D \varepsilon_{ij}^*(\underline{x}) \bar{\sigma}_{ij} dV = \int_D (M_{ijkl}(\underline{x}) - M_{ijkl}^h) \bar{\sigma}_{ij} \bar{\sigma}_{kl} dV = 2D (\bar{U}_c - \bar{U}_c^h),$$

in other words, the right-hand side of (5.126) is **minimized**.

From (5.126) follows the theorem: among all the symmetric second-order tensors, the *real solution to the strain polarization tensor* $\hat{\varepsilon}_{ij}^*$ renders the following functional minimum:

$$(5.132) \tilde{J}(\underline{\hat{\varepsilon}}^*) = \frac{1}{2} \bar{M}_{ijkl}^h \bar{\sigma}_{ij} \bar{\sigma}_{kl} - \frac{1}{2D} \tilde{H}(\underline{\hat{\varepsilon}}^*) + \frac{1}{2D} \int_D M_{ijkl}^p(\underline{x}) \gamma_{ij}(\underline{x}) \gamma_{kl}(\underline{x}) dV(\underline{x}),$$

and the minimum value of the functional gives the strain energy density of the heterogeneous material under the traction boundary condition (5.110):

$$(5.133) \min \{ \tilde{J}(\underline{\hat{\varepsilon}}^*) \} = \bar{U}_c = \frac{1}{2} \bar{M}_{ijkl} \bar{\sigma}_{ij} \bar{\sigma}_{kl}.$$

The *Hashin-Shtrikman variational principle* states that if M_{ijkl}^p is negative semi-definite, the functional (5.132) simplifies to

$$(5.134) \tilde{J}(\underline{\hat{\varepsilon}}^*) = \frac{1}{2} \bar{M}_{ijkl}^h \bar{\sigma}_{ij} \bar{\sigma}_{kl} - \frac{1}{2D} \tilde{H}(\underline{\hat{\varepsilon}}^*),$$

due to the attribute

$$(5.135) \int_D M_{ijkl}^p(\underline{x}) \gamma_{ij}(\underline{x}) \gamma_{kl}(\underline{x}) dV(\underline{x}) \leq 0.$$

Similarly as shown in 'Hashin-Shtrikman variational principle under displacement boundary conditions', the dual pair of the Hashin-Shtrikman variational principle for given traction boundary conditions *can be derived* based on the *minimum potential energy* principle.

Among all the kinematically admissible eigenstrain fields, the *real solution to the strain polarization tensor* $\hat{\underline{\underline{\epsilon}}}_{ij}^*$ renders the following functional maximum:

$$(5.136) J(\hat{\underline{\underline{\epsilon}}}_{ij}^*) = \frac{1}{2} \bar{M}_{ijkl}^h \bar{\sigma}_{ij} \bar{\sigma}_{kl} - \frac{1}{2D} \tilde{H}(\hat{\underline{\underline{\epsilon}}}_{ij}^*) - \frac{1}{2D} \int_D L_{ijkl}^p(\underline{x}) \gamma_{ij}(\underline{x}) \gamma_{kl}(\underline{x}) dV(\underline{x}),$$

and the maximum value of the functional gives the strain energy density of the heterogeneous material under the traction boundary condition (5.110):

$$(5.137) \max \{J(\hat{\underline{\underline{\epsilon}}}_{ij}^*)\} = \bar{U}_c = \frac{1}{2} \bar{M}_{ijkl} \bar{\sigma}_{ij} \bar{\sigma}_{kl}.$$

The *Hashin-Shtrikman variational principle* states that if M_{ijkl}^p is positive semi-definite, or, equivalently, L_{ijkl}^p is negative semi-definite, the functional (5.136) simplifies to

$$(5.138) J(\hat{\underline{\underline{\epsilon}}}_{ij}^*) = \frac{1}{2} \bar{M}_{ijkl}^h \bar{\sigma}_{ij} \bar{\sigma}_{kl} - \frac{1}{2D} \tilde{H}(\hat{\underline{\underline{\epsilon}}}_{ij}^*),$$

due to the attribute

$$(5.139) \int_D L_{ijkl}^p(\underline{x}) \gamma_{ij}(\underline{x}) \gamma_{kl}(\underline{x}) dV(\underline{x}) \leq 0.$$

5.3 Determination of effective moduli

In this chapter, several methods for determining the effective moduli of heterogeneous materials are presented. All of these approaches are based on Eshelby's single inclusion method, though one can find multiple-inclusion methods also in the literature.

5.3.1 Basic ideas of micromechanics for effective properties

Our main goal is to find the overall elastic moduli of a heterogeneous material based on known values of the effective moduli of the matrix and of the inhomogeneities, and the volume fractions of them. In the previous section it was shown that the effective stiffness tensor can easily be obtained from the global or local concentration tensors. On the other hand, the exact values of these concentration tensors are not easy to obtain. In this chapter different methods are shown to evaluate approximations for the concentration tensors.

When developing the concentration tensors, a common solution is to use Eshelby's solution in conjunction with the equivalent inclusion method. First, let us assume that a composite material is subjected to either *displacement boundary condition*

$$(5.140) \underline{u}|_s = \underline{\underline{\epsilon}}^0 \underline{x},$$

or *traction boundary condition*

$$(5.141) \underline{\underline{\sigma}} n \Big|_s = \underline{\underline{\sigma}}^0 n ,$$

where $\underline{\underline{\varepsilon}}^0$ and $\underline{\underline{\sigma}}^0$ are constant second-order tensors and their Voigt forms $(\underline{\underline{\sigma}}^0, \underline{\underline{\varepsilon}}^0)$ are related to the stiffness tensor $(\underline{\underline{L}}_0)$ by

$$(5.142) \underline{\underline{\sigma}}^0 = \underline{\underline{L}}_0 \underline{\underline{\varepsilon}}^0 .$$

If the material under consideration would completely filled with the matrix material with elastic stiffness $\underline{\underline{L}}_0$ and all the inhomogeneities were absent, the strain and stress field inside the material would equal to $\underline{\underline{\varepsilon}}^0$ and $\underline{\underline{\sigma}}^0$, respectively. Once the inhomogeneities appear inside this material, the uniform strain field near the r -th inhomogeneity is perturbed because of the r -th inhomogeneity itself and the existence of the other inhomogeneities as well. This perturbation can be modelled as if the isolated r -th inhomogeneity were embedded into a matrix that already bears its own strain $\underline{\underline{\varepsilon}}^0$ and the influence of the other inhomogeneities –that **do not appear in our model** any more– can be accounted for by assuming that the matrix material is somewhat different from the actual matrix. The stiffness tensor of this fictitious matrix material will be denoted by $\hat{\underline{\underline{L}}}_0$ (Figure 52).

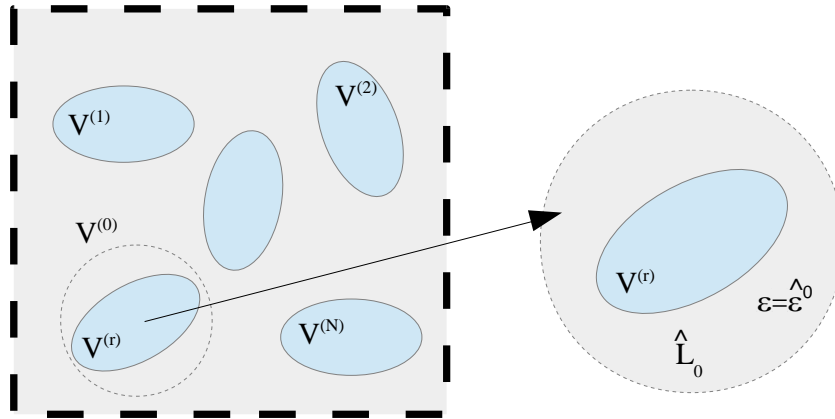


Figure 52 The strain field and the stiffness tensor of the fictitious matrix material around an isolated inhomogeneity

The problem can be restated as follows: an ellipsoidal inhomogeneity Ω_r with stiffness tensor $\underline{\underline{L}}_r$ is embedded in a matrix with stiffness tensor $\hat{\underline{\underline{L}}}_0$ which was subjected to a uniform strain $\underline{\underline{\varepsilon}}^0$ prior to the inhomogeneity was embedded. Proper values for $\hat{\underline{\underline{L}}}_0$ and $\underline{\underline{\varepsilon}}^0$ shall be found such that the stress and strain in Ω_r are the same as that in the r -th inhomogeneity in the actual problem. The solution can be found using Eshelby's solution for the equivalent inclusion problem. In this case the equivalent inclusion equation becomes

$$(5.143) \underline{\underline{L}}_r (\underline{\underline{\varepsilon}}^0 + \underline{\underline{\varepsilon}}_r^{pt}) = \hat{\underline{\underline{L}}}_0 (\underline{\underline{\varepsilon}}^0 + \underline{\underline{\varepsilon}}_r^{pt} - \underline{\underline{\varepsilon}}_r^*),$$

where, according to Eshelby's solution

$$(5.144) \underline{\underline{\varepsilon}}_r^{pt} = \hat{\underline{\underline{S}}}_r \underline{\underline{\varepsilon}}_r^* .$$

$\hat{\underline{\underline{S}}}_r$ is the Eshelby tensor calculated from the fictitious elastic stiffness tensor $\hat{\underline{\underline{L}}}_0$ and the geometry of the r -th inhomogeneity Ω_r . Substituting the Eshelby solution into the equivalent inclusion equation results in the eigenstrain to simulate the effect of the heterogeneous material in the r -th inhomogeneity

$$(5.145) \underline{\underline{\varepsilon}}_r^* = \left(\left(\underline{\underline{L}}_r - \hat{\underline{\underline{L}}}_0 \right) \hat{\underline{\underline{S}}}_r + \hat{\underline{\underline{L}}}_0 \right)^{-1} \left(\underline{\underline{L}}_r - \hat{\underline{\underline{L}}}_0 \right) \hat{\underline{\underline{\varepsilon}}}^0.$$

Hence, the total strain in the r -th inhomogeneity is

$$(5.146) \underline{\underline{\varepsilon}}_r = \hat{\underline{\underline{\varepsilon}}}^0 + \underline{\underline{\varepsilon}}_r^{pr} = \hat{\underline{\underline{\varepsilon}}}^0 + \hat{\underline{\underline{S}}}_r \underline{\underline{\varepsilon}}_r^* = \hat{\underline{\underline{T}}}_r \hat{\underline{\underline{\varepsilon}}}^0$$

with

$$(5.147) \hat{\underline{\underline{T}}}_r = \left(\underline{\underline{I}} + \hat{\underline{\underline{S}}}_r \hat{\underline{\underline{L}}}_0^{-1} \left(\underline{\underline{L}}_r - \hat{\underline{\underline{L}}}_0 \right) \right)^{-1}.$$

The stress field in the r -th inhomogeneity is

$$(5.148) \underline{\underline{\sigma}}_r = \underline{\underline{L}}_r \underline{\underline{\varepsilon}}_r = \underline{\underline{L}}_r \hat{\underline{\underline{T}}}_r \hat{\underline{\underline{\varepsilon}}}^0.$$

The ultimate question, that differ in the following methods is how to determine the fictitious quantities $\hat{\underline{\underline{L}}}_0$ and $\hat{\underline{\underline{\varepsilon}}}^0$.

5.3.2 Eshelby method

If the inhomogeneities in a composite are **far from each other**, in other words, the composite material is dilute, the interactions between the inhomogeneities can be neglected. Thus, the r -th inhomogeneity can be treated as if it were embedded in the matrix material with its actual stiffness tensor $\underline{\underline{L}}_0$ which was previously subjected to a uniform strain $\underline{\underline{\varepsilon}}^0$ (Figure 53).

Therefore,

$$(5.149) \hat{\underline{\underline{L}}}_0 = \underline{\underline{L}}_0$$

and

$$(5.150) \hat{\underline{\underline{\varepsilon}}}^0 = \underline{\underline{\varepsilon}}^0.$$

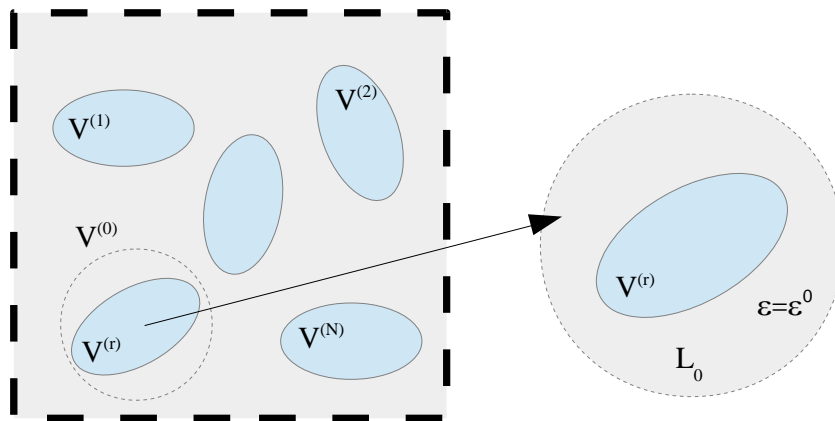


Figure 53 Eshelby's estimation

The Eshelby tensor computed from the actual properties of the matrix and the geometry of the r -th inhomogeneity Ω_r is

$$(5.151) \hat{\underline{\underline{S}}}_r = \underline{\underline{S}}_r .$$

The total strain inside the r -th inhomogeneity:

$$(5.152) \underline{\underline{\varepsilon}}_r = \underline{\underline{\varepsilon}}^0 + \underline{\underline{\varepsilon}}_r^{pt} = \underline{\underline{\varepsilon}}^0 + \underline{\underline{S}}_r \underline{\underline{\varepsilon}}_r^* = \underline{\underline{T}}_r \underline{\underline{\varepsilon}}^0 ,$$

with

$$(5.153) \underline{\underline{T}}_r = \left(\underline{\underline{I}} + \underline{\underline{S}}_r \underline{\underline{L}}_0^{-1} \left(\underline{\underline{L}}_r - \underline{\underline{L}}_0 \right) \right)^{-1} .$$

Assuming that the material is subjected to displacement boundary condition (5.140) and applying the average strain theorem (5.22) resulting in $\bar{\underline{\underline{\varepsilon}}} = \underline{\underline{\varepsilon}}^0$, equation (5.152) can be rewritten in the form

$$(5.154) \underline{\underline{\varepsilon}}_r = \underline{\underline{T}}_r \bar{\underline{\underline{\varepsilon}}} ,$$

where $\bar{\underline{\underline{\varepsilon}}}$ is the average strain over the entire heterogeneous body. Comparing this equation to (5.32) one can see that the global strain concentration tensor for Ω_r is

$$(5.155) \underline{\underline{A}}_r = \underline{\underline{T}}_r .$$

Substituting into (5.31) yields the Eshelby estimate of the effective stiffness tensor. Please note that this approximation is valid only for heterogeneous materials with *very low volume fraction of inhomogeneities*, that is why this estimation is called also as the dilute concentration method:

$$(5.156) \bar{\underline{\underline{L}}} = \underline{\underline{L}}_0 + \sum_{r=1}^N c_r \left(\underline{\underline{L}}_r - \underline{\underline{L}}_0 \right) \underline{\underline{A}}_r = \underline{\underline{L}}_0 + \sum_{r=1}^N c_r \left(\underline{\underline{L}}_r - \underline{\underline{L}}_0 \right) \left(\underline{\underline{I}} + \underline{\underline{S}}_r \underline{\underline{L}}_0^{-1} \left(\underline{\underline{L}}_r - \underline{\underline{L}}_0 \right) \right)^{-1} .$$

Now let us consider the case when the heterogeneous body is subjected to *given traction boundary condition* (5.141). In this case the average strain $\bar{\underline{\underline{\varepsilon}}}$ is no longer equal to $\underline{\underline{\varepsilon}}^0$, where

$$(5.157) \underline{\underline{\varepsilon}}^0 = \underline{\underline{M}}_0 \underline{\underline{\sigma}}^0 .$$

However, the average stress theorem holds, therefore $\bar{\underline{\underline{\sigma}}} = \underline{\underline{\sigma}}^0$. Substituting (5.157) into (5.154) yields

$$(5.158) \underline{\underline{\sigma}}_r = \underline{\underline{L}}_r \underline{\underline{\varepsilon}}_r = \underline{\underline{L}}_r \underline{\underline{T}}_r \underline{\underline{M}}_0 \bar{\underline{\underline{\sigma}}} ,$$

where $\bar{\underline{\underline{\sigma}}}$ is the average stress over the entire heterogeneous body. The global stress concentration tensor for the r -th inhomogeneity from (5.34):

$$(5.159) \underline{\underline{B}}_r = \underline{\underline{L}}_r \underline{\underline{T}}_r \underline{\underline{M}}_0 .$$

The Eshelby estimate of the effective compliance tensor of the composite from (5.33):

$$(5.160) \quad \underline{\underline{M}} = \underline{\underline{M}}_0 + \sum_{r=1}^N c_r (\underline{\underline{M}}_r - \underline{\underline{M}}_0) \underline{\underline{B}}_r = \underline{\underline{M}}_0 + \sum_{r=1}^N c_r (\underline{\underline{M}}_r - \underline{\underline{M}}_0) \underline{\underline{L}}_r \underline{\underline{T}}_r \underline{\underline{M}}_0 .$$

Finally, let us check the consistency of the Eshelby estimation by examining the connection between the stiffness and the compliance tensor, that is whether their product yields the identity matrix:

$$(5.161) \quad \underline{\underline{M}} \underline{\underline{L}} = \underline{\underline{I}} + O(c_r^2) .$$

The error of the estimation is of order c_r^2 , which means the Eshelby approximation is consistent only up to the first order of the volume fraction of the inhomogeneities. Please note that not only the volume fraction but the geometry of the inhomogeneities is also taken into consideration through the Eshelby tensor, but the distribution and the interaction between them is neglected.

5.3.3 Mori-Tanaka method

Let us consider the r -th inhomogeneity in a composite material. The stiffness tensor $\underline{\underline{L}}_r$ ($r > 0$) is affected by the other inhomogeneities through the stress and strain field of the matrix material. Though the elastic field in the matrix changes from point to point, the averages $\underline{\underline{\varepsilon}}_0$ and $\underline{\underline{\sigma}}_0$ represent a good approximation at each position inside the matrix if the **inhomogeneities are randomly distributed** and are **of large number**:

$$(5.162) \quad \underline{\underline{\varepsilon}}_r = \frac{1}{\Omega_r} \int_{\Omega_r} \underline{\underline{\varepsilon}} dV ,$$

$$(5.163) \quad \underline{\underline{\sigma}}_r = \frac{1}{\Omega_r} \int_{\Omega_r} \underline{\underline{\sigma}} dV .$$

Due to the random distribution and large number of inhomogeneities, we can assume that taking out the r -th inhomogeneity and substituting with the matrix material will not influence the averaged value of the elastic field over the matrix material, and therefore the overall mechanical behavior of the heterogeneous sample. Mori-Tanaka determined the concentration tensors of the r -th inhomogeneity by considering the heterogeneity in question as an *ellipsoidal inhomogeneity* Ω_r with stiffness tensor $\underline{\underline{L}}_r$ embedded in the matrix of stiffness tensor $\underline{\underline{L}}_0$ which had been previously subjected to uniform strain $\underline{\underline{\varepsilon}}_0$ before the inhomogeneity was embedded (Figure 54). Thus,

$$(5.164) \quad \hat{\underline{\underline{L}}}_0 = \underline{\underline{L}}_0$$

and

$$(5.165) \quad \hat{\underline{\underline{\varepsilon}}}_0 = \underline{\underline{\varepsilon}}_0 .$$

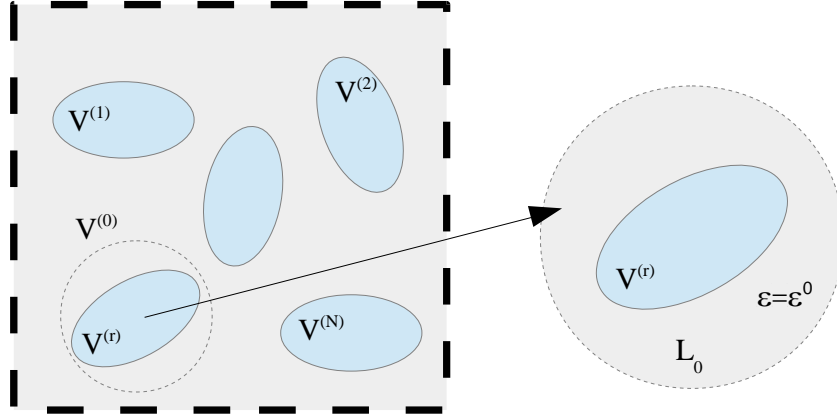


Figure 54 The Mori-Tanaka approach

The Eshelby tensor is computed with the actual stiffness tensor of the matrix, hence

$$(5.166) \hat{\underline{\underline{S}}}_r = \underline{\underline{S}}_r .$$

The only *difference* between the Eshelby and Mori-Tanaka methods is the *value* of the *previously induced strain* in the matrix. With the help of this strain tensor we can take into account the *perturbing effect* on the r -th inhomogeneity of the other inhomogeneities embedded in the matrix. The Eshelby method applies $\hat{\underline{\underline{\varepsilon}}}^0 = \underline{\underline{\varepsilon}}^0$, which is the strain in the matrix in the absence of any inhomogeneities. The Mori-Tanaka method assumes this strain field to be $\hat{\underline{\underline{\varepsilon}}}^0 = \bar{\underline{\underline{\varepsilon}}}_0$, where the averaged value of the strain is computed when all the inhomogeneities are present in the matrix. Otherwise, the latter method also does not take into account the other inhomogeneities, only the one in question.

The total strain inside the r -th inhomogeneity:

$$(5.167) \underline{\underline{\varepsilon}}_r = \bar{\underline{\underline{\varepsilon}}}_0 + \underline{\underline{\varepsilon}}_r^{pl} = \bar{\underline{\underline{\varepsilon}}}_0 + \underline{\underline{S}}_r \underline{\underline{\varepsilon}}_r^* = \underline{\underline{T}}_r \bar{\underline{\underline{\varepsilon}}}_0 ,$$

with

$$(5.168) \underline{\underline{T}}_r = \left(\underline{\underline{I}} + \underline{\underline{S}}_r \underline{\underline{L}}_0^{-1} (\underline{\underline{L}}_r - \underline{\underline{L}}_0) \right)^{-1} .$$

There is a great difference between (5.152) and (5.167): the previous one relates the total strain in the r -th inhomogeneity to the averaged strain of the whole material, while the latter one connects the total strain in Ω_r with the averaged strain in the surrounding matrix. Thus, in case of the Eshelby method we get the *global strain concentration* tensor, while the Mori-Tanaka yields the *local strain concentration* tensor:

$$(5.169) \underline{\underline{G}}_r = \underline{\underline{T}}_r .$$

From (5.37) the global strain concentration tensor:

$$(5.170) \underline{\underline{A}}_r = \underline{\underline{G}}_r \left(c_0 \underline{\underline{I}} + \sum_{r=1}^N c_r \underline{\underline{G}}_r \right)^{-1} = \underline{\underline{T}}_r \left(\sum_{r=0}^N c_r \underline{\underline{T}}_r \right)^{-1} .$$

Substituting into (5.31) yields the Mori-Tanaka estimate of the effective stiffness tensor:

$$(5.171) \quad \underline{\underline{\bar{L}}} = \underline{\underline{L}}_0 + \sum_{r=1}^N c_r (\underline{\underline{L}}_r - \underline{\underline{L}}_0) \underline{\underline{A}}_r = \sum_{r=0}^N c_r \underline{\underline{L}}_r \underline{\underline{T}}_r \left(\sum_{r=0}^N c_r \underline{\underline{T}}_r \right)^{-1}.$$

In order to determine the effective compliance tensor with the help of the Mori-Tanaka method, substituting

$$(5.172) \quad \underline{\underline{\bar{\varepsilon}}}_0 = \underline{\underline{M}}_0 \underline{\underline{\bar{\sigma}}}_0$$

into (5.167) yields

$$(5.173) \quad \underline{\underline{\sigma}}_r = \underline{\underline{L}}_r \underline{\underline{\varepsilon}}_r = \underline{\underline{L}}_r \underline{\underline{T}}_r \underline{\underline{M}}_0 \underline{\underline{\bar{\sigma}}}_0$$

The local stress concentration tensor for the r -th inhomogeneity from (5.36):

$$(5.174) \quad \underline{\underline{H}}_r = \underline{\underline{L}}_r \underline{\underline{T}}_r \underline{\underline{M}}_0.$$

The global stress concentration tensor from (5.38) is therefore

$$(5.175) \quad \underline{\underline{B}}_r = \underline{\underline{H}}_r \left(c_0 \underline{\underline{I}} + \sum_{r=1}^N c_r \underline{\underline{H}}_r \right)^{-1} = \underline{\underline{L}}_r \underline{\underline{T}}_r \underline{\underline{M}}_0 \left(\sum_{n=0}^N c_n \underline{\underline{L}}_n \underline{\underline{T}}_n \underline{\underline{M}}_0 \right)^{-1}.$$

The Mori-Tanaka estimate of the effective compliance tensor of the composite from (5.33):

$$(5.176) \quad \underline{\underline{\bar{M}}} = \underline{\underline{M}}_0 + \sum_{r=1}^N c_r (\underline{\underline{M}}_r - \underline{\underline{M}}_0) \underline{\underline{B}}_r = \sum_{r=0}^N c_r \underline{\underline{T}}_r \left(\sum_{n=0}^N c_n \underline{\underline{L}}_n \underline{\underline{T}}_n \right)^{-1}.$$

Examining the consistency of the Mori-Tanaka method yields

$$(5.177) \quad \underline{\underline{\bar{M}}} \underline{\underline{\bar{L}}} = \underline{\underline{I}}$$

for any c_r .

5.3.4 Self-consistent methods for composite materials

Let us assume that we know the effective properties $\underline{\underline{\bar{L}}}$ and $\underline{\underline{\bar{M}}}$ of the composite material under consideration. In case of heterogeneous materials with large number of inhomogeneities, if one inhomogeneity is removed from the matrix, the overall mechanical properties of the material will remain the same. It is conceivable that the effect of the applied loads and the other inhomogeneities on the r -th heterogeneity can be interpreted as if the r -th inhomogeneity was embedded in the matrix with stiffness tensor $\underline{\underline{\bar{L}}}$ that had been subjected to the uniform strain $\underline{\underline{\bar{\varepsilon}}}$ previously (Figure 55). Hence, the solution will be computed from the values

$$(5.178) \quad \hat{\underline{\underline{L}}}_0 = \underline{\underline{\bar{L}}},$$

$$(5.179) \quad \hat{\underline{\underline{\varepsilon}}}_0 = \underline{\underline{\bar{\varepsilon}}}$$

and

$$(5.180) \quad \hat{\underline{\underline{S}}}_r = \underline{\underline{\bar{S}}},$$

where the Eshelby tensor is dependent on the overall elastic properties of the composite material.

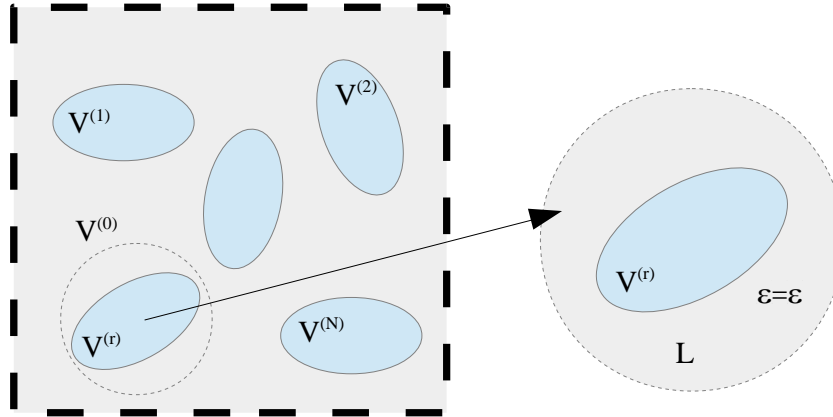


Figure 55 The self-consistent method

The total strain in the r -th inhomogeneity:

$$(5.181) \underline{\underline{\varepsilon}}_r = \underline{\underline{\varepsilon}} + \underline{\underline{\varepsilon}}_r^{pt} = \underline{\underline{\varepsilon}} + \underline{\underline{S}} \underline{\underline{\varepsilon}}_r^* = \underline{\underline{T}}_r \underline{\underline{\varepsilon}},$$

with

$$(5.182) \underline{\underline{T}}_r = \left(\underline{\underline{I}} + \underline{\underline{S}} \underline{\underline{L}}^{-1} (\underline{\underline{L}}_r - \underline{\underline{L}}) \right)^{-1}.$$

The stress field in the r -th inhomogeneity becomes

$$(5.183) \underline{\underline{\sigma}}_r = \underline{\underline{L}}_r \underline{\underline{\varepsilon}}_r = \underline{\underline{L}}_r \underline{\underline{T}}_r \underline{\underline{\varepsilon}} = \underline{\underline{L}}_r \underline{\underline{T}}_r \underline{\underline{M}} \underline{\underline{\sigma}}.$$

It is easy to see that the global strain and stress concentration tensors, respectively, are the following:

$$(5.184) \underline{\underline{A}}_r = \underline{\underline{T}}_r,$$

$$(5.185) \underline{\underline{B}}_r = \underline{\underline{L}}_r \underline{\underline{T}}_r \underline{\underline{M}}.$$

The improved values of the elastic stiffness and compliance tensors are, respectively:

$$(5.186) \underline{\underline{L}} = \underline{\underline{L}}_0 + \sum_{r=1}^N c_r (\underline{\underline{L}}_r - \underline{\underline{L}}_0) \underline{\underline{A}}_r = \underline{\underline{L}}_0 + \sum_{r=1}^N c_r (\underline{\underline{L}}_r - \underline{\underline{L}}_0) \underline{\underline{T}}_r,$$

$$(5.187) \underline{\underline{M}} = \underline{\underline{M}}_0 + \sum_{r=1}^N c_r (\underline{\underline{M}}_r - \underline{\underline{M}}_0) \underline{\underline{B}}_r = \underline{\underline{M}}_0 + \sum_{r=1}^N c_r (\underline{\underline{M}}_r - \underline{\underline{M}}_0) \underline{\underline{L}}_r \underline{\underline{T}}_r \underline{\underline{M}}.$$

The self-consistent method is therefore an *implicit method*, which results in a better approximation but it requires some numerical iterative technique.

Checking the *consistency* of this method yields

$$(5.188) \underline{\underline{M}} \underline{\underline{L}} = \underline{\underline{I}}$$

for any c_r .

In the previous sections we considered only composite materials, that is there was a distinct matrix material in which the inhomogeneities were embedded. In case of *polycrystalline* materials, there is no such matrix phase, therefore *all the inhomogeneities* are of the *same significance*. There is a self-consistent method developed for polycrystalline materials, which can be found in the literature that also yields implicit equations for the effective properties of the heterogeneous material, applying Hill's constraint tensor for the solution.

5.3.5 Differential schemes

There is another approach to determine the effective properties of a *relatively dilute composite material* with quite high accuracy. Let us consider first the matrix material with stiffness tensor $\underline{\underline{L}}_0$. Add a small amount (of volume fraction Δc) of inhomogeneities with elastic stiffness $\underline{\underline{L}}_1$. The effective stiffness tensor $\underline{\underline{L}}^{(1)}(\Delta c, \underline{\underline{L}}_0)$ can be computed from the elastic properties of the matrix ($\underline{\underline{L}}_0$) and the volume fraction of the inhomogeneities (Δc). In the next step add a small amount (Δc) of inhomogeneities to the composite material gained in the first step, but now the matrix material will bear the stiffness tensor $\underline{\underline{L}}^{(1)}(\Delta c, \underline{\underline{L}}_0)$. Thus, one can compute the elastic stiffness tensor $\underline{\underline{L}}^{(2)}(\Delta c, \underline{\underline{L}}^{(1)})$ of the newly created composite material with the volume fraction $2 \cdot \Delta c$ of inhomogeneities. These steps are to be continued until the actual volume fraction of inhomogeneities is reached. This method yields differential equations for the effective properties of the composite material as functions of the volume fraction of the inhomogeneities. This is the so-called **differential method**.

Assuming that the heterogeneous material consists only of two phases ($N = 1$): one kind of inhomogeneities embedded into the matrix phase, the effective stiffness tensor can be written in the form

$$(5.189) \quad \underline{\underline{L}}(c_1) = \underline{\underline{L}}_0 + c_1 (\underline{\underline{L}}_1 - \underline{\underline{L}}_0) : \underline{\underline{A}}_1(\underline{\underline{L}}_0),$$

where $\underline{\underline{A}}_1(\underline{\underline{L}}_0)$ indicates the dependence of the global strain concentration tensor on the elastic stiffness of the matrix phase and the symbol $:$ denotes the tensor product¹¹. The connection between the average strain in the inhomogeneities and the entire composite material:

$$(5.190) \quad \bar{\underline{\underline{\varepsilon}}}_1 = \underline{\underline{A}}_1(\underline{\underline{L}}_0) : \bar{\underline{\underline{\varepsilon}}}.$$

Assuming that the effective stiffness tensor $\underline{\underline{L}}(c_1)$ is known at the volume fraction

$$(5.191) \quad c_1 = \frac{\Omega_1}{\Omega_0 + \Omega_1},$$

¹¹ The tensor product is defined in case of fourth-order tensors $\underline{\underline{A}}$ and $\underline{\underline{B}}$ as $\underline{\underline{A}} : \underline{\underline{B}} = A_{ijmn} B_{nmkl} = C_{ijkl}$.

where Ω_0 and Ω_1 are the volumes of the matrix and the inhomogeneities, respectively. Now, let us consider a *fictitious matrix* with stiffness tensor $\underline{\underline{L}}(c_1)$ and add to this matrix a small amount $\Delta\Omega_1$ of inhomogeneities with the volume fraction $\frac{\Delta\Omega_1}{\Omega_0 + \Omega_1 + \Delta\Omega_1}$.

For such small amount of additional inhomogeneities the effective stiffness tensor can be determined from (5.189):

$$(5.192) \quad \underline{\underline{L}}(c_1 + \Delta c_1) = \underline{\underline{L}}(c_1) + \frac{\Delta\Omega_1}{\Omega_0 + \Omega_1 + \Delta\Omega_1} (\underline{\underline{L}}_1 - \underline{\underline{L}}(c_1)) : \underline{\underline{A}}_1(\underline{\underline{L}}(c_1)),$$

where Δc_1 denotes the increment of the volume fraction in the composite material due to the addition of inhomogeneities of volume $\Delta\Omega_1$. The total volume fraction in the composite material at this step is

$$(5.193) \quad c_1 + \Delta c_1 = \frac{\Omega_1 + \Delta\Omega_1}{\Omega_0 + \Omega_1 + \Delta\Omega_1},$$

therefore the increment is

$$(5.194) \quad \Delta c_1 = \frac{(1 - c_1)\Delta\Omega_1}{\Omega_0 + \Omega_1 + \Delta\Omega_1}.$$

Substituting into (5.192) yields

$$(5.195) \quad \frac{\underline{\underline{L}}(c_1 + \Delta c_1) - \underline{\underline{L}}(c_1)}{\Delta c_1} = \frac{1}{1 - c_1} (\underline{\underline{L}}_1 - \underline{\underline{L}}(c_1)) : \underline{\underline{A}}_1(\underline{\underline{L}}(c_1)).$$

In the limit of $\Delta c_1 \rightarrow 0$, a first-order differential equation is derived:

$$(5.196) \quad \frac{d\underline{\underline{L}}(c_1)}{dc_1} = \frac{1}{1 - c_1} (\underline{\underline{L}}_1 - \underline{\underline{L}}(c_1)) : \underline{\underline{A}}_1(\underline{\underline{L}}(c_1)),$$

with the initial condition

$$(5.197) \quad \underline{\underline{L}}(c_1) \Big|_{c_1=0} = \underline{\underline{L}}_0.$$

The dual pair of the above differential equation and initial condition consists of the elastic compliance tensor of the composite material:

$$(5.198) \quad \frac{d\underline{\underline{M}}(c_1)}{dc_1} = \frac{1}{1 - c_1} (\underline{\underline{M}}_1 - \underline{\underline{M}}(c_1)) : \underline{\underline{B}}_1(\underline{\underline{M}}(c_1)),$$

$$(5.199) \quad \underline{\underline{M}}(c_1) \Big|_{c_1=0} = \underline{\underline{M}}_0,$$

where the global stress concentration tensor of the inhomogeneity $\underline{\underline{B}}_1$ is defined as

$$(5.200) \quad \underline{\underline{M}}(c_1) = \underline{\underline{M}}_0 + c_1 (\underline{\underline{M}}_1 - \underline{\underline{M}}_0) : \underline{\underline{B}}_1(\underline{\underline{M}}_0).$$

Making use of the Eshelby estimation yields

$$(5.201) \underline{\underline{A}}_1(\bar{\underline{\underline{L}}}(c_1)) = \underline{\underline{T}}_1 \Big|_{\underline{\underline{L}}_0 = \bar{\underline{\underline{L}}}(c_1)} = \left(\underline{\underline{I}} + \underline{\underline{S}}_1 \left(\bar{\underline{\underline{L}}}^{-1} \underline{\underline{L}}_1 - \underline{\underline{I}} \right) \right)^{-1},$$

where all the quantities with an overbar are dependent on the volume fraction c .

The differential equation becomes

$$(5.202) \frac{d\bar{\underline{\underline{L}}}}{dc_1} = \frac{1}{1-c_1} \left(\underline{\underline{L}}_1 - \bar{\underline{\underline{L}}} \right) \left(\underline{\underline{I}} + \underline{\underline{S}}_1 \left(\bar{\underline{\underline{L}}}^{-1} \underline{\underline{L}}_1 - \underline{\underline{I}} \right) \right)^{-1},$$

with the initial condition

$$(5.203) \bar{\underline{\underline{L}}}(0) = \underline{\underline{L}}_0.$$

The Mori-Tanaka method combined with the differential approach defines the global strain concentration tensor of the inhomogeneities as

$$(5.204) \underline{\underline{A}}_1(\bar{\underline{\underline{L}}}(c_1)) = \underline{\underline{T}}_1 \left((1-c_1) \underline{\underline{I}} + c_1 \underline{\underline{T}}_1 \right)^{-1} \Big|_{\underline{\underline{L}}_0 = \bar{\underline{\underline{L}}}(c_1)}.$$

The differential equation at the Mori-Tanaka approach:

$$(5.205) \frac{d\bar{\underline{\underline{L}}}}{dc_1} = \frac{1}{1-c_1} \left(\underline{\underline{L}}_1 - \bar{\underline{\underline{L}}} \right) \underline{\underline{T}}_1 \left((1-c_1) \underline{\underline{I}} + c_1 \underline{\underline{T}}_1 \right)^{-1} \Big|_{\underline{\underline{L}}_0 = \bar{\underline{\underline{L}}}(c_1)},$$

with the initial condition (5.203).

It is clearly visible that the differential schemes yield a set of *highly nonlinear ordinary differential equations*, which can only be solved with the help of numerical techniques.

6 Analytical and numerical homogenization

6.1 Analytical homogenization

In this section, I compute the effective stiffness tensor and therefore, the effective Young's modulus and Poisson's ratio of a heterogeneous material consisting of a distinct matrix material in which ellipsoidal inhomogeneities are embedded. The calculation is based on some of the analytical homogenization methods presented in the previous sections, namely I applied the *Voigt upper* (5.57) and *Reuss lower bounds* (5.58), and the *Eshelby* (5.156) and *Mori-Tanaka estimations* (5.171).

In order to compute the effective material properties for any given input parameter, I wrote a *Matlab*TM code with input data including the volume fraction c_i , Young's modulus E_i and Poisson's ratio ν_i of phases $i = 0, \dots, N$, where $i = 0$ always refers to the matrix phase. The Eshelby and Mori-Tanaka estimations take into account the geometry of the inhomogeneities by involving the fourth-order Eshelby-tensor S_{ijkl} in the analytical methods. Formulae for the Eshelby tensor (3.33) for specially shaped inhomogeneities are given in function of the I -integrals (3.42)-(3.44) in (Mura, 1987). My analytical results are based on the Eshelby tensor computed with the help of a *Matlab*TM code developed by Chunfang Meng (Meng, Heltsley,

& Pollard, 2012; Meng & Pollard, 2014). This code evaluates the solutions by Eshelby for the quasi-static elastic fields inside an ellipsoidal inhomogeneity with arbitrary semi-axial lengths a_1, a_2, a_3 ($a_1 > a_2 > a_3$) and in the surrounding infinite elastic body. The inhomogeneity and the matrix are both of homogeneous and isotropic materials, and the interface between them is perfectly bonded.

6.1.1 Two-phase heterogeneous material

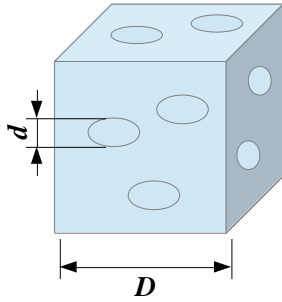


Figure 56 Representative volume element of concrete

First, I examine a block of concrete with the size of $100 \times 100 \times 100$ mm, that is, I consider the RVE of concrete (Bojtár, 2014) consisting of two different phases (Figure 56). The matrix material is portland cement and the inhomogeneities are ellipsoidal-shaped aggregates with ≈ 10 mm average length of semi-axes. Therefore, the condition on the ratio between the micro- and macroscale length to be sufficiently small is satisfied:

$$\frac{d}{D} \approx \frac{20}{100} = 0.2.$$

The known material properties E (Young's modulus) and ν (Poisson's ratio) of the individual phases must be converted into a 6-by-6 elastic stiffness matrix of isotropic material:

$$(6.1) \quad L_{ijkl} = \frac{E}{(1+\nu)(1-2\nu)} \begin{bmatrix} 1-\nu & \nu & \nu & 0 & 0 & 0 \\ \nu & 1-\nu & \nu & 0 & 0 & 0 \\ \nu & \nu & 1-\nu & 0 & 0 & 0 \\ 0 & 0 & 0 & 1-2\nu & 0 & 0 \\ 0 & 0 & 0 & 0 & 1-2\nu & 0 \\ 0 & 0 & 0 & 0 & 0 & 1-2\nu \end{bmatrix}.$$

Hence, the two individual elements of the matrix can be computed from

$$(6.2) \quad L_{12} = \frac{E\nu}{(1+\nu)(1-2\nu)},$$

$$(6.3) \quad L_{11} = \frac{1-\nu}{\nu} L_{12}.$$

We talk about particle-reinforced materials if the ratio of the semi-axes of ellipsoids are not too high: $\frac{a_i}{a_j} \approx 1 \div 10$ ($i \neq j$). Isotropic materials have infinite planes of symmetry, that is, the

material properties are independent of the orientation. Particle-reinforced materials are assumed to be isotropic materials. This behaviour is not to be mistaken with the different strengths (compressive and tensile strength) of concrete with respect to the type of loading. Though, in general, concrete without any reinforcement is a particle-reinforced material, in my calculations, I also applied ellipsoids with high semi-axes ratio acting as small fibers, which resulted in a fiber reinforced composite. According to (Barbero, 2014), a transversely

isotropic material has one axis of symmetry, and in case of a unidirectional fiber reinforced composite, the fiber direction can be considered as an axis of symmetry if the fibers are randomly distributed in the cross-section. Since the Eshelby-tensor cannot take into account the orientation of the inhomogeneity, only the shape of it, let us suppose that all the fibers have the same orientation. The basic assumption of the presented homogenization methods was the random distribution of inhomogeneities in the matrix material, therefore, both requirements are satisfied to consider the investigated concrete as a transversely isotropic material. The only problem is the fact, that homogenization methods work with the given material stiffness matrices of the individual phases, which were originally considered to be isotropic materials. Furthermore, the Eshelby-tensor is also calculated for isotropic materials.

First, I have to convert the fourth-order material stiffness tensor L_{ijkl} into a 6-by-6 elastic stiffness matrix such that

$$(6.4) \quad \sigma_{ij} = L_{ijkl} \varepsilon_{kl},$$

where σ_{ij} and ε_{ij} are the stress and strain tensors, respectively. Due to the minor symmetry of the material stiffness tensor $L_{ijkl} = L_{jikl} = L_{ijlk} = L_{jilk}$ and the symmetry of the stress and strain tensors $\sigma_{ij} = \sigma_{ji}$ and $\varepsilon_{ij} = \varepsilon_{ji}$, the fourth-order tensor can be converted into a 6-by-6 matrix and the second-order tensors can be written in vectorial form following Voigt notation. The equation (6.4) can be rewritten as

$$(6.5) \quad \underline{\sigma} = \underline{L} \underline{\varepsilon}.$$

The indices of the second-order tensors (ij) and the fourth-order tensors ($ijkl$) in contracted form:

$$(6.6) \quad \begin{bmatrix} (11) \\ (22) \\ (33) \\ (23) \\ (13) \\ (12) \end{bmatrix} = \begin{bmatrix} (1111) & (1122) & (1133) & (1123) & (1113) & (1112) \\ (2211) & (2222) & (2233) & (2223) & (2213) & (2212) \\ (3311) & (3322) & (3333) & (3323) & (3313) & (3312) \\ (2311) & (2322) & (2333) & (2323) & (2313) & (2312) \\ (1311) & (1322) & (1333) & (1323) & (1313) & (1312) \\ (1211) & (1222) & (1233) & (1223) & (1213) & (1212) \end{bmatrix} \begin{bmatrix} (11) \\ (22) \\ (33) \\ (23) \\ (13) \\ (12) \end{bmatrix},$$

which I applied in the Matlab™ code as well.

The elastic stiffness matrix of isotropic materials :

$$(6.7) \quad \underline{\underline{L}} = \begin{bmatrix} L_{11} & L_{12} & L_{12} & 0 & 0 & 0 \\ L_{12} & L_{11} & L_{12} & 0 & 0 & 0 \\ L_{12} & L_{12} & L_{11} & 0 & 0 & 0 \\ 0 & 0 & 0 & \frac{L_{11} - L_{12}}{2} & 0 & 0 \\ 0 & 0 & 0 & 0 & \frac{L_{11} - L_{12}}{2} & 0 \\ 0 & 0 & 0 & 0 & 0 & \frac{L_{11} - L_{12}}{2} \end{bmatrix}.$$

Therefore, the elastic modulus of an isotropic material:

$$(6.8) \quad E = L_{11} - \frac{2L_{12}^2}{L_{11} + L_{12}},$$

the Poisson's ratio:

$$(6.9) \quad \nu_{12} = \frac{L_{12}}{L_{11} + L_{12}},$$

and the shear modulus:

$$(6.10) \quad G = \frac{L_{11} - L_{12}}{2}.$$

It is very important that the formulae for effective properties in homogenization methods are given in function of fourth-order tensors. Thus, when calculating the inverse of 6-by-6 matrices in contracted form, one has to apply the formula given in footnote '4' on page 34.

About the geometry of the inhomogeneities, I applied both spheres, where the radius equals to the semiaxes of an ellipsoid ($a_1 = a_2 = a_3$) and spheroids, that is, such ellipsoids, that are generated from rotating an ellipse about one of the axes of the ellipsoid. There are two types of spheroids: the *oblate spheroid* (Figure 57), where the axis of rotation is the minor axis, hence its size is $a_1 = a_2 > a_3$, and it is a flat ellipsoid. The other type is the *prolate spheroid* (Figure 58), where the ellipse is rotated about the major axis of the ellipsoid, therefore $a_1 > a_2 = a_3$ producing an elongated ellipsoid. The sections with normal vector parallel to the axis of rotation are always circles (disks).

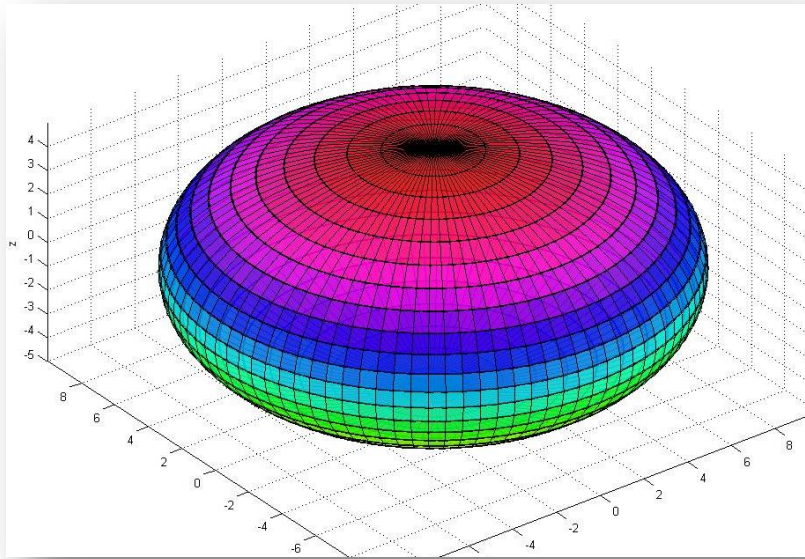


Figure 57 *Oblate spheroid*

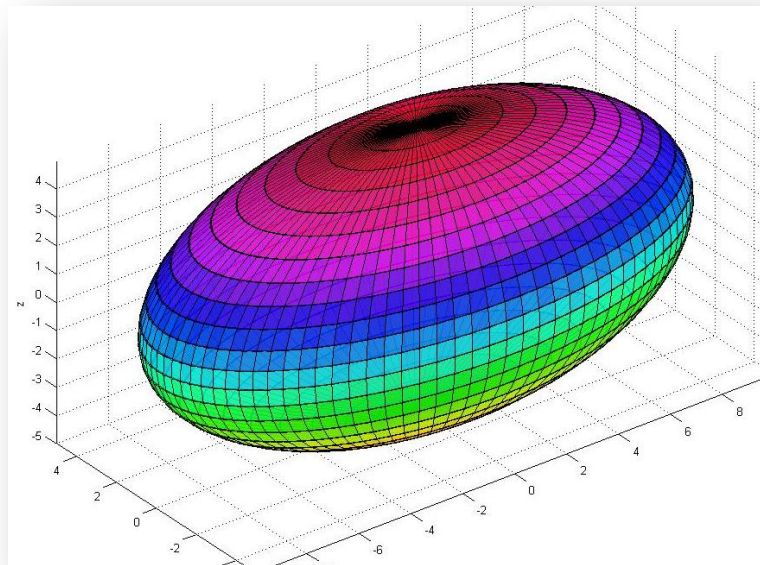


Figure 58 *Prolate spheroid*

When the ratio of major to minor semi-axes $\frac{a_1}{a_3}$ tends to infinity, the oblate spheroid becomes a *penny-shape* inhomogeneity (Figure 59), which is the usual geometric model of cracks, and the prolate spheroid becomes a *needle-type* inhomogeneity (Figure 60), that can be interpreted as fiber reinforcements (steel, carbon, glass, etc.).

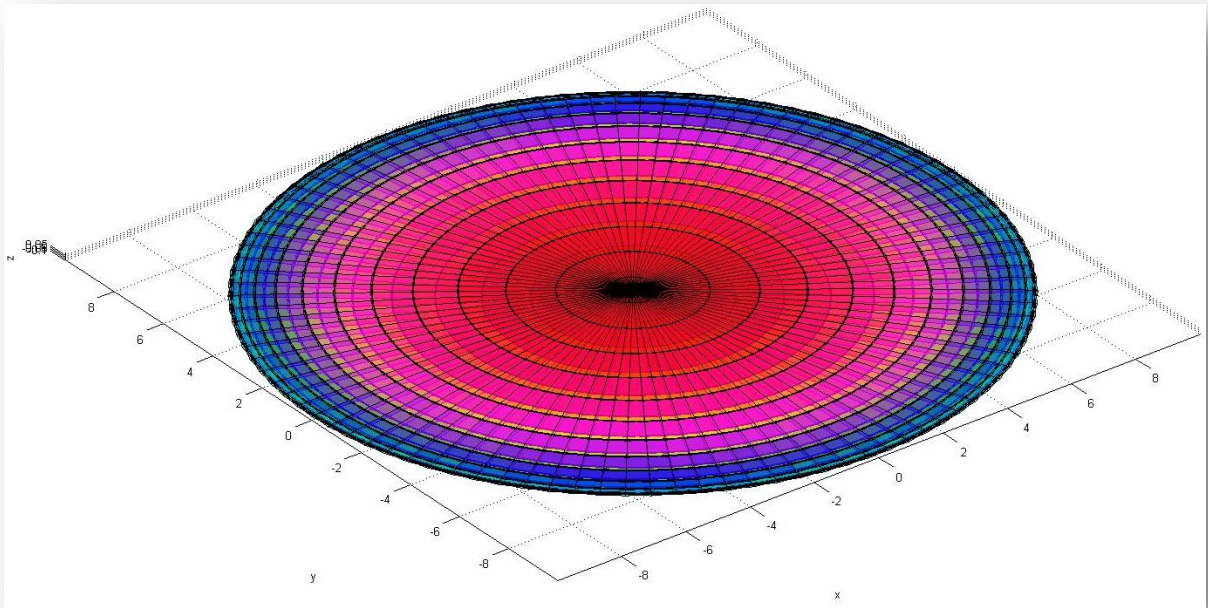


Figure 59 Penny-shape spheroid

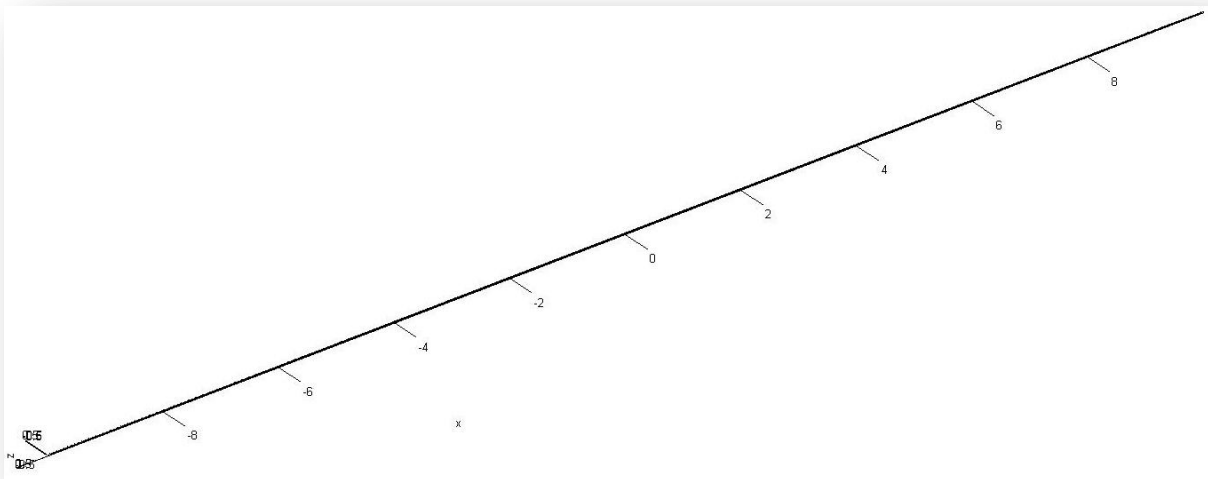


Figure 60 Needle-type spheroid

When examining spheres, the Matlab™ code computing the Eshelby tensor only works with different lengths of semi-axes $a_1 > a_2 > a_3$, and calculates the I -integrals for spheres, if both

$$\frac{a_1 - a_2}{a_1} < 10^{-6} \text{ and } \frac{a_2 - a_3}{a_1} < 10^{-6} \text{ are satisfied.}$$

With the help of analytical methods, I investigate the change in the effective elastic modulus, Poisson's ratio and shear modulus of the heterogeneous material by varying one of the input data while fixing the others.

The material properties I applied in case of portland cement: $E = 20 \div 35$ GPa , $\nu = 0.15$. As for the aggregates, the engineering properties are dependent on the type of the applied material. From common gravel to basalt, the Young modulus can be $E = 1 \div 100$ GPa and the Poisson's ratio $\nu = 0.1 \div 0.4$. In most of my calculations, I set the properties of aggregates to result in a strong inhomogeneity, i.e. $E_{\text{matrix}} \approx 20$ GPa $< E_{\text{inhomogeneity}} \approx 30$ GPa . In general, the volume fraction of cement is $20 \div 40\%$, thus, the volume fraction of aggregates is $80 \div 60\%$, which means the dominant phase in the heterogeneous material is the aggregate. One might expect that the Poisson's ratio of the examined concrete to be $\nu = 0.1 \div 0.2$ and the Young's modulus to be $E = 17 \div 25$ (35) GPa , where the highest values are reached in case of very stiff aggregates.

6.1.1.1 Effect of volume fraction

The fixed input data:

$$a_1 = 10 \text{ mm}, a_2 = 9.999999 \text{ mm}, a_3 = 9.999998 \text{ mm} ,$$

$$E_0 = 20 \text{ GPa}, \nu_0 = 0.15 ,$$

$$E_1 = 30 \text{ GPa}, \nu_1 = 0.2 ,$$

where the conditions to calculate with I -integrals for spheres are satisfied. The initial volume fractions:

$$c_0 = 0.2, c_1 = 0.8 .$$

In all the calculations, the subscript '0' refers to the matrix phase, and '1' to the inhomogeneity, i.e. to the cement and aggregates, respectively.

The results can be seen in Figure 61:

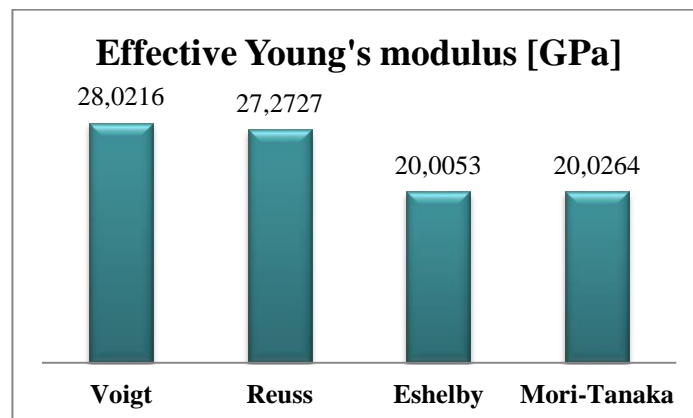


Figure 61 Effective properties in case of spherical inclusions

The Eshelby and Mori-Tanaka methods are suspected of yielding bad results, since the Reuss estimations produces a lower bound of the effective Young's modulus, and the volume fraction of the strong inhomogeneities are four times greater, than that of the softer matrix, so the overall elastic modulus should be closer to 30 GPa, than to 20 GPa. Since the Eshelby and

Mori-Tanaka method uses the Eshelby-tensor dependent on the geometry of the inhomogeneity, let us approximate the sphere by an ellipsoid:

$$a_1 = 10 \text{ mm}, a_2 = 9.9 \text{ mm}, a_3 = 9.8 \text{ mm},$$

and the results (Figure 62):

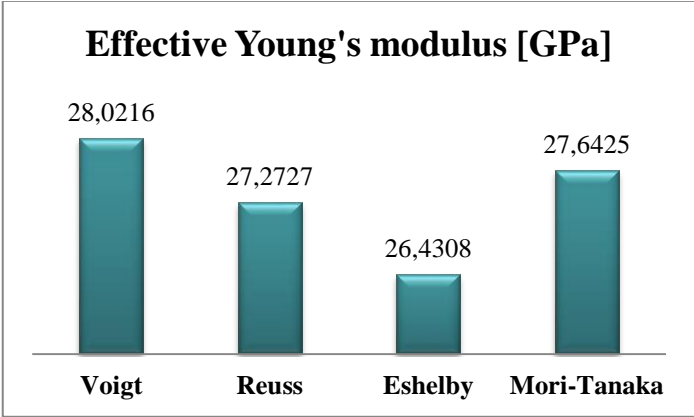


Figure 62 Effective properties in case of ellipsoidal inclusions

It is clearly visible, that the Eshelby tensor for spheres does not yield correct results, hence, I will concentrate only on ellipsoidal inhomogeneities. The Mori-Tanaka estimation is between the permitted bounds, yet the Eshelby approximation still falls behind the Reuss lower bound. Anyhow, let us increase the volume fraction of the matrix while fixing the geometry and the engineering constants of the composite (Figure 63):

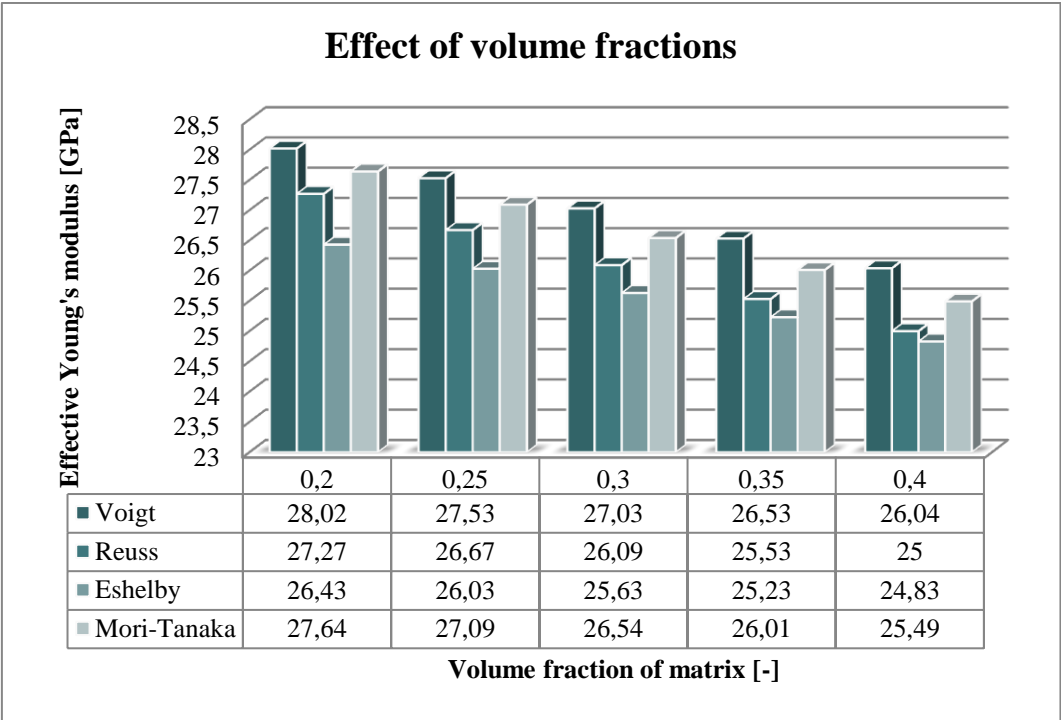


Figure 63 Effect of volume fractions on overall material properties

Due to the increase of the volume fraction of the softer material to twice of its original value, the overall elastic modulus decreases to approximately 90% of its initial value. What is quite

interesting is that the difference between the Reuss lower bound and the Eshelby estimate decreases from 3.2% to 0.7%, which means that the Eshelby method yields better results in case of dilute composites. Apart from concrete, if the volume fractions of each phase were 50-50%, the effective modulus resulted by the Eshelby method would already exceed the Reuss lower bound.

The other engineering constant, Poisson's ratio follows the same tendency as Young's modulus. Since the shear modulus can be calculated from these two as

$$(6.11) \quad G = \frac{E}{2(1+\nu)},$$

and the change in the elastic modulus is 'faster' than that of the Poisson's ratio, the shear modulus will also be linearly dependent on the elastic modulus. In other words, if the Young's modulus increases, then the Poisson's ratio and hence, the shear modulus increase as well.

6.1.1.2 Effect of Young's modulus

The fixed input data:

$$a_1 = 10 \text{ mm}, a_2 = 9.9 \text{ mm}, a_3 = 9.8 \text{ mm},$$

$$E_1 = 30 \text{ GPa}, \nu_1 = 0.2, \nu_0 = 0.15,$$

$$c_0 = 0.4, c_1 = 0.6.$$

Since the most accurate results of the Eshelby approximation come from a dilute concentration of inhomogeneities, I set their volume fraction to be the smallest possible. By increasing the value of the elastic modulus of cement, the change in the overall modulus can be seen in Figure 64.

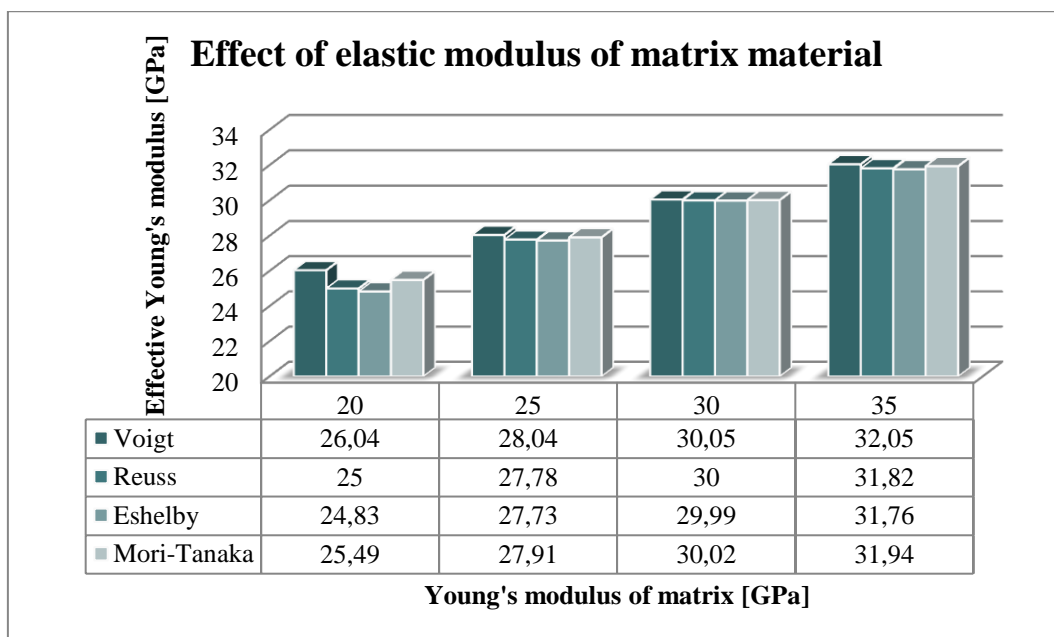


Figure 64 Effect of elastic modulus of matrix material on effective material properties

It is clearly visible that the smaller the difference in the material property of the distinct phases, the closer the estimations are. For example, in case of homogeneous material, when both the inhomogeneities and the matrix bear the elastic modulus of $E_0 = E_1 = 30$ GPa, the 0.2% difference between the Voigt upper bound and the Eshelby estimation is due to the rounding errors of the computation.

The same tendency can be seen when fixing the material properties

$$E_0 = 20 \text{ GPa}, \nu_0 = 0.15, \nu_1 = 0.2,$$

Increasing the Young's modulus of the heterogeneity in the interval $E_1 = 10 \div 50$ GPa (Figure 65):

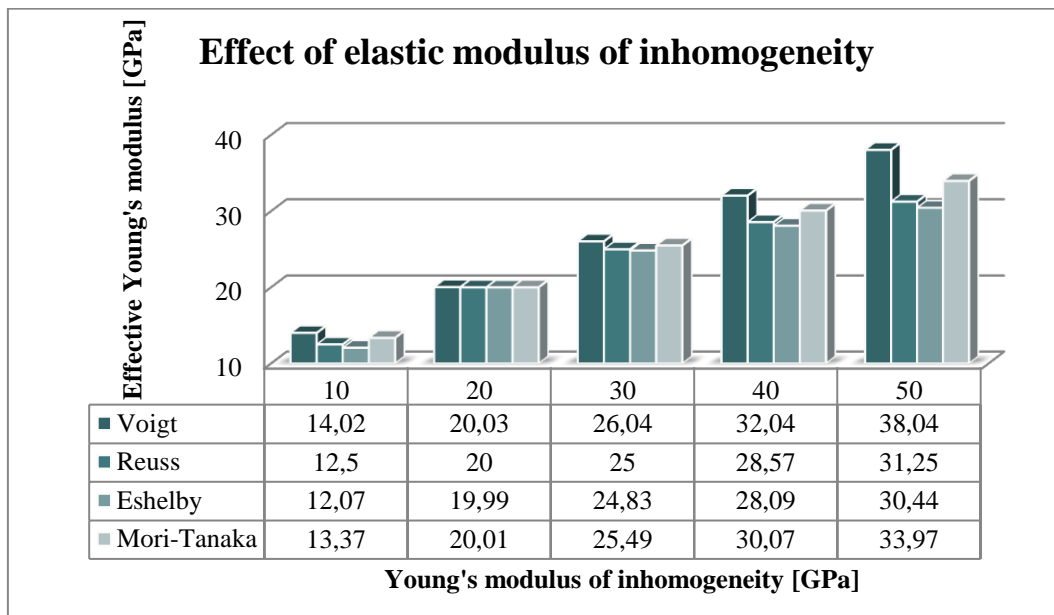


Figure 65 Effect of elastic modulus of inhomogeneity on effective material properties

It is also to be noticed, that the quality of the applied aggregates have great effect on the overall material properties of the heterogeneous material. A stiff aggregate like crushed rock ($E_1 = 50$ GPa) contributes to the macroscale behavior of the concrete as it will bear 2.5 times larger stresses with the same deformations than a concrete with five times softer aggregates ($E_1 = 10$ GPa). In this configuration, the connection between the changes in the elastic

modulus of inhomogeneity and the heterogeneous material:
$$\frac{\Delta E_{\text{effective}}}{\Delta E_1} = \frac{1}{2}.$$

On the other hand, the difference between the estimated overall moduli at a particular value of Young's modulus of inhomogeneity is quite large. In the last column, the Voigt upper bound shows an overall elastic moduli 25% larger than the Eshelby approximation.

6.1.1.3 Effect of size of inhomogeneity

The Eshelby- and Mori-Tanaka approximation needs the geometry of the inhomogeneity as an input data, therefore let us investigate the effect of the size of inhomogeneity on the overall elastic modulus (Figure 66) of the material, when

$$E_0 = 20 \text{ GPa}, \nu_0 = 0.15,$$

$$E_1 = 30 \text{ GPa}, \nu_1 = 0.2,$$

$$c_0 = 0.4, c_1 = 0.6,$$

and the ratio between the semi-axes are held to be constant.

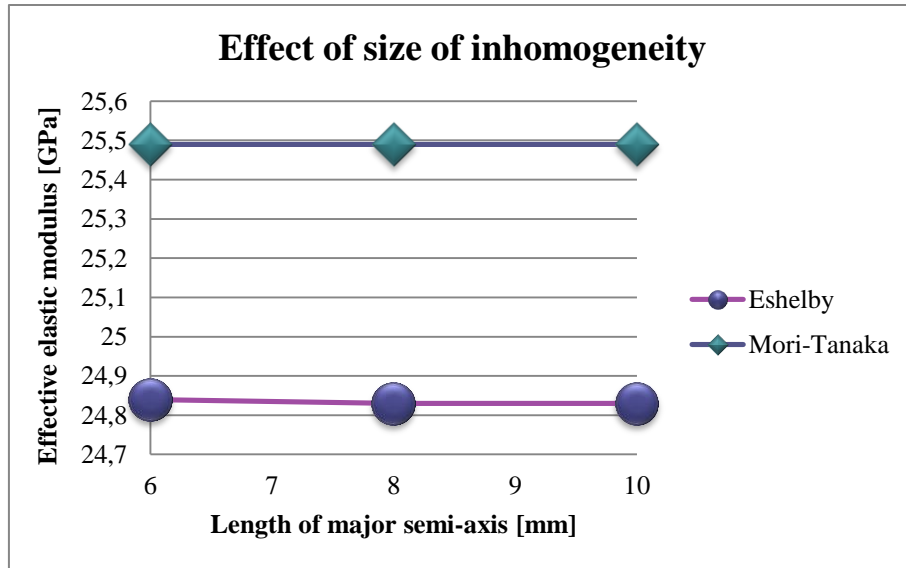


Figure 66 Effect of size of inhomogeneity at constant value of volume fractions

Since the Eshelby tensor is only dependent on the shape of the inhomogeneity, that is, on the ratio between the semi-axes, the overall properties does not change when we consider the same volume fraction of larger and smaller inhomogeneities of the same shape.

Now, let us see the change in the effective material properties (Figure 67) when decreasing the size of the inhomogeneities while fixing their shape, but this time, the volume fraction of them shall be decreased simultaneously, while the volume fraction of the matrix is increased:

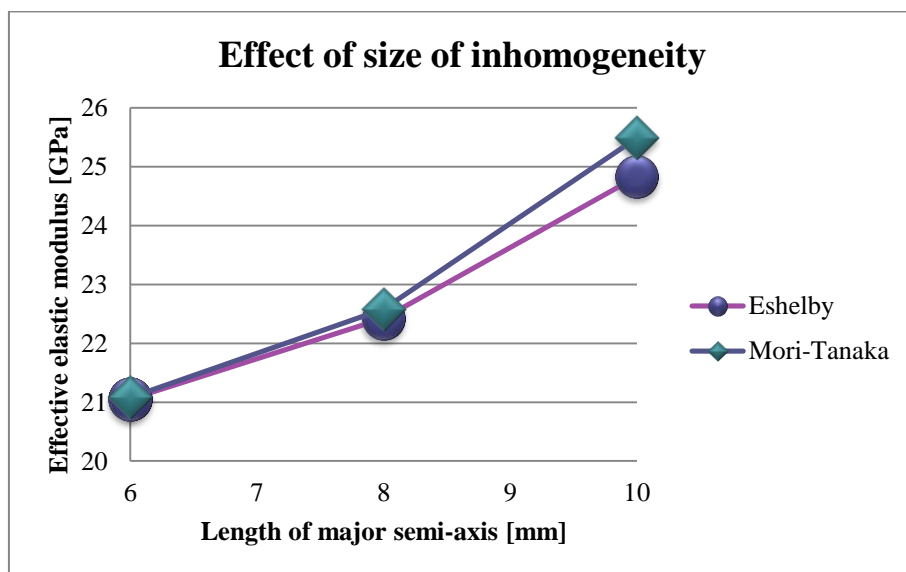


Figure 67 Effect of size of inhomogeneity while varying the value of volume fractions

As it can be seen in Figure 63, the change in the volume fraction yields an approximately linearly dependent change in the effective properties. Since the volume fraction is a cubic function of the length of semi-axes, the function in Figure 67 can be estimated by a higher-order polynomial.

6.1.1.4 Effect of shape of inhomogeneity

Let us consider an initial configuration with properties

$$E_0 = 20 \text{ GPa}, \nu_0 = 0.15,$$

$$E_1 = 30 \text{ GPa}, \nu_1 = 0.2,$$

$$c_0 = 0.4, c_1 = 0.6,$$

and follow the changes in the overall elastic modulus by varying the shape of the inhomogeneity. First, the heterogeneity is an oblate spheroid (Figure 57) with lengths of semi-axes

$$a_1 = 10 \text{ mm}, a_2 = 9.9 \text{ mm}, a_3 = 8 \text{ mm}.$$

By increasing the ratio of major to minor semi-axes $\frac{a_1}{a_3} = 1.25$ to $\frac{a_1}{a_3} = 100$, the oblate

spheroid becomes a penny-shaped inhomogeneity (Figure 59). During the calculations, I change the length of the minor axis only, and hence, the volume fractions as well (Figure 68).

In case of $\frac{a_1}{a_3} = 100$ the volume fractions become $c_0 = 0.994$, $c_1 = 0.006$. This cannot be a possible model for real concrete, still the changes in the effective properties can be observed.

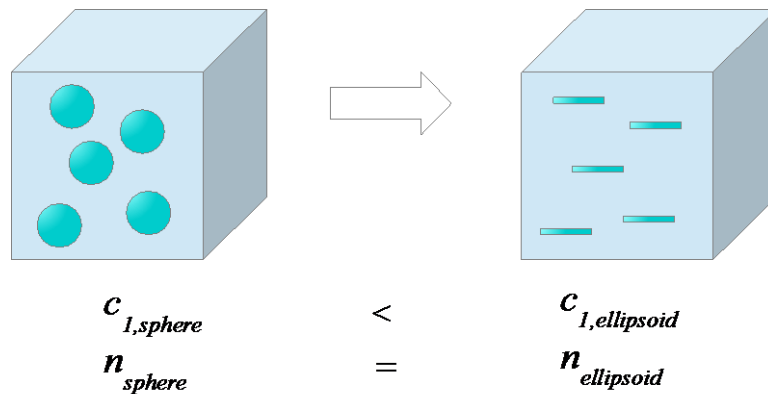


Figure 68 Changing the shape of inhomogeneities at constant number of heterogeneities

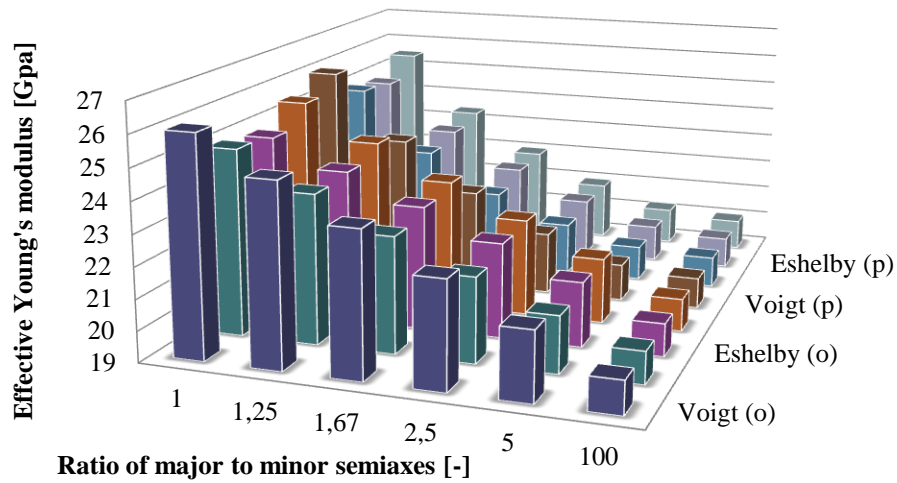
I also examine prolate spheroids (Figure 58) with initial size of

$$a_1 = 10 \text{ mm}, a_2 = 8 \text{ mm}, a_3 = 7.9 \text{ mm}.$$

The change in the ratio $\frac{a_1}{a_3}$ is the same as in case of oblate spheroids, but this time, $\frac{a_1}{a_3} = 100$

results in needle-type inhomogeneities (Figure 60).

Effect of geometry of inhomogeneity



	1	1,25	1,67	2,5	5	100
■ Voigt (o)	26,04	24,84	23,64	22,43	21,22	20,06
■ Reuss (o)	25	23,81	22,73	21,74	20,83	20,04
■ Eshelby (o)	24,83	23,92	23	22,07	21,09	20,06
■ Mori-Tanaka (o)	25,49	24,31	23,2	22,15	21,11	20,06
■ Voigt (p)	26,04	23,84	22,23	21,02	20,2	20
■ Reuss (p)	25	22,9	21,58	20,69	20,13	20
■ Eshelby (p)	24,83	23,16	21,91	20,92	20,2	20
■ Mori-Tanaka (p)	25,49	23,39	21,97	20,93	20,2	20

Figure 69 Effect of shape of inhomogeneity on the effective material properties

The first column in Figure 69 shows the heterogeneous material with the spherical-shaped inhomogeneities as a guideline. The upper part of the chart consists of the results coming from the heterogeneous material with oblate-spheroids, and the lower part from that with prolate-spheroids. Both of them tend to the value of the elastic modulus of the matrix ($E_0 = 20 \text{ GPa}$), since the volume fraction of the inhomogeneities tends to zero. The diagram in Figure 70 shows that the change can be approximated by a higher-order polynomial. The solid lines indicate the lower and upper bounds for the oblate (o) and prolate (p) cases. Excluding the spherical-shaped heterogeneities, the Eshelby and Mori-Tanaka methods yield values between these bounds, hence they work properly. According to these results, considering a constant number of inhomogeneities, those who have an almost spherical shape, yield the highest overall elastic modulus. Please note, that in this case, the number of the inhomogeneities were fixed, hence, by having smaller and more distorted heterogeneities, their volume fraction will decrease strongly.

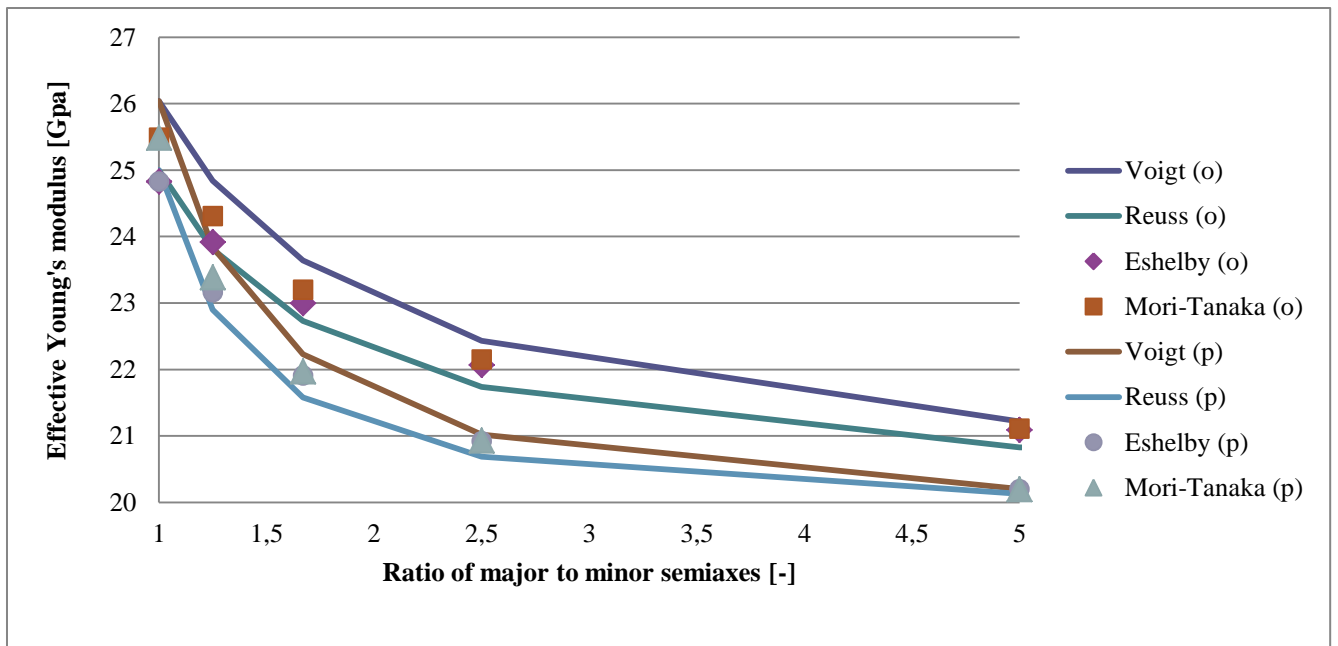


Figure 70 Effect of oblate (o) and prolate (p) spheroidal inhomogeneities

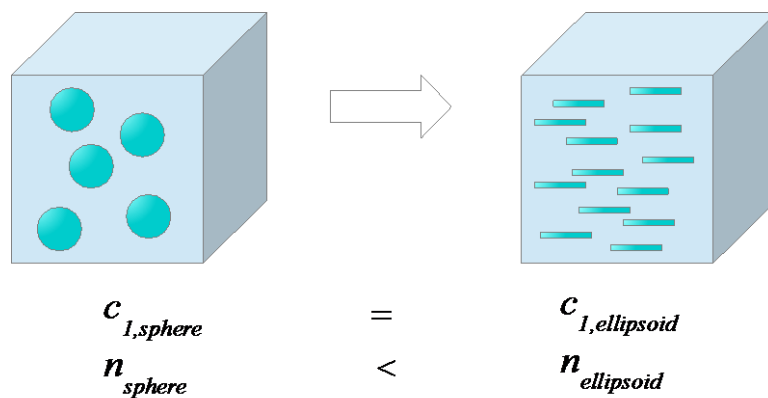


Figure 71 Changing the shape of inhomogeneities at constant value of volume fraction of heterogeneities

Now let us consider the case, when the *volume fraction of the inhomogeneities is held constant* (Figure 71), and the smaller their size – and simultaneously the more distorted their shape – , the higher their number inside the examined RVE of concrete (Figure 72):

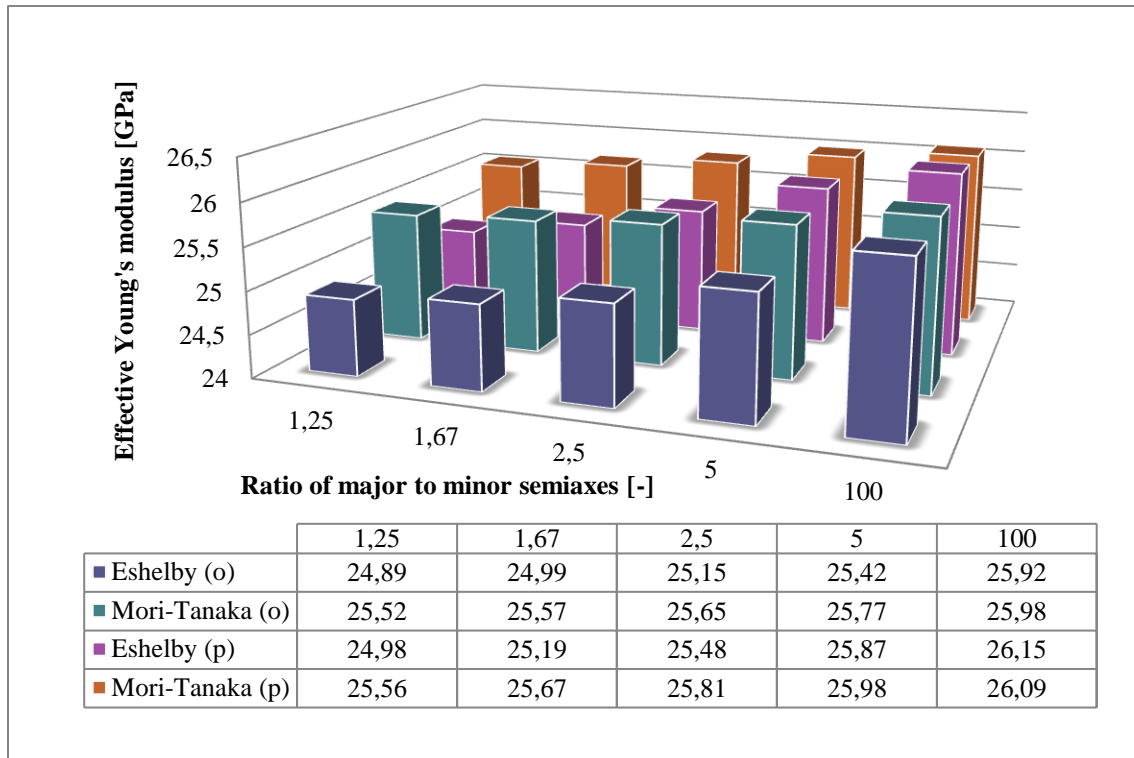


Figure 72 Effect of shape of inhomogeneity at constant value of volume fractions

It is quite interesting, that in case of given volume fraction of aggregates, the penny-shaped and needle-type heterogeneities yield the stiffest concrete. On the other hand, the difference between the cases when $\frac{a_1}{a_3} = 1.25$ and $\frac{a_1}{a_3} = 100$ is only 4.5% at the Eshelby method and 2% at the Mori-Tanaka approximation. It can also be seen that the prolate spheroids result in higher values of macroscale properties.

6.1.2 Three- and four-phase heterogeneous material

With the help of three-phase model (Figure 73), I will consider the effect of voids inside the concrete. Phase ‘0’ refers to portland cement, phase ‘1’ to ellipsoidal shaped aggregates and phase ‘2’ to spherical voids. The size of aggregates:

$$a_1 = 10 \text{ mm}, a_2 = 6.1 \text{ mm}, a_3 = 6 \text{ mm},$$

and that of voids:

$$a_1 = 0.5 \text{ mm}, a_2 = 0.49 \text{ mm}, a_3 = 0.48 \text{ mm}.$$

The material properties and volume fractions:

$$E_0 = 20 \text{ GPa}, \nu_0 = 0.15,$$

$$E_1 = 30 \text{ GPa}, \nu_1 = 0.2,$$

$$c_0 = 0.4, c_1 = 0.55, c_2 = 0.05.$$

In case of voids, the Reuss lower bound cannot be calculated, since it needs the inverse of the material stiffness matrix of each phase, therefore the existence of voids leads to singularities. The difference between the two-phase model and the three-phase model can be seen in Table 1:

Table 1 Results of a three-phase model

		Effective elastic modulus (GPa)		
		Voigt	Eshelby	Mori-Tanaka
c_2	0	26,04	25,19	25,67
	0,05	24,53	22,84	22,94

When considering 5V% of voids in concrete, the effective Young’s modulus decreases to 90% of its original value.

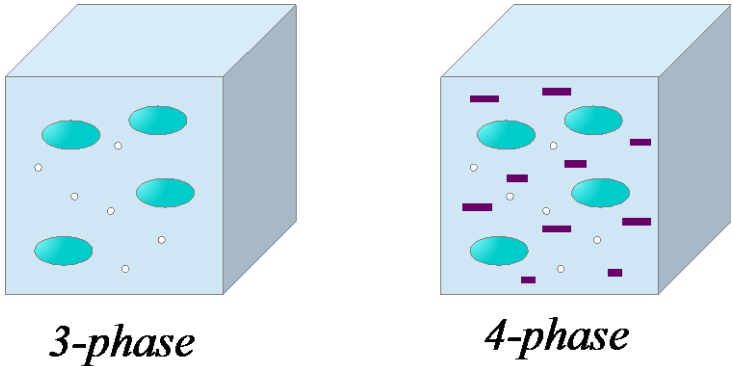


Figure 73 Three- and four-phase models of heterogeneous materials

Finally, I examine the overall material property of a steel fiber-reinforced concrete as a four-phase heterogeneous model (Figure 73) with the same input data presented above, complemented by

$E_3 = 200 \text{ GPa}, \nu_3 = 0.3,$
 $c_3 = 0.03,$ therefore $c_1 = 0.52,$
 $a_1 = 1 \text{ mm}, a_2 = 0.002 \text{ mm}, a_3 = 0.001 \text{ mm}.$

The steel fibers are modelled as needle-type inhomogeneities. The results (Table 2):

Table 2 Results of a four-phase model

				Effective elastic modulus (GPa)		
				Voigt	Eshelby	Mori-Tanaka
c_2	0	c_3	0	26,04	25,19	25,67
	0,05		0	24,53	22,84	22,94
	0,05		0,03	29,86	28,78	29,03

Adding 3V% of steel fibers to the concrete results in approximately 25% increase in the value of the overall elastic modulus.

Summarizing the results of analytical homogenization, the problem of all methods is the lack of ability to take into account the orientation and the real distribution of the inhomogeneities inside the RVE. The size of the heterogeneities (Figure 66) is considered only by the condition between the micro-length d and macro-length D as $\frac{d}{D} \ll 1$. Neither can the analytical solution take into account the number of inhomogeneities and the distance between them. These methods assume the heterogeneities to be normally distributed throughout the RVE, hence, for example the problem of segregation in concrete cannot be investigated.

The Eshelby estimation can only be used in case of dilute concentration of heterogeneities, otherwise it falls behind the lower bound predicted by the Reuss approximation. Moreover, the higher the ratio of the elastic moduli of individual phases, the larger the difference between the results of the analytical methods. Hence, better bounds would be useful when predicting the overall material properties of heterogeneous materials.

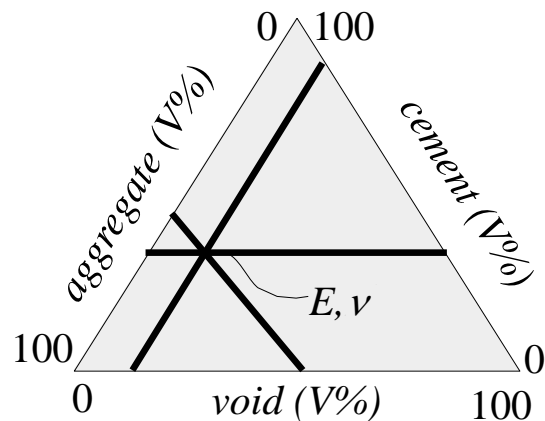


Figure 74 Expected effective material properties of concrete with given volume fractions of cement, aggregates and voids

The advantage of the analytical solutions is obtaining quick results from few input data. There is no need to build a numerical model, which is quite time-consuming, not to mention the computational time of a three-dimensional finite element calculation. A lot of phases can be incorporated in one model, with different material properties and/or shapes. It can be applied at preparing laboratory experiments (Figure 74), at designing new materials or developing already existing ones. Semi-empirical analytical homogenization methods would also be reasonable, by fitting them to results coming from experiments.

6.2 Numerical homogenization

In the previous section I computed the overall material properties of a heterogeneous material based on analytical formulae derived in (Qu & Cherkaoui, 2006). In the following, I show the calculation of overall material stiffness matrix $\underline{\underline{L}}$ using finite element software (Barbero, 2014). The results will be compared to that of the analytical homogenization.

6.2.1 Derivation of overall material properties by numerical homogenization

The effective material stiffness matrix of a transversely isotropic composite material can be derived from column to column. As it was shown at the analytical homogenization, due to the random microstructure of a heterogeneous material, the behaviour of the material is presumed to be transversely isotropic.

Obviously, I could examine anisotropic materials as well, but in numerical homogenization, I could not derive its material stiffness matrix because of the large number of unknowns. Furthermore, anisotropic materials provide greater strength and stiffness than isotropic materials, but the extra strength gained in one direction results in weaker material in other directions. Regarding concrete – that I have already investigated –, this behaviour does not hold.

In case of numerical homogenization, the heterogeneous material is the same concrete as before, with phase '0' referring to the matrix, i.e. portland cement, '1' to the aggregates, '2' to the microvoids and '3' to the steel fibers. The applied material properties:

$$E_0 = 20 \text{ GPa}, \nu_0 = 0.15, E_1 = 30 \text{ GPa}, \nu_1 = 0.2, E_3 = 200 \text{ GPa}, \nu_3 = 0.3 .$$

When studying the behaviour of concrete, considering the existence of microvoids as well, any discontinuities shall be avoided, therefore voids are assumed to be very weak inhomogeneities and the engineering constants are set to be

$$E_2 = 0.01 \text{ GPa}, \nu_2 = 0.01 .$$

The geometry of the investigated material is the same block of $100 \times 100 \times 100 \text{ mm}$, that is the RVE of concrete. The random microstructure can be modeled as a fictitious periodic microstructure.

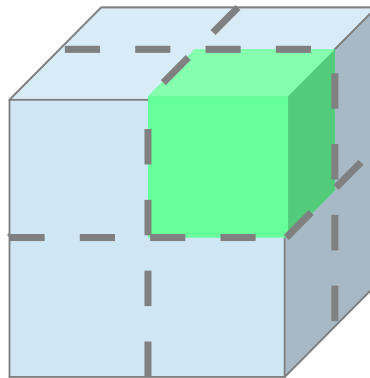


Figure 75 The symmetry of the RVE

Due to this fictitious periodicity and the overall geometry of the RVE, there are three symmetry planes that cut the RVE into 8 blocks of $50 \times 50 \times 50 \text{ mm}$ (Figure 75). Hence, it is convenient to model only this smaller block of composite material by applying symmetry boundary conditions on the surfaces connecting to the other blocks.

The connection between the averaged stresses $\bar{\sigma}_{ij}$ and strains $\bar{\varepsilon}_{ij}$ over the RVE are given with the help of the effective elastic stiffness matrix of transversely isotropic materials as

$$(6.12) \quad \begin{bmatrix} \bar{\sigma}_1 \\ \bar{\sigma}_2 \\ \bar{\sigma}_3 \\ \bar{\sigma}_4 \\ \bar{\sigma}_5 \\ \bar{\sigma}_6 \end{bmatrix} = \begin{bmatrix} L_{11} & L_{12} & L_{13} & 0 & 0 & 0 \\ L_{12} & L_{11} & L_{13} & 0 & 0 & 0 \\ L_{13} & L_{13} & L_{33} & 0 & 0 & 0 \\ 0 & 0 & 0 & L_{44} & 0 & 0 \\ 0 & 0 & 0 & 0 & L_{44} & 0 \\ 0 & 0 & 0 & 0 & 0 & \frac{L_{11} - L_{12}}{2} \end{bmatrix} \begin{bmatrix} \bar{\varepsilon}_1 \\ \bar{\varepsilon}_2 \\ \bar{\varepsilon}_3 \\ \bar{\varepsilon}_4 \\ \bar{\varepsilon}_5 \\ \bar{\varepsilon}_6 \end{bmatrix},$$

where the symmetry axis is axis '3' and the stresses and strains are in Voigt form.

Therefore, the transverse elastic modulus:

$$(6.13) \quad E_T = E_1 = E_2 = (L_{11} - L_{12}) \frac{(L_{11}L_{33} + L_{12}L_{33} - 2L_{13}^2)}{(L_{11}L_{33} - L_{13}^2)},$$

the longitudinal elastic modulus:

$$(6.14) \quad E_L = E_3 = L_{33} - \frac{2L_{13}^2}{L_{11} + L_{12}}.$$

The longitudinal Poisson's ratio:

$$(6.15) \quad \nu_{13} = \frac{L_{13}}{L_{11} + L_{12}},$$

and the transversal Poisson's ratio:

$$\nu_{12} = \frac{L_{12}L_{33} - L_{13}^2}{L_{11}L_{33} - L_{13}^2}.$$

The shear modulus in transversal plane:

$$(6.16) \quad G_{12} = \frac{L_{11} - L_{12}}{2}.$$

In this paper, I will not compute the longitudinal shear modulus, but it is defined by

$$(6.17) \quad G_{13} = G_{23} = L_{44}.$$

The basic idea of evaluating the effective stiffness matrix using numerical homogenization is to subject the RVE of an applied strain ε_{ij}^0 , and from the resulting stress field, the elements of the elastic stiffness matrix can be calculated. The boundary conditions on displacements:

$$(6.18) \quad u_i(a_1, y, z) - u_i(0, y, z) = a_1 \varepsilon_{i1}^0, \quad \begin{cases} 0 \leq y \leq a_2 \\ 0 \leq z \leq a_3 \end{cases},$$

$$(6.19) \quad u_i(x, a_2, z) - u_i(x, 0, z) = a_2 \varepsilon_{i2}^0, \quad \begin{cases} 0 \leq x \leq a_1 \\ 0 \leq z \leq a_3 \end{cases},$$

$$(6.20) \quad u_i(x, y, a_3) - u_i(x, y, 0) = a_3 \varepsilon_{i3}^0, \quad \begin{cases} 0 \leq x \leq a_1 \\ 0 \leq y \leq a_2 \end{cases}.$$

In (6.18)-(6.20) $a_j \varepsilon_{ij}^0$ is the displacement needed to produce strain ε_{ij}^0 over distance a_j . According to the average strain theorem given in (5.22), the applied strain ε_{ij}^0 on the boundary of the RVE equals to the volume average of the resulting strain field inside the RVE:

$$(6.21) \quad \bar{\varepsilon}_{ij} = \frac{1}{V} \int_V \varepsilon_{ij} dV = \varepsilon_{ij}^0.$$

Since the connection between the average stresses and strains are given as (6.12), the effective material stiffness tensor can be generated by solving four elastic models of the RVE subjected to the displacement boundary conditions given in (6.18)-(6.20). If the applied strain ε_{ij}^0 is of unit magnitude, the i -th element of averaged stress $\bar{\sigma}$ computed by the finite element software determines directly the (i, j) -th element of the effective material stiffness matrix:

$$(6.22) \quad \underline{\underline{L}}(i, j) = \bar{\sigma}(i) = \frac{1}{V} \int_V \sigma(i)(x, y, z) dV \quad \text{with } \varepsilon_j^0 = 1,$$

where the applied strain ε_{ij}^0 is also converted into Voigt form ε_i^0 .

The integrals (6.22) are evaluated in each element of the numerical model of RVE using the Gauss-Legendre quadrature. The finite element software computes the average stresses and the volumes for every element. From (6.22), applying $\varepsilon_1^0 = 1$ determines $\underline{\underline{L}}(i, 1)$, i.e. the first column of $\underline{\underline{L}}$. Taking into account the symmetry of the RVE, the boundary conditions of the first load set:

$$(6.23) \quad \left. \begin{array}{l} u_1(a_1, y, z) = a_1 \\ u_1(0, y, z) = 0 \\ \sigma_{12}(a_1, y, z) = 0 \\ \sigma_{12}(0, y, z) = 0 \\ \sigma_{13}(a_1, y, z) = 0 \\ \sigma_{13}(0, y, z) = 0 \end{array} \right\}, \quad \left. \begin{array}{l} u_2(x, a_2, z) = 0 \\ u_2(x, 0, z) = 0 \\ \sigma_{21}(x, a_2, z) = 0 \\ \sigma_{21}(x, 0, z) = 0 \\ \sigma_{23}(x, a_2, z) = 0 \\ \sigma_{23}(x, 0, z) = 0 \end{array} \right\}, \quad \left. \begin{array}{l} u_3(x, y, a_3) = 0 \\ u_3(x, y, 0) = 0 \\ \sigma_{31}(x, y, a_3) = 0 \\ \sigma_{31}(x, y, 0) = 0 \\ \sigma_{32}(x, y, a_3) = 0 \\ \sigma_{32}(x, y, 0) = 0 \end{array} \right\}.$$

The displacement boundary conditions of computing the second column $\underline{\underline{L}}(i, 2)$ by applying $\varepsilon_2^0 = 1$:

$$(6.24) \quad \left. \begin{array}{l} u_1(a_1, y, z) = 0 \\ u_1(0, y, z) = 0 \end{array} \right\}, \quad \left. \begin{array}{l} u_2(x, a_2, z) = a_2 \\ u_2(x, 0, z) = 0 \end{array} \right\}, \quad \left. \begin{array}{l} u_3(x, y, a_3) = 0 \\ u_3(x, y, 0) = 0 \end{array} \right\}$$

and that of computing the third column $\underline{\underline{L}}(i, 3)$ by applying $\varepsilon_3^0 = 1$:

$$(6.25) \left. \begin{array}{l} u_1(a_1, y, z) = 0 \\ u_1(0, y, z) = 0 \end{array} \right\}, \left. \begin{array}{l} u_2(x, a_2, z) = 0 \\ u_2(x, 0, z) = 0 \end{array} \right\}, \left. \begin{array}{l} u_3(x, y, a_3) = a_3 \\ u_3(x, y, 0) = 0 \end{array} \right\}$$

The fourth and fifth columns are not considered here, and the sixth column can be calculated from the elements of the first three columns.

6.2.2 The applied numerical model

During numerical homogenization, I use the finite element software Mechanical APDL version 14.5 by Ansys™. I write *macrofiles* in which the input parameters can be changed regarding the size of the concrete block, the size of the inhomogeneities, the shape of the inhomogeneities and the material properties.

In details, the input parameters are the size of the inhomogeneities, namely the radius of sphere, and in case of ellipsoids, the ratio between major and minor semi-axes. The size of the concrete block is $50 \times 50 \times 50$ mm in every case. The material properties are given with their material stiffness matrices, which were computed from the engineering constants using the Matlab™ code I generated at the analytical homogenization.

I applied element type SOLID186 (Figure 76), which is a higher-order 20-node solid element. At every nodes, the degrees of freedom are the translations in the nodal x, y, z directions. It is suitable for structural solids with irregular mesh, hence, it is convenient to apply in the numerical homogenization of composite materials.

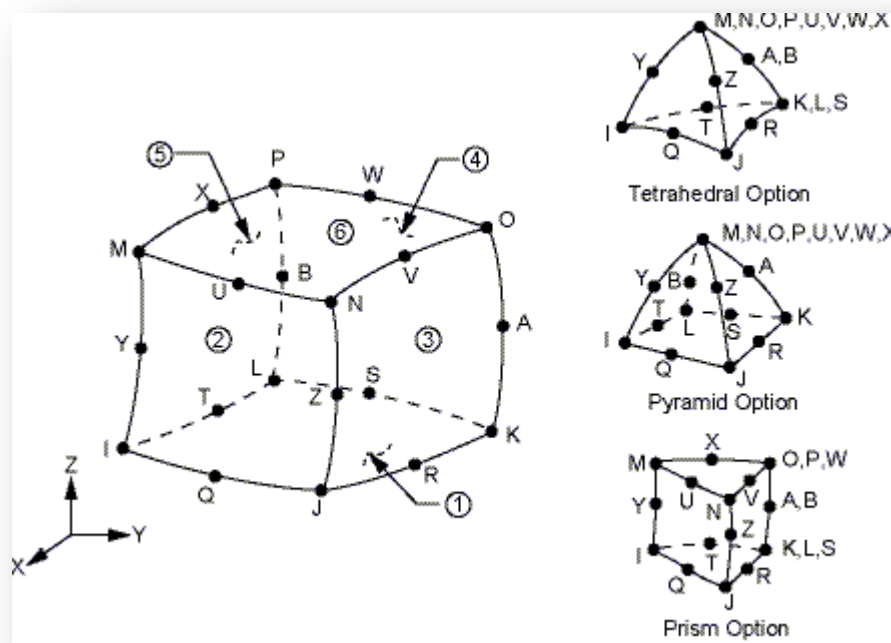


Figure 76 SOLID186 element type

When creating the geometry, first I generated eight pieces of quarter-spheres in the corners of the block of concrete, and one sphere in the middle of the block, then I created the block itself, intersecting the quarter-spheres that resulted in one-eighth of spheres in the corners. If

the inhomogeneities are of ellipsoidal shape, the spheres have to be rescaled by altering the position of their surrounding areas.

First, I divide the lines into six sections, which will be the starting point of meshing the volumes. The difficult geometry of the matrix can only be meshed by applying free meshing with tetrahedral shaped elements. The meshing of the volumes of inhomogeneities are done next. The material properties are rendered to each phase in this step of modelling.

The three different sets of boundary conditions are defined as three loadsteps, and finally, a static analysis is carried out for each loadstep. An additional macro file calculates the effective stiffness matrix based on (6.22). It reads the element volumes and element stresses of the finite element analysis, multiplying them and integrating along the total volume, and finally dividing by the total volume of the concrete block.

6.2.3 Two-phase model

6.2.3.1 Effect of volume fraction

In this section, I examine the behavior of a heterogeneous material considering spherical inhomogeneities. The radii of the spheres are set to result in volume fractions of inhomogeneities $c_1 = 0.6$, $c_1 = 0.7$ and $c_1 = 0.8$, respectively. The geometry of the block (Figure 77) and the heterogeneities (Figure 78):

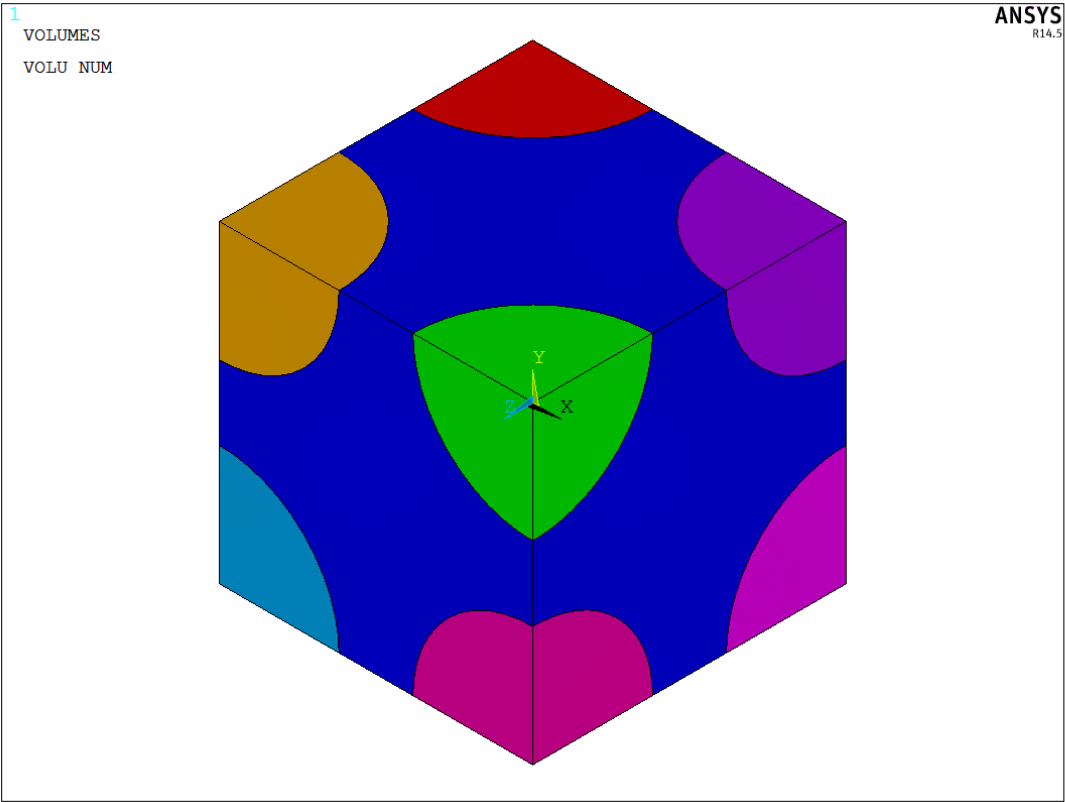


Figure 77 The examined block of composite material

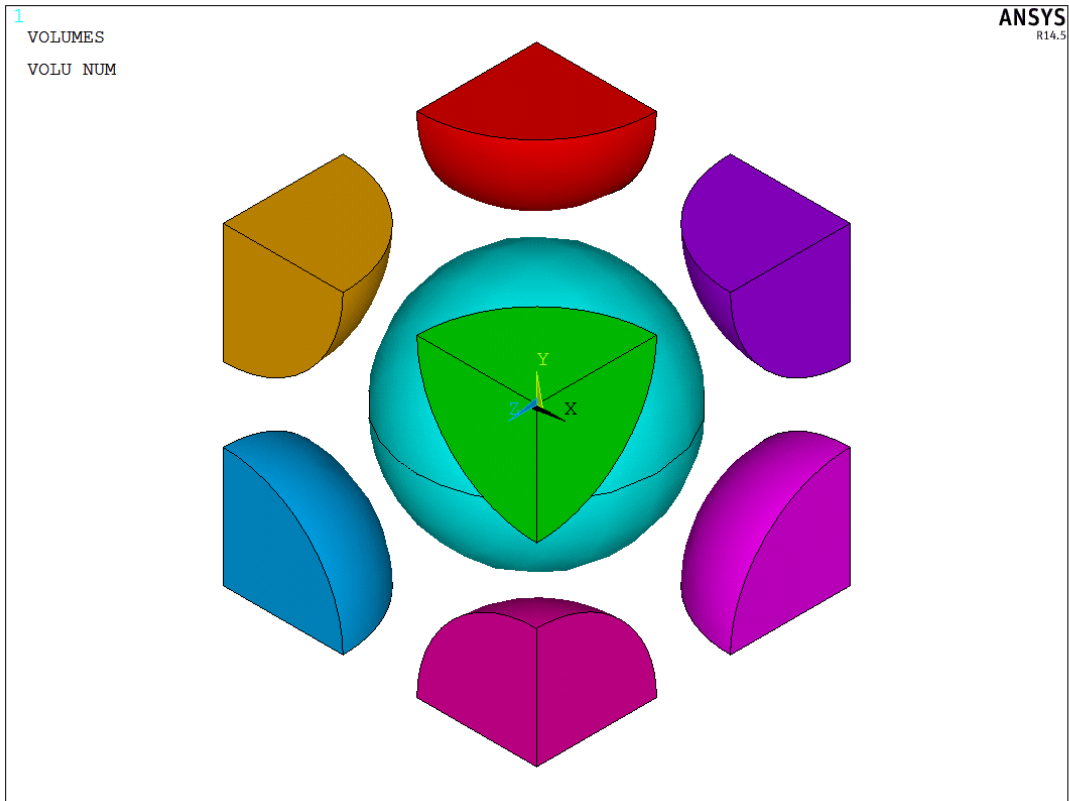


Figure 78 The fictitious distribution of spherical inhomogeneities

The results coming from finite element analysis (FEA) are compared to that of the analytical homogenization (Figure 79):

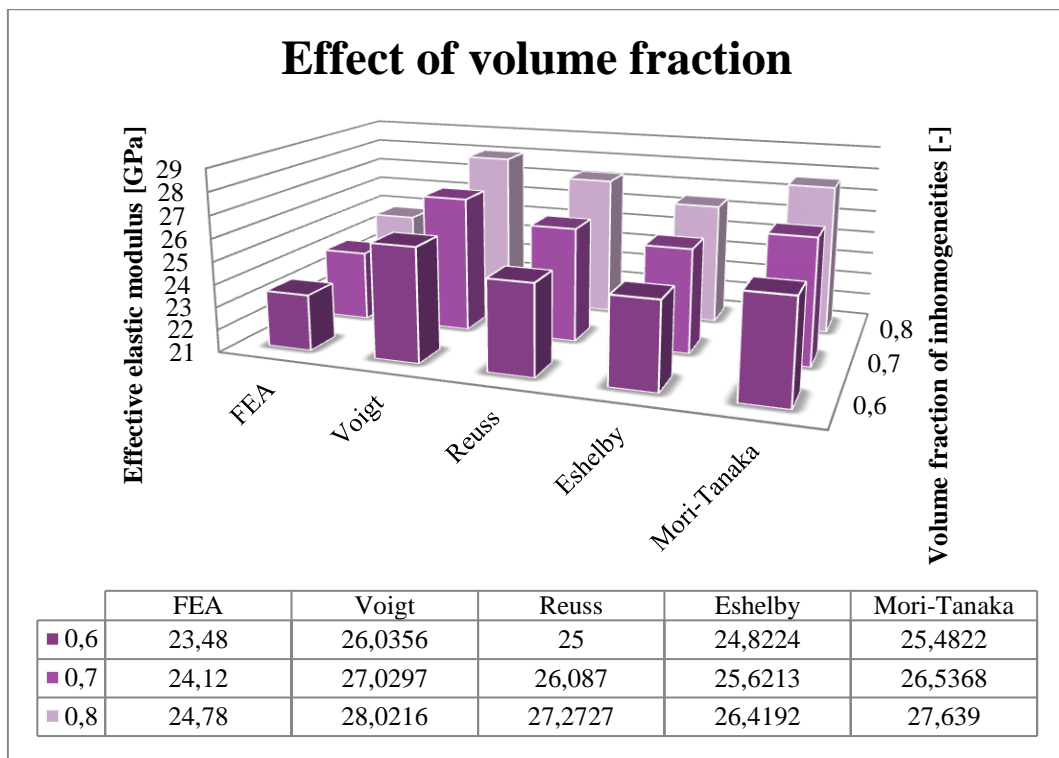


Figure 79 Effect of volume fraction of inhomogeneities on overall elastic modulus of heterogeneous material

The analytical results overestimate the effective engineering properties of the composite material under consideration. The *numerical analysis can take into account the whole set of inhomogeneities*, including their *positions*, their *sizes* and *shapes*, therefore their effect on each other, the *interaction between them* when examining the behaviour of the heterogeneous material under prescribed boundary conditions. In Figure 80, we can see the x, y, z components of the resulting stress field of the three loadsteps, i.e. unit displacements in x, y, z directions, respectively ($c_1 = 0.8$). The stress field characterizes the stiffness of the material.

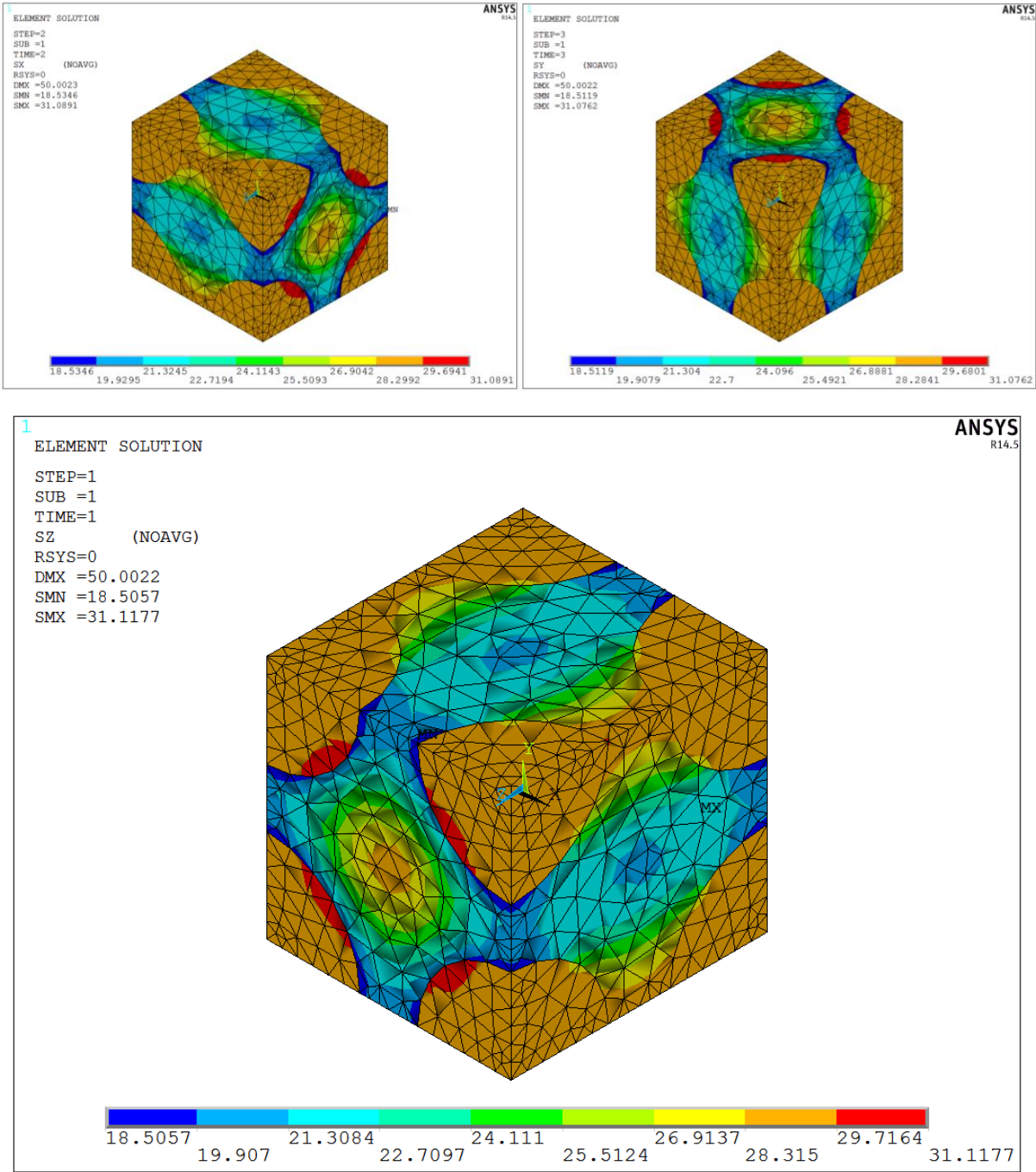


Figure 80 The x, y, z components of stress field inside RVE under unit displacements in x, y, z directions, respectively

Between the particles, parallel to the applied displacements, there is a ‘bridging’ effect that stiffens the cement material. Otherwise, inside the matrix the governing value is close to the value of the elastic modulus of cement, meaning the particles have no stiffening effect in this part of the composite material. Inside the inhomogeneities, some softening can be observed, and these effects considered in the numerical solution result in an overall Young’s modulus smaller than in case of analytical homogenization.

6.2.3.2 Effect of shape of inhomogeneities

In the following, I compare results coming from heterogeneous materials with inhomogeneities of spherical ($a_1 = a_2 = a_3$), oblate spheroidal ($a_1 > a_2 = a_3$) and prolate spheroidal ($a_1 < a_2 = a_3$) shapes. The volume fraction of heterogeneities $c_1 = 0.6$ is held constant, while the ratio of major to minor semi-axes is $\frac{a_1}{a_3} = 1.25$, $\frac{a_1}{a_3} = 1.67$ and $\frac{a_1}{a_3} = 2.5$, respectively. With this size of RVE and volume fraction of heterogeneities, larger values of ratio $\frac{a_1}{a_3}$ cannot be investigated, since they simply cannot fit into this RVE.

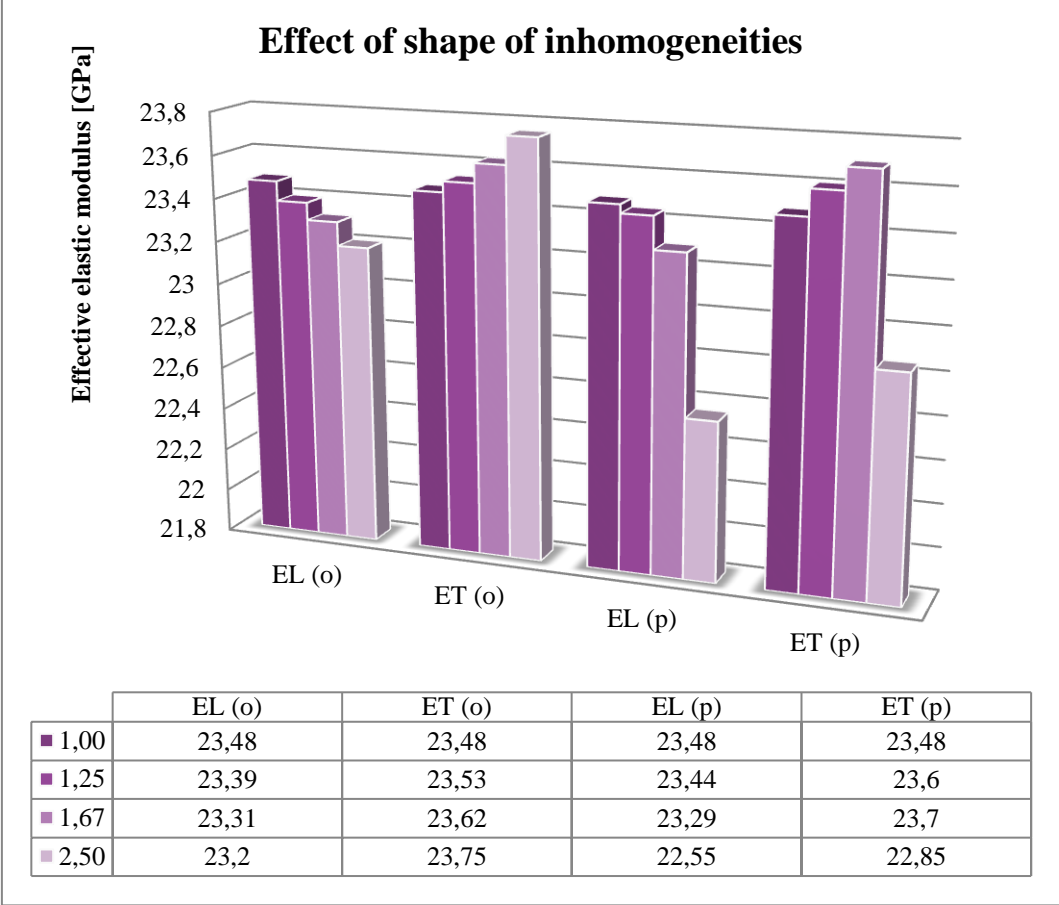


Figure 81 Effect of shape of inhomogeneities on overall Young’s modulus of heterogeneous material

In Figure 81, the numerical homogenization results of a material containing oblate (o) and prolate (p) spheroidal heterogeneities can be seen. The major axes of the spheroids are parallel to the global x axis and the longitudinal (EL) elastic modulus belongs to the global z axis

(Figure 82). When the major to minor axis ratio is of unit magnitude, the spheroids become spheres and all four values of Young’s modulus are the same. It is obvious that when changing the shape of the spheroids, a decrease in the value of the longitudinal elastic modulus implies an increase in that of the transversal elastic modulus. The difference between an oblate and a prolate spheroid at small $\frac{a_1}{a_3}$ ratios, like the applied ratios, is negligible.

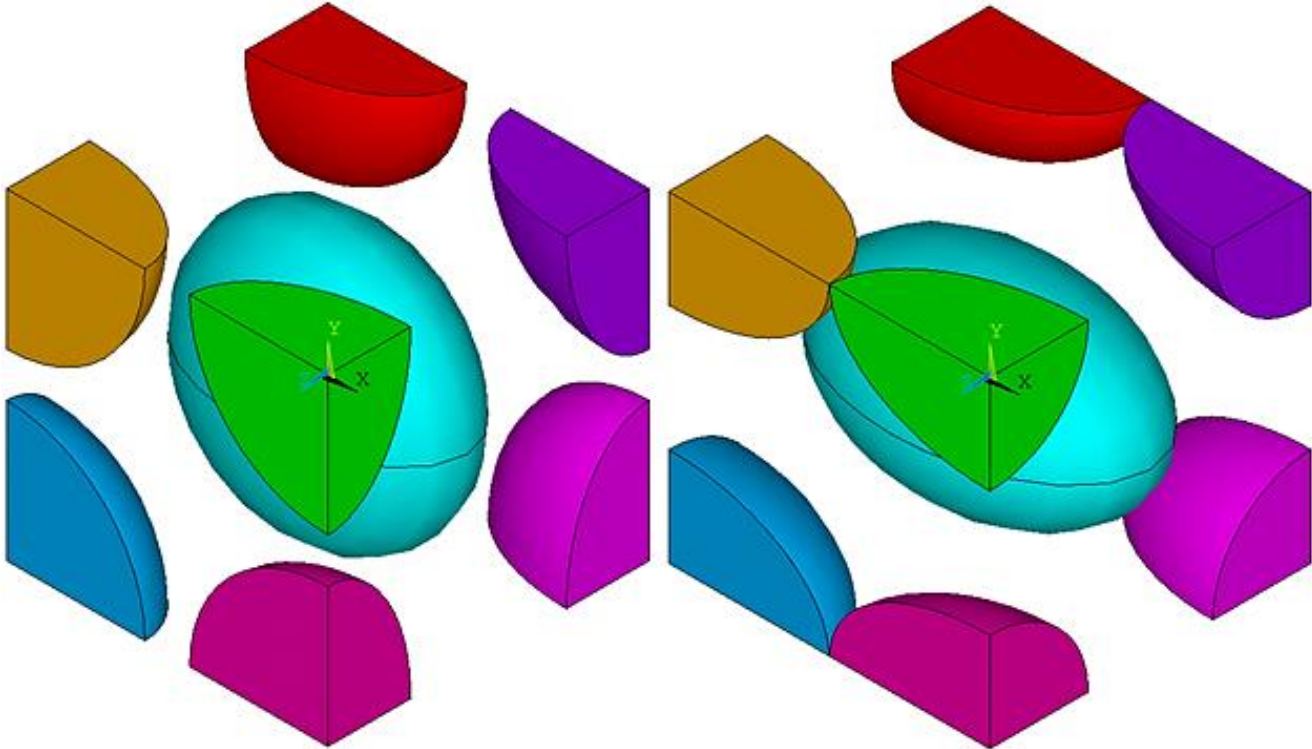


Figure 82 Oblate and prolate spheroidal inhomogeneities

The last columns of the diagram (Figure 81) at prolate spheroids show discrepancy in the behaviour of the model. It can be explained by the fact that prolate spheroids of volume fraction $c_1 = 0.6$ and ratio $\frac{a_1}{a_3} = 2.5$ do not fit inside the block of $50 \times 50 \times 50$ mm of the heterogeneous material. Hence, I had to modify the geometry by generating only four pieces of one-eighth of spheroids in the four corners at the ends of two space diagonals of the block (Figure 83).

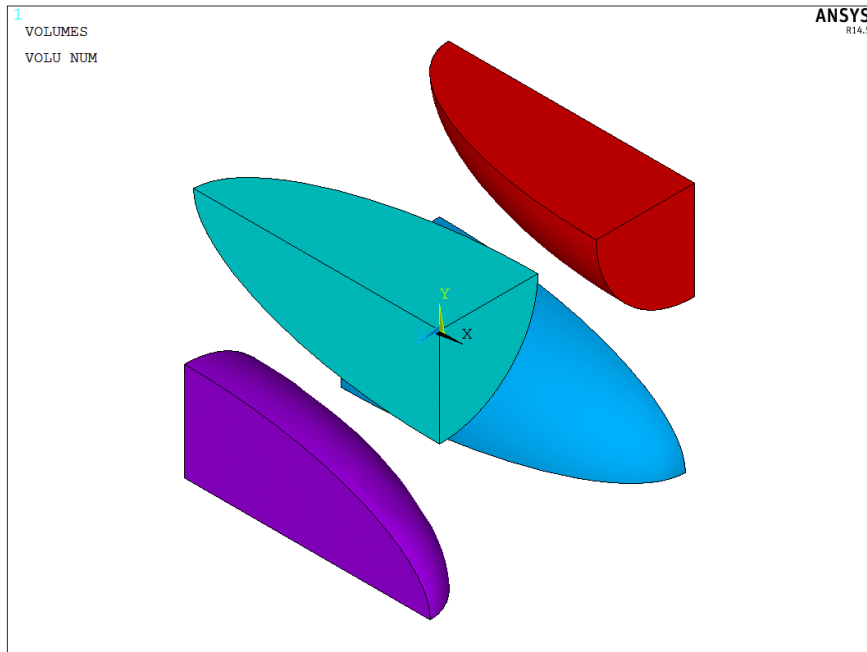


Figure 83 *Modified geometry of spheroids with large major-to-minor axis ratio*

We can see in Figure 84, that due to this necessary modification of geometry, the numerical model cannot take into account the stiffening effect between the particles parallel to the applied displacements (Figure 85) which explains the incorrect results in Figure 81.

I note that the numerical homogenization can take into account the interaction of the particles, but only if their positions and distribution over the volume is set properly, otherwise they yield poor results comparing to the analytical methods. In order to correct the results, a completely different geometric model regarding the distribution of inhomogeneities would be necessary.

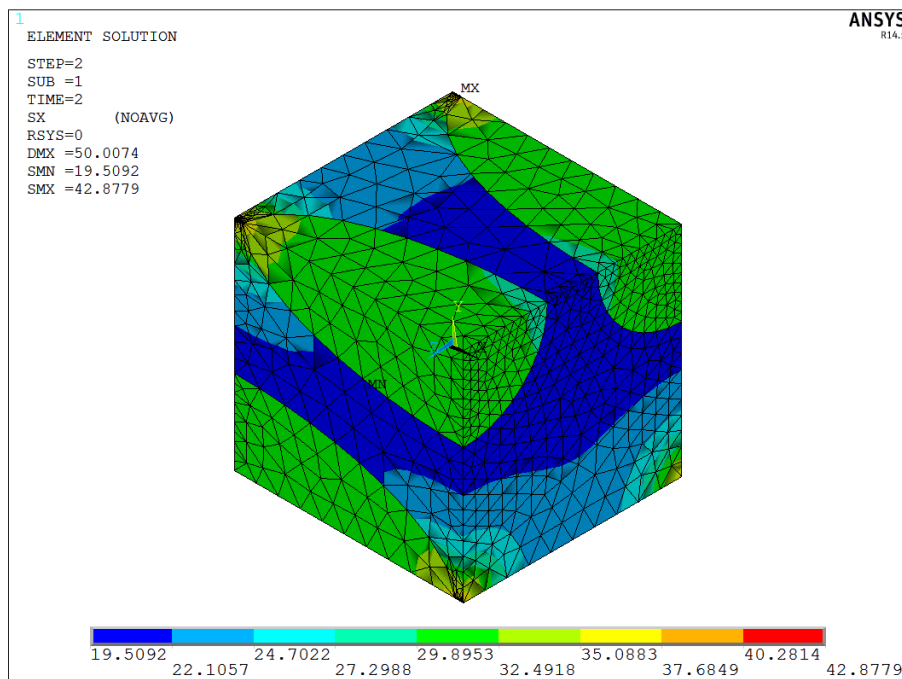


Figure 84 *The inaccuracy of the modified geometry*

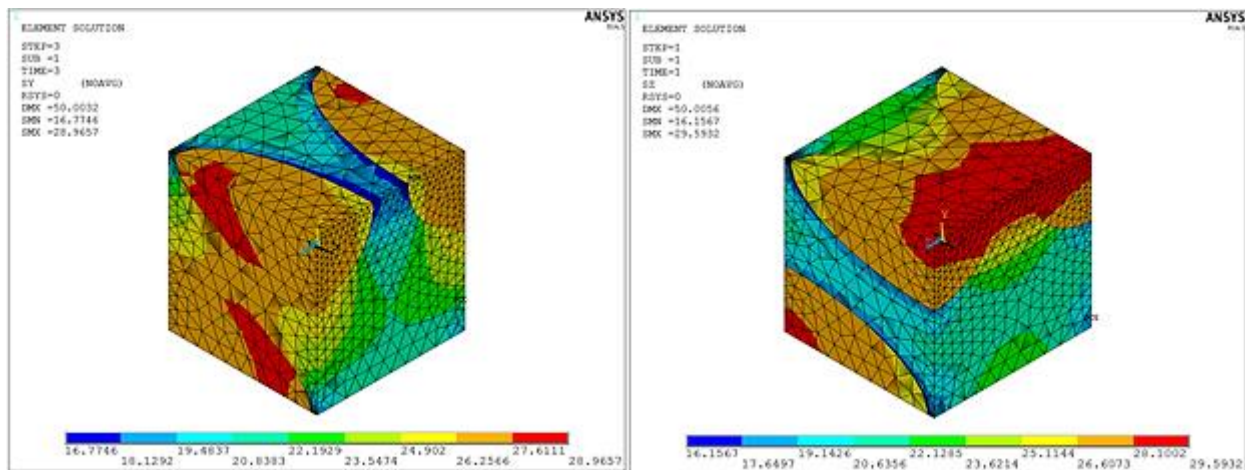


Figure 85 The modified numerical model under unit displacements parallel to the minor axes of spheroid

6.2.4 Three- and four-phase model

In the three-phase model, I consider spherical voids as inhomogeneities embedded in a matrix with material properties originated from the results of two-phase models in the previous section. In other words, the three-phase numerical model is a two-phase model, where the material properties of the matrix are the overall material properties of a two-phase composite consisting of cement and aggregates. The original two-phase model consists of prolate spheroidal inhomogeneities with major-to-minor ratio of semi-axes of 1.67 and their volume fraction is 60V%. The three-phase model considers the microvoids in concrete by applying very weak inhomogeneities ($E_3 = 0.01$ GPa, $\nu_3 = 0.01$). The volume fraction of microvoids is $c_2 = 0.05$ and the results are compared to that of the analytical homogenization in Table 3:

Table 3 Effective elastic modulus of a three-phase model

		Effective elastic modulus (GPa)				
		FEA (l)	FEA (t)	Voigt	Eshelby	Mori-Tanaka
c_2	0	23,29	23,69	26,04	25,19	25,67
	0,05	21,96	21,96	24,53	22,84	22,94

Due to the existence of microvoids, the effective elastic modulus of concrete decreases by 5.7%, 7.3%, 6.5%, 5.8%, 9.3%, 10.6% according to the finite element analysis (longitudinal and transversal values), and to the Voigt-, Eshelby- and Mori-Tanaka estimation, respectively. Hence, the latter two analytical methods overestimate the deteriorating effect of microvoids.

The four-phase model – similarly to the three-phase model –, applies inhomogeneities in a matrix material, i.e. it is a special type of two-phase model, where the material properties of the matrix come from the results of the three-phase model presented above. Phase ‘3’ refers to the steel reinforcing fibers with volume fraction of $c_3 = 0.03$, and with a prolate spheroidal shape where the ratio of major to minor axis is 10. The numerical results can be compared to the effective properties of the same heterogeneous material computed from analytical homogenization methods (Table 4):

Table 4 Effective elastic modulus of a four-phase model

				Effective elastic modulus (GPa)				
				FEA (l)	FEA (t)	Voigt	Eshelby	Mori-Tanaka
c_2	0	c_3	0	23,29	23,69	26,04	25,19	25,67
	0,05		0	21,96	21,96	24,53	22,84	22,94
	0,05		0,03	23,94	24,09	29,86	28,78	29,03

The geometry had to be modified again, since the fibers are needle-type inhomogeneities, but it resulted again in an inaccurate behaviour of the numerical model (see Figure 84). The increase in the elastic modulus compared to the three-phase model: 9.0%, 9.7%, 21.7%, 26.0%, 26.5%; and to the two-phase model: 2.8%, 1.7%, 14.7%, 14.25%, 13.1%, according to the finite element analysis (longitudinal and transversal values), and to the Voigt-, Eshelby- and Mori-Tanaka estimation, respectively. Clearly, the numerical homogenization yields incorrect results, since the fibers should be of larger number and be distributed over the whole volume in a more realistic way.

In numerical homogenization, the real distribution and shape of inhomogeneities can be modelled quite precisely, however, the definition of geometry is extremely time-consuming. In general, the analytical methods overestimate the effective properties, but they yield a steady, therefore reliable set of effective properties.

7 Summary

The aim of this work was to introduce the mesolevel mechanical modeling of heterogeneous materials by understanding its mathematical and micromechanical background. Furthermore, another purpose of this paper was presenting examples for both analytical and numerical solutions of the disturbing effect of the presence of inhomogeneities in the elastic field of a heterogeneous material and of homogenization methods.

The mathematical background is based on the application of integral theorems and Green's functions which is useful at the solution of inhomogeneous boundary value problems. The main idea of the mechanical background of mesolevel modeling is to take into account the disturbing effect of distinct phases of a heterogeneous material in the elastic field of the material.

The comparative study of the analytical and numerical results of the elastic field of a heterogeneous material containing an ellipsoidal shaped inhomogeneity under applied loading showed that the analytical solution based on the application of Green's functions, and on Eshelby's equivalent inclusion method yields surprisingly exact results without the time-consuming process of building a numerical model. Of course, the correctness of the resulting elastic field is dependent on the mesostructure of the heterogeneous material, i.e. it varies in case of particle- and fiber-reinforced materials.

With the help of homogenization methods, I computed the effective material properties of concrete given that the material properties and the volume fractions of the additives are known. Comparing the analytical and numerical solutions, I observed that the analytical methods cannot take into account the interaction between the individual phases of the heterogeneous material, thereby they need some further improvement. On the other hand, they give an extremely fast result from very few input data, hence I would recommend to use them for example at concrete plants to predict the strength of concrete based on the always changing quality of applied additives.

Summarizing my experiences described above, the scope of this paper was satisfactorily achieved, moreover, such questions arised during this work that I would like to answer hereafter. In the future, I would like to address my studies to *higher-order computational homogenization* (Geers, Kouznetsova, & Brekelmans, 2011).

The development of computational methods allows us to apply so-called *unit cell methods* in multiscale modeling. These methods provide information on the effective material properties by fitting the averaged microscopical elastic fields, resulting from the analysis of a microstructural representative unit cell subjected to prescribed loading, on macroscopic phenomenological constitutive equations. When a macroscopic behaviour becomes non-linear, this approach face great difficulties, therefore the presented homogenization techniques cannot be applied in case of large deformations or complex loading paths, moreover they cannot account for the geometrical and physical changes in the microstructure.

Another type of modelling techniques is the *variational multi-scale method*. The weak form of the governing equations is separated into a coarse (macro-) and fine (micro-) scale part on the basis of suitable assumptions on the fine scale field. The point of this method is to

eliminate the fine scale part from the obtained formulation, but it is highly dependent on the assumptions made a priori.

The most recent technique is the *two-scale computational homogenization*, based on the solution of a nested boundary problem on both scale. *First-order computational homogenization* includes the *first-order gradients of the macroscopic displacement field*, hence, they can take into account large displacements as well. At this technique, assumptions for the macroscopic constitutive behaviour are not required, they are obtained from the solution of the microscopic boundary value problem. Since the microscale problem is a classical boundary value problem, any of the known appropriate methods (finite element method, boundary element method, etc.) can be used.

The *second-order computational homogenization* can take into account the size-effects of microstructural constituents, and can deal with more than simple first-order deformation modes (tension, compression, shear and their combinations) of microstructural cells. The basic idea is to use the Taylor-series expansion of a classical nonlinear deformation map to determine the macroscopic kinematics through *not only its deformation gradient tensor*, but also the *Lagrangian gradient of the deformation gradient tensor*. Hence, this method is ‘deformation driven’, since the macroscopic stresses are ensued from the macroscopic deformation-gradient tensor. After solving the classical boundary value problem obtained at the microscale, the results can be transformed back to the structural level with the help of averaging theorems.

Bibliography

- Asaro, R. J., & Barnett, D. M. (1975). The non-uniform transformation strain problem for an anisotropic ellipsoidal inclusion. *J. Mech. Phys. Solids*(23), 77-83.
- Asaro, R. J., & Lubarda, V. A. (2006). *Mechanics of Solids and Materials*. Cambridge University Press.
- Barbero, E. J. (2014). *Finite Element Analysis of Composite Materials Using ANSYS*. CRC Press.
- Barnett, D. M. (1972). The precise evaluation of derivatives of the anisotropic elastic Green's functions. *Phys. stat. sol.*(49), pp. 741-748.
- Bojtár, I. (2014, January). Material Models. Lecture 4: The basic properties of the material models. Microstructurally based constitutive equations. Budapest.
- Dyson, F. W. (1891). The potentials of ellipsoids of variable densities. *Q. J. Pure and Appl. Math.*(25), 259-288.
- en.wikipedia.org*. (n.d.).
- Eshelby, J. D. (1951). The force on an elastic singularity. *Phil. Trans. Roy. Soc.*, A244, pp. 87-112.
- Eshelby, J. D. (1957). The determination of the elastic field of an ellipsoidal inclusion, and related problems. *Proc. Roy. Soc.*, A241, pp. 376-396.
- Eshelby, J. D. (1959). The elastic field outside an ellipsoidal inclusion. *Proc. Roy. Soc.*, A252, pp. 561-569.
- Eshelby, J. D. (1961). Elastic inclusions and inhomogeneities. (I. N. Sneddon, & R. Hill, Eds.) *Progress in Solid Mechanics 2*, pp. 89-140.
- Ferrers, N. M. (1877). *An elementary treatise on spherical harmonics and subjects connected with them*. London: MacMillan and Co.
- Geers, M., Kouznetsova, V., & Brekelmans, M. (2011). Scale transitions in solid mechanics based on computational homogenization. *CISM Advanced School*. Udine.
- Hashin, Z. (1988). The differential scheme and its applications to cracked materials. *J. Mech. Phys. Solids*, 36, 719-734.
- Hashin, Z., & Shtrikman, S. (1961). Note on a variational approach to the theory of composite elastic materials. *J. Franklin Inst.*, 271, pp. 336-341.
- Hashin, Z., & Shtrikman, S. (1963). A variational approach to the theory of the elastic behaviour of multiphase materials. *J. Mech. Phys. Solids*, 11, 127-140.
- Hill, R. (1963). Elastic properties of reinforced solids: some theoretical principles. *J. Mech. Phys. of Solids*, 11, 357-372.
- Hill, R. (1965). A self-consistent mechanics of composite materials. *J. Mech. Phys. Solids*, 13, 213-222.

- Hooke, R. (1987). *Micrographia* (facsimile ed.). Lincolnwood: Science Heritage Ltd.
- Kepler, J. (1966). *On the Six-cornered Snowflake*. (C. Hardie, Ed., & C. Hardie, Trans.) Oxford: Clarendon Press.
- Khachaturyan, A. G. (1967). Some questions concerning the theory of phase transformations in solids. *Sov. Phys. Solid State*(8), 2163-2168.
- Lalena, J. N. (2006). From quartz to quasicrystals: probing nature's geometric patterns in crystalline substances. *Crystallogr. Rev.*, pp. 125-180.
- mathworld.wolfram.com*. (n.d.).
- Meng, C., & Pollard, D. D. (2014, October). Eshelby's solution for ellipsoidal inhomogeneous inclusions with applications to compaction bands. *Journal of Structural Geology*, 67, 1-19.
- Meng, C., Heltsley, W., & Pollard, D. D. (2012, March). Evaluation of the Eshelby solution for the ellipsoidal inclusion and heterogeneity. *Comput. Geosci.*, 40, 40-48.
- Mindlin, R. D. (1953). Force at a point in the interior of a semi-infinite solid. *Midwestern Conf., Solid Mech.*, (pp. 56-59).
- Mori, T., & Tanaka, K. (1973). Average stress in matrix and average elastic energy of materials with misfitting inclusions. *Acta Metall.*, 21, 571-574.
- Moschovidis, Z. A. (1975). Two ellipsoidal inhomogeneities and related problems treated by the equivalent inclusion method. Evanston: Northwestern University.
- Mura, T. (1964). Periodic distribution of dislocations. *Proc. Roy. Soc.*, A280, pp. 528-544.
- Mura, T. (1987). *Micromechanics of defects in solids*. Dordrecht: Martinus Nijhoff Publishers.
- Mura, T., & Kinoshita, N. (1971). Green's functions for anisotropic elasticity. *phys. stat. sol.*(47), pp. 607-618.
- Mura, T., & Koya, T. (1992). In *Variational Methods in Mechanics*. New York: Oxford University Press.
- Muskhelishvili, N. I. (1953). *Some Basic Problems of the Mathematical Theory of Elasticity*. Noordhoff.
- Nemat-Nasser, S., & Hori, M. (1993). In *Micromechanics: Overall Properties of Heterogeneous Materials*. New York: North-Holland.
- Newton, I. (1730). *Opticks: or a Treatise on the Reflexions, Refractions, Inflexions and Colours of Light* (4th English ed.). London: William Inngs.
- Orowan, E. (1944). Discussion of the significance of tensile and other mechanical test properties of metals. *Proceeding of the Institute of Mechanical Engineers*, 151, pp. 134-146.
- Qu, J., & Cherkaoui, M. (2006). *Fundamentals of Micromechanics of Solids*. John Wiley & Sons, Inc.

- Seo, K., & Mura, T. (1979). The elastic field in a half space due to ellipsoidal inclusions with uniform dilatational eigenstrains. *J. Appl. Mech.*, 46, 568-572.
- Tadmor, E. B., & Miller, R. E. (2011). *Modeling Materials: Continuum, Atomistic and Multiscale Techniques*. Cambridge, United Kingdom: Cambridge University Press.
- Tanaka, K., & Mura, T. (1982). A theory of fatigue crack initiation at inclusions. *Metall. Trans.*(13A), pp. 117-123.
- Timoshenko, S. P., & Goodier, J. N. (1934). *Theory of Elasticity*. McGraw-Hill Book Company.
- Torquato, S. (2001). *Random Heterogeneous Materials: Microstructure and Macroscopic Properties*. New York: Springer.
- Truesdell, C. (1960, February). The Principles of Continuum Mechanics. 5. The Socony Mobile Oil Company, Inc.
- Willis, J. R. (1975). The interaction of gas bubbles in an anisotropic elastic solid. *J. Mech. Phys. Solids*(23), 129-138.
- Willis, J. R. (1977). Bounds and self-consistent estimates for the overall properties of anisotropic composites. *J. Mech. Phys. Solids*, 25, 185-202.
- Willis, J. R. (1981). Variational and related methods for the overall properties of composites. *Adv. Appl. Mech.*, 21, 1-78.